UNIVERSITY OF Southampton

University of Southampton Research Repository
ePrints Soton

Copyright © and Moral Rights for this thesis are retained by the author and/or other copyright owners. A copy can be downloaded for personal non-commercial research or study, without prior permission or charge. This thesis cannot be reproduced or quoted extensively from without first obtaining permission in writing from the copyright holder/s. The content must not be changed in any way or sold commercially in any format or medium without the formal permission of the copyright holders.

When referring to this work, full bibliographic details including the author, title, awarding institution and date of the thesis must be given e.g.

AUTHOR (year of submission) "Full thesis title", University of Southampton, name of the University School or Department, PhD Thesis, pagination

http://eprints.soton.ac.uk

UNIVERSITY OF SOUTHAMPTON

FACULTY OF PHYSICAL SCIENCES AND ENGINEERING

Electronics and Computer Science

Reliability and interconnections for printed circuits on fabrics

by

Komolafe Abiodun Oluwaseyi

Thesis for the degree of Doctor of Philosophy

12th May 2016

UNIVERSITY OF SOUTHAMPTON

ABSTRACT

FACULTY OF PHYSICAL SCIENCES AND ENGINEERING

Electronics and Computer Science

Thesis for the degree of Doctor of Philosophy in

RELIABILITY AND INTERCONNECTIONS FOR PRINTED CIRCUITS ON FABRICS

Komolafe, Abiodun Oluwaseyi

E-textiles are specially engineered textiles that perform intelligent functions such as sensing and actuation. They find useful applications in medicine, the military, fashion and entertainment. However the durability of these textiles is limited by mechanical failure resulting in degradation of the electrical performance of the electronic circuits incorporated into them when they are exposed to stresses from washing and bending which leave the host textile undamaged.

This thesis investigates the methods for improving the durability and wearability of printed circuits on fabrics with an initial review of the state of the art interconnection technologies and integration techniques for adding electronic capabilities to fabrics. The durability solutions for e-textiles in the literature are examined to identify their limitations and potential for achieving durable e-textiles. A preliminary assessment of the durability of a printed e-textile fabricated by screen printing is conducted to empirically identify the failure modes that result from washing the e-textile.

Consequently, a theoretical model for characterising the bending behaviour of printed e-textiles is developed to locate the neutral axis (NA) position where printed circuits integrated to fabrics can be positioned to improve their durability. The model integrates Pierce's fabric cantilever test with the classical beam theory to predict the NA positions of four screen printed e-textiles based on different blends of polyester/cotton/lycra fabric. Modelling and empirical results show that piezoresistive strain gauges, screen printed as conductors within ±1 % distance from these NA positions, show approximately 0.3 % and 10 % change in electrical

resistance for a bending radius of 5 mm and five washing cycles respectively. This contrasts to the corresponding changes of the 37 % and 400 % in the resistance of the strain gauges positioned at a 65 % distance to the NA.

This thesis also examines the use of photolithography and thin film deposition techniques to integrate functional thin film circuits with resolution down to 30 µm on fabrics. The advantages of flexible substrates such as Kapton over polymer coated fabrics for adding these fine circuits to fabrics is discussed. A 0.8 mm wide electronic plastic strip containing micron-scale components such as LEDs is fabricated to demonstrate the technology. The strip is 40 % of the size of the state of the art offering better concealment in fabrics.

Contents

List of tables

List of figures

DECLARATION OF AUTHORSHIP

I, Komolafe Abiodun Oluwaseyi declare that this thesis and the work presented in it are my own and has been generated by me as the result of my own original research.

Reliability and interconnections for printed circuits on fabrics

I confirm that:

1. This work was done wholly or mainly while in candidature for a research degree at this University;

2. Where any part of this thesis has previously been submitted for a degree or any other qualification at this University or any other institution, this has been clearly stated;

3. Where I have consulted the published work of others, this is always clearly attributed;

4. Where I have quoted from the work of others, the source is always given. With the exception of such quotations, this thesis is entirely my own work;

5. I have acknowledged all main sources of help;

6. Where the thesis is based on work done by myself jointly with others, I have made clear exactly what was done by others and what I have contributed myself;

7. Parts of this work have been published as listed in section 1.4 of this thesis.

Signed: .....

Date: 12th May 2016

Acknowledgements

I thank God Almighty for His continued grace, favour and guidance during my PhD program, without which I'd be lost. I am also deeply grateful to my supervisors, Prof. Steve Beeby, Dr. John Tudor and Dr. Russell Torah who had all been of immense help, support and encouragement during the program. I am particularly grateful to Prof. Steve Beeby who funded a huge part of my PhD through his leadership grant.

I must also recognise my Pastor, Rev. Charles Ajai-ajagbe who showed me so much great care, attending both my physical and spiritual needs throughout my PhD program. Huge thanks also goes to all my church members, CB, Eela, Mrs Orekoya, Sister Judith and my pastor, Pastor Kunle Bello. I would like to thank all my colleagues in the Smart fabric group, Ahmed, Zhuo, Zihao, Dr. Yi Li 1 and 2, Dr. Kai, Yang, Zeeshan, Nursabirah, Joseph, Marc, Dr. Jerry and Sasi even to those who joined the group towards the end of my program, Menlong, Jinjie, Monika and Olivia.

Final thanks goes to my Parents, my siblings and my aunty Shade who have all been supportive though my program. Thanks goes to them for their financial and moral support to ensure this PhD was a success.

Nomenclature

Acronyms/abbreviations

ASTM – American Standard for Testing of Materials

Bari – a commercial 65 % / 35 % polyester- cotton fabric

BS – British Standards

CBT – Classical beam theory

CPW – Coplanar waveguides

DC – Direct current

ECG/EKG – Electrocardiogram

EMG – Electromyography

EN – European Standards

EOG – Electrooculography

Escalade – A commercial 16 % /46 % /38 % polyester-cotton-lycra fabric

FLC – Four layer composite

FR-4 – A grade of fire or flame retardant fibreglass reinforced epoxy laminates

Fabink UV-IF-1 – A commercial thermoplastic polyurethane paste

Fabink UV-IF-010 – A commercial thermoplastic elastomer polyurethane paste

Fabink TC-PolyPR1 – A commercial piezo-resistive paste

GND – Ground

ISO – International Standardisation Organisation

Lagonda – A commercial 30 % /40 % /30 % polyester-cotton-lycra fabric

MC – Mesh count

NB – Negative bending

NBI – Negative bending based on modelling the interface layer effect on a fabric

NMP – N-Methyl-2-pyrrolidone

PB – Positive bending

PBI – Positive bending based on modelling the interface layer effect on a fabric

PDMS – Polydimethylsiloxane

PET – Polyethylene terephthalate

PS – Particle size

TPU – Thermoplastic polyurethane

TPI – Tiny programming interface

SG – Strain gauge

SMA – Sub-miniature Version A

UV – Ultraviolet

Parameters

A – Surface area of a film or material

B – Bending modulus

β – Bimodular ratio of a fabric

δ – Distance between the central axis and the neutral axis

E – Young's modulus

EI – Flexural rigidity or stiffness

E_r – Reduced modulus

E_A – Young's modulus of the top layer of a bilayer composite

E_B – Young's modulus of the bottom layer of a bilayer composite

E_I – Young's modulus of indenter

E_i – Young's modulus of the i^{th} layer in a multilayer composite

E_T – Tensile modulus of a material

E_C – Compressive modulus of a material

ε – Bending strain

ε_t – Theoretical strain

ε_{tl} – Theoretical strain based on modelling of the interface layer effect on fabric

ε_p – Empirical strain

e_i – Young's modulus ratio of the i^{th} layer and the 1st sub-layer in the bottom or top layer

e_A – Young's modulus ratio of the top layer and the 1st sub-layer in the top layer

e_B – Young's modulus ratio of the bottom layer and the 1st sub-layer in the bottom layer

F – Applied force

G – Bending rigidity

GF – Gauge factor

H_A – Thickness of top layer of a bilayer

H_B – Thickness of bottom layer of a bilayer

h – Thickness of a layer within a multilayer composite

h_T – Optimised thickness of a layer in a multilayer composite

h_i – Thickness of the i^{th} layer in a multilayer composite

I – Moment of inertia

k – Relative modular difference of a fabric

L – Bending length of a fabric

l – Length of a conductor

M – Bending moment

n – Fractional change in the neutral axis from its initial central axis position

η – Asymmetric factor of a fabric

θ – Bending angle of fabric or composite

σ – Bending stress

ρ – Electrical resistivity of a material

R – Electrical resistance

ΔR – Change in electrical resistance

R_a value – Average surface roughness

R_{sq} – Sheet resistance

r – Bending radius

s – Extension in a material or film

t – Thickness of a conductor

t_i – Ratio of the thickness of the i^{th} layer and the 1st sub-layer in the bottom or top layer

t_w – Mesh thickness

V_{CC} – Power supply pin

υ – Poisson ratio

υ_I – Poisson ratio of indenter

W – Weight per unit area of a fabric

w – Width of a conductor

x – Width of a layer within a composite

$\overline{y}$ or NA – Neutral axis

Units

eV – Electron volts

torr – Atmospheric pressure unit

Å/s – Angstrom per second

F - Farads

nF – NanoFarads

pF – PicoFarads

μm – Micro-meter

mm – Milli-meter

nm – Nanometer

ml – Millilitres

mA – Milli-amperes

Ω/□ or Ω/sq. – Ohm per square

Ω/m – Ohm per meter

Ω m – Ohm meter

kΩ – kilo ohms

Pa - Pascal

MPa – Mega-Pascal

GPa – Giga Pascal

Oz – Ounce

rpm – Revolutions per minute

dB – Decibels

Hz – Hertz

MHz – Mega Hertz

GHz – Giga Hertz

V - Volts

US energy – Unit for the ultrasonic energy during wire-bonding

CHAPTER 1
INTRODUCTION

1.1 Motivation: Integration and durability of electronic circuits on textiles

For certain applications in areas such as fashion and entertainment, the military and the bio-medicals [1, 2], electronic systems perform vital intelligent functions. It is often advantageous for these to be mobile, personalized and unobtrusively accessible to their users anywhere and anytime without hindering user mobility. Electronic textiles (or e-textiles) are an attractive approach because textiles are widely used and universally worn by individuals. The challenge then becomes how to reliably and unobtrusively incorporate electronic functionalities into the textile.

Early integration ideas exploited the reasonable low weight of existing portable devices and were embodied in commercial products like the entertainment ICD (industrial Clothing Design) + suit from Levi Strauss and Philips Electronics [3], figure 1.1(a, b), and the healthcare LifeShirt by Vivometrics [4], figure 1.1c. While existing electronic solutions were easily inserted into their host garment, the following design flaws became evident:

a. Enclosed devices were rigid and lack the flexibility typical of textiles.

b. Device packaging made the garments heavy, bulky and aesthetically diminished.

c. Garments became uncomfortable to wear especially over a lengthy period of time.

d. Garments often required delicate handling since attached devices are fragile and would not normally survive impact stresses (such as collision or fall) that normal textiles would withstand.

e. Devices had to be detached before the garment could be washed and in some cases a level of technical ability was required to reassemble them.

(a) (b) (c)

(a) The ICD+suit by Levi and Philips Electronics (2000)[3] (b) Attached headphone and mouthpiece [2] (c) LifeShirt by Vivometrics, 2001 [4]

Figure 1.1: Early integration of electronics into textiles

These flaws led to research on E-Textiles where novel techniques are investigated for embedding and packaging electronics on textiles, and more importantly, for developing flexible and elastic electrical interconnections necessary for building electronic circuits directly on textiles.

E-textiles are textiles that are functionalized to perform a specific electronic activity in addition to their primary purpose e.g. clothing. They can be realized by replicating the rigid printed circuit boards (PCBs) found in most electronics on textiles using interconnection technologies that do not significantly affect the traditional characteristics of textiles such as flexibility, feel, breathability, and robustness (e.g. surviving washing). Some emerging e-textile prototypes shown in figure 1.2, use traditional textile production techniques such as weaving [5], knitting [6], embroidery [7] and screen printing [8], and the printing techniques used in the fabrication of conventional PCBs such as evaporation [9] and etching [10]. These techniques use electrically conductive yarns or threads [7] and electrically conductive films and laminates [8, 9] as electrical interconnections respectively. While passive components such as resistors and capacitors [8], have also been fabricated with these interconnection technologies, electronic components (such as LEDs, microcontrollers etc.) are mainly integrated on fabrics using electrically conductive adhesives [8], and rigid or flexible interposer circuits [11].

(a) The early e-textile prototype, Georgia Tech wearable motherboard in 2002 [5] based on conductive fibres

(b) VTAMN remote health monitoring e-textile prototype in 2004 based on woven and embroidered conductive yarns [7]

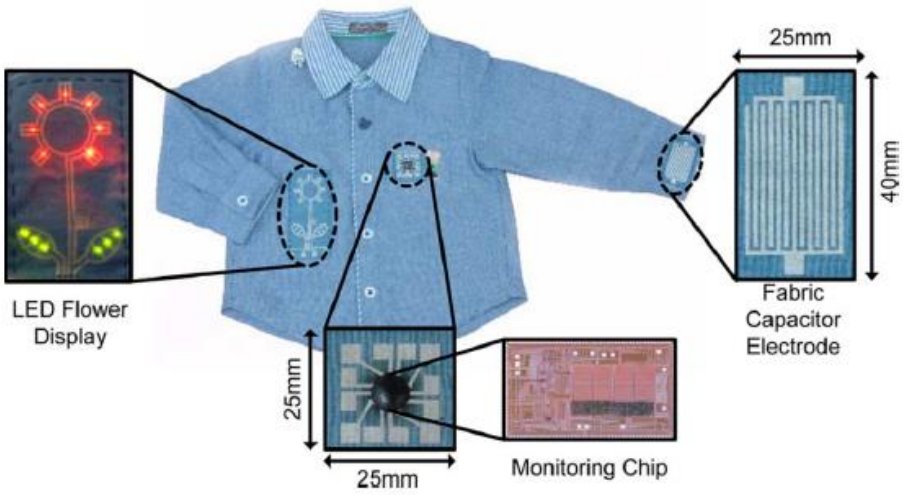

(c) Planar-fashionable circuit board with capacitive sensor, chip and LED display in 2010 based on screen printed conductive films [8]

Figure 1.2: Some emerging e-textile prototypes

The durability of these e-textiles is still significantly affected by mechanical stresses from typical washing or general use that standard textiles can endure. Consequently, commercial products are still few and far between [12] and there are no universal standards for designing and manufacturing e-textiles despite the preponderance of target applications [13].

The state of the art solutions on e-textile durability use new interconnect materials of improved tensile strength and flexibility [14] and apply polymeric encapsulations to protect the interconnections and electronics [8, 14] from oxidation, abrasion or washing effects.

1.2 Scope and objectives of thesis

This research aims to realise durable and reliable printed interconnects on textiles and investigates the integration of electronic components to these interconnects. This will be applied in the design of printed LED and temperature sensing garments which are useful in fashion, military and biomedical applications.

To achieve this, the following objectives are outlined:

1. Preliminary assessment of the mechanical challenges to the design and durability of printed electronics on textiles based on a wash test of a screen printed LED circuit on a fabric.
2. Modelling of the neutral axis, NA of printed textile composites based on classical beam theory to obtain equations for:
    a. Optimizing the interconnect position to or in close proximity to the neutral axis of the textile composite.
    b. Easy determination of the requisite thickness for each layer of the textile composite.
3. Experimental verification of model results from the bending induced changes in the electrical resistance of a piezo-resistive strain gauge that is screen printed on or close to NA of its e-textile composite based on modelled thickness values.

4. Contrast the durability of interconnects positioned on and away from the NA of their e-textiles due to a bending stresses at a radius of 5×10^{-3} m and washing of at least five cycles.
5. Investigate the packaging of electronics inside the yarn itself which will provide further mechanical protection.
6. Develop an example temperature sensor circuit using thin metal films on Kapton.

1.3 Statement of novelty

The novelties arising from the research described in this thesis are as follows:

1. The derivation of an asymmetric factor, η through an analytical model that better approximates the elastic and bending behaviour of a woven fabric.
2. The identification of multiple neutral axis, NA positions in woven fabrics as opposed to the singular NA position theorised in the classical beam theory (CBT).
3. The introduction of the asymmetric factor, η into the generic NA equation of classical beams to theoretically predict and empirically verify the neutral axis positions of the screen printed e-textiles from four different woven fabrics.
4. A simplified analytical approach and equation for calculating the requisite thicknesses of the constituent layers of an N-layered e-textile ($N \geq 2$). These thicknesses position the interconnect layer of the e-textile on the NA.
5. Durable screen printed interconnects on different polyester/cotton textile blends that exhibited less than 1 % change in electrical resistance during and after a single cycle of positive and negative bending around a 5 mm bending radius. This significantly betters the 200 % change in resistance reported in literature under similar testing conditions.

6. Durable interconnects with less than 10 % change in electrical resistance after five washing cycles. This betters the 57 % change in resistance reported in literature for interconnects under conditions.

7. Fabrication of a temperature sensor circuitry on a Kapton strip which can be assembled into an electronic yarn. The sensor is responsive to temperature changes with 5 °C and 45 °C. The electronic strip is 2.5 times smaller than the state of the art.

1.3.1 Publications

The publications resulting from this work are:

1. Komolafe, A. O., Torah, R. N., Yang, K., Tudor, J., & Beeby, S. (2015, May). Durability of screen printed electrical interconnections on woven textiles. In Electronic Components and Technology Conference (ECTC), 2015 IEEE 65th (pp. 1142-1147). IEEE.

2. Komolafe, A.O., Torah, R.N., Tudor, J., & Beeby, S. P. The effect of the elastic properties of fabrics on the durability of screen printed e-textiles by neutral axis engineering. (To be submitted)

1.4 Thesis Outline

The rest of this report is structured as follows:

Chapter 2 discusses the state of the art in the integration of electronics on textiles. The chapter is divided into two main sections which review the interconnection technologies and electronic component integration on textiles respectively.

Chapter 3 introduces the process of screen printing while focusing on the factors that affect the quality of printed interconnections on textiles and the design guidelines for printing interconnections on textiles. Screen printed LED circuits were also experimented and evaluated as a platform for understanding the challenges of e-textile design.

Chapter 4 discusses the neutral axis engineering of screen printed patterns on textiles. In chapter 5, the implications of the bending characteristics of woven fabrics on electrical interconnections is investigated while chapter 6 discusses the

performance of interconnects that are optimised on the NA when they are subject to bending and washing stresses.

In chapter 7, the fabrication of fine interconnections of higher resolution than screen printed interconnections is discussed. These interconnections are fabricated on plastic substrate and cut into strips so that they can be woven into fabrics.

The conclusion and future work are detailed in Chapter 8.

CHAPTER 2
E-TEXTILES REVIEW

2.1 Defining E-textiles

There is currently no standard definition for "*Electronic textiles*" (E-textiles). The term varies in its use and meaning when often replaced with associated terms like Technical textiles, Textronics, Interactive textiles, Smart or Intelligent textiles [15]. Hence several authors [2], [15–19] have coined their own definitions and in most cases within the context of their research. While this lack of standard is not ideal in itself, it is common with newly developing fields and *"E-textiles"* is no exception. However as a common ground, e-textile researchers seek to integrate pervasive electronic and computational elements into clothing with the ultimate target of developing technologies that will ensure an entirely textile based electronic integration [10]. At the moment, the state of art is still far from this target.

This work adopts the following definition by Joanna Berzowska [18] which succinctly captures the working understanding of e-textiles as relayed in this research:

"*Electronic textile is defined as a textile substrate that incorporates capabilities for sensing (biometric or external), communications (usually wireless), and power transmission and an interconnection technology which allows sensors or devices such as information processing devices to be networked together within a Fabric*".

2.1.1 Challenges to e-textile technology

The following research questions arise from the adopted e-textile definition [18]:

a. How to implement durable and reliable electrical interconnections for electronic components.
b. How to realize and integrate the electronic (passive or active) components on fabrics
c. How to supply power the components.
d. How to package of the entire system so that it satisfies consumer needs.

This chapter first discusses how these issues are being tackled with newly developed electrical interconnection technologies with emphasis on the potential of each of these interconnections for e-textiles. This is followed by a review on the integration techniques for hardware electronics on textiles.

2.2 Electrical interconnections for e-textiles

Electrical interconnections are necessary for transmitting information and/or energy within an electronic circuit on a textile substrate [20]. Wireless signal transmission can be expedient for e-textiles since it potentially limits the use of physical interconnections between electronic components to occasions where it is only necessary. It is also possible to wirelessly transfer power to these components but the technology is nascent and still limited to short transmission distance [21-24].

Consequently physical electrical interconnections are best suited for e-textiles. New electrical interconnects vis-a-vis their integration technologies on textiles are investigated since the use of traditional interconnections like poly-vinyl-chloride (PVC) coated copper wires alter the feel and handle of the textile significantly.

The emerging interconnects are reviewed below under three broad interconnection categories – electrically conductive yarns/threads, electrically conductive films and laminates.

2.2.1 Electrically conductive yarns and threads

A yarn is a continuous strand of textile fibres consisting of long or short fibres that are twisted or otherwise held together. Threads are small diameter yarns that are spun to a considerable length for sewing fabrics [25].

Electrically conductive yarns are a conductive composite comprising of the non-conductive yarns from polyester, cotton fibres etc. and metal wires such as gold, nickel, stainless steel, silver etc. These materials can be blended into three classes of conductive yarns namely metal-wrapped yarns, metal-filled yarns and metal yarns [26].

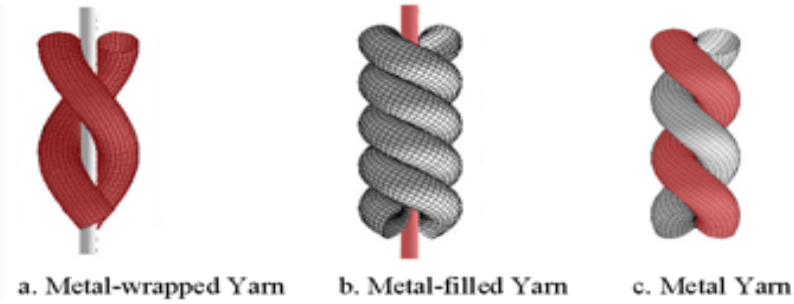

Figure 2.1: Structures of conductive yarns, metal wires are shown in red [26]

In metal-wrapped yarns, one or more metal wires are spun around a strand of a non-conductive yarn as in figure 2.1a. For metal-filled yarns, the core is a metal wire that is wrapped with non-conductive yarns as shown in figure 2.1b. In metal yarns, neither the metal nor the fibre yarn is the core. Rather finely drawn metal fibres are interlocked with strands of the non-conductive yarns, figure 2.1c or with another strand of metallic fibres in which case, the yarn is only composed of metal wires and otherwise referred to as "*full metal yarns*". In general, the electrical conductivity of these yarns is dependent of the ratio of the conductive to non-conductive fibres contained in them.

Post et.al [7] contrasted the conductivities of different blends of stainless steel yarns that are biologically inert and resistant to washing or sweat. The yarn composed of polyester fibres and short stainless steel fibres performed best under machine sewing but offered the lowest conductivity of 0.5 Ω/m. Yarns composed of 100% steel fibres produced the best conductivity 0.01 Ω/m, they were only sewable when short stainless steel fibres were used. Yarns with full continuous stainless-steel fibres were rigid and impossible to sew due to its low elasticity [7]. The major disadvantage of these yarns is the difficulty in interfacing them with electronic components [7]. More importantly, metal yarns can be generally hard to work with due to their rigidity [27].

Metal coated yarns/threads are more flexible but less conductive than metal yarns. This is because metallic coatings in them are not densely packed as the metal fibres in metal yarns. Buechley et al. [27] reported machine sewable silver plated nylon yarns of conductivities of 50 Ω/m and 270 Ω/m but these resistances can be too high for many device applications distributed over large areas [28]. The major drawback for metal coated threads is the quick degradation in their conductivity which results from the poor adhesion the coatings to the textile fibres [21, 29].

2.2.1.1 Enabling technologies for conductive yarns/threads on textiles

Electrically conductive yarn/thread interconnections are implemented on fabrics using any of weaving, knitting, sewing and embroidery.

- **Weaving**

Weaving is a textile production technique in which two distinct orthogonal yarns or threads are interlaced with each other to produce what is called a "*Weave*". The threads or yarns laced in the longitudinal direction are called the Warp while the lateral threads are called the Weft or Filling as shown in figure 2.2a.

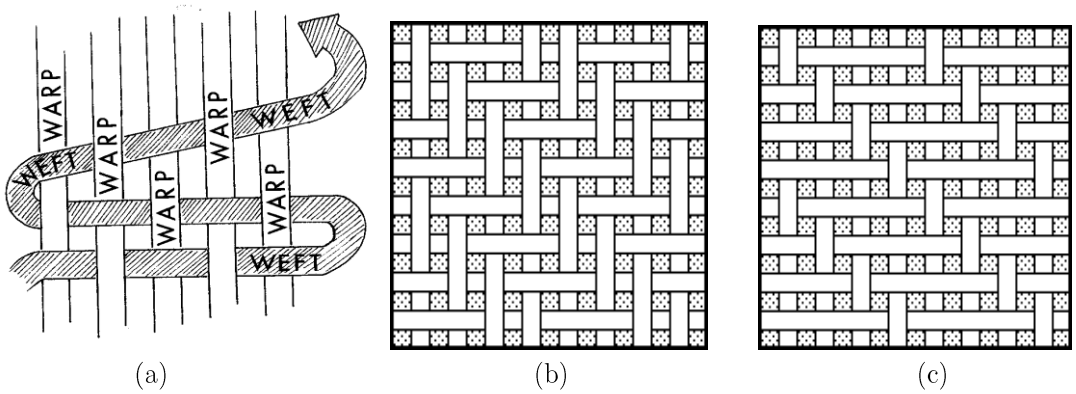

Figure 2.2: Weaving patterns: (a) plain weave [30], (b) twill weave [31], (c) satin weave [31].

Three types of weaves are common; plain weave, twill weave and satin weave. In plain weave, each and every weft yarn goes alternately under and over the warp yarn across the width of the fabric, figure 2.2a. For a twill weave, every weft yarn goes alternately over every other warp yarn as shown in figure 2.2b while in satin weave, the weft yarn floats over several warp yarns before interlacing with a warp yarn, figure 2.2c. In like manner, conductive threads or yarns are also woven into textiles to generate conductive paths or conductive fabrics [32, 33] using conventional weaving machines such as the jacquard shedding system [34].

Post et al. [7] reported a woven metallic silk organza fabric, figure 2.3a, that was used as interconnection lines for a microcontroller circuit, figure 2.3b. The organza consisted of a plain silk yarn placed in the warp direction and a metal-yarn composed of silk yarn wrapped around a thin metal (gold or copper or silver) foil in the weft direction. The metal yarn had a conductivity of around 10 Ω/m but was too fragile to be machine sewn without breaking its electrical continuity.

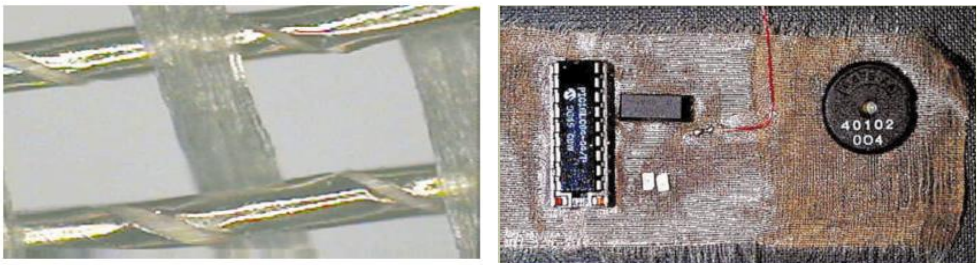

(a) (b)

Figure 2.3: (a) Metallic silk organza (b) Microcontroller circuit based on metallic silk organza

Jung et al. [35–37] also reported the use of conductive threads for a functional digital music player prototype jacket. The authors replaced some warp yarns of a polyester fabric with parallel and electrically isolated silver coated copper wires as shown in figure 2.4. The electrical isolations by laser treatment of specific sites allowed the soldering of electronics to the wires. The conductivity and the durability of the thread was not reported.

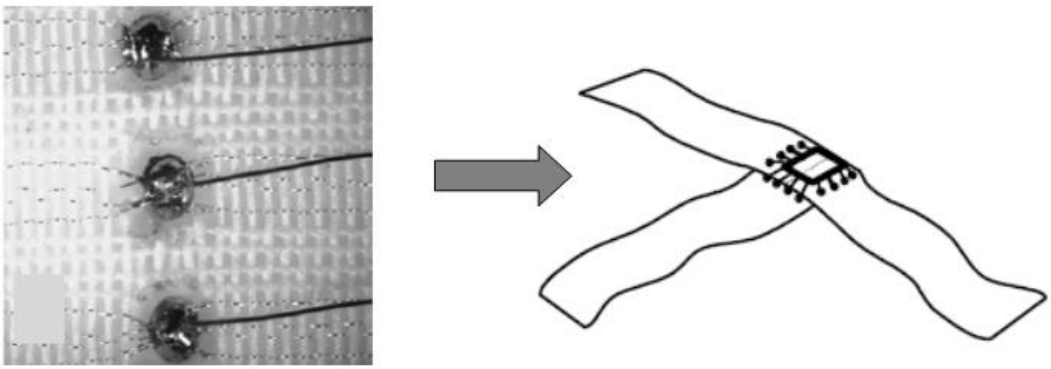

Figure 2.4: Polyester fabric with some warp yarns replaced with conductive threads and attached to an electronic circuit [35-37].

Locher et al. [32] also introduced a 90 µm thick PETEX, a woven hybrid textile substrate embedded with thin copper wires (coated with polyurethane varnish) in both weft and warp directions, figure 2.5a, offering conductivities of 15.7 Ω/m and 17.2 Ω/m respectively. It was used as interconnections between two SMA adapters. The PETEX structure is best suited for use with interposer circuits. Its main drawback is the potential design complexities in its wiring structure especially for applications where the maximum allowable current and voltage drop is higher than the ratings of its thin copper wires [32].

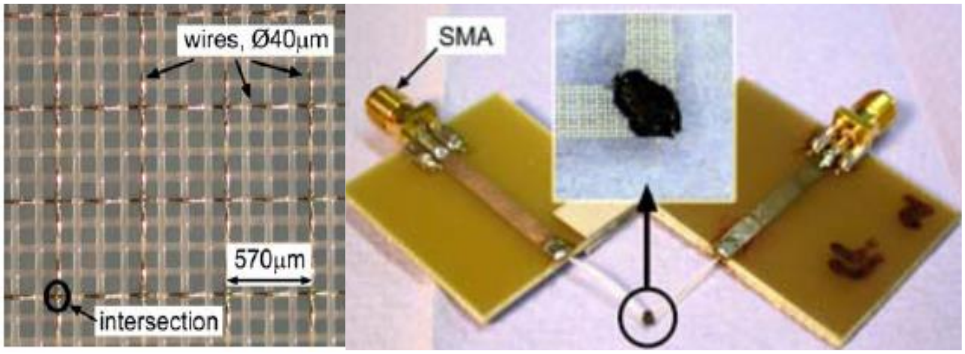

(a) (b)

Figure 2.5: (a) Hybrid textile substrate, PETEX (b) Textile connected SMA adapters [32]

- **Knitting**

In knitting, a thread or yarn is used to form a series of interlocking loops as shown in figure 2.6. These interlocking loops called "*knits*" are usually made using needles.

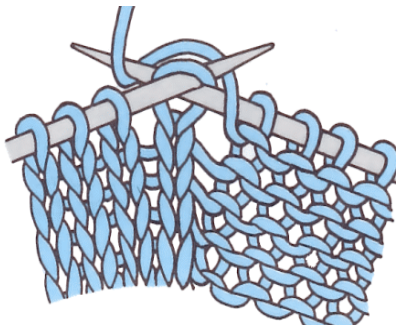

Figure 2.6: Knitting pattern [38]

A bio-clothe, figure 2.7, for health monitoring using a WEALTHY patented interface was realized by knitting stainless steel yarns and viscose textile yarn based on tubular intarsia technique [39]. The cloth consisted of knitted insulated conductive tracks, piezoresistive yarn sensors and electrodes. Soleimani et al. [40] also implemented a two-electrode switch by knitting copper-sulphide (CuS) polyester yarn and a non-conductive polyester yarn to establish conductive pathways between the two sensing electrodes.

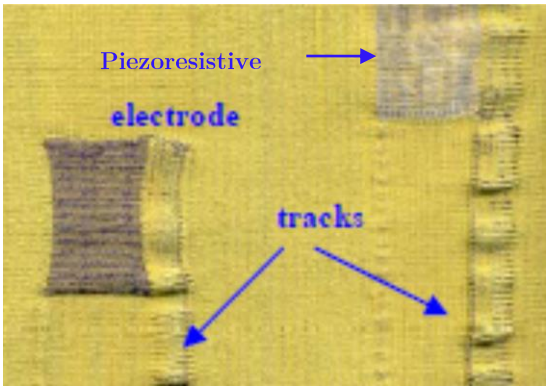

Figure 2.7: Knitted conductive tracks and sensors, the WEALTHY interface [39]

Interconnects made from knitting are able to stretch because they are not as tightly interlaced as woven patterns. However transmission lines created through knitting is expected to exhibit variable impedance characteristics due to opening and closing of the conductive loops [34].

- **Sewing and Embroidery**

Sewing and embroidering are very similar but distinct technologies. The major difference is that sewing is used for joining textiles while embroidery is used for decorating [41]. The art of embroidering uses threads to form decorative patterns on one cloth. The embroidery of conductive threads is generally referred to as E-broidery [7].

(a) (b)

Figure 2.8: (a) Fully integrated EKG shirt with embroidered interconnections [42], (b) Two contactless embroidered sensors integrated into a vest. Wiring was done with embroidery and conductive woven yarns (White ribbons) [44]

Linz et al. [42, 43] designed a fully integrated EKG (Electrocardiogram) shirt by embroidering a low conductivity yarn (silver-coated polyamide multifilament yarn)

of resistance 500 Ω/m. The shirt consisted of three electrodes, an EKG module on a flexible polyimide substrate with embroidered wiring linking the electrodes and the EKG module as shown in figure 2.8a. Contactless EMG (Electromyography) sensors on textile figure (figure 2.8b) for analysis of muscle activity were also produced from the embroidery of conductive threads [44].

Noury et al. [45] have woven and embroidered a metal filled yarn comprising stainless steel wires and silk on a cotton shirt to fabricate a prototype communicating undergarments for remote medical monitoring, figure 2.9.

(a) (b)

Figure 2.9: (a) Woven stainless-steel wires on fabric used as bus for the VTAMN health monitoring system [45] (b) The embroidered sinusoidal wiring [45]

Buechley et al. [10, 46] have sewn stainless steel thread into a shirt, figure 2.10a, to electrically connect 140 LEDs in a wearable and fashionable LED display matrix (figure 2.10b). The authors attempted three different techniques to make the sewn conductive traces durable. The first technique was termed "couching" where electrically insulating thread were sewn over the conductive tracks in a zigzag pattern, figure 2.11a. Under a contact pressure, the sewn thread peeled off the conductor beneath and hence is not a suitable approach for insulating tracks that will come into frequent contact. The second approach which involved gluing non-conductive textile patches over the sewn conductors, figure 2.11b–c, provided better insulation but the insulated area became stiffer. This approach alters the textural and elastic properties of the fabric. Fabric paints that were applied on the conductive lines had similar disadvantages and also diminished the aesthetics of the fabric.

(a) (b)

Figure 2.10: (a) Sewn stainless steel interconnect patterns (b) Wearable LED display matrix [10, 46]

(a) (b) (c) (d)

(a) Crouching stitch made with the thread (b & c) The blue cloth in (c) ironed-on the pink conductor in b, (d) Painted conductor traces

Figure 2.11: Insulation for conductive threads [10, 46]

2.2.1.2 Implications of conductive yarns for e-textile applications

Conductive yarns/threads offer acceptable conductivity and flexibility, and are also suitable for mass e-textile production since they can be integrated using conventional textile production techniques [47]. However, their positioning will be restricted by the structure of the fabric which are typically manufactured by weaving and knitting. This ultimately limits the design freedom for realizing electronic circuits on the fabrics [34] because circuits must now be tailored along the linear path the conductive yarns follow, that is, the warp and weft weave of the fabric [48]. Moreover, the long-term stability at the point of intersection of the warp and weft conductive yarns in the textile is also constrained by the high strains imposed on them by their integration process. Only metal coated textile yarns of resistances more than 15 Ω/m could reliably survive industrial weaving [28]. Similarly, the electrical contacts formed at the warp-weft intersections in the weave show unstable contact resistances especially when the morphology and tension of the yarns around these contacts are altered whenever the fabric deforms [28]. This

presents a significant challenge in adapting the conductive yarns into clothes using traditional textile processes especially where complex circuitry is inevitable.

Furthermore, the integration technology for conductive yarns and threads limit the optimization of their durability to encapsulation techniques based on insulating materials such as fabric paints, non-conductive threads and fabrics etc. These either alter the physical and textural properties of the textile or are still unreliable under stresses such as abrasion and bending [47]. Conductive threads or yarns are interlocked together almost sinusoidally in and out the fabric. This makes it impractical to locate them on the neutral axis of the e-textile.

2.2.2 Electrically conductive films

These are categorized into conductive thin and polymer thick films:

2.2.2.1 Conductive thin films

Deposition methods such as metal plating, sputtering and thermal evaporation have been used to achieve thin layers of conductive materials on textiles. Also thin film interconnections are also realized in the form of electrically conductive laminates.

- **Metal Plating**

Electro-less plating is the most reported metal plating techniques for fabrics. Electro-less plating involves the deposition of metal on a material by dipping it in a chemical solution. It is an autocatalytic process which continues deposition even after the material appears coated with metal. This technique differs from electroplating in that it does not require an external voltage supply. Electroplating is a purely electrolytic process that requires a power supply [49].

Cho et.al [48, 50-51] reported an electro-less plated Cu/Ni polyester fabric that was used as earphone transmission lines for an mp3 player. Other metal plated interconnects reported in literature are summarized in Table 2.1. With thick encapsulations, metal-plated interconnects show improved durability but after washing the resistance changes by more than 500%. Metal plated textiles and fibres exhibit limited washability [29].

- **Thermal evaporation and sputtering depositions**

Thermal evaporation is the condensation of thermally vaporized or evaporated atoms from a target material (such as copper, gold and aluminium) on to a substrate in a vacuum chamber [52]. This is a low cost process which also offers a deposition rate as high as 1000 Å/s.

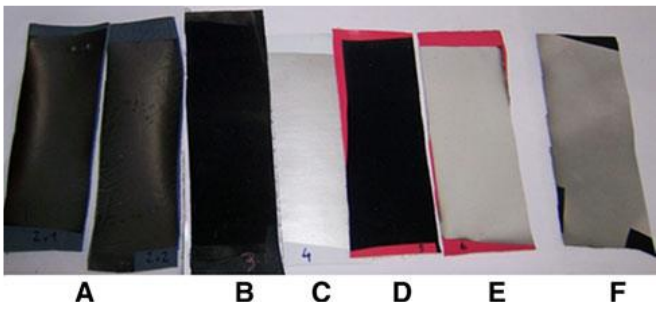

Figure 2.12: Evaporated aluminium on coated and uncoated textiles. Sample A-B are uncoated synthetic and natural leather, samples C – D are woven doubly and singly coated with PVC and E – F are PU coated woven and knitted fabrics [9]

Silva et al. [9] successfully evaporated a 300 nm thick aluminium onto polymer coated and uncoated textile substrates, figure 2.12, achieving low electrical resistivity of 10^{-7} Ωm. After 100 cycles of cyclical extension, a resistivity change of less than 180 % was reported for the PVC coated substrates. However, their findings also showed that the adhesion of evaporated films are poor and that the surface of textile may need to be treated to improve adhesion. This is not the case with sputtering deposition. Sputtering involves the momentum transfer of physically vaporized atoms from a target surface to a substrate after bombarding the target with energetic atomic particles, usually ions of a gaseous material accelerated in an electric field. While sputtering is an expensive process that require more capital equipment [157], it offers excellent adhesion. Hegemann et al, [29] reported the good performance of silver sputtered PET (Poly-Ethylene Terephthalate) fibres when subjected to a tensile strain of up to 7 % and cycle strains of 5 % suggesting they can withstand fibre processing techniques such as weaving, knitting and embroidering. Although the PET fibres lasted 30 washing cycles each performed at 40 °C for 1 hr, its change in surface resistivity was in the order of magnitude of 10^4.

- **Electrically conductive flexible laminates**

Conductive laminates are flexible plastic substrates that are cladded on one or both sides with thin sheets or films of metals.

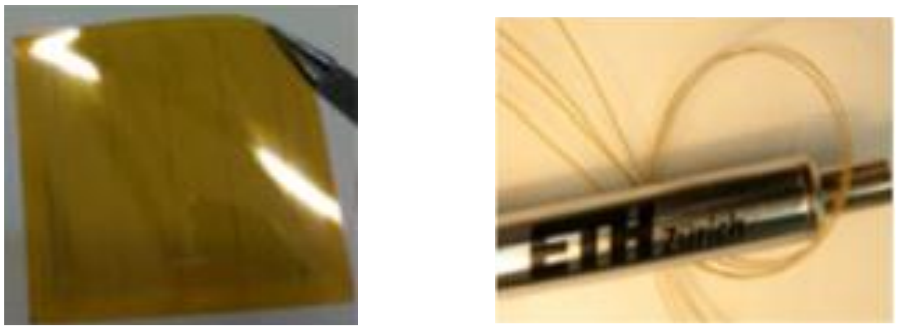

(a) (b)

Figure 2.13: E-fibre fabrication. (a) Patterned flexible plastic substrate (b) The substrate is cut into e-fibres [53]

Zysset et al. [53, 54] reported the fabrication of e-fibres using flexible plastic substrates with electronic components such as single transistors, electrical interconnections, sensors and contact pads for attachment of microchips. The circuit design was selectively patterned on the deposited metallic films on the substrate using photolithography and wet-etching techniques [55]. The patterned substrate was then cut into thin fibres using a wafer saw, figure 2.13 and were interconnected using conductive threads.

2.2.2.2 Enabling technologies for conductive thin films on fabrics

Thin-film coated fabrics or fibres have been integrated onto textiles using etching [10] or weaving, knitting, sewing and embroidery [29].

- **Etching**

It is the selective removal of unwanted parts on a substrate [43] with the use of chemicals or lasers [46, 49]. Buechley et al. [10, 27, 46] laser etched a Sn/Cu (tin-copper) plated fabric which was ironed on to another fabric to realize a fabric PCB and an LED bracelet, figure 2.14. Shin et al. [56] also etched a 35 µm thick copper foil and glued it on polyester fabric to realize interconnections for a 16-bit microcontroller circuit and a flexible textile wristwatch, figure 2.15.

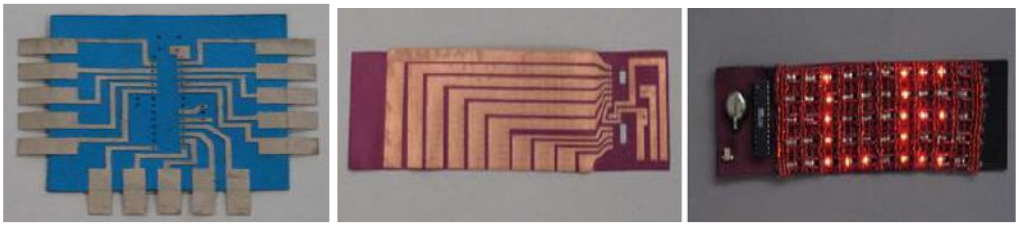

(a) (b) (c)

Figure 2.14: (a) Fabric PCB for microcontroller [10] (b) Fabric PCB for LED bracelet (c) LED bracelet [10]

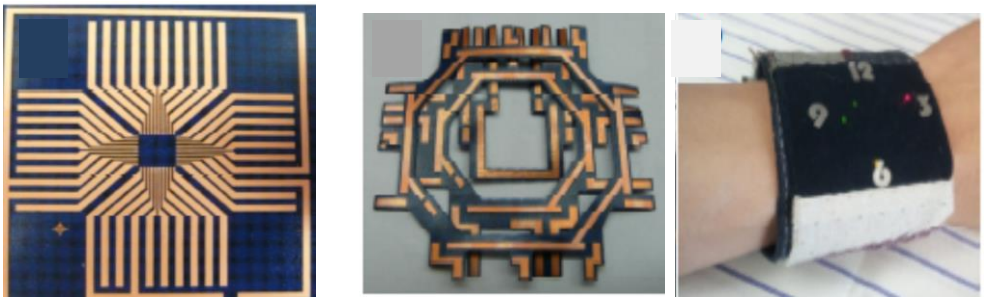

(a) (b) (c)

Figure 2.15: (a) Etched circuit of a 16-bit microcontroller [56] (b) Textile wristwatch etched circuit [56] (c) Textile wristwatch

Stretchable horse-shoe patterned interconnects for textiles were fabricated within the EU project STELLA (Stretchable ELectronics for Large Area applications) by embedding and encapsulating the etched interconnects within a screen printed PDMS (poly-dimethyl-siloxane) on knitted and woven fabrics as shown in figure 2.16 [57 - 60].

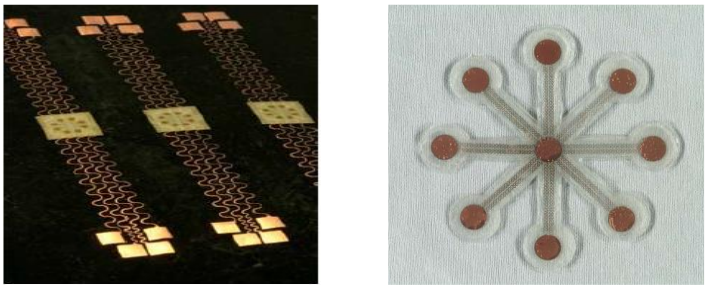

(a) (b)

Figure 2.16: (a) Stretchable interconnects from STELLA project [59] (b) Stretchable interconnect incorporated to a knitted fabric with PDMS [57]

The major disadvantage of the etch technique is the amount of the conductive material wasted during the process and this can become prohibitive when expensive materials like gold or silver are used.

- **Weaving of e-fibres**

Takamatsu et al. [61] fabricated a fabric LED array by weaving e-fibres as shown in figure 2.17.

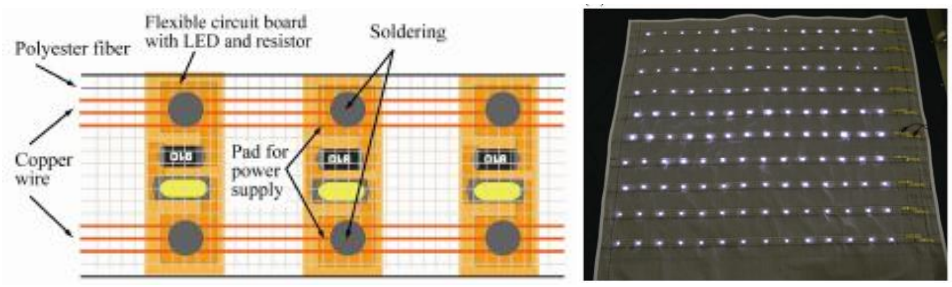

(a) *(b)*

Figure 2.17: (a) Process description for integrating plastic strips to textiles, (b) A functional array of LED plastic strips woven on textiles [61]

Zysset et al. [53] also reported a 100 mm long and 45 mm wide prototype temperature sensitive undershirt fabricated by weaving conductive threads and temperature sensing e-fibres into textile, in the weft and warp directions respectively, figure 2.18a. Parallel e-fibres were connected with conductive threads using a conductive glue. The woven fabric survived five washing cycles at 30 °C for 47 minutes per cycle and 100 tensile strain cycles of strains up to 10 % before failure. Although the sensing patch survived a bending radius of 0.75 mm it failed at a radius of 170 µm due to poor adhesion between the plastic and the metal. This bending radius is representative of what is encountered during the weaving process and hence poses a significant hurdle for commercial integration of plastic strips into e-textiles [54].

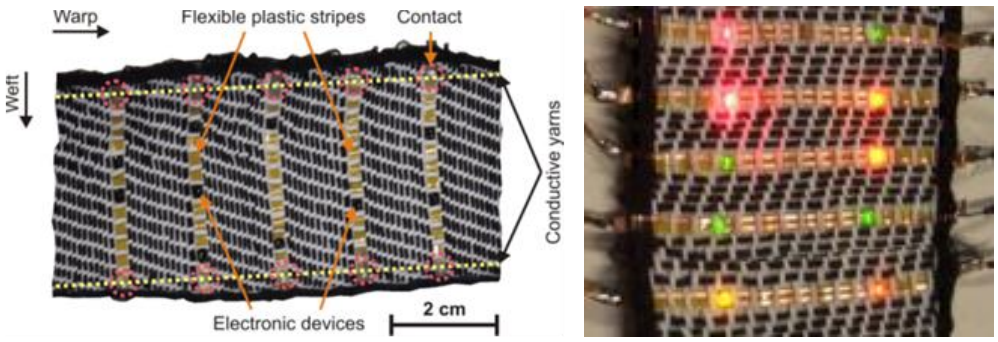

(a) *(b)*

Figure 2.18: (a) The temperature sensing textile band [53] (b) LED patch based on e-fibres [54]

Cherenack et al. [55] addressed this by improving the adhesion between the metal and Kapton substrate which lowered the bending radius of the e-fibres to a critical value of 120 µm, below which the e-fibre failed. The adhesion was improved by replacing the commercial copper-clad substrate with a thin copper-film of 500 nm thickness deposited on a bare DuPont Kapton substrate [53]. This improvement was demonstrated with a woven LED patch, figure 2.18b.

2.2.2.3 Implications of conductive thin films for e-textiles

In Table 2.1, the advantages of fabricating thin films on flexible plastic substrates such as Kapton over fabrics are highlighted but the technologies that produce an almost seamless integration between the flexible plastics and textiles are still required for e-textiles. The durability results summarized in Table 2.1 indicate that at the moment, the best performance from thin films are achievable with deposited thin-films on plastic substrates. Although the weaving of plastic strips into fabrics and the sandwiching these flexible conductive plastics on fabrics with polymers have been reported, these technology must still be improved so as to be able to properly mask the textural difference between flexible plastics and fabrics during integration.

Table 2.1: Comparison of the advantages fabrics and Kapton for thin film interconnections

Comparison	**Fabric**	**Kapton**
Surface treatment	Required to eliminate surface roughness and improve electrical performance of films [9, 151]	Required to only improve adhesion [152, 153]
Textural feel	Can be slightly affected by the polymer interface and encapsulations [99]	Plastic feel are usually mitigated by placing them with fabric yarns [53] or by sandwiching them on a fabric between polymers [59]
Flexibility	Flexible but depending on thicknesses of the polymer interface and encapsulation [94]	Very flexible because substrates are usually thinner than fabrics [55]
Integration into textile	Not required since the thin film are directly fabricated on the fabric [9]	Processes such as like weaving [55], screen printing [60] are still required to integrate them into fabrics.
Compatibility with thin film fabrication processes	Compatibility still uncertain. While thin films have been used to make fabrics conductive [9, 151], they are yet to be used to achieve printed circuits on fabrics.	Very compatible because Kapton is the standard substrate for flexible printed circuits which are mainly fabricated using thin film processes [154]
Durability	Thin films deposited directly on fabrics lack durability [29].	They are more durable, surviving up to 100 cycles and 5 washing cycles [53].

Table 2.2: Durability Tests for conductive thin films on textiles

	Materials		Interconnect Pattern	Wash Test		Encapsulation	Abrasion Test	Performance index
Authors	Substrate Type	Conductor Type	Pattern Type	Before (initial value)	After /Washing temperature	Material/Method	Result	
J. Cho et al [50-51].	Polyester (Ripstop and Mesh Type)	I) Cu/Ni Electro-less plated fabric	Transmission line	**Ripstop Material** i) UN – 0.035 Ω/sq. ii) SE – 0.035 Ω/sq. iii) DE – 0.035 Ω/sq.	**Ripstop Material** i) UN – 70.0174 Ω/sq after 5 laundering cycles. ii) SE – 21.750 Ω/sq. after 5 laundering cycles iii) DE – 0.062 Ω/sq. after ten (10) laundering cycles	**Material:** Polyurethane Tape **Method**: Hot air welding	**Ripstop material** i) Resistance Increase from initial value of 0.23 Ω/sq. to 0.53 Ω/sq.	Low
				Mesh Material i) UN – 0.097 Ω/sq. ii) SE – 0.097 Ω/sq. iii) DE – 0.097 Ω/sq. UN – Un-encapsulated SE – Singly Encapsulated DE – Doubly Encapsulated	**Mesh Material** i) UN –10.504 Ω/sq. after 2 laundering cycles ii) SE – 10.650 Ω/sq. after 2 laundering cycle iii) DE – 5.063 Ω/sq. after ten(10) laundering cycles Laundry performed at 20 °C.		**Mesh Material** i) Resistance increase from initial value of 0.29 Ω/sq. to 15.09 Ω/sq. Final Resistances obtained after 10000 abrasion cycles based on Martindale test.	
Slade et al. [26, 62]	Woven Ribbons (Samples 1 and 2)	i) Ni/Cu/Ag plated yarn		i) 0.0040 Ω/sq. for sample 1 ii) 0.0032 Ω/sq. for sample 2	**Sample 1** i) 0.0073 Ω/sq. after 10 washing cycles ii) 0.0090 Ω/sq. after 50 washing cycles **Sample 2** i) 0.0042 Ω/sq. after 10 dry-cleaning cycles ii) 0.0057 Ω/sq. after 50 dry cleaning cycles		N/A	Good
T. Vervust et al. [57-60]	i) Knitted Fabric (Polyester + Elastane) ii) Woven Fabric (Polyester + Carbon)	Copper foil	Horse-Shoe interconnects	Not Reported	Survives 50 wash Cycles at 40 °C. (only by observation)	**Material**: PDMS **Method**: Screen Printed on pattern	I) Withstood more than 30 % elongation at 100 N force on Woven substrate. ii) Withstood 140 % elongation at 100 N on Knitted substrate	High

	Materials		Interconnect Pattern	Wash Test		Encapsulation	Tensile Test	Performance index
Authors	Substrate Type	Conductor Type	Pattern Type	Before (initial value)	After/Washing temperature	Material/Method	Result	
Silva et. al [9]	Synthetic leather (Sample A), Woven textile + PVC coating on both sides. (Sample B)	Thermally evaporated Aluminium	Rectangular conductor	None	None	None	i) **Sample A**: Resistance change of 700 % over 3mm extension at 40 N ii) **Sample B:** Resistance change of 25 % over 3mm extension at 50 N	Fair
Hegemann et al. [29]	PET fibres	i) Ag-plated PET fibres ii) Ag-sputtered PET fibres	-	i) 10 Ωsq. – Ag plated ii) 10 Ωsq. – Ag sputtered	i) 10^5 Ωsq. after 15 washes (for Ag plated PET) ii) 10^5 Ωsq. after 25 washes (for Ag Sputtered PET) Washing was for 1 hr at 40 °C	None	Tensile test: Ag sputtered PET survived 7 % tensile strain before cracking Cyclic Test Ag sputtered PET survived 5 % tensile strain,	Low
Buechley et al. [10, 46]	Cotton	I) Copper (Cu) plated fabric ii) Tin/Copper (Sn/Cu) plated fabric	Fabric PCB	**Un-Insulated** i) 11.7 Ω - 0.6 Ω (for Cu traces) ii) 0.6 Ω - 0 Ω (for Sn/Cu traces **Insulated** i) 2.6 Ω - 0.7 Ω (for Cu traces) ii) 1.2 Ω - 0.4 Ω (for Sn/Cu traces) All traces have length 100m and width in the range 3 mm-20 mm	**Un-Insulated** i) >400 MΩ - 790 kΩ (for Cu traces) ii) 2.3 Ω - 0.4 Ω (for Sn/Cu traces **Insulated** i) 3.3 Ω - 0.9 Ω (for Cu traces) ii) 1.5 Ω - 0.4 Ω (for Sn/Cu traces) Results obtained after five (5) washing cycles at 20 °C.	**Material**: Cotton fabric **Method**: By Ironing cotton and an adhesive on conductive pattern	Not Reported	Fair
Slade et al. [26, 62]	Cotton, Foils	i) Copper (Cu) plated fabric ii) Tin/Copper (Sn/Cu) plated fabric		N/A	Both coated fabric (Cu-coated and Sn/Cu) lost 98 % conductivity. Result obtained after Ten (10) washing cycles		N/A	Low
S. Shin et al. [56]	Polyester	Copper foil	16-bit RHA contact pads	0.01 Ω/cm	Not Reported	N/A	i) 0.01 Ω/cm after stretching at 21 kg/cm^2	Moderate

2.2.2.4 Conductive polymer thick films

Conductive thick films can be broadly categorized into electrically conductive polymers and composite inks.

Intrinsically conductive polymers (ICPs) conduct electricity because their molecular chain structure contain fully conjugated sequences of double bonds which have low ionisation potential and a high electronic affinity. Hence excess charges are created in ICPs using reducing agents (electron donors) or oxidizing agents (electron acceptors) [63]. Examples of ICPs are polyaniline, polyactelylene, polypropylene, polypyrrole etc. However, ICPs offer insufficient conductivity levels unlike metallic inks and may require inert atmospheres since they are highly susceptible to ambient humidity and very reactive with oxygen [64]. Doping have been used to increase the conductivity of ICPs by forming polymers such as PEDOT:PSS (poly (3, 4-ethylenedioxythiopene (PEDOT), poly(styrene sulfonic acid), (PSS)), but this was at the expense of their flexibility [65].

Conductive composite inks typically contain conductive fillers or particles and a binder system which hold the particles together. The binder system usually comprises a resin (e.g. phenolic or epoxy resins) and a compatible solvent which dissolves it. Metal particles or flakes such as silver, nickel, or copper can be used as then conductive fillers. Often referred to as polymer thick films (PTF), these inks have a typical curing temperature between room temperature and 170 °C which most textiles can withstand [66].

Table 2.3: Typical sheet resistivity of PTF inks [68]

Ink	Sheet resistivity for 25 µm thick film, Ω /□
Silver (Ag flakes)	0.01 – 0.1
Silver mixture	0.1 – 1.0
Nickel – copper	1.0 – 10.0
Carbon	10.0 – 100+

The conductivity of PTF films are obtained by measuring of the sheet resistivity, at a specific thickness. This is the resistance per unit square area, (i.e. the resistance of a printed conductor divided by the ratio of its length and width) [67]. The typical sheet resistivity of common PTF inks are shown in table 2.3 [68].

Silver-based inks are common due to their high conductivity even after oxidization. Copper-based inks are also a good alternative but copper easily oxidizes with prolonged exposure to ambient conditions and loses its conductivity after oxidation [69]. To prevent this, copper is usually silver-plated [65]. Silver migration can also occur with purely silver inks; a failure mechanism that happens when silver is able to migrate between two close polarized silver conductors due to increased air humidity or applied voltage. To prevent this, several blends of silver inks like carbon-silver blends and palladium-silver inks are used. The addition of carbon to silver inks only retards the effect and while palladium is a definitive solution, but is an expensive option [64]. Other conductive inks include carbon inks [70] and nickel inks [71, 72]. Carbon inks have high resistivity and are basically used for high resistance applications like resistors [70].

In general, the conductivity of PTF inks depends on the ratio of the metal to polymer content in the ink. Increasing the polymer content improves flexibility of the ink but reduces the electrical conductivity [65].

2.2.2.5 Enabling technologies for integrating thick films on fabrics

Thick films are integrated on fabrics by printing methods such as screen printing, inkjet printing and dispenser printing. The advantage of printing is that it is an additive process that can enable the direct production of electronic circuit patterns on specific local areas on textiles using conducting inks.

Inkjet and dispenser printing are both direct write techniques that require no form physical screens or stencils. Pattern creation on a substrate is achieved by following a predefined digital layout. Electrical interconnections based on inkjet printing have been demonstrated in [73 - 75] however nothing has been reported about the durability of these interconnections. Moreover inkjet printing is only possible with a very narrow range of inks of specific rheological properties (i.e. ink flow characteristics such as (i) low viscosity to enable easy expulsion of ink from the nozzle and (ii) a surface tension high enough to prevent unwanted dripping from the nozzle but low enough to ensure ejected droplets break away easily from the nozzle [64, 73]. While dispenser printing is unlimited by these shortcomings, the technology is still nascent and the durability of its interconnections are also very much uncertain [76 - 79].

This review therefore focuses on the screen printing technique and the state of the art approach for enhancing the durability of its interconnections.

- **Screen printing**

The screen printing process described in figure 2.19, starts by depositing a volume of ink on the printing screen. The ink is dragged across the screen by a squeegee which presses the screen into contact with the substrate and in the process forces ink onto the substrate (which is a fabric in this case) through the open areas of the screen. As the screen behind the squeegee snaps back from the fabric, the screen pattern is transferred to the fabric [80]. For multilayer printing, the pattern on the screen must be properly aligned with the initial pattern on the substrate to avoid any misalignment. The screen printing process is discussed in great detail in section 3.3.

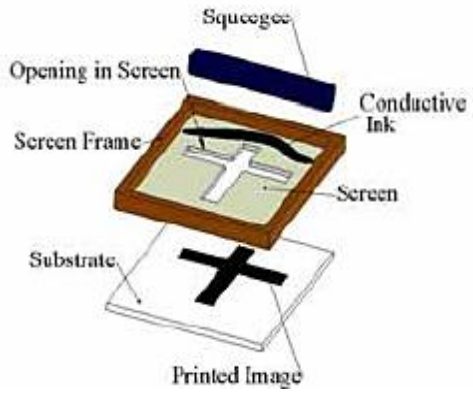

Figure 2.19: Illustration of the screen printing [81]

Researchers have screen printed conductors and electrodes on textiles for health monitoring which compare significantly in performance with the commercial alternatives. Merritt et al. [11, 82] developed active carbon-rubber electrodes circuit consisting 1 mm wide interconnect wires which were screen printed on opposite sides of a nonwoven polyester-nylon textile as shown in figure 2.20.

The active electrodes which were designed to monitor ECG (Electrocardiogram) rhythms produced a comparable performance to commercial Ag/AgCl electrodes during an ECG test. The interconnect wires were realized from a commercial silver ink CMI 112-15, and protected with a screen printed electrically insulating dielectric ink, CMI 115–30 to improve durability and prevent cracks along the conductive tracks. Both inks were cured at 100 °C but the curing time was not reported.

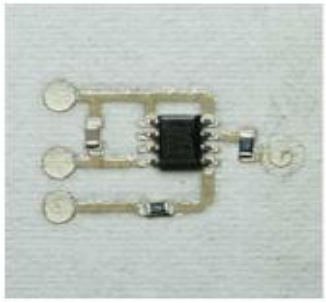

Figure 2.20: Screen printed fabric electrode [82]

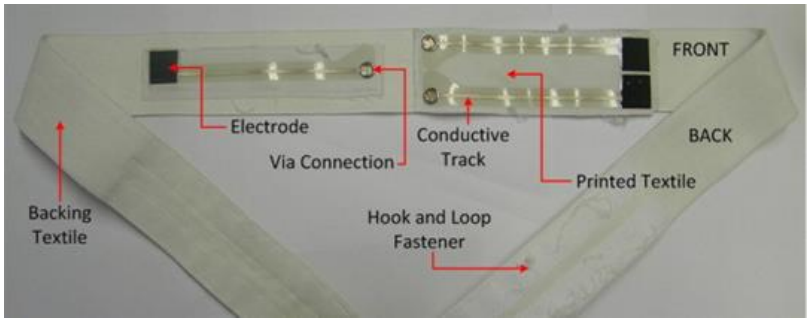

(a) An ECG chest band on Escalade fabric [83]

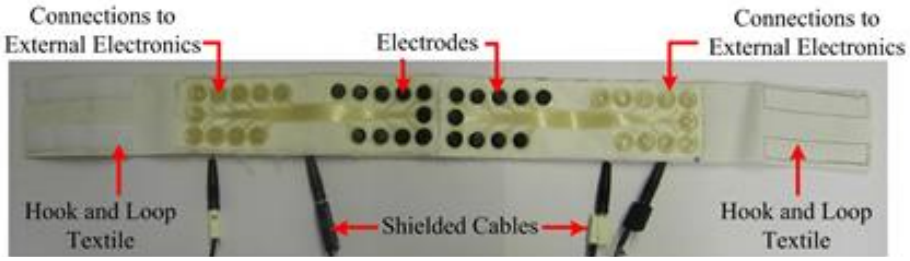

(b) Textile headband for facial EMG and EOG monitoring on Escalade fabric [84]

(c) Fabric electrode array on polyester cotton fabric [85]

Figure 2.21: Screen printed fabric electrodes at University of Southampton, UK

Similarly, at the University of Southampton, researchers screen printed conductive pathways for several stencil-printed carbon-rubber electrodes for ECG monitoring [83], facial EMG and EOG monitoring [84] and for functional electrical stimulation (FES) that assists movement of patients with central nervous system lesions [85], figure 2.21. The conductors were 5 µm thick and were realized using Fabink-TC-AG4001 and DuPont 5000 silver pastes which were thermally cured at 120 °C for 10 minutes. The conductors were sandwiched between two UV-curable and screen printed polyurethane layers on the fabrics to limit the effect of bending strains on the conductors.

- **Substrate-ink challenges with printed interconnections**

In investigating the suitability of nonwovens for e-textiles, Karaguzel et al. [67, 86, 87] reported how the electrical characteristics of three different silver inks (CMI 112-15, DuPont 5025 and DuPont 5096) with different rheological properties were affected by the surface characteristics of three different nonwoven textiles (Evolon, DuPont's Tyvek and Resolution Print Media (RPM)). The authors did this by screen printing coplanar waveguides with the silver inks. Coplanar wave guides (CPW) are interconnect lines used for propagating electromagnetic signals in a preferred direction in space at a certain frequency [88] because they offer less dispersion of signals. They consist of a centre strip, usually a signal plane of width, W, and thickness, t, patterned on a dielectric substrate at a distance, S, from two ground planes of equal thickness, t parallel to and in the plane of the strip as illustrated in figure 2.22 [88].

Results from a TDR (Time Domain Reflectometry) profile and a DC resistance measurement of their screen printed CPW lines shown in figure 2.23, indicated a high viscosity was essential in retaining more of the ink on the surface of the

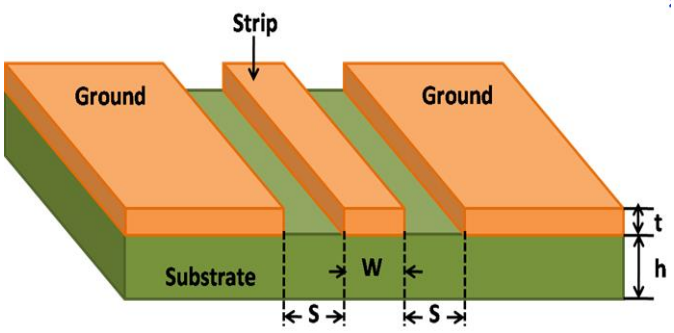

Figure 2.22: Cross section of a coplanar waveguide [89]

nonwovens. Of all their inks, the creative materials ink, CMI 112-15 had the highest viscosity and silver content, and produced more continuous and conductive transmission lines on the nonwovens. Characteristic impedances between 135 Ω and 95 Ω for signals from track widths varying from 600 µm to 1200 µm were reported at an average thickness of 41 µm.

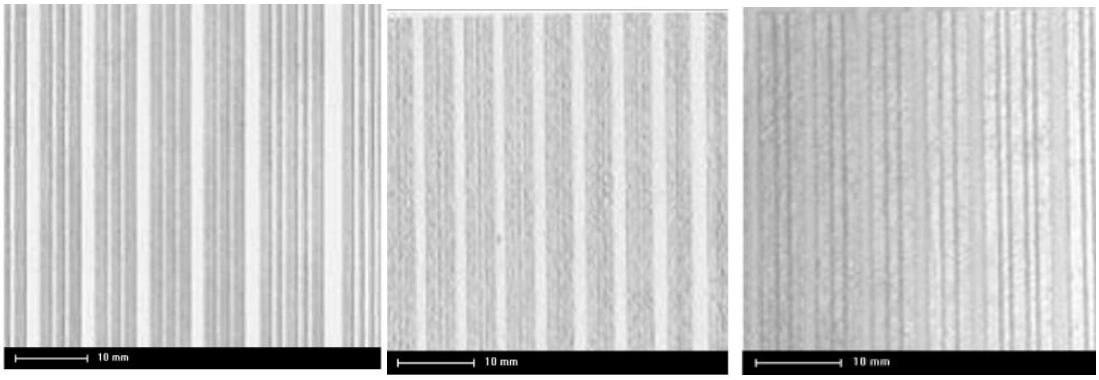

(a) Tyvek Substrate (b) Evolon Substrate (c) RPM Substrate

Figure 2.23: Screen-printed coplanar waveguides on three different substrates [86]

Kim et al. [8] screen printed 10 µm thick CPWs of characteristic impedances between 180 Ω and 230 Ω on woven polyester substrate. The silver transmission lines were encapsulated with a liquid molding epoxy to improve robustness. When tested with a high frequency network analyser for high and low frequencies up to 3 GHz and 100 MHz, their 15 cm long printed transmission line produced a reliable signal transmission with a -3 dB frequency response of 80 MHz.

These findings demonstrate that the interaction of the conductive ink with the surface properties of the textile is critical for achieving printed interconnections on textiles. A dissimilarity between the substrate material and the polymer type contained in conductive inks, a high metal to polymer volume content and high curing temperatures are factors identified to contribute to poor adhesion of conductors to textiles [90]. The authors also showed that the higher the porosity of the textile or substrate, the higher the variation in the thickness of the printed conductor irrespective of the viscosity of the ink. This was evaluated by printing silver conductors on paper, PVC (Polyvinyl Chloride), polyethylene terephthalate (PET) and textile (50 % polyamide and 50 % cotton) substrates. Textile and paper substrates were most porous, showing a variation of ±5 µm in the thickness of the silver conductors as against the ±3 µm on the other substrates. Despite this, the

sheet resistance of conductors on all substrates was still between 0.04 Ω/□ and 0.13 Ω/□ for average thicknesses between 35 µm and 10 µm.

Araki et al. [91] studied the adhesion strength and conductance of polyurethane (PU) and polychloroprene (PC) based silver pastes that were mask printed on polymeric, cellulosic, PC and PU substrates upon stretching and folding. Silver inks with binders matching their substrate type were found to have better adhesion and better conductivity upon stretching, figure 2.24.

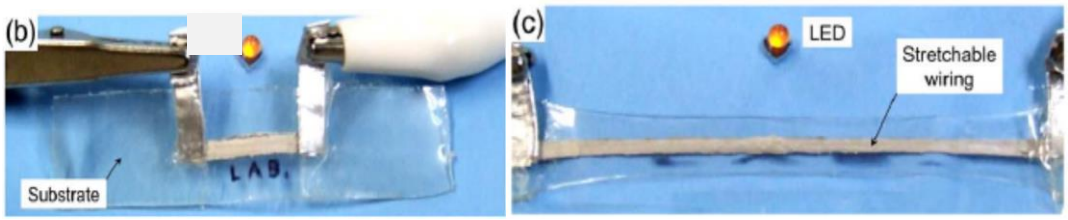

Figure 2.24: LED circuit based on stretchable wires [91]

In [92], the impact of the mechanical properties of the textiles on the durability of screen printed conductors was also investigated. Silver conductors on an elastic polyester/spandex fabric showed higher changes in resistance relative to those on the less elastic fabric (without spandex) despite plastic deformation of the fabric (without spandex) at 19 % strain. At strains > 30 %, resistance measurements from the elastic fabric were unreliable due to voids in the fabric after extension.

- **Optimizing printed interconnections for low stress response**

It is evident from this review that screen printed interconnects on textiles have been widely studied. Screen printed interconnects realized directly on fabrics as shown in figure 2.25, are quick to lose their conductivity under external stresses as arising from, for example, washing. Other stresses such as bending, abrasion and flexing also significantly affect the durability of these interconnects as shown in Table 2.4.

In addressing this, commercial inks such as Creative materials CMI 112-15 or DuPont 5025 which offer better elastic (or tensile) and electrical properties under these conditions were initially tested. Experimental results from Karaguel et.al [86, 87], Kazani et al [93], Kim et al. [8], Merilampi et al. [90, 92] and Araki et al. [91] all indicate that the electrical reliability of these inks are adversely affected when the substrate and ink properties are not properly matched. Some of the properties

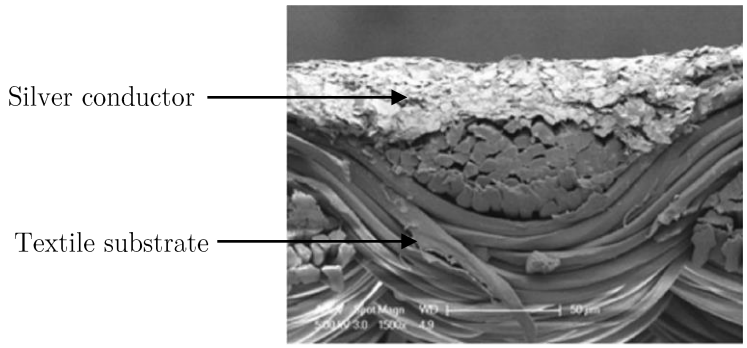

Figure 2.25: Screen-printed silver conductor directly on textile surface [8].

to consider include the elasticity of fabrics and inks, surface roughness and porosity of the fabrics, adhesive strength between the ink and the substrate, and the ink viscosity and formulation. However, while inks of better flexibility and tensile strength are desirable or necessary for certain applications, these characteristics are often achieved by trading-off the mechanical resilience of the ink for its electrical conductivity i.e. changing the ink formulation. For expensive inks like silver, the cost of evaluating the compatibility of the inks and fabrics also makes this approach undesirable.

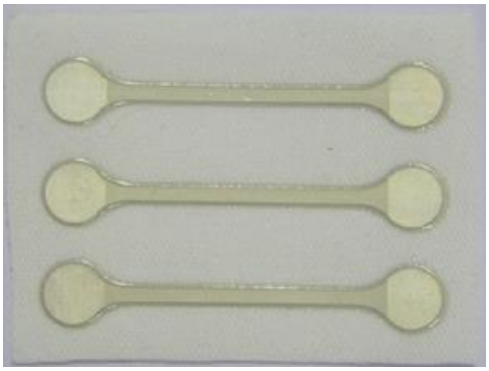

Figure 2.26: Polymeric encapsulation of screen-printed silver conductors [93].

Low-cost waterproof polymers have also been investigated in order to protect the conductors, figure 2.26. Conductors are either directly encapsulated with the polymer or sandwiched within two polymers on the fabric to enhance their durability. This method structurally modifies the printed composite and improves the mechanical durability of the conductor without compromising its electrical properties.

Table 2.4: Durability tests for conductive thick films on textiles from literatures between 2005 and 2014.

	Materials		Printed Pattern	Wash Test (Range of Results Reported over all substrate Selections) of Encapsulated Patterns		Encapsulation	Tensile Test	Abrading Test (Range taken over all substrate selections)	Performance index
Authors	Substrate Type	Ink type/ application	Pattern Type	Before (initial value)	After /Washing temperature	Material/Method of Application	Result	Final Results	
Merritt et al. [11]	Nonwoven (PES-Nylon) PES -polyester	Ink type: Silver (CMI 112-15) Application Screen printing	Electrode	Not Reported	Failed after five (5) wash Cycles Washing Conditions not Reported	**Material:** Dielectric material CMI 115-30 **Method** Screen printed on traces	Not Reported	Not Reported	Low
Kazani et al. [93]	Woven (PES, Cotton, Viscose (CV), CO/PES, PES/CV)	Silver (Electrodag PF 410 and DuPont 5025)	Square-shaped Conductor	i) 0.032 Ω/sq for Electrodag ink ii) 0.010 Ω/sq for DuPont	i) 0.171 Ω/sq at 40 ± 3 °C for Electrodag ink ii) 0.074 Ω/sq at 40 ± 3 °C for DuPont Ink All obtained over 20 wash cycles with Van Der Pauw Resistance Method []	**Material:** Thermoplastic Polyurethane **Method**: Laminated on Conductive pattern	Not Reported	i) 0.036 Ω/sq – 0.234 Ω/sq for Electrodag ink ii) 0.022 Ω/sq – 0.396 Ω/sq for DuPont ink All obtained via Martindale test	Moderate
Karaguzel et al. [87]	Nonwoven (Tyvek, Evolon and RPM)	Silver (CMI 112-15,DuPont 5025 and 5096 inks)	Coplanar Waveguide Lines	i) 2.2 Ω to 8.1 Ω (over all inks) for Evolon Substrate ii) 2.2 Ω to 3.0 Ω (over all inks) for Tyvek substrate	i) 7.8Ω to 80Ω (over all inks) for Evolon substrate based on ISO 6330 standard ii) Failed (over all inks) for Tyvek All obtained after 25 wash-cycles using Digital Multimeter.	**Material:** Thermoplastic Polyurethane **Method**: Laminated on Conductive pattern	Not Reported	Not Reported	Moderate
Kim et al. [8]	Woven (Polyester)	Silver (CSP-3163)	Coplanar Waveguide Lines	4.6 Ω	I) Approximately 9.2 Ω (Washing conditions not reported) Obtained after 50 wash cycles based on Four-Point Probe Technique	**Material:** Thermoplastic Polyurethane **Method**: Laminated on Conductive pattern	i). Withstood a force of 300 N in the x or y direction ii) 380 N force diagonally with an extension of 28 mm	Not Reported	High

Kazani et al. [96]	Nonwoven (PU Foam, PES)	Silver (DuPont-Epoxy resin, Acheson-PES resin, Sun Chemical-PES resin, Sun Chemical–Epoxy Resin)	Square-shaped Conductor	i) 0.002 Ω/sq -0.011 Ω/sq (over all inks) for PU foam ii) 0.001 Ω/sq – 0.014 Ω/sq (over all inks) for PES substrate	i) 0.0129 Ω/sq to 2.263 Ω/sq (over all inks) for PU foam ii) 0.0125 Ω/sq to > 2.263 Ω/sq (over all ink) for PES substrate. All obtained after 60 dry cleaning Cycles (30 °C Washing temp.) for 45 minutes. Van Der Pauw technique was used to measure resistance	**Material:** Thermoplastic Polyurethane **Method**: Laminated on Conductive pattern	Not Reported	Not Reported	High
Merillampi et al. [90]	Paper, Polyimide, PET, PVC,	Silver (Polymeric ink–Epoxy Resin, One component silver ink – PES resin, PES-based silver ink)	Square-shaped conductor, Different line-width conductors	0.01 Ω/sq - 0.04 Ω/sq (for all inks over all substrates)	Not Reported	N/A	i) 200 Ω to 60 kΩ at 75 % strain (Over all inks) on PVC substrate ii) 10-15 % increase in resistance on PET substrates after 10000 bending cycles	Not reported	Low
Araki et al. [91]	PU(Polyurethane) and PC (Polychloroprene) substrates	Silver (PU-based and PC-based silver)	Line Conductor for LED circuit	i) 2.8×10^{-4} Ωcm (PU-pattern on PU-Substrates) ii) 2.1×10^{-5} Ωcm (PC-pattern on PC-Substrates) * Patterns not encapsulated*	Not reported	N/A	i) 0.1 Ωcm after 400 % strain (still lights an LED) for PU patterns ii) 2.4 Ωcm and 1.3×10^{3} Ωcm for 600 % strain and beyond for PU-Conductors iii) 4.3×10^{-2} Ωcm after 40 % strain and complete failure after 60 % strain for PC-Conductors	Not Reported	High
Inoue et al. [97]	Silicone	Silver (based on silicone-binder)	Super-flexible wire	Not reported	Not reported	N/A	i) 0.2 kΩ - 5 kΩ after 100-180 % elongation	Not Reported	Moderate

Yang et al. [98]	65% Polyester/ 30% Cotton fabric	Silver (DuPont 5043)	Line conductor of lengths 20 mm and 30 mm Width, 1mm Thickness = ~10 µm	Not reported	**Nominal Changes in resistance** ~40 % change in resistance for 20 mm long sample ~ 70 % change in resistance for 30 mm long sample All values obtained after 20 washing cycles consisting of Washing at 30 °C for 39 minutes. Spin speed = 1000 rpm Drying at 50 °C for 30 minutes Baking at 120 °C for 10 minutes	**Material:** Thermoplastic Polyurethane (Fabink-UV-IF020 and Fabink-UV-IF1) **Method**: Screen printed as interface and encapsulation for the conductor	Bending test 200 % change in resistance due to internal and external bending Single cycle at a bending radius of 5 mm	Not Reported	High
Paul et al. [94]	Escalade	Silver (Fabinks AG-TC-4001)	Line conductor of length, 40mm Width, 3mm Thickness = 5 µm	~ 5 Ω 35 samples were washed	~ 12 Ω After 10 washing cycles at 40 °C for 58 minutes. Spin speed = 1200 rpm 34 of 35 samples survived.	**Material:** Thermoplastic Polyurethane (Fabink-UV-IF020 and Fabink-UV-IF1) **Method**: Screen printed as interface and encapsulation for the conductor	Bending test Escalade: 20 % change in resistance after internal and external bending 100 cycles at a bending radius of 3 mm	Not Reported	High

Polymers used as encapsulants are directly printed above the conductors for protection against abrasion and oxidation upon exposure to air and water. Epoxy [8], dielectric ink [11] and thermoplastic polyurethane (TPU) [83 - 85] encapsulants have been reported. Encapsulated conductors show increases of up to 335 % [67, 87] and 100 % [8] in their initial electrical resistances after 25 and 50 washing cycles respectively. Kazani et al. [93] also reported TPU encapsulated square-shaped silver conductors with 434 % increment in sheet resistance after 20 washing cycles at 40 ˚C for 22 minutes per cycle. The better performance of the conductors after 50 cycles of washings While the encapsulated conductors performed better than the un-encapsulated ones which did not survive at all, the small change in the resistance of conductors after 50 wash cycles relative to the change obtained after 25 cycles could indicate that the conductive ink CHANGSUNG CORP. CSP-3163 that was used for the 50 wash cycle test is more resilient to flexural stresses than the CMI 112-15 ink that was used in the 25 wash cycle test. Since the authors did not give the encapsulation thicknesses for these conductors, the better performance of the CSP-3163 conductor could also be attributed to using a thicker encapsulation than what was used for the CMI 112-15 conductor.

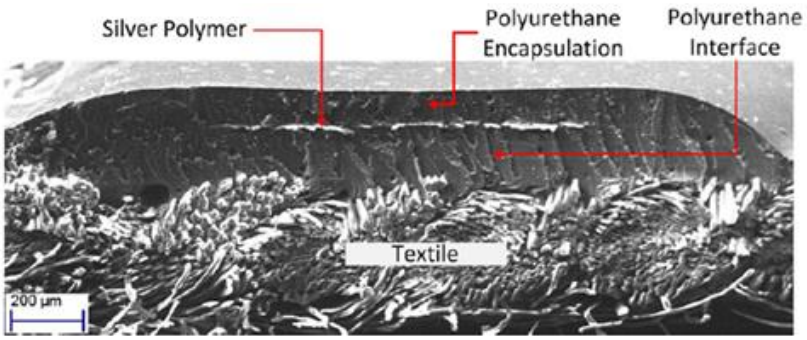

Figure 2.27: Screen-Printed conductors sandwiched between two polymeric layers, the interface and encapsulation layers [94].

In the case of conductors being sandwiched between two polymer layers as shown in figure 2.27, this can increase their flexibility and reduce their printed thicknesses and hence the fabrication cost. In this case, the polymer is used as an interface between the fabric and the conductor, and as an encapsulant on the conductor. As an interface, the polymer eliminates the surface roughness and porosity of the fabric that would normally require thicker deposits of conductive inks to fill up. The average thicknesses of conductors printed directly on fabric is typically between 20

and 45 µm [8, 67]. The use of an interface layer means much thinner conductive layers can be printed. Reported interface materials include acrylic resin [99], silicone [99], and polyurethane coatings [96, 99] which were screen printed or laminated on fabrics to realize four and six-layer composite (FLC and SLC) structures. Acrylic coatings were shown to give poor performances under tensile and bending stresses unlike like silicone and polyurethane [99]. Yang et al. [98] realized a 10 µm thick silver conductor on a polyurethane interface. This interface material was also used to encapsulate the conductor in their six layer composite (SLC) structure because of its good waterproof property. The 20 mm × 1 mm sized conductor had a 40 % change in initial resistance after 20 washing and drying cycles.

The addition of polymer interface and encapsulating layers has been shown to improve the durability of screen printed conductors. This structural modification does, however, mean that externally induced stresses will be internally distributed within a printed composite. Internal stresses could affect the resistance of a conductor if it is not located in the region of minimal stress. Paul et al [94] examined this by empirically varying the printed thicknesses of polyurethane (interface and encapsulation) to correctly position a 5 µm thick silver conductor (20 mm × 3 mm) within FLC and SLC structures. Minimal changes in the electrical resistances of conductors that were accurately positioned within the composite was reported after several cycles of cyclic bending at a 3 mm radius. Increases as small as a 20 % change in the electrical resistance of conductors in both FLC and SLC structures on Lagonda fabric were reported after 50 and 100 cycles of internal (positive) and external (negative) cyclic bending respectively as shown in figure 2.28. Inaccurately positioned conductors in both composites had increases of up to 100 % and 400 % respectively.

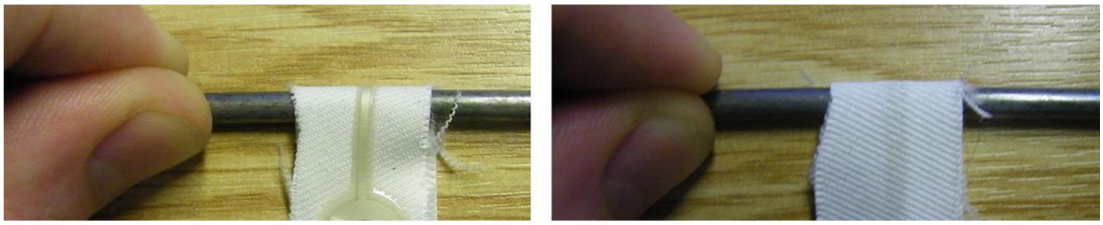

Figure 2.28: Screen-printed conductors in external (left) and internal (right) bending orientations [93]

The model implemented by the authors was unable to identify the location of the neutral axis because of the complex mechanical properties of the textile. Consequently, the requisite polymer thicknesses were only empirically obtained.

2.2.3 Conclusions

Electrically conductive yarns/threads, and conductive films and laminates are the state of the art interconnect solutions available for e-textiles. The performance of these interconnects is affected by the external stresses in their application environments. The use of polymeric encapsulations limit the effect of these stresses and can optimize conductor performance by locating it on the neutral axis of the e-textile. With conductive threads/yarns this is impractical because they are layered across all stress planes within the e-textile. While the durability of the thick films is still a major concern for e-textiles, the significant progress achieved in the past decade in the improved durability of thick films demonstrates they are potential interconnections for e-textiles.

This review has identified the scope of this work to the mathematical and empirical characterization of the durability of conductive films (based on screen printing) and laminates. To this end, this work investigates a model for characterising the mechanical properties of fabrics and the screen printed composites.

2.3 Modelling of the mechanical properties of screen printed e-textiles

Following from the review in section 2.2.2.5, a screen printed e-textile can be defined as a multilayer composite that primarily consists of a fabric substrate, an interface, electrical interconnections (or circuit) and an encapsulation as shown in figure 2.29.

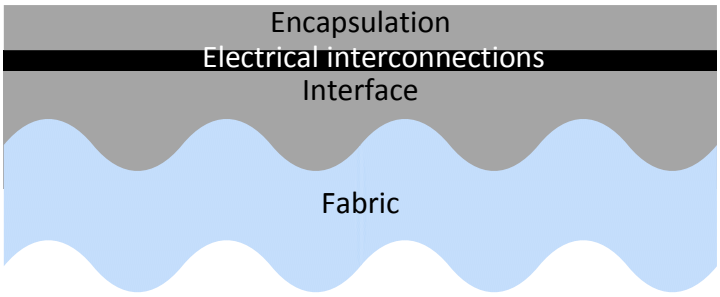

Figure 2.29: Cross sectional view of a screen printed e-textile composite

The review indicates that a reasonable amount of empirical research has gone into improving the durability of such e-textiles against washing, bending and tensile stresses as summarised in Table 2.4 (see page 33). Theoretical models for characterising the mechanical behaviour of these e-textiles under such stresses are still unreported. Although several models based on analytical, numerical and finite element modelling techniques are available for characterising the mechanical properties of fabrics [100 – 110] and textile composites (i.e. textile reinforced polymer matrices) [111 – 114], some of these are complicated by the different structural geometries of fabrics (knitted, woven, braided etc.) and by the type of loading on the fabric [103]. These factors i.e. the fabric structure and the loading conditions account for the different mechanical behaviours of fabrics and their composites such as tensile extensibility, shearing, bending, twisting, and stiffness [105]. An unsophisticated theoretical model is still necessary for predicting the behaviour of screen printed e-textiles under such stresses so as to optimise their design and performance in real applications.

In Table 2.4, three primary stresses, washing, tensile and bending are shown to potentially limit the durability of screen printed e-textiles during use. In fact, these can be reduced to tensile and bending stresses, since the washing action is largely dominated by the flexing (or bending) of a fabric in a washing machine [115 – 117]. The simplest approach to modelling the bending (and/or tensile) of a screen printed e-textile is with the Pierce's fabric cantilever test developed in 1930 [118]. This model is popular for its simplicity and for its high correlation to subjective measurements such as draping, appearance and tailorability [101, 104, 105]. Although the Pierce's model does not account for the nonlinearity of fabrics, it is still considered the standard to measure the two-dimensional bending of fabrics [109]. It measures the bending rigidity of the fabric based on a simple calculation of the bending length, weight and thickness of the fabric. The model has birthed several testing systems such as the Kawabata Evaluation system (KES) [119], the Fast Assurance by Simple Testing (FAST)-2 bending meter [119], the Shirley bending tester [109] amongst others [119].

Yu et al [110] characterised the nonlinearity in the bending of fabrics based on the classical beam theory (CBT) model. While the CBT assumes a linear bending behaviour of beams and characterises the beam in tension and compression with the same elastic modulus, fabrics show significantly different elastic properties in

tension and compression. To account for this dissimilar fabric behaviour in the CBT model, the authors characterised the fabric with different elastic modulus in tension and compression. This led to the derivation of an asymmetric factor that quantifies the nonlinearity of the fabric. The asymmetric factor was used in conjoint with finite element simulation and a cantilever test to obtain a drape shape of fabrics that correlated with experimental results. A potential benefit of CBT to the modelling the screen printed e-textile is the concept of the neutral axis. This is a position within a beam or multilayer where all strains or stresses are practically zero. The implication of this is that electrical interconnections (or circuits) in a screen printed e-textile can be positioned on the neutral axis to improve the durability of the e-textile. While this neutral axis theory has not been demonstrated on textile composites, this has been successfully demonstrated on a six layered flexible nano-electronic structure based on a polyethersulfone substrate [120].

Consequently in this work screen printed e-textiles will be modelled by integrating the Pierce's bending of fabrics with the classical beam theory which also compensate for the nonlinearity in the fabric bending. Moreover the beam theory and the Pierce's model were reported to show better correlations of 5 % and 11 % with finite element simulations of a fabric cantilever. This is in contrast to the 61% of the model based on the ASTM D1388 standard for measuring fabric stiffness [108].

2.4 Integrating electronics on textiles based on conductive films

Three levels of integration of electronics on traditional textiles are possible namely direct, embedded and textile electronic integration, figure 2.30.

The direct integration of classical electronics on textiles is a system-level integration which entails enclosing application-specific off-the-shelf electronic products and their wired interconnections into textiles. It is the easiest form of integration but it has limitations in the bulkiness and discomfort of the host-garment as detailed in Chapter One. On the other hand, embedded and textile electronics integrations are both component-level integration in which case the textile becomes the substrate on which the electronics are fabricated rather than as a container for already existing electronic solutions. Both techniques utilize the interconnection technologies discussed in section 2.2 but differ in the type of electronic components integrated on the textile.

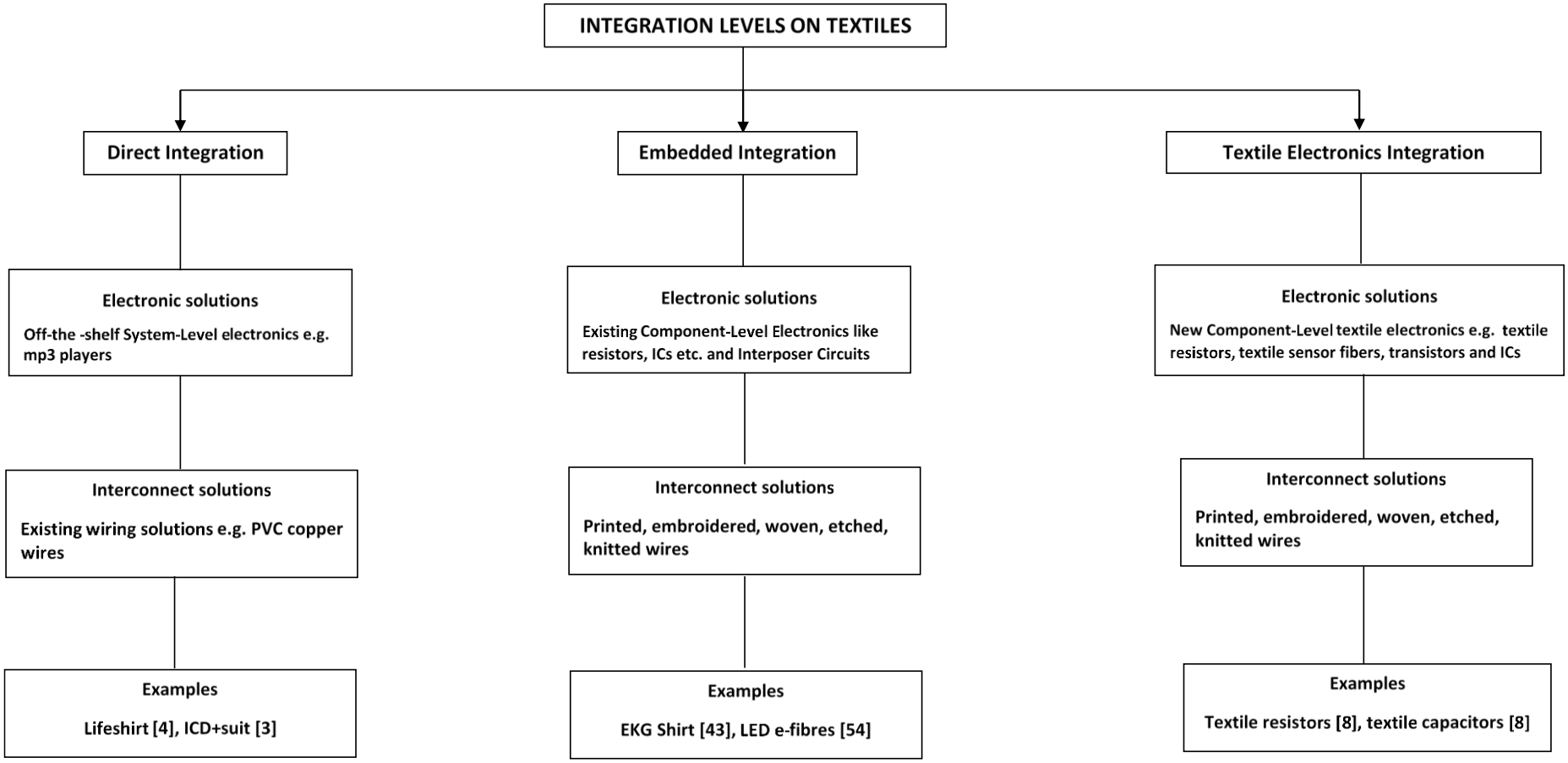

Figure 2.30: Integration levels of e-textiles

In embedded integration, conventional passive components such as resistors, capacitors and active components such as microchips (or ICs) are used to incorporate electronic functionality in textiles. Associated challenges to attaching such electrical components into a garment include [121]:

a. Almost all fabrics are made from polymers, which have a melting temperature well below the typical soldering temperatures (for example polyesters melt within 150 °C – 260 °C [122]). Hence high temperature soldering of components (i.e. hard and soft soldering occur at temperatures greater than and less than 450 °C respectively [50]) is not compatible with these textiles.

b. Most wearable computer systems that have electrical components incorporated into clothing lose their flexibility and do not drape naturally on the body [7, 121]

c. Electrical components must be connected in such a way that they are safe from environmental factors like moisture and that they remain attached and electrically connected to the textile substrate after the garment has been washed [7, 121].

The current solutions offered in literature to these problems include stapling component lead frames on conductive threads [7], the use of low temperature solders, micro spot-welding [7] or conductive adhesives [82] (especially for surface mount components) and electronic sequins [10] for mounting electronic components directly on the fabric. Interposer circuits [35, 82] (electronic circuits developed on flexible substrates such as Kapton) have also been directly sewn or glued on textiles to indirectly attach the components as discussed in page 19.

In textile electronics integration, an all-textile electronic components and interconnections are incorporated into the textile and this can be a viable solution to the problems associated with the embedded technique. Passive textile components in resistors, capacitors and inductors have already been demonstrated [8] while active components like sensors, integrated circuits (ICs) are yet to be realized. The fabrication of such textile-based active components constitutes another research focus in electronic textiles called Fibertronics which is regarded as the building-in of electronic blocks such as transistors into yarns [19]. However this

technology is still primitive due to the limited scope of current knowledge. Although, the fabrication the fibre "Field Effect Transistors" (FETs) based on a woven technology have been reported [123, 124], it has not been really implemented in real applications.

Nonetheless, the advantages of the embedded and textile electronic integration over the direct integration of packaged solutions include the increased flexibility and potential stretchability and washability of integrated electronics with garment, better textural comfort of integrated garment and also the minimal increase in garment/textile weight after integration.

2.4.1 Prototypes based on embedded integration

C. R. Merritt et al. [11] used conductive adhesive (CMI 119-05 and CMI 119-44 mixed at 100:2.3) to directly attach on a polyester-nylon fabric, surface mount 100 kΩ and 200 kΩ resistors, 10 nF capacitor and an SO-8 amplifier to a screen printed silver active electrode circuit. The attached components were further encapsulated, figure 2.31 with Hysol FP4460 which was cured for 4 hrs at 130 °C.

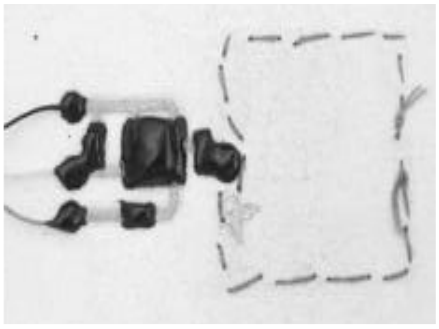

Figure 2.31: Encapsulated surface mount components attached using conductive adhesives [11]

The authors also developed an interposer circuit (developed on a 0.005 inch thick FR-4 with 0.5 oz. copper cladding and a gold finish) for the same design where similar components were attached on the FR-4 substrate using a conductive epoxy, CW2400 (Circuit works). The interposer circuit was designed to connect the surface mount devices due to the feature size limitations (pitch mismatch) of the direct attach approach for surface mount components. Unlike the direct attach approach where the interconnecting lines were screen printed, conductive yarns were used as the interconnect lines of the interposer circuit in figure 2.32a. The circuit was also

encapsulated with a glob-top encapsulant as in figure 2.32b for protection from environmental effects like moisture.

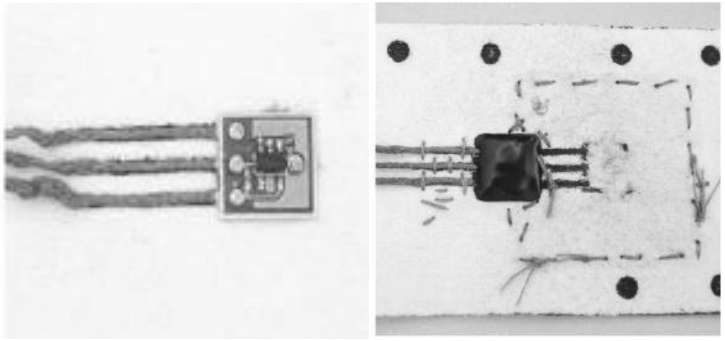

(a) (b)

Figure 2.32: (a) Interposer circuit with attached components [11] (b) Encapsulated interposer circuit [11]

The performance of the interposer circuit electrode patch in figure 2.32 was compared to that of the direct-attach electrode circuit patch in figure 2.31 after both were hand stitched to larger sheets of Evolon. After five wash cycles and one drying, the direct-attach circuit failed due to the cracks formed at the interconnection lines and contact pads while the interposer circuit was reported to pass the wash test. The authors however did not mention the washing conditions.

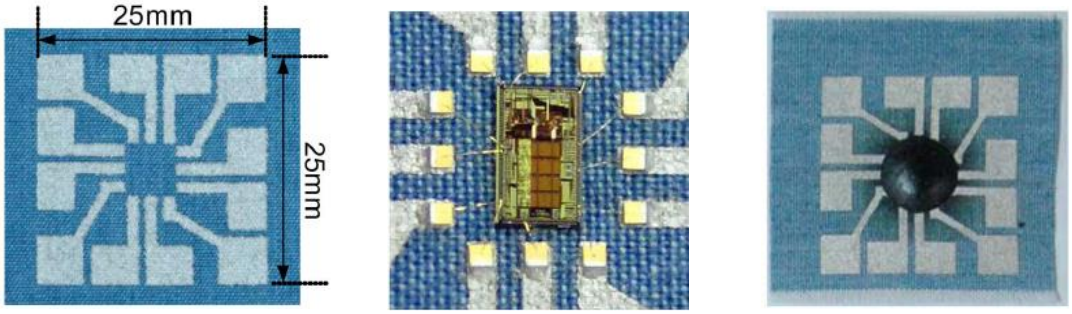

(a) (b) (c)

Figure 2.33: (a) Screen printed lead frame, (b) Unpackaged chip glued to frame (c) Molded silicon package [8, 123]

Kim et al [8] also attached an unpackaged die on a screen printed lead frame shown in figure 2.33a. The unpackaged chip was glued on the printed lead frame then gold wire was bonded to the pads of the chip and to the lead frame, figure 2.33b. The chip was then coated with a liquid molding epoxy to provide robust protection against potential pressure on the packaged chip, figure 2.33c. The molded package had dimensions of 1 cm $\times$ 1 cm and a height around 2.2 mm - 2.5 mm. A tensile

strength tested performed on the molded silicon chip in figure 2.33c strained the package along the x, y and the diagonal directions using a maximum load of 85.1 N/cm, 85.2 N/cm and 99.3 N/cm respectively. The package/bonding remained unbroken in each case until the fabric itself got torn after experiencing a total strain of 19.5 %, 27.2 % and 26.8 % in the x, y and diagonal directions respectively.

2.4.2 Prototypes based on textile electronics integration

In place of traditional passive components on textiles, Kim et al. [8] screen printed an 85 Ω resistor of width and space of 1 mm each and thickness 10 µm as shown in figure 2.34a. Square and octagonal shaped inductors of inductances 577 nH at 10 MHz and 970 nH at 10 MHz respectively were also printed (figures 2.34 b, c).

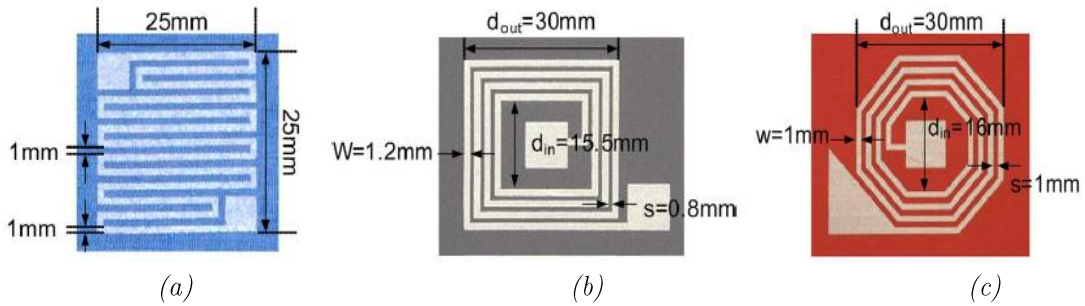

Figure 2.34: Screen printed (a) 85Ω resistor, (b) inductor, 577nH at 10MHz (c) inductor, 970nH at 10MHz; (dout = outer diameter, din = inner diameter, w = line width) [8, 123]

The authors also fabricated three different capacitors with screen printing using different types of fabric, figure 2.35. The type A parallel plate capacitor used a denim fabric of thickness 320 µm as the dielectric between the screen printed ink electrodes. The capacitor has an area of 35 × 20 mm^2 and a capacitance of 50 pF.

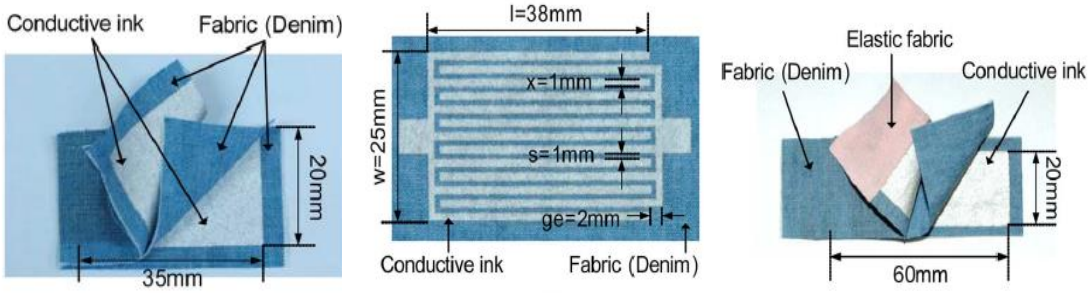

Figure 2.35: Three types of screen printed capacitors [8, 123]

The type B capacitor was an interdigitated capacitor with six fingers of length and width of 38 mm and 1 mm respectively. The finger gap x, the end gap "ge", terminal width w, substrate height h and the dielectric constant, were 1 mm, 2 mm, 25 mm, 320 µm, and 4.0 respectively. Its capacitance was 10 pF. The type C capacitor is also a parallel plate capacitor but it differs from the type A capacitor because of the elastic fabric used at both ends of the plates. Due to the elastic nature of this fabric, the capacitance of this capacitor can vary when stretched from 10 to 100 pF.

2.5 Discussion

Current techniques, based on the above literature review, for integrating electrical components on textiles are still very much based on laboratory prototypes, their effectiveness and durability in real applications is challenging.

The direct attachment of classical components on textiles using low temperature solder and micro-spot welding is challenged with the problem of biocompatibility [121] resulting from the potential exposure of the body to solder (usually lead-based solders). Also, due to the rigid nature of the solders, they are more prone to failure in flexible applications. In addition, both processes can be time consuming especially for complex electronic-textile applications where several components are to be attached.

Although, the use of conductive adhesives offer instantaneous processing i.e. attachment of components [121] there is a major concern on the longevity of its adhesive strength in the face the real stresses and strains caused by washing, bending and stretching of the fabric. There is also the minor problem on how it can be neatly dispensed on textile substrate without affecting the textile aesthetics. The packaged electronic components with threaded leads [7], which can be embroidered on the textile also offer an easy form of incorporating components on textiles however, the process required to achieve such threaded leads is complicated. Also the durability of the bonded fine conductive threads used in such threaded components, even after encapsulation is still uncertain for real applications. This also applies to the unpackaged silicon die [8, 125, 126] which are integrated on textiles to eliminate the rigid packaging of conventional ICs or microchips.

Interposer circuits (flexible or rigid) [43, 127] are usually used for indirectly attaching components with fine footprints and small pitch sizes on textiles. Although they offer better and easy integration especially for condensed circuits on textiles, the circuit boards are rigid and even for flexible rigid boards there is still textural mismatch.

Finally, the use of rigid passive components is bypassed by fabricating them directly on textiles [7] using the interconnection technologies discussed in section 2.3.1. As with interconnect patterns, electrical reliability still needs to be improved so that electronic characteristics of fabricated components do not vary in circuit applications. Hence, screen printed interconnections are initially fabricated on fabric in Chapter 3 for a preliminary assessment of their reliability after washing.

CHAPTER 3
THE FABRICATION OF E-TEXTILES BY SCREEN PRINTING

3.1 Introduction

This chapter presents the empirical investigation into the durability of screen printed circuits on fabrics and identifies the fabrication challenges. Ten LED and resistor circuits were realized on a 65 % / 35 % polyester cotton Bari fabric by using screen printed silver interconnections sandwiched between two the interface and encapsulation layers. The Bari fabric (see datasheet in appendix A for physical properties) was selected because of its extensive use in garment industries and for its potential for e-textile applications [95]. The durability of the printed circuits were evaluated by performing 3 wash cycles and the conclusions resulting from the experiment are used to pave the direction for the rest of this work.

3.2 The screen printing technology

Screen printing is a traditional process in the textile industry for reproducing artistic patterns on textiles. It also doubles as the low cost fabrication process that is widely used in the electronics industry for realizing thick-film circuits [81]. This conveniently makes screen printing the ideal technique for replicating printed circuits on textiles.

In this work, the commercial DEK 248 semi-automatic screen printer, figure 3.1 is used to screen print the LED and resistor circuits on Bari fabric. While printed circuits such as the LED circuits maybe easily replicated on woven fabrics with screen printing, the functionality and/or long-time reliability of the circuits can be limited by poor printing resolution and quality.

3.3 Resolution of screen printing

Resolution refers to the smallest possible feature size, i.e. line widths and spacing, that is transferrable onto the fabric from a screen or mask. A good resolution gives

Figure 3.1: Semi-automatic DEK-248 screen printer

a high print quality (i.e. accurately defined lines and spacings) and allows for denser circuit patterns to be realized. The resolution for screen printing is typically around 100 µm but with specialized screens that have high dense mesh structures and special surface treatment, resolution can be as high as 20 µm [128].

In general, the resolution of screen printing is controlled by the following parameters:

1. Ink rheology
2. Printing screen characteristics like its mesh count; mesh and emulsion thickness and the mesh material.
3. Printing process parameters such as print speed, separation and snap-off distance and squeegee pressure.
4. Surface roughness of the fabric.

These parameters served as a guide for the following:

a. Selection of inks

b. Selection of screen properties

c. Selection of printing parameters

d. Minimizing of surface roughness effects

3.3.1 Selection of inks

The deformation and flow characteristics of an ink under pressure, i.e. its rheology, determines its suitability for screen printing. Screen printable inks exhibit thixotropic or shear-thinning behaviour which means they increase and decrease in viscosity at low and high shear rates respectively [129]. This property enables a highly viscous ink to become fluid enough to pass through a screen mesh during printing, and to return to their original viscosity once the screen has snapped back thereby maintaining the printed geometry [66]. Pudas et al. [130] showed that inks with high viscosity and internal cohesion yielded the best printing while low viscous pastes yielded patterns with poor resolution since they bled on the substrate during the printing.

Table 3.1: Viscosity and electrical characteristics of inks

Ink	Fabink UV-IF1	Electrodag PF-410
Supplier	Smart Fabinks Ltd.	Nor-cote International Inc.
Ink type	Thermoplastic polyurethane	Polymeric silver
Viscosity @ 25 °C (Pa.s) (Brookfield, 10 rpm)	4.7	17.5
Sheet resistance @ 25 µm film thickness (Ω/□)	-	< 0.025

Nonetheless, the suitable range of ink viscosity range for screen printing is reportedly from 1 Pa.s to 50 Pa.s at 25 °C [131]. This is reflected in the viscosities of the inks chosen for this experiment as shown in table 3.1. The chosen commercial conductive ink, Electrodag PF-410, has a conductivity of 0.025Ω/□ which is sufficient for this experiment.

3.3.2 Selection of screen properties

Screen properties such as the mesh count, mesh material, the mesh and emulsion thicknesses of the screen, can also affect print quality.

The mesh count is the number of apertures (i.e. meshes) in a screen per linear inch [66] or the number of threads per inch of the screen [132]. A screen with a high mesh count produces finer line-width and line spacing unlike a low mesh-count screen which produces coarse patterns. The appropriate mesh count (MC) for a

screen depends on the ink to be printed and it is usually specified by the ink manufacturer. The particle size (PS) of the ink, figure 3.2, can also be used to estimate MC using equation 3.1 provided the mesh thickness, t_w (i.e. the thickness of each wire strand in the screen) is known [133].

$$PS = \frac{1}{MC} - t_w \tag{3.1}$$

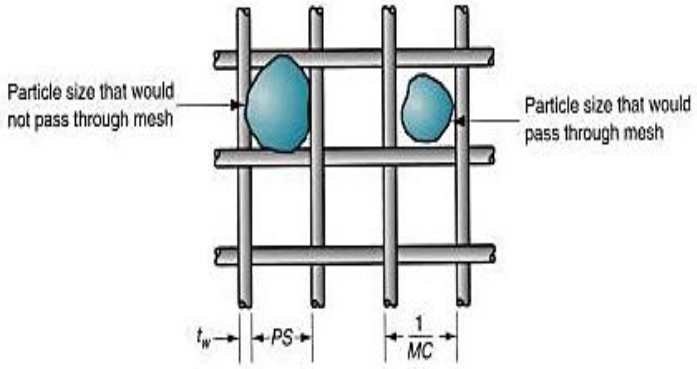

Figure 3.2: Screen mesh for sorting particle sizes [133]

The mesh thickness, t_w and the thickness of emulsion used to block off the undesired mesh areas also determines the amount of squeegee pressure to be exerted on the screen during printing [81]. The typical value of "t_w " is 150 µm but as this value increases, the screen becomes thicker and rigid hence the squeegee pressure increases. By reducing the emulsion thickness, mesh thickness t_w and selecting a flexible mesh material for the screen, the pressure can be reduced.

Four different screens were used in this experiment and the characteristics of each is shown Table 3.2. The interconnect screen was designed for printing a monolayer of the Electrodag PF-410 silver ink which contained silver particles of sizes of ≤ 3 µm [93]. To minimize the weight of the screen, the smallest mesh thickness was chosen from the available screens at MCI precision Ltd, the screen supplier. For monolayer printing, a polyester mesh material was suitable largely because it costs half the price of using a stainless steel. With $t_w = 30\ \mu m$ and $PS = 3\ \mu m$, an estimate mesh count of $MC = 303\ meshes/cm$ was obtained from equation (3.1). Therefore the standard mesh count of 305 meshes/cm (i.e. 120 threads/inch) was selected. The same properties were chosen for the encapsulation screen but with a higher emulsion thickness of 20 µm to ensure a thicker encapsulation (i.e. protection) for the silver interconnect.

Table 3.2: Selected screen properties for screen printing

Screens	Ink	Mesh material	Mesh count	Emulsion
Test screen	Fabink UV-IF1	Stainless Steel	250 meshes/cm	40 µm
Interface	Fabink UV-IF1	Stainless Steel	250 meshes/cm	40 µm
Interconnect	Electrodag PF-410	Polyester	305 meshes/cm	5 µm
Encapsulation	Fabink UV-IF1	Polyester	305 meshes/cm	20 µm

The interface and test screens also printed the Fabink UV-IF1 and following from the review in Chapter 2, screen printed interfaces are usually the thickest of the all the printed layers on fabrics. Therefore to reduce the printing time the screens had a reduced mesh count, an emulsion thickness of 40 µm and a more durable mesh material. Selection of printing parameters

The printing process parameters include the squeegee pressure, printing speed and the snap-off distance (i.e. print gap), figure 3.3. These parameters can be controlled to ensure a repeatable printing process. On the DEK-248 printer, these parameters were set as shown in Table 3.3.

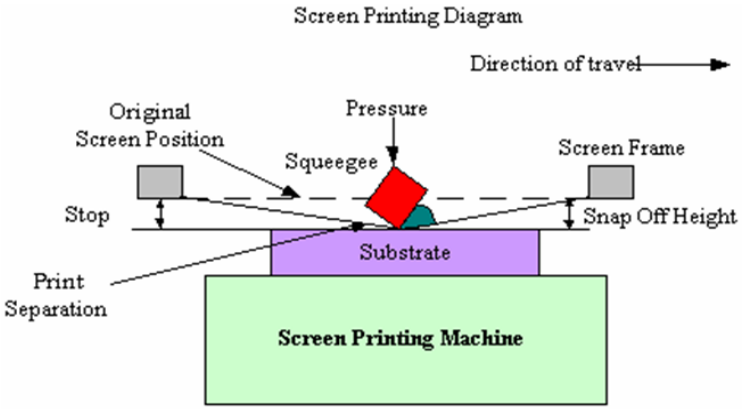

Figure 3.3: Screen printing process parameters [107]

Generally, the pressure the squeegee exerts on the screen depends on the tension and mesh material in the screen and must therefore be carefully chosen so as not to damage the screen or wear out the squeegee [81]. In this case, the squeegee pressure was set to 6 kPa.

Conversely, the print speed depends on the thixotropic behaviour of the chosen ink. The highest possible speed for printing the ink is recommended to reduce printing

time and to prevent thinning the ink than it should be during printing. When the ink is thinned, its viscosity reduces and it can become watery which will lead to bleeding i.e. the spreading of the ink outside printed areas of the substrate [134]. A printing speed of 70 mm/s was found suitable for all the inks selected in this work.

Table 3.3: Printing settings on DEK-248 semi-automatic screen printer

Screen printer parameters	**Settings**
Snap-off height (print gap)	1.1 mm
Snap-off height test range	0.7mm – 1.1 mm
Squeegee Speed (forward & Backward)	70 mm/s
Squeegee Pressure	6.0 kPa
Print type	Flood print
Front print limit	119 mm
Rear print limit	327 mm

The snap-off height, also the print gap is the distance between the bottom of the screen and the top of the substrate.

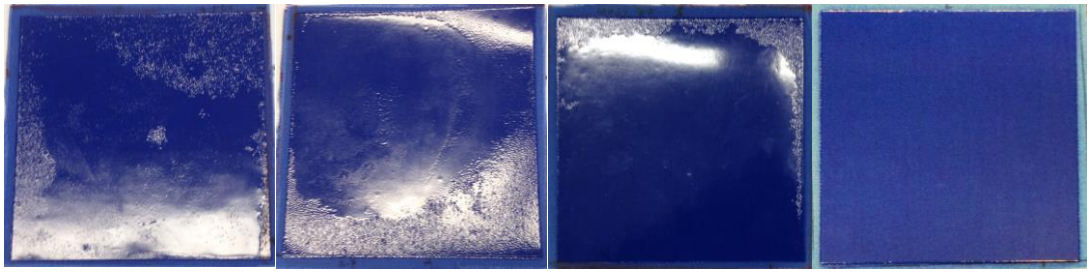

(a) *(b)* *(c)* *(d)*

Figure 3.4: Resolution and print quality of 100 mm x 100 mm rectangular samples after nine (9) prints at snap-off heights of 0.7 mm, 0.9mm, 1.0mm and 1.1mm respectively.

The print gap should be small enough to allow the screen to make good contact with the substrate. The gap height was determined by test printing a 100 mm x 100 mm rectangular pattern at different print gaps ranging from 0.7 mm to 1.1 mm. The best rectangular pattern was obtained at 1.1 mm, (figure 3.4 sample d).

3.3.3 Minimizing surface roughness effects

Woven fabrics have uneven and porous surfaces due to their weave pattern. That potentially causes a thickness variations or discontinuities along a printed pattern

as in figure 3.4. The surface of the polyester cotton fabric, Bari used in this work shows the sinusoidal and interlocking weave structure that is typical of a woven fabric, figure 3.5.

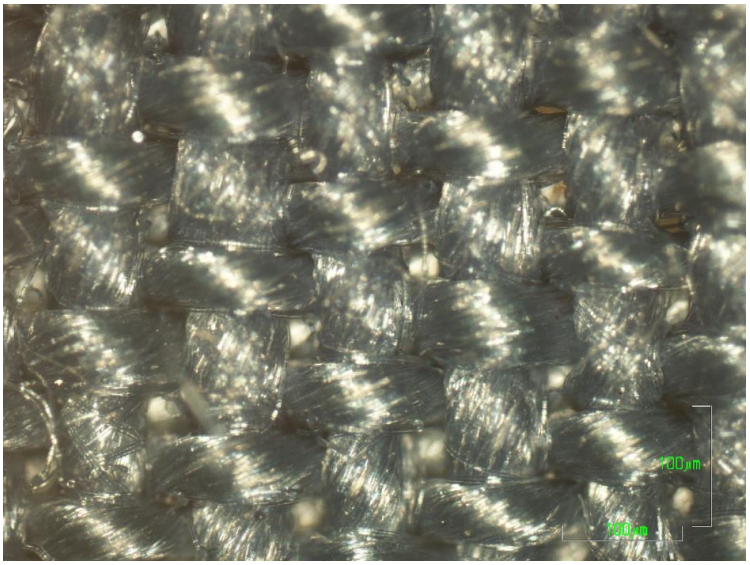

Figure 3.5: Weave structure of the Bari fabric showing its porosity and uneven surface

With a 2-D surface profile, vertical displacements relative to a reference position on the surface of the fabric can be obtained and used to estimate its average roughness R_a using equation 3.2 [135]

$$R_a = \frac{1}{n}\sum_{i=1}^{n} S_i \tag{3.2}$$

Where S_i is the surface displacement at a profiled point "i", and "n" is the total number of profiled points.

The R_a value calculated for the Bari fabric was 30.7 µm based on results from the commercial 2-D Tencor P-11 surface profiler which profiled $n = 20000$ points on the fabric over a scan length of 8000 µm, figure 3.6. Despite this high degree of roughness, it is still possible to realize functional circuits on the fabric by printing more layers of the conductor [92] but for e-textiles, this is a problem when expensive inks are used and/or flexibility is essential. It is then necessary to reduce the surface roughness of the fabric to a minimum by treating its surface.

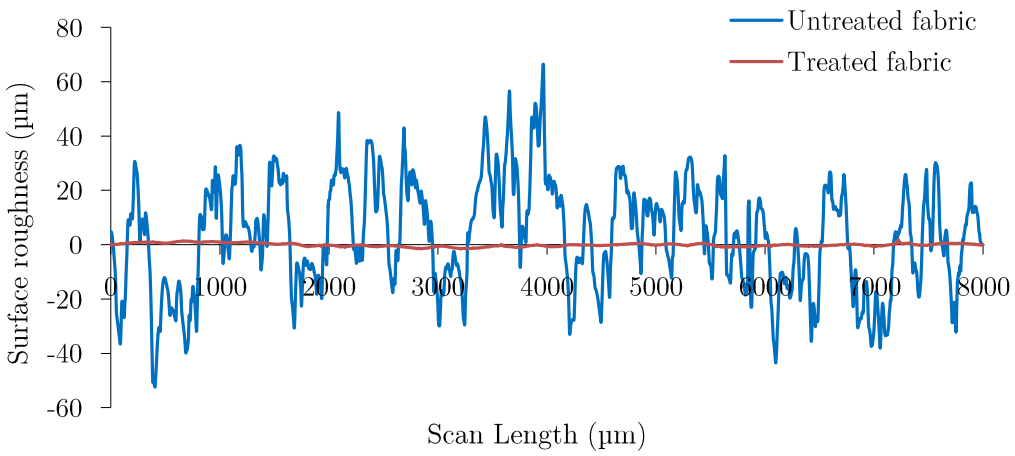

Figure 3.6: 2-D surface topology of the Bari fabric and the TPU interface layer

3.3.4.1 The interface layer

The use of thermoplastic films and coatings are the two approaches common for treating the surface of fabrics. These materials are smoothening layers which interface the fabric and the printed circuit. They are used to also modify other surface properties of the fabric such as its surface energy, porosity and water proof property.

Fabrics can be laminated with thermoplastic polyurethane (TPU) films to create a surface that is smooth enough for screen printing. While this can be achieved with relatively small film thicknesses (since the TPU-film thickness can be as low as 25 µm), tailoring the film by lamination to the design layout of the circuit can be very cumbersome especially for microcircuits of line-widths and spacings less than 0.5 mm [94].

The Microflex Project at the University of Southampton introduced screen printed interfaces using coatings such as polyurethanes which are easily tailored to the design layout of a printed circuit. Although the printed interface thickness is higher, the fabric is still flexible, interfacing material is not over-used and printed circuits are easily localized on the host textile.

Consequently, the TPU Fabink UV-IF1 paste was screen printed on Bari fabric, figure 3.4d. At an average printed interface thickness of 211 µm measured from a micrometre, the R_a value of the fabric was significantly reduced to 0.5 µm from its

initial 30.7 µm. Figure 3.6 depicts this reduction by contrasting the surfaces of the fabric and the TPU interface layer.

3.4 Design guidelines for interconnects: The stress and strain considerations

Interconnect patterns in rigid printed circuits can always assume any type of geometry since they are only meant for static applications. In flexible circuits, the interconnect geometry is crucial to its durability. Simple design guidelines have been reported for flexible circuits [136] and although the production process is based on etching, they provide a platform for designing interconnect patterns on textiles.

It is recommended that sharp corners, (right or acute angles) are avoided in the circuit routing. This is to mitigate potential issues of stress risers (stress concentration points) at the interface between perpendicular conductors.

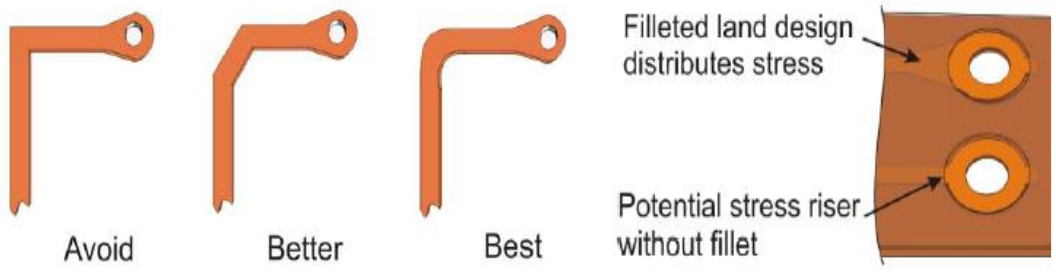

Figure 3.7: Geometrical considerations for routing interconnects [116]

A radius at such interface best provides a smooth transition between the conductors, figure 3.7c. Similarly, at the interface of between contact pads and conductors, the conductors should be flared into the contact pads using fillets as shown in figure 3.7d.

3.4.1 Design of printing screen

Patterns on the interface, interconnect and encapsulation screens were designed using a Tanner EDA software tool, L-Edit, figure 3.8. LED circuit patterns of varying line-widths and PCB footprints of a 14-pin microcontroller were designed on a 150 mm x 150 mm Bari fabric. Two square-shaped conductors of different areas were also designed. The alignment marks on each screen were designed to ensure easy and proper positioning of layers during the multi-layer printing as

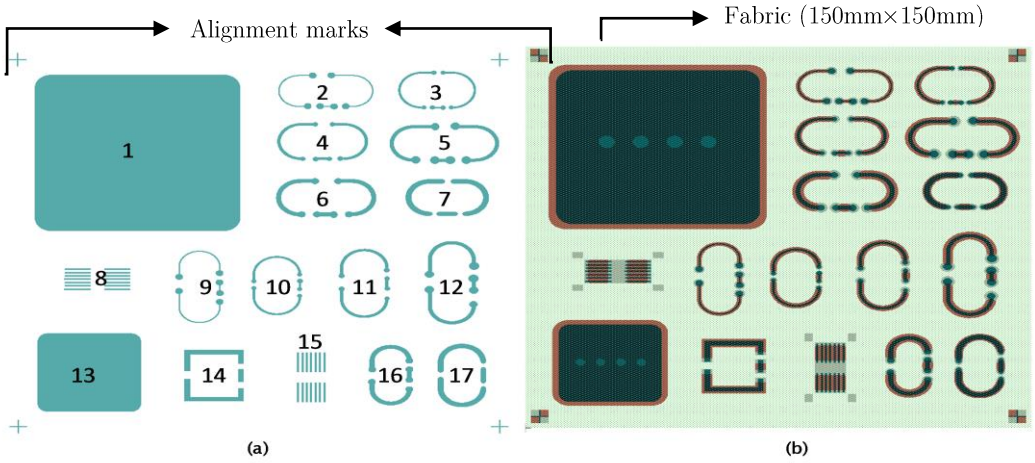

Figure 4.2: (a) Screen Layout for the Interconnect layer (b) Layout of entire Layers when Printed

(a) *(b)*

Figure 3.8: L-EDIT screen layout (a) Patterns on interconnect screen (b) Composite pattern for the screens

Table 3.4: Interconnect screen patterns and their dimensions

Pattern no	**Printed pattern**	**Dimensions**
1	Square Conductor	60 mm×60 mm
2 and 9	LED Circuit	0.2 mm line width
3 and 10	LED Circuit	0.5 mm line width
4 and 11	LED Circuit	0.75 mm line width
5 and 12	LED Circuit	1 mm line width
13	Square Conductor	30 mm×30 mm
14	Square LED Circuit	1.5 mm line width
6 and 16	LED Circuit	1.25 mm line width
7 and 17	LED Circuit	1.5 mm line width
8 and 15	IC contact pads	0.4 mm line-width, 0.9 mm line spacing

depicted in the composite layout, figure 3.8b. Also, the contact pads for attaching electronic devices and power supply cable were designed without encapsulation to allow easy access.

The interconnect dimensions are shown in Table 3.4. The line-widths of the LED circuits was varied to find the minimum line-width that can be achievable with the screen. The line-widths for the interface and encapsulation patterns were also slightly increased so that the interconnect patterns to just lie in the middle of each and are completely sandwiched within them as shown in figure 3.8b. This also accommodates patterns that slightly bleed out after printing.

3.5 The fabrication process

The fabrication process as shown in figure 3.9 is split into two categories namely, the screen printing and component attachment processes. These are described as follows:

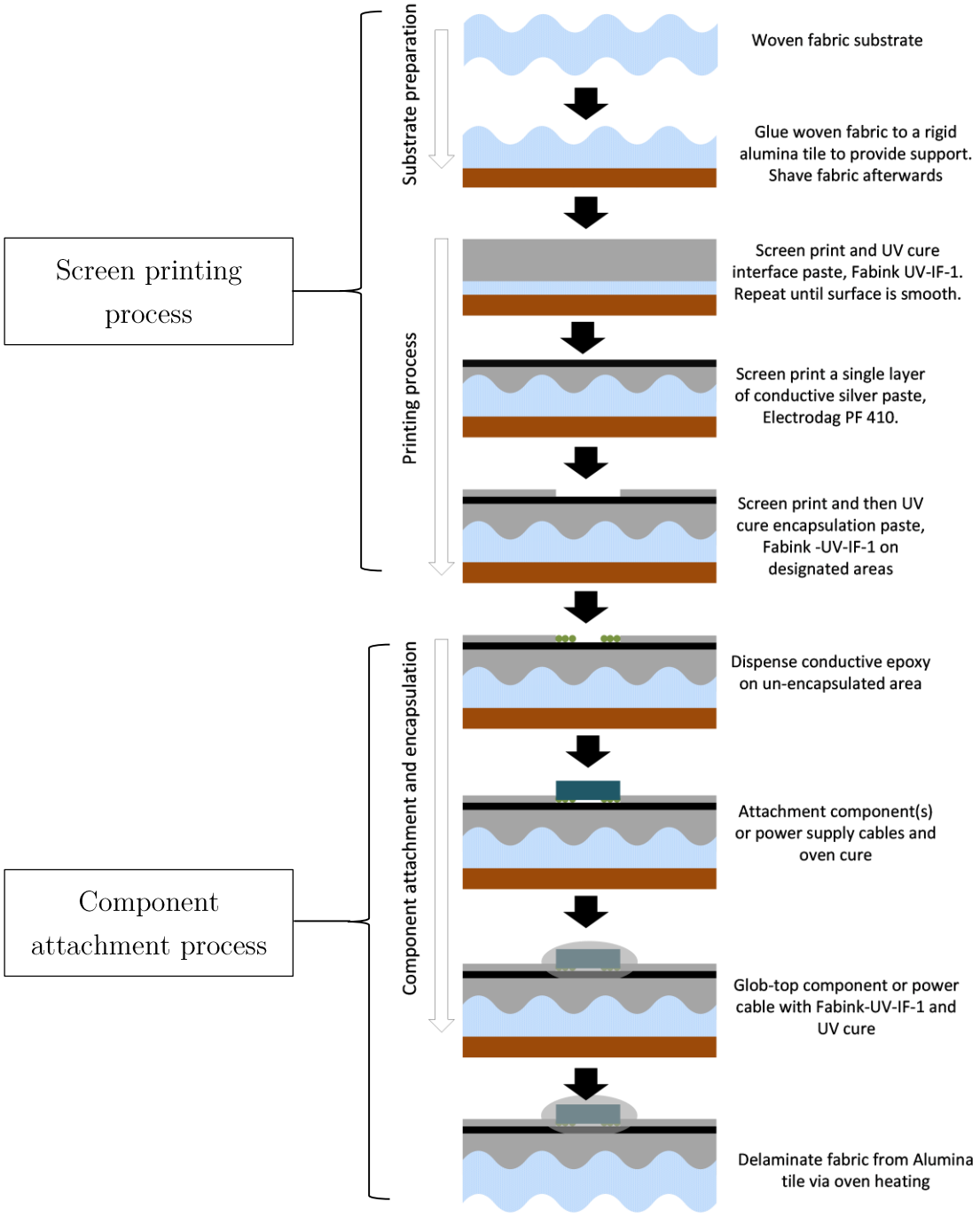

Figure 3.9: Fabrication process flow chart

3.5.1 The screen printing process

The Bari fabric was first adhesively bonded to a flat alumina tile. This ensures consistency in the prints and to also enable proper alignment of the printed layers. Afterwards, the textile was shaved with a rotary shaver to remove any standing fibre strands that contribute to the surface roughness of the fabric.

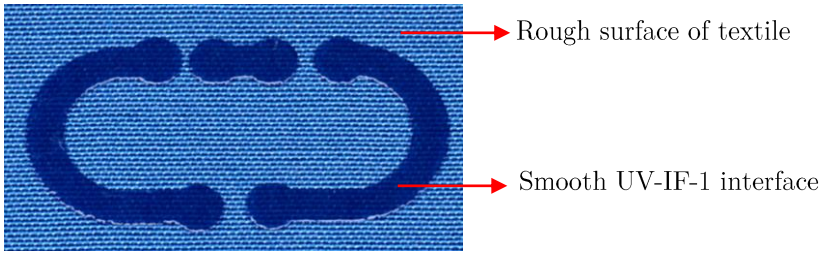

Figure 3.10: Interconnect screen patterns and their dimensions

The interface layer was realized in 4 prints consisting of 6-4-2-2 depositions of the Fabink UV-IF1 ink on the Bari fabric respectively. The smoothening effect of the interface on fabric is clearly shown in figure 3.10. Each print was UV cured for 60 seconds. The average interface thickness from seven measurements was 124 µm, Table 3.5.

Table 3.5: Screen printed layers and their thickness measurements (thickness taken over seven micrometre measurements)

Layers	**Material**	**Curing method**	**Measured thickness**
Substrate	Bari Fabric		324 µm
Interface layer	Fabink UV-IF1 ink	Oven cure, 125°C 15 mins	124 µm
Interconnect Layer	Electodag PF-410 silver ink	Ultraviolet (UV), 60 secs	10 µm
Encapsulation Layer	Fabink UV-IF1 ink	Ultraviolet (UV), 60 secs	28 µm

The LED circuit was printed on interface in a single print consisting only one deposition of the Electrodag PF-410 silver ink. The print was oven-cured at 125 °C for 15 minutes. An average thickness of 10 µm was measured. Finally the encapsulation layer was printed in a single print consisting 2 depositions of Fabink UV-IF1 ink. The print was UV-cured for 60 seconds. An average thickness of 28 µm was measured. Figure 3.11 shows the composite structure.

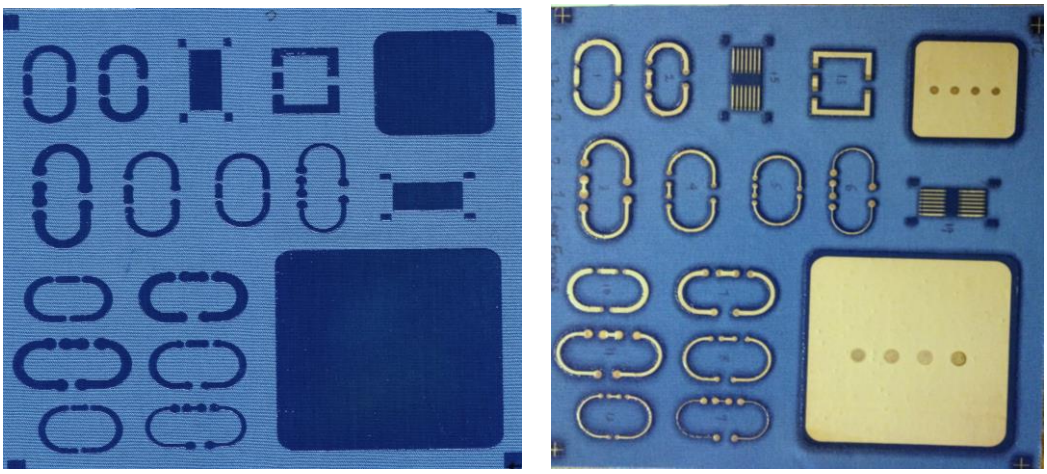

(a) (b)

Figure 3.11: (a) Interface Layer on Fabric, (b) Printed silver and encapsulation on the interface

3.5.1.1 Resolution of the screen printed circuits

All the patterns were well defined on the fabric except for the LED circuit with line width 200 µm which was difficult to achieve repeatedly with accuracy, figure 3.12. This suggests that the 305 mesh/cm mesh count of the interconnect screen was not sufficient to achieve that resolution. Consequently, screens with higher mesh counts will be better suited for patterns with linewidths ≤ 200 µm.

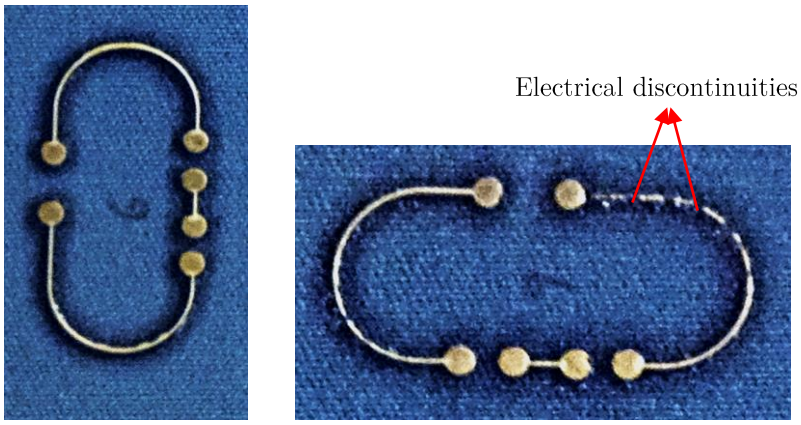

Sample A *Sample B*

Figure 3.12: Poor and inconsistent resolution of LED circuits of 200 µm

3.5.2 Component attachment process

Surface-mount green LEDs and 470 Ω resistors with dimensions 3.2 mm x 1.6 mm x 1.1 mm, and 3.2 mm x 1.6 mm x 0.6 mm supplied by RS components were attached to the printed patterns using a silver-loaded epoxy adhesive and left to

cure at room temperature for twenty-four hours. Similarly in figure 3.13, 240 µm-thick wires were also glued to the contact pads and the edge of the LED, with the same epoxy so as to ensure power supply into the circuit and to estimate circuit resistance respectively.

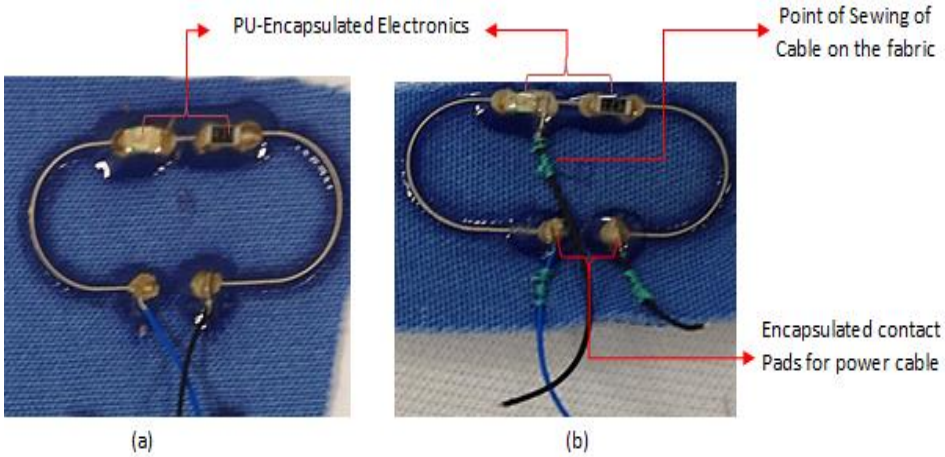

Figure 3.13: (a) Un-sewn and (b) sewn cable attachments on LED circuits

It was also dried for the same period of time. The attached electronics and the wires were then encapsulated with a Fabink UV-IF1 glob top which was dispensed with a syringe and UV-cured for sixty seconds immediately after application so as to prevent it from bleeding out.

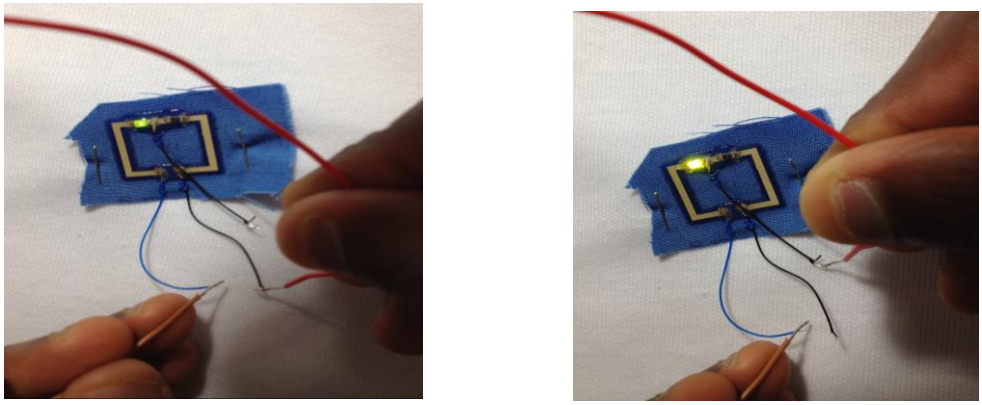

(a) Connected without by-passing the resistor *(b) Connected by by-passing the resistor*

Figure 3.14: Functional LED circuit (before washing)

Following this encapsulation, the wires were sewn onto the fabric, figure 3.13b to provide mechanical support to the joints especially when the sample undergoes washing. Figure 3.14 shows the functional LED circuit after being supplied with a dc current of 3 mA driven by a voltage of 2.5 volts.

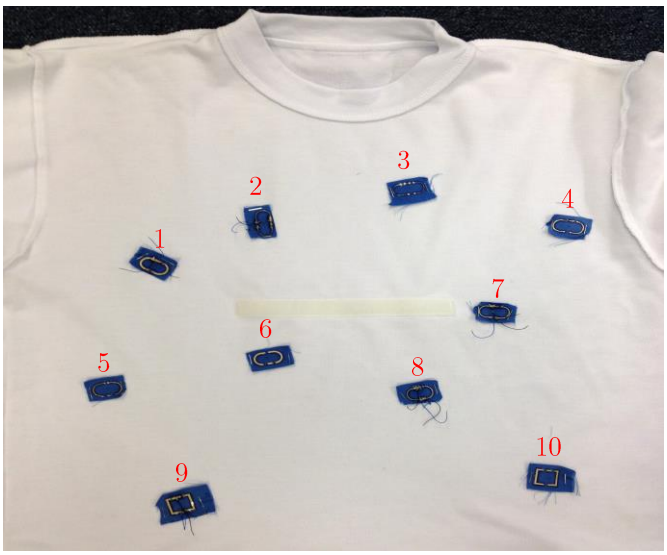

Figure 3.15: Stapled circuits on T-Shirt

Table 3.6: Description of stapled circuits on the shirt

Circuits	Type	Line-width	Encapsulated	Threaded cables
1	LED circuit	1.5 mm	Yes	No
2	LED circuit	0.2 mm	Yes	Yes
3	Resistor circuit	0.2 mm	No	No
4	Resistor circuit	0.75 mm	No	No
5	Resistor circuit	0.5 mm	No	No
6	Resistor circuit	1.5 mm	No	No
7	LED circuit	0.75 mm	Yes	Yes
8	LED circuit	0.5 mm	Yes	Yes
9	Square LED circuit	1.5 mm	Yes	Yes
10	Square resistor circuit	1.5 mm	No	No

3.6 Wash test

To replicate practical applications, ten textile circuit patches described in Table 3.6 were randomly stapled to a white shirt as shown in figure 3.15 for the wash test. Similarly for real conditions, the shirt was washed alongside two other shirts in a commercial Beko washing machine WME7247W at 30 °C for 49 minutes with a 1000 rpm spin dry. A total of 3 wash cycles is reported.

3.6.1 Results and discussion

All the circuits (both the LED and the resistor circuits) survived the first wash with all components still well attached. The LED circuits were still functional as well. No noticeable break in the interconnect lines was observed.

The second wash resulted in the failure of the component – interconnect (C–I) adhesive bond and cracks in both the encapsulation and interconnect layers of some of the circuits. In circuit 1, the unsewn black power cable as shown in figure 3.16a was weakened and almost peeled off. Although the LED circuit was still functional when powered as shown in figure 3.16b, small cracks were also noticed along the silver interconnect just around the mounted LED but the TPU encapsulation appeared unaffected.

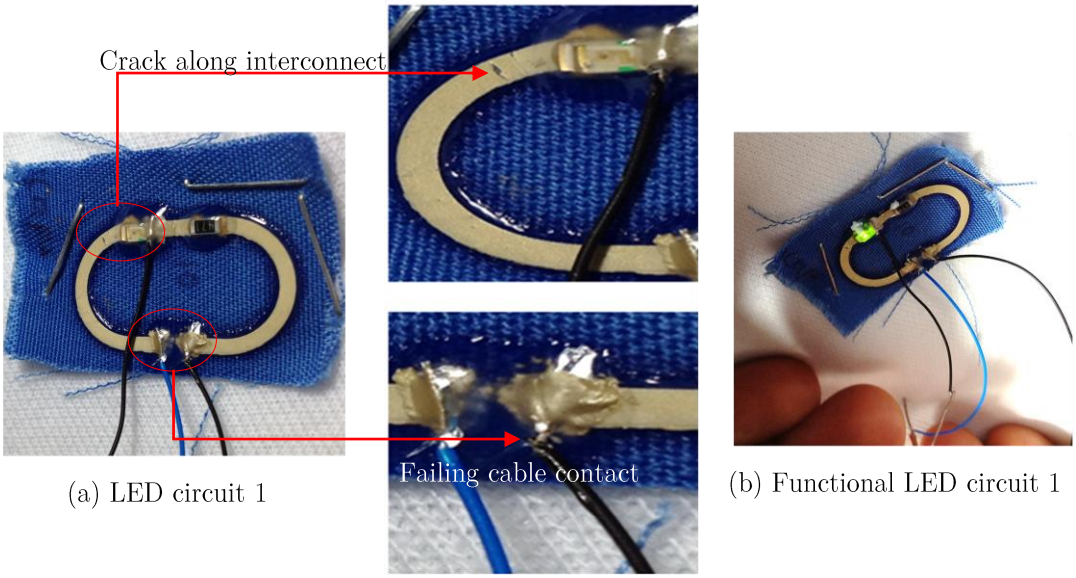

(a) LED circuit 1

(b) Functional LED circuit 1

Figure 3.16: LED circuit 1 after 2nd wash

LED circuit 8 completely failed after the second washing. A crack (location 1, figure 3.17) in the in the encapsulation which also led to the split the interconnect path just between the mounted resistor and the LED was observed. The TPU encapsulation became brittle largely due to its water absorption [95]. Another crack, (location 2) which was seen just at end of the encapsulation. The encapsulation layer peeled off the fabric hence peeling the interconnect layer with it.

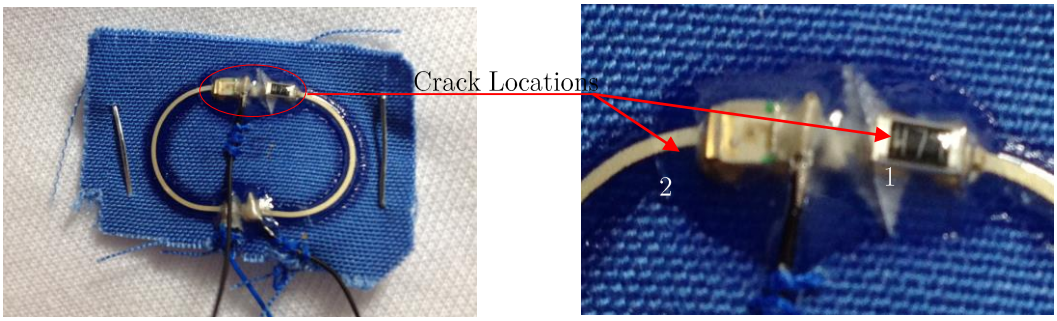

Figure 3.17: Crack Locations in LED circuit 8 after 2nd Wash

The brightness of circuit 2 reduced after the second washing (by observation). This likely resulted from an increase in circuit resistance and poor contact between the power terminals and the components. It was difficult to measure the circuit resistance since it was encapsulated. Other LED circuits (7 and 9) remained functional.

Figure 3.18: The resistors in circuit 3 still firmly attached after 2nd wash but with discontinuity along the silver conductor

The C–I adhesive bond in some of the un-encapsulated circuits were also weakened. In circuits 4 and 6, the solder at one leg of the resistor terminals was broken unlike in circuit 3, where all resistors remained firmly attached but with broken conductive track, as in figure 3.18.

The third wash severed the already weakened connection of the unsewn black cable in circuit 1. In addition, a crack was also observed in the area between the resistor and the LED due to the break in the encapsulation. However, the components still remained firmly attached to the circuit, figure 3.19.

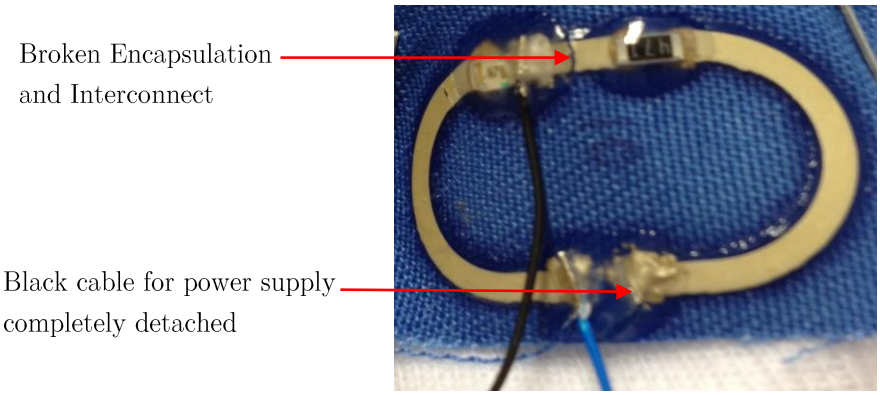

Figure 3.19: Crack Location in circuit 1 after 3rd Wash

Similarly in circuit 7, the blue power cable, figure 3.20 was peeled off the interconnect contact pad despite being sewn to the fabric. This failure is largely due to the weakening of the encapsulation layer and also can probably be as a result of poor soldering of the wire to the contact pad before encapsulation and sewing.

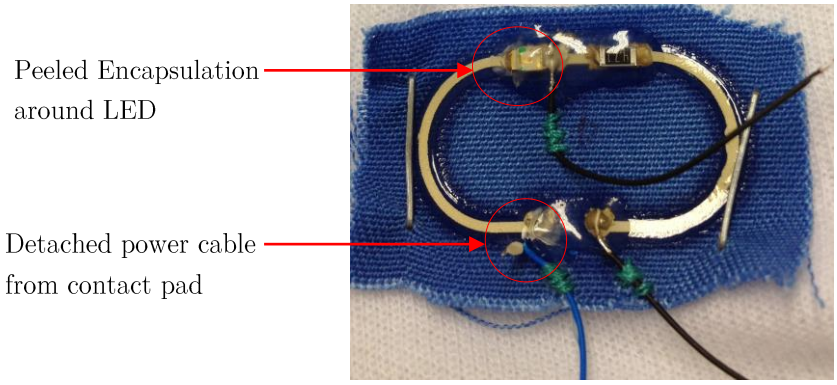

Figure 3.20: Faults in circuit 7 after 3rd Wash

The components and the power cable in circuit 2 were still firmly attached after the third wash however the LED became even dimmer than it was after the 2nd wash. Probable causes for this include the further increase in circuit resistance and weakening in the contact or jointing between the LED and its printed terminals. For the three washes, the square LED circuit, circuit 9 remained functional with all components firmly attached and the LED lighting very bright as in figure 3.14. In this case, the soldering appeared to have been better and circuit well encapsulated unlike the others which might be a reason for its survival. The resistors in the un-encapsulated circuits 3, 4 and 6 remained as they were after the second wash.

Circuits 5 and 10 have not been studied because their components removed before washing started. This happened because they were not encapsulated hence they peeled off during the delamination of the fabric substrate from the alumina tile.

Table 3.7 summarises the wash test results as follows:

Table 3.7: Summary of wash test results

Circuits	**Type**	**Encapsulated**	**Result**
1	LED circuit	Yes	Power cable weakened after second wash but failed completely after the 3rd wash. Encapsulation also cracked after 3rd wash.
2	LED circuit	Yes	Circuit survived three washes but LED lighting became very dim that it was barely seen.
3	Resistor circuit	No	Resistors remained attached after the 2nd wash but cracks were noticed along the silver tracks.
4	Resistor circuit	No	Adhesive failed at one of the two terminals of the resistor that was bonded to the circuit.
5	Resistor circuit	No	Failed before washing during the delamination of fabric from the alumina tile
6	Resistor circuit	No	Resistors remained attached after the 2nd wash but cracks were noticed along the silver tracks.
7	LED circuit	Yes	Failed after the third wash due to the peeling of the power cable from the circuit.
8	LED circuit	Yes	Failed after the 3rd wash due to a crack in the encapsulation layer and in the silver tracks
9	Square LED circuit	Yes	Survived the three wash cycles. Circuit appeared to be better encapsulated than the others.
10	Square resistor circuit	No	Failed before washing during the delamination of fabric from the alumina tile

The table showed that encapsulated circuits lasted until the third wash before failing completely unlike the un-encapsulated circuits that failed only after the second wash. While most of the encapsulated circuit failed after the 3rd wash mainly due to the poor water proof property of the Fabink UV-IF-1 encapsulation, the results however indicate the importance of a proper encapsulation to the durability of e-textiles.

3.6.1.1 Discussion: Problems arising from experiment

The problems identified from the wash test are as follows:

1. *Increase in circuit resistance*:

   A continuous increase in circuit resistance not only introduces design challenges but also degrades the electrical characteristics of the circuit as evidenced by the dimmed LED lighting observed in circuit 2 after the 2nd and 3rd wash cycles.

2. *Water absorption of interface and encapsulation material*:

   The experiment demonstrated the importance of encapsulations for printed circuits having recorded 100 % failures for un-encapsulated circuits (circuits 3, 4 and 6) after the 2nd wash cycle, figure 3.18. While encapsulated circuits performed better, the water absorption of the encapsulation material initiated other failures. The Fabink-UV-IF-1 encapsulation have been shown to absorb roughly 20 % of water when completely immersed in it [95]. This in turn makes the material brittle and prone to cracking as shown in figure 3.17. It also weakens its interfacial bond with the underlying surface which can potentially break the electrical continuity within a circuit, figure 3.19.

3. *Interfacial failures at the joints*:

   This largely occurs between power cables and printed terminals, and components and printed terminals. The threading and encapsulation of the power cables to the substrate have shown minimal failure rate by limiting the stress induced at the joint between the cable and the printed terminals. Only one of the four tested circuits (circuits 2, 7, 8 and 10) failed.

   To minimize failure of the adhesive bonding the component (LED or resistor) with the printed terminals, a Fabink-UV-IF-1 glob-top encapsulation was dispensed across the joints. However, the glob-topping proved to be a temporal solution to encapsulating components due to failures arising at its interfaces which results in the peeling of the glob-top and/or with the breaking circuital lines, figure 3.20. Other recorded failures were largely due the weakening of the adhesive strength of the silver-loaded epoxy adhesive by the washing stresses and/or the failures along on encapsulation which translate into these joints. The silver loaded epoxy used in this work

had an adhesive shear strength between 70 – 140 kg/cm^2 [137]. This suggests conductive adhesives that provide a better adhesive strength will be crucial for integrating components on printed circuit.

3.6.1.2 Proposed solutions

To address the problems the following solutions are proposed:

1. *Printing on the neutral axis:*

   From the review in chapter, it can be concluded that the resistance of a circuit increases when the conductive path (i.e. interconnection) is subjected to stress. In multilayer printed composites such as the LED circuits, the magnitude of the induced stress will vary across the printed layers especially as the composite flexes or bends. Conductors must therefore be carefully located in the region of minimal stress within the printed composite.

2. *Waterproof interfaces and encapsulation:*

   Kai et al. [95] reported a new and highly hydrophobic polyurethane material, Fabink UV-IF-010 that absorption rate of 0.3 % when fully immersed in water. However, the material has a lower surface energy than the Fabink UV-IF-1 and therefore materials other than the Fabink-UV-IF-1 will not strongly adhere to it. This means a thin layer of the UV-IF-1 must be printed to improve adhesion. This changes the structure of the e-textile from a four layer composite (FLC) to the six layer composite (SLC) structure in figure 3.21.

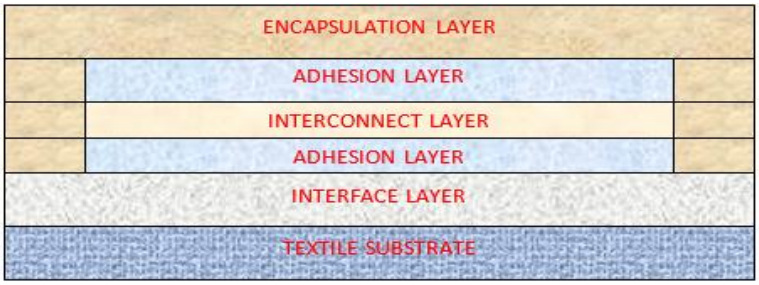

Figure 3.21: Cross section of the six layer composite (SLC) e-textile

3. *Anisotropic adhesives:*

   The use of the isotropic silver loaded conductive adhesive meant that the components could only bonded to the substrate at their contact pads

therefore leaving a considerable portion of the component un-bonded. In bonding the entire bottom area of the component, its adhesion can be improved. Anisotropic adhesives offer this advantage since their unidirectional conduction allow them to be applied to the entire component area other than the contact pads. Therefore the anisotropic adhesive Elecolit 3061 supplied by Eurobond Adhesives Limited will be used be in further experiments.

3.7 Conclusions

This chapter investigated the durability of screen printed circuits by subjecting fabricated samples to a wash test. The results indicated that encapsulated printed circuits showed better durability against washing unlike un-encapsulated circuits.

However, to improve on this durability, it is still important to understand the mechanical actions of a fabric in a washer and separately examine the effect of each mechanical action on the durability of e-textiles. Yun et al [116] categorised these mechanical actions into three fabric movements consisting of sliding, falling and rotation. These movements especially the falling action impact the loaded fabric by flexing (or bending) it and also ensure that the fabric is properly immersed in the detergent solution during washing [115, 116].

Consequently, the next chapter focuses on improving the durability of printed circuits against a bending action of a printed e-textile.

CHAPTER 4
NEUTRAL AXIS ENGINEERING OF PRINTED E-TEXTILES

4.1 Introduction

This chapter attempts to improve the durability of printed e-textiles in bending by investigating the positioning of electrical interconnections on or in close proximity to the neutral axis, NA of e-textiles where they will experience zero stress. It examines the applicability of the classical beam theory (CBT) in calculating the thicknesses of the different layers contained in e-textile structure depicted in figure 3.21 that are needed to position the interconnect on the NA. It also evaluates the effects of the elastic and geometric properties of the different layers contained in the e-textile on the NA position and the stiffness of the e-textile. The NAs calculated from the CBT model based for a three and four layer composite structure of Kapton and polyester cotton fabric are experimentally verified by measuring the resistance change in bending of the strain gauges screen printed on these NA positions respectively.

4.2 The concept of the neutral axis: The beam theory

The preceding chapters indicate that the stresses induced in printed e-textiles during use cause mechanical failures and a degradation of the electrical resistance of the printed electrical interconnections after at least three cycles of washing and bending. Nevertheless, this degradation can be minimised by positioning their electrical interconnections on the NA of the e-textile; a point within the e-textile where all normal strains and stresses are non-existent based on CBT [138].

However the CBT model simplifies the mechanical behaviour of a beam to only pure bending and assumes that shearing deformation and beam deflections are negligible. But depending on the loading and geometric structure of a fabric, mechanical properties such as tensile extensibility, shearing, bending and twisting can be exhibited by a fabric [105]. While the stresses consequent of these mechanical properties may influence the mechanical behaviour of screen printed e-textiles, the

assumptions of the CBT are also extended in this work for modelling screen printed e-textiles for initial investigations. This reasoning is based on review in section 2.3 which identifies the bending stress (comprising of tensile and compressive stresses) as the primary stress to limit the durability of such e-textiles. Therefore to assess the suitability of beam theory to e-textile design it needs to be decided whether or not printed e-textiles comprising a fabric substrate and some printed polymeric layers can be treated as beams?

A beam is defined by Huston et al. [139] as any structure whose length, l is an order of magnitude (i.e. 10 times) larger than the cross sectional dimensions, that is;

$$l > 10\,y \quad and \quad l > 10\,x \tag{4.1}$$

Where y and x represent the height (depth) and width of the beam respectively. The screen printed e-textiles reviewed in section 2.2.2.5 fall within this definition. So a printer fabric can be considered to be a beam.

Further when in use, fabrics are also subject to any, or a combination, of the three principal loadings theoretically associated with beams:

i. Axial or longitudinal loads, in which case the beam experiences either compression or tension

ii. Transverse loads which subjects the beam to bending

iii. Torsional loads which twists the beam.

Hence before fabricating an e-textile, it is imperative to know its NA position during the e-textile design so that interconnects can be printed on, or close to, the NA during fabrication. This model will also be useful for rapid prototyping of printed e-textiles.

4.2.1 Importance of the neutral axis to e-textiles

Although this work primarily focuses on using the beam theory to locate the NA of screen printed e-textiles, the stress distribution across the constituent layers of the e-textile is also investigated. This is particularly relevant when the functional or active layer needs to be optimised for maximum stress response. This is the case with energy harvesting e-textiles such as piezoelectric shoe insoles or carpets where the piezo-layer must be located as far as possible from the NA to harvest maximal

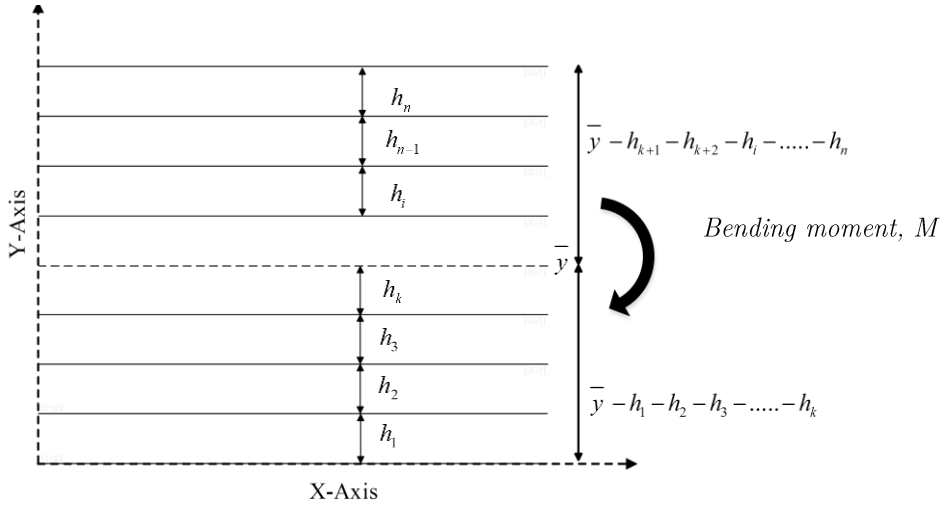

Figure 4.1: The neutral axis of a multilayer beam

energy. Also in the design of e-textiles containing more than one functional layer, this also helps in optimising the positions of these layers for desired stress response.

4.3 Locating the neutral axis of a printed e-textile

The e-textile in figure 3.21 can be approximated to a multilayer beam shown in figure 4.1 whose NA, $\bar{y}$ is the interconnect layer. If $\bar{y}$ is chosen such that the position of other layers in beam are measured relative to it, then from Ballas' model [140] on piezoelectric multilayer beams, $\bar{y}$ can be obtained using (see appendix B.1):

$$\bar{y} = \frac{\sum_{i=1}^{n} E_i x_i h_i \left(2\sum_{j=1}^{i} h_j - h_i \right)}{2\sum_{i=1}^{n} E_i x_i h_i} \tag{4.2}$$

Where E_i, x_i and h_i represent the elastic modulus, width and thickness of the i^{th} layer of the beam respectively.

4.3.1 The method for measuring the elastic modulus of materials

A tensile test is one of common industrial techniques for measuring the elastic properties of materials [141]. It involves applying a controlled tension or force on a clamped material, with the equipment shown in figure 4.2, until it fails. In the linear regime of its stress-strain profile shown in figure 4.3, elastic deformation

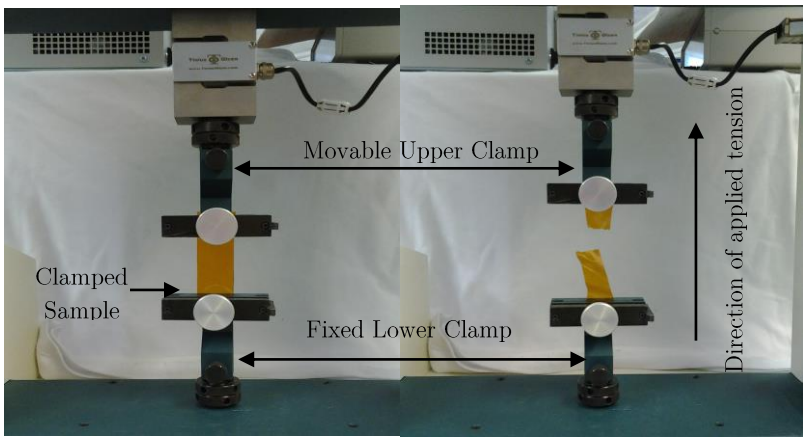

(a) Before loading (b) After unloading

Figure 4.2: Tensile testing of Kapton on Tinius Olsen's H25KS benchtop tester

occurs. The slope of the graph gives the elastic modulus of material which is based on Hooke's law of elasticity given by equation 4.3.

$$E = \frac{stress, \sigma}{strain, \varepsilon} = \frac{\frac{Force, F}{Cross\,sectional\,Area, A}}{\frac{extension, s}{length, l}} = \frac{Fl}{As} \tag{4.3}$$

In the second regime, viscoelastic deformation occurs in which case the fabric slowly returns to its initial length after unloading for a certain relaxation time. In the third phase, the fabric permanently deforms before it eventually breaks [143].

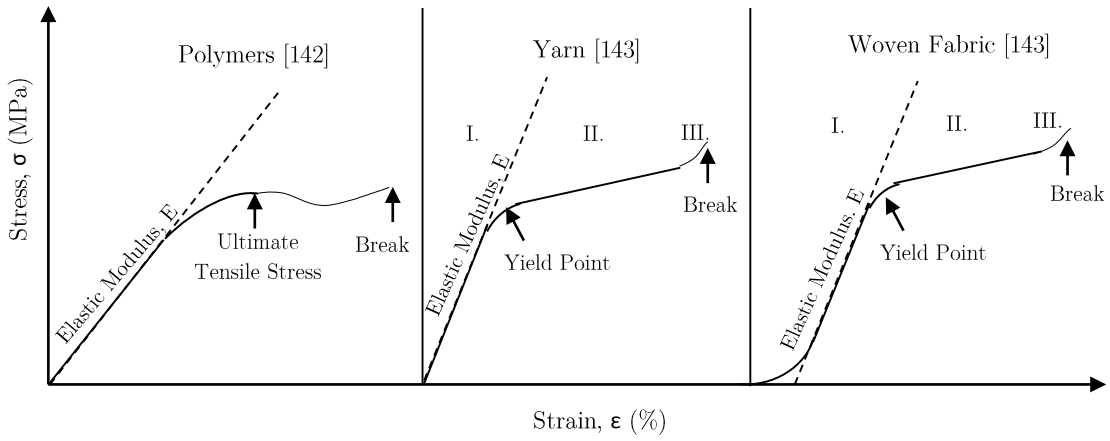

Figure 4.3: Stress-strain diagrams of different materials

Dumb-bell shaped specimens are typically used for tensile testing. But based on the BS EN ISO 13934-1:1999 standard for the tensile testing of fabrics and, the ASTM D882 and EN ISO 527-3 standards for the tensile testing of thin plastic strips that

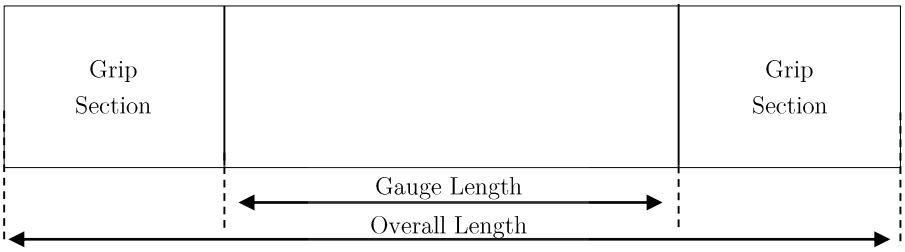

Figure 4.4: Description of specimen for tensile testing

are less than 1 mm thick, rectangular specimens were used. This is because the materials to be tested fall within the specification of these standards. The rectangular strip as shown in figure 4.4, is divided into three sections namely:

i. **Grip sections**: These sections provide clamping for the specimen to be tested. The lower clamp is usually fixed while the upper clamp is movable which allows for tension or compression stress in the material when moved up or down.

ii. **Gauge section**: The change in length of the gauge section gives the extension in the material after the test.

Tensile tests are unsuitable for some thick film materials that are fragile and hence easily prone to cracking such as the 100 µm thick Electrodag PF 410 silver conductor shown in figure 4.5.

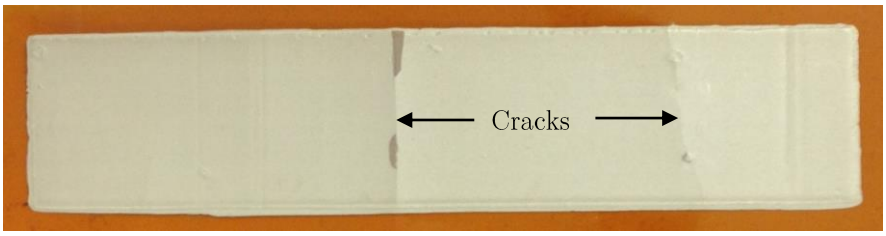

Figure 4.5: Cracks on a 100 µm thick Electrodag PF 410 silver on Kapton

The nano-indentation technique is one way of measuring the elastic modulus of such coatings [123]. During the indentation process, the tip of the indenter indents the material surface with a loaded force and penetrates into the sample to a certain depth, shown in figure 4.6. Both parameters are recorded as a function of time to obtain the load – displacement plot for the sample. However, the modulus measured in this way is referred to as a reduced modulus, E_r which is related to the elastic moduli, E and E_I of the material and indenter respectively by [144]:

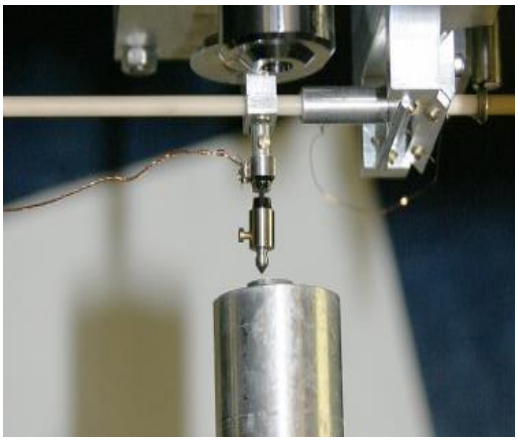

Figure 4.6: The Berkovich Indenter [145]

$$\frac{1}{E_r} = \frac{1-\upsilon_I^2}{E_I} + \frac{1-\upsilon^2}{E} \tag{4.4}$$

Where υ and υ_I are the Poisson ratios of the material and indenter respectively.

4.3.2 Elastic modulus measurement of materials in the e-textile

The Tinius Olsen's H25KS benchtop tester, pictured in figure 4.2 was used to obtain the elastic modulus of the materials shown in Table 4.1 except for Fabink-TC-PolyPR1 which was indented with the Berkovich nano-indenter in figure 4.6 because of its brittleness. The polymer samples for testing were stencil printed (screen printing with an unmeshed screen) on a poly-tetra-fluoroethylene, PTFE substrate which enabled them to be easily removed after curing.

Table 4.1: Elastic modulus of materials

Classification	Materials	Thickness	Width	Gauge length	Overall length	[1]Average Elastic modulus, E
Substrates	Bari fabric	324 µm	3 cm	5.5 cm	10 cm	400 ± 20 MPa
	Kapton	75 µm				3 ± 0.5 GPa
Polymers	Fabink UV-IF-1	250 µm	2 cm	3.5 cm	8 cm	100 ± 30 MPa
	Fabink UV-IF-010	285 µm				2.8 ± 1 MPa
	Fabink TC-PolyPR1	100 µm	10 mm	10 mm		3.25 ± 0.9 GPa

[1] Elastic modulus was averaged over five samples.

The dimensions of the tensile tested materials are given in Table 4.1 and these were chosen to easily suit the sample holders of the tensile equipment. Five samples of each material were tested to minimise measurement errors. Their elastic modulus values, correct to the tolerances shown in Table 4.1, were calculated from the force-extension profiles shown in figure 4.7 using equation 4.3.

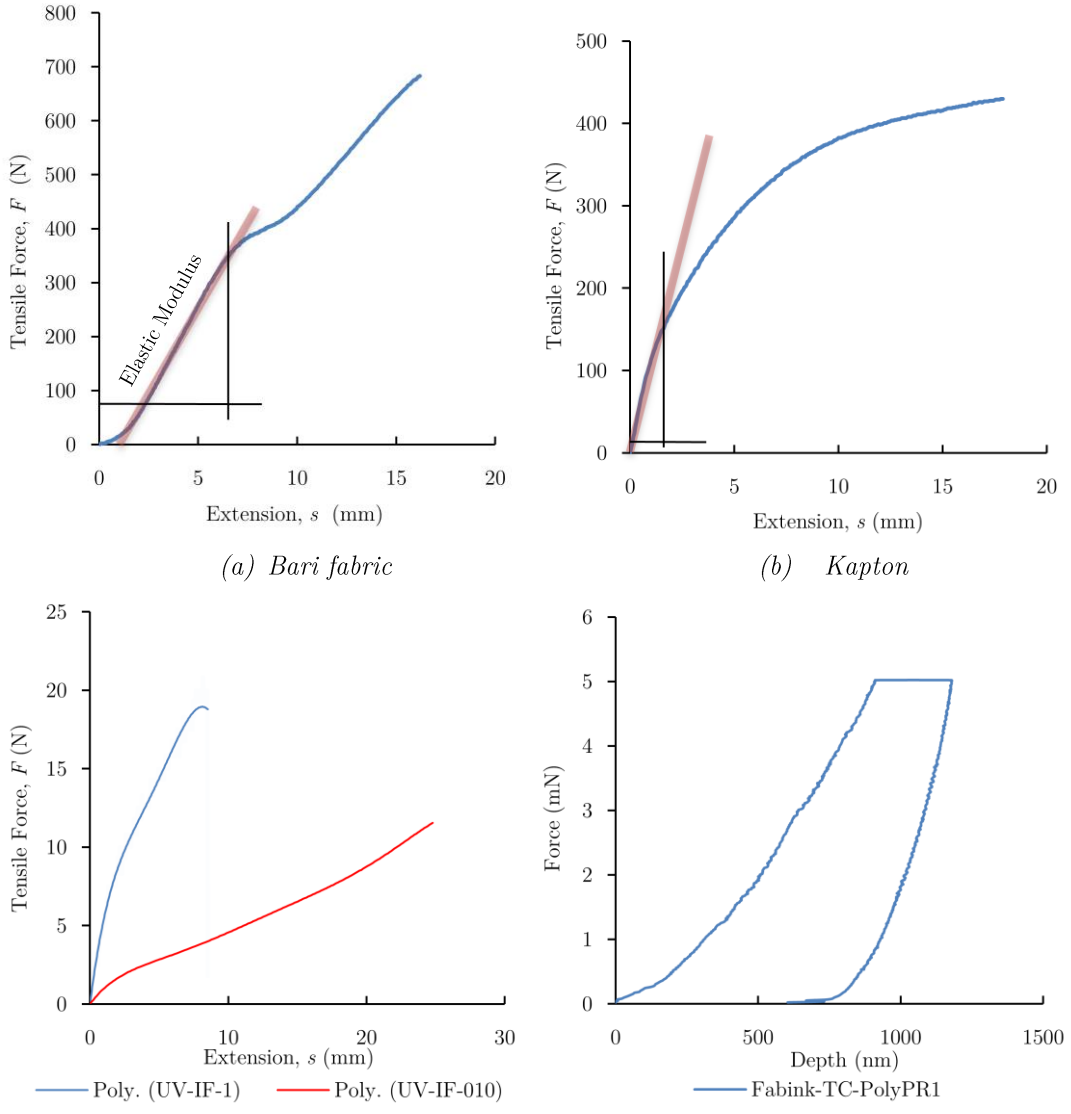

(a) Bari fabric *(b) Kapton*

(c) Fabink UV-IF-1 and Fabink UV-IF-010 *(d) Fabink TC-PolyPR!*

Figure 4.7: Force - extension profiles of substrate and polymer materials

The reduced modulus of the Fabink-TC-PolyPR1 was automatically calculated by from the nano-indenter after twenty indentations. This equals the elastic modulus

of the material in equation 4.4 under plane strain conditions for the thin layer (i.e. $\upsilon = 0$) since the diamond indenter has high modulus of 1.141TPa [146].

4.4 Numerical modelling of the neutral axis of a printed e-textile

For simplicity, the layers of the e-textile are assumed to be of equal width, x which can be the case when the e-textile is not necessarily desired to be completely waterproof (i.e. water can penetrate slightly from the sides). Therefore equation 4.2 becomes:

$$\overline{y} = \frac{\sum_{i=1}^{n} E_i h_i \left(2\sum_{j=i}^{i} h_j - h_i \right)}{2\sum_{i=1}^{n} E_i h_i} \; ; \quad \forall \; x_i = x \tag{4.5}$$

This reduces the parameters for calculating $\overline{y}$ to E and h. An understanding of the relationship between these parameters and the NA position pre-informs the choice and range of materials that can be used to easily:

i. Position the interconnections on the NA of an e-textile during fabrication.

ii. Optimise an e-textile without significantly compromising its textile properties such as flexibility during fabrication.

Table 4.2: Initial material properties of a multilayer beam on Kapton substrate

Classification	Sub-layer	Material	Elastic Modulus		Initial Thickness	
Bottom layer	Substrate	Kapton	E_1	3.0 GPa	h_1	75 µm
	Interface,	Fabink UV-IF- 010	E_2	2.8 MPa	h_2	15 µm
	Bottom adhesion	Fabink UV-IF-1	E_3	100 MPa	h_3	15 µm
Interconnect layer	Interconnect	Piezoresistive carbon paste, Fabink-TC-PolyPR1	E_4	3.25 GPa	h_4	5 µm
Top layer	Top adhesion	Fabink UV-IF-1	E_5	100 MPa	h_5	15 µm
	Encapsulation	Fabink UV-IF- 010	E_6	2.8 MPa	h_6	15 µm
	Interconnect position		**Neutral axis position**			
	110 µm		43 µm			

This understanding is enabled by a numerical analysis of equation 4.5 which was undertaken in MATLAB to investigate how the independent changes to the E and h values of each layer will affect the NA position of the e-textile. The values of E and h, that will place the interconnect on the NA are also investigated. These values are called the optimised elastic modulus and thickness values respectively. First, the initial material properties of the e-textile are defined in Table 4.2. To avoid the irregular mechanical properties of woven fabrics reported in [94], Kapton was used as the substrate. The interconnect layer is 105 µm from the substrate and 62 µm away from the NA which is located 43 µm from the substrate as calculated from equation 4.4.

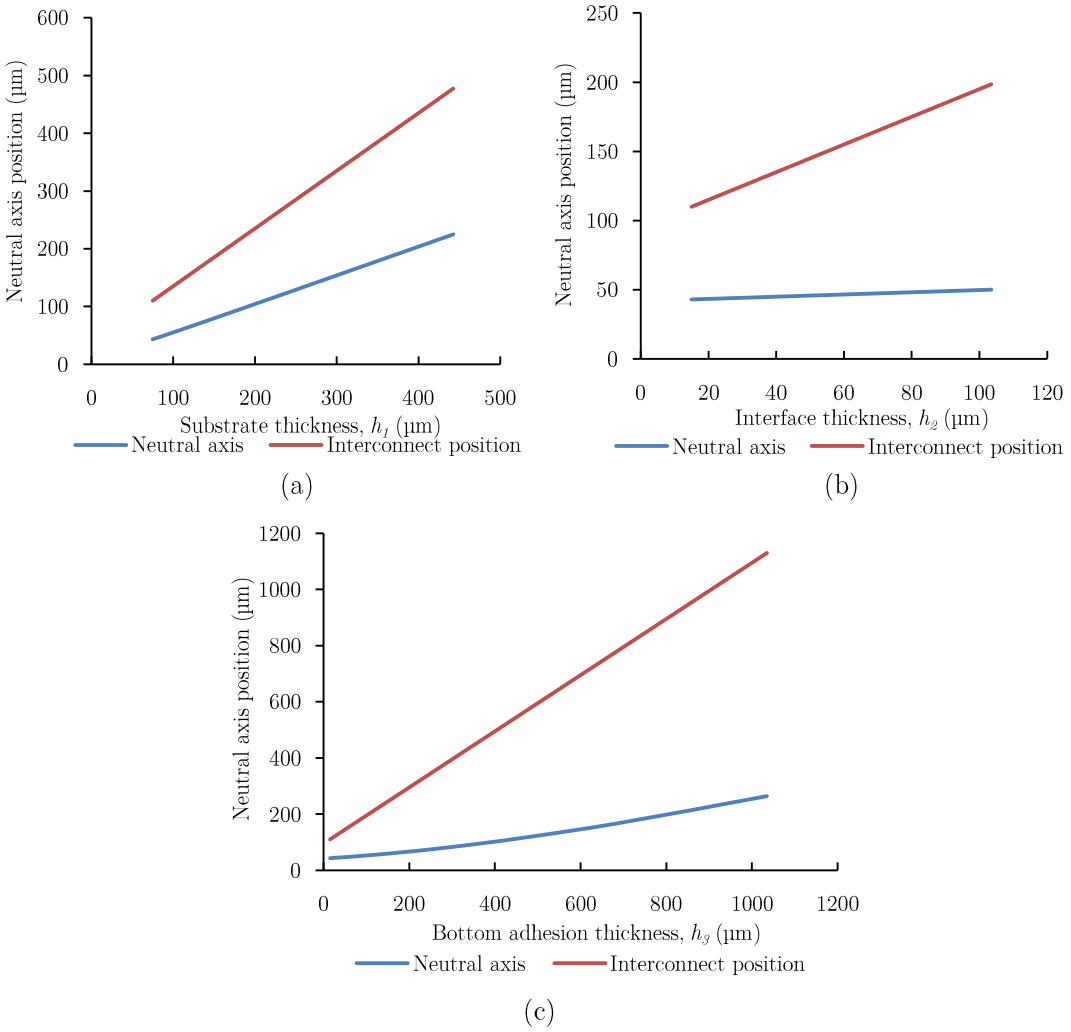

Figure 4.8: The NA and interconnect positions at different (a) substrate, (b) interface and (c) bottom adhesion thickness values using initial elastic modulus values.

4.4.1 Effect of the thickness and elastic modulus values of the bottom and interconnect materials on the neutral axis

The increase in the thicknesses h_1, h_2 and h_3 of the substrate, interface and the bottom adhesion layers separates the NA from the interconnect position as respectively shown in figures 4.8 (a, b & c). The blue and red lines represent the positions of the layer whose thickness is modified and the interconnect in the e-textile. Similar divergence is also observed with increasing values of E_1, the substrate elastic modulus, and decreasing values of E_2, E_3, and E_4 of the interface, bottom adhesion and interconnect materials respectively as shown in figure 4.9 (a, b, c & d). Conversely, the distance between the NA and the interconnect layer reduces.

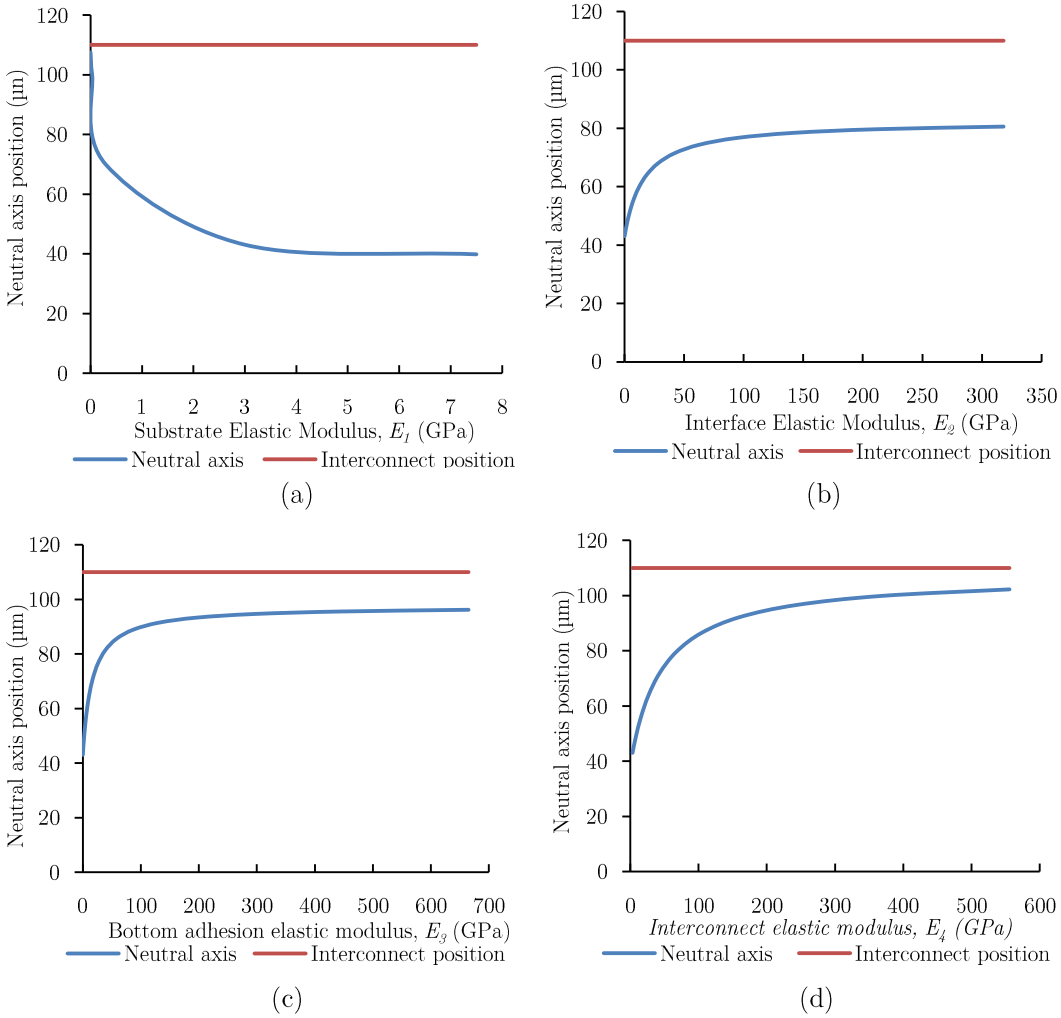

Figure 4.9: Effect of varying the elastic modulus of (a) substrate (b) interface (c) bottom adhesion and (d) interconnect layers on the neutral axis position with the layer thickness unchanged.

For locating interconnects on the NA, these results imply either:

(a) A replacement of the substrate with an elastomeric polymer whose elastic modulus in the order of $E \leq 0.1$ MPa [147]. For example the distance between the NA and the interconnect layer reduces to 3 µm as $E_1 \rightarrow 0$. While such polymers maybe flexible, they lack the textural feel of textiles.

(b) A replacement of any of the interface, bottom adhesion and interconnects materials with stiff materials in the order of $E > 320$ GPa which typify materials like ceramics, metallic alloys and glasses as shown in figure 4.10 [148]. Using such materials will trade-off the flexibility of the e-textile. Figure 4.9 also discounts this approach because the reduction in the NA – interconnect distance from 43 µm when $E_2 = 100$ MPa and $E_4 = 3.25$ GPa, to 10 µm when E_2 increased to 320 GPa or to 29 µm when $E_4 = 555$ GPa indicates that the interconnect can still be located away from the NA after using such high elastic modulus materials and at thicknesses as small as 15µm. In contrast to their initial values, the high values of the final E_2 and E_4 also shows that the increase in stiffness of the bottom layer materials is not necessarily commensurate with the rate at which the NA-interconnect distance reduces.

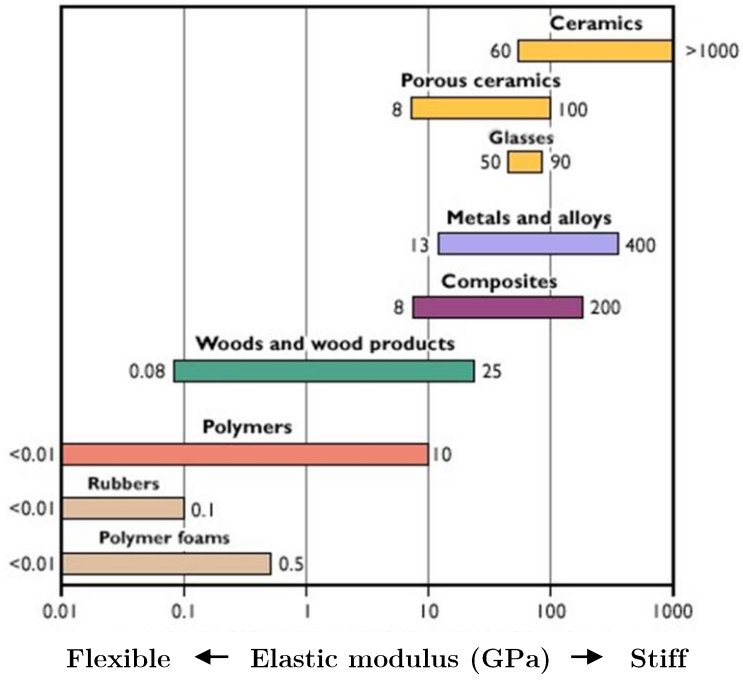

Figure 4.10: Elastic modulus (stiffness) values of common materials [148]

4.4.2 Effect of the thickness and elastic modulus values of the top layer materials on the neutral axis

Figure 4.11 (a, b) shows that positions of the NA and the interconnect layer become exactly the same when the thickness of the top adhesion, h_5 or encapsulation, h_6, reaches the optimised value respectively. This occurs at the intersection between the NA and interconnect lines when $h_5 = 550$ µm and $h_6 = 3300$ µm.

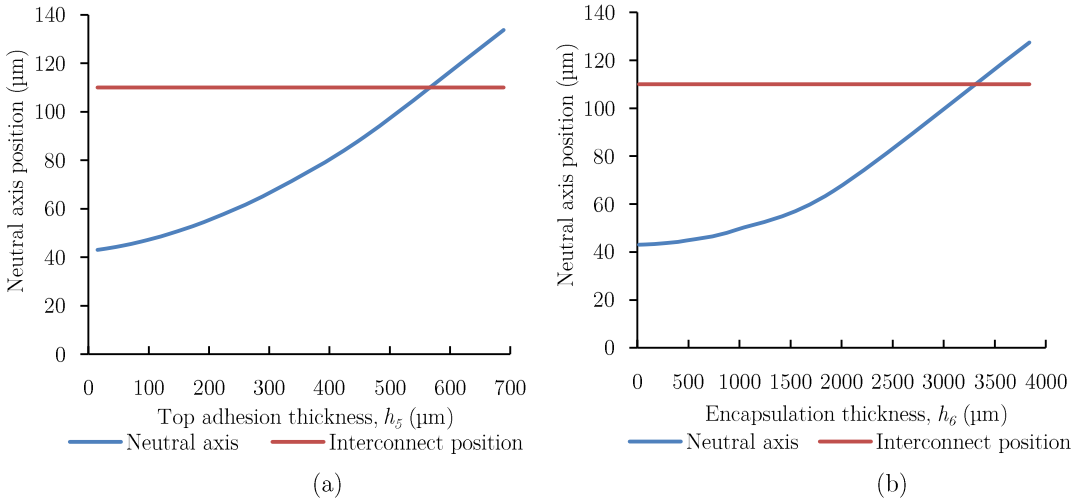

Figure 4.11: Effect of varying in thickness of (a) top adhesion and (b) encapsulation layers on the neutral axis position, with the elastic modulus unchanged.

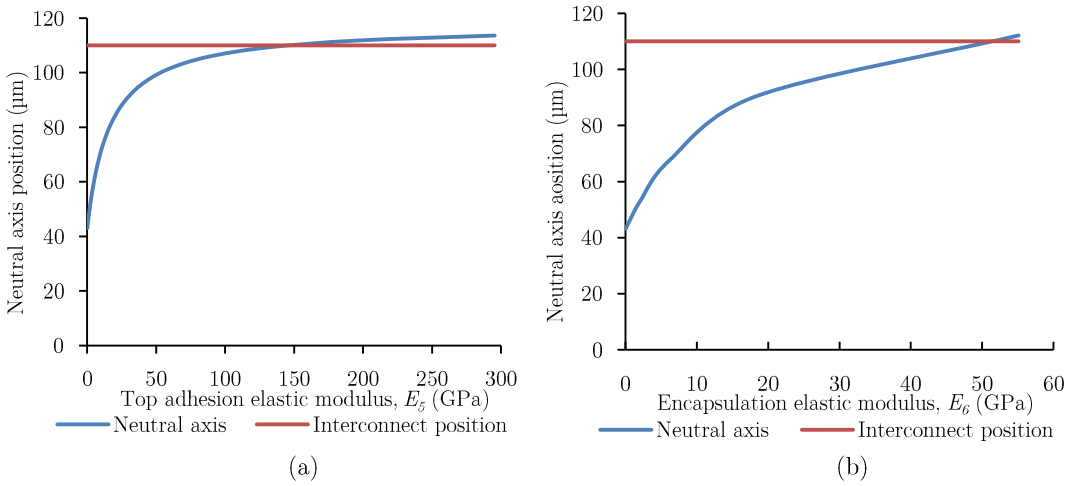

Figure 4.12: Effect of varying the elastic modulus of (a) top adhesion and (b) encapsulation layers on the neutral axis position, with the thickness unchanged.

Since the top adhesion material, $E_5 = 100$ MPa is stiffer than the encapsulation material, $E_6 = 2.8$ MPa, it can be concluded that by using a reasonably stiff polymer to encapsulate an interconnect, the optimised encapsulation thickness can be

significantly minimised. This is evidenced by the optimised value of h_5 which is 2750 µm less than that of h_6. This also ensures that the total thickness of the e-textile is curtailed to a practical minimum as best as possible. Figure 4.12 (a, b) also shows that when E_5 = 50 GPa or E_5 = 150 GPa, the optimised values of h_5 and h_6 can both be as small as 15 µm. Since these modulus values typify rigid materials as is shown in figure 4.10, it is still essential to optimise the e-textile for optimal flexural stiffness. This compromises between achieving small optimised encapsulation thickness with polymers of elastic modulus as high as 100 MPa ≤E ≤ 10 GPa and high optimised encapsulation with polymers of elastic modulus as low as E ≤ 2.8 MPa. This is discussed in much detail in section 4.5.1.

4.4.3 Inferences from the numeric modelling of the neutral axis

- The thicknesses of the sub layers contained in the bottom layer as described in Table 4.2 should be low as practically possible. At high thicknesses, the interconnect layer drifts further away from the NA as shown in figures 4.8 (a, b &c).
- It is better and easier to modify the thicknesses of the sub-layers in the top layer of the e-textile than those of the bottom layer. This is portrayed in figures 4.8 c and 4.9 c where the interconnect layer was not positioned on the NA despite increasing the thickness and elastic modulus of the bottom adhesion layers to 700 GPa and 1 mm respectively. This is contrasted in figure 4.11 where the interconnect layer was positioned on the NA by only increasing the thickness and elastic modulus of the top adhesion layer to 100 MPa and 0.55 mm respectively.
- The more elastic the fabric (or substrate) is, the lower the top layer thickness required to engineer the interconnect layer on the NA. Figure 4.9a showed that as the elastic modulus of the substrate is reduced down to the order of E ≤ 0.1 MPa, the optimised thickness of the top adhesion and encapsulation layers which constitute the top layer were each still as small as 15 µm.
- The stiffer the materials in the top layer, the lower the optimised thickness. When elastomers (E ≤ 1 MPa) are used, the optimised thickness can be as high as 3.3 mm and for higher elastic modulus polymers (100 MPa ≤ E ≤ 10

GPa) such as thermoplastic polyurethanes i.e., optimising thickness of less than 0.55 mm are achievable depending of the elastic properties of the bottom layer [147].

- The e-textile should be optimised for minimal flexural stiffness when choosing between using stiff and elastic materials for the sub layers of the top layer.

4.5 Analytical modelling of the neutral axis of a printed e-textile

This analytic model characterises the elastic behaviour of the top and bottom layers of the e-textile making it possible to calculate the values of E and h for the materials in the top layer.

Consider a bilayer material whose bottom and top layers are bounded by the neutral axis. If E_B and E_A represent the elastic modulus of these layers, and H_B and H_A their respective thicknesses, then these parameters can be related by [120]:

$$H_A = \frac{\sqrt{E_B}}{\sqrt{E_A}} \times H_B \tag{4.6}$$

Equation 4.6 is explained in figure 4.13 by showing how the optimised thickness and elastic modulus of the top layer can be chosen relative to a bottom layer of known elastic property i.e. thickness and elastic modulus of the bottom sub-layers.

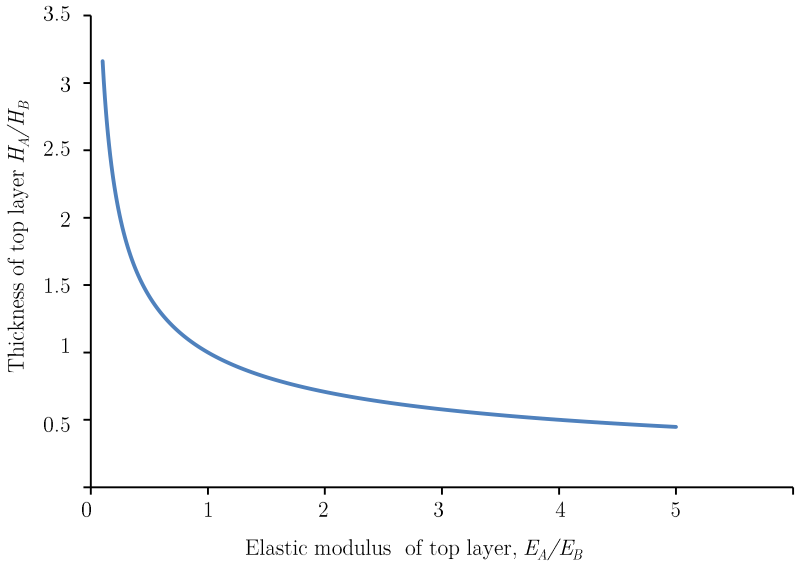

Figure 4.13: Relationship between the elastic modulus and thickness of top Layer

In comparison with the e-textile classifications in Table 4.2, the bottom and top layers of the bilayer are further divided into "*q*" and "*n-q*" sub-layers whose elastic properties are effectively characterised by E_B and E_A using equation 4.7. This was derived from equations 4.5 and 4.6 as (see appendix B.2):

$$E_B = \sum_{i=1}^{q} E_i t_i \left(2\sum_{j=1}^{q} t_j - t_i \right); \quad \left\{ \sum_{i=1}^{q} t_i = 1; \quad t_i = \frac{h_i}{H_B} \right. \tag{4.7a}$$

$$E_A = \sum_{i=q+1}^{n} E_i t_i \left(2\sum_{j=q+1}^{i} t_j - t_i \right); \quad \left\{ \sum_{i=q+1}^{n} t_i = 1; \quad t_i = \frac{h_i}{H_A} \right. \tag{4.7b}$$

Where E_i, h_i and t_i are the elastic modulus, thickness and thickness ratio of the i^{th} layer in the e-textile respectively.

The values of E_B and E_A are defined as:

$$E_B \in \{E_1, ..., E_q\} \tag{4.8a}$$

$$E_A \in \{E_{q+1}, ..., E_n\} \tag{4.8b}$$

The equation for calculating the optimised thicknesses of the sub-layers is derived from equation 4.7 as follows:

$$e_B = \sum_{i=1}^{q} e_i t_i \left(2\sum_{j=1}^{q} t_j - t_i \right); \quad \left\{ e_B = \frac{E_B}{E_1}; \; e_i = \frac{E_i}{E_1}; \; \forall \; i \le q, \right. \tag{4.9a}$$

$$e_A = \sum_{i=q+1}^{n} e_i t_i \left(2\sum_{j=q+1}^{i} t_j - t_i \right); \quad \left\{ e_A = \frac{E_B}{E_1}; \; e_i = \frac{E_i}{E_{q+1}}; \; \forall \; q+1 \le i \le n, \right. \tag{4.9b}$$

Where e_i and t_i are the elastic modulus and thickness ratios of the sub-layers, and e_A and e_B are the elastic modulus ratios in the bilayer material as defined in equation 4.8.

For example:

By assuming the empirical values of E and h for the sub-layers in the six layer composite (SLC) e-textile are as defined in Table 4.1, then the optimised thicknesses for materials in the top layer can be obtained from equation 4.9b by:

$$t_5 = \sqrt{\frac{e_A - e_6}{1 - e_6}} \quad (4.10a)$$

$$t_6 = 1 - \sqrt{\frac{e_A - e_6}{1 - e_6}} \quad (4.10b)$$

So that:

$$h_5 = t_5 \times H_A \quad (4.11a)$$

$$h_6 = t_6 \times H_A \quad (4.11b)$$

Note: Equations 4.9 and 4.10 assume that the interconnect layer is the neutral axis and has a negligible thickness so that $h_4 \approx t_4 \approx 0$.

Setting $H_B = 105$ µm, then from (4.7a), $E_B = 2.76$ GPa.

Inserting H_B and E_B into (4.6), we get $H_A = 712$ µm.

Based on equation 4.8 and the inferences in 4.4.3, the elastic moduli of the top layer materials should be chosen close to the higher modulus material so as to reduce the optimised thicknesses of the top layer and e-textile. Here $E_A = 60$ MPa.

From equation (4.9b), we get $e_A = (E_A/E_5) = 0.6$; $e_6 = (E_6/E_5) = 0.028$.

Inserting e_A and e_6 into (4.11), we obtain $t_5 = 0.767$; $t_6 = 0.233$

So that $h_5 = 546$ µm and $h_6 = 166$ µm.

The calculated optimised thicknesses for other chosen values of E_A indicate that as the value of E_A increases, the optimised thickness value is reduced as shown in Table 4.3 when the E_A and H_A values are compared. The table compares the stiffness of a SLC e-textile before and after the optimisation of the elastic moduli and thicknesses of its bottom and top layer materials. The table is divided into three sections - the initial material property, the various elastic modulus only and thickness only variations of the e-textile. The elastic modulus only section shows the optimised elastic modulus values of composites 2-5 while the thickness only section shows the optimised thicknesses of composites 6-10. A comparison of the flexural stiffness values of the optimised composites using equation 4.12 shows the beam stiffness is always increased after a composite has been optimised.

Table 4.3: The normalized flexural stiffness (where width, $x = 1\mu m$) of a six-layer e-textile. The asterisked cells represent the parameter changed. In composites 1 and 3, the interconnect layer is still away at the neutral axis position.

	Bottom layer						Neutral axis		Top layer				Modular ratio			Total Thickness		Thickness ratio					Apparent Modulus		Beam Stiffness
	Substrate		Interface		Bottom adhesion		Interconnect		Top Adhesion		Encapsulation		Bottom Layers		Top Layer	Bottom Layer	Top layer	Bottom Layer			Top Layer		Bottom layer	Top Layer	
	E_1 (GPa)	h_1 (µm)	E_2 (MPa)	h_2 (µm)	E_3 (MPa)	h_3 (µm)	E_4 (GPa)	h_4 (µm)	E_5 (MPa)	h_5 (µm)	E_6 (MPa)	h_6 (µm)	e_2 ($\times 10^{-3}$)	e_3 ($\times 10^{-3}$)	e_6 ($\times 10^{-3}$)	H_B (µm)	H_A (µm)	t_1	t_2	t_3	t_5	t_6	E_B (GPa)	E_A (MPa)	EI µNm²
Initial Material Properties (Calculated Neutral Axis = 43µm)																									
1	3	75	2.8	15	100	15	3.25	5	100	15	2.8	15	0. 933	33.33	28	105	30	0.714	0.143	0.143	0.5	0.5	-	-	431
Elastic Modulus Variation Only																									
2	*3 $\times 10^{-3}$	75	2.8	15	100	15	3.25	5	100	15	2.8	15	933.3	33.33 $\times 10^{3}$	28	105	30	0.714	0.143	0.143	0.5	0.5	2.21×10^{-3}	27.1	0.25
3	3	75	*300 $\times 10^{3}$	15	100	15	3.25	5	100	15	2.8	15	100 $\times 10^{3}$	33.33	28	105	30	0.714	0.143	0.143	0.5	0.5	-	-	529
4	3	75	2.8	15	100	15	3.25	5	*150 $\times 10^{3}$	15	2.8	15	0. 933	33.33	0.02	105	30	0.714	0.143	0.143	0.5	0.5	2.76	37.5 $\times 10^{3}$	591
5	3	75	2.8	15	100	15	3.25	5	100	15	*50 $\times 10^{3}$	15	0. 933	33.33	500 $\times 10^{3}$	105	30	0.714	0.143	0.143	0.5	0.5	2.76	37.5 $\times 10^{3}$	816
Thickness Variation Only																									
6	3	75	2.8	15	100	15	3.25	5	100	15	2.8	*3300	0. 933	33.33	28	105	3315	0.714	0.143	0.143	0.005	0.995	2.76	2.77	34,423
7	3	75	2.8	15	100	15	3.25	5	100	*474	2.8	*1270	0. 933	33.33	28	180	1744	0.714	0.143	0.143	0.272	0.728	2.76	10	8823
8	3	75	2.8	15	100	15	3.25	5	100	*532	2.8	*475	0. 933	33.33	28	120	1007	0.714	0.143	0.143	0.528	0.472	2.76	30	6253
9	3	75	2.8	15	100	15	3.25	5	100	*546	2.8	*166	0. 933	33.33	28	120	712	0.714	0.143	0.143	0.767	0.233	2.76	60	6033
10	3	75	2.8	15	100	15	3.25	5	100	*550	2.8	15	0. 933	33.33	28	105	565	0.714	0.143	0.143	0.973	0.027	2.76	95.23	5981

$$EI = \frac{1}{12}\sum_{i=1}^{n} E_i x_i h_i^3 \qquad (4.12)$$

EI is the flexural stiffness and I is the moment of inertia of the e-textile which is a measure of its resistance to rotation about an axis.

For example, the normalised stiffness (i.e. when x = 1 µm) of the un-optimised composite 1 is 431 µNm² at a total thickness of 135 µm. Results from modifying only the elastic modulus of the bottom layer materials show about 90 % increase in the initial stiffness and this will require printable polymers of $E > 50$ GPa which is currently impractical because polymers only have elastic modulus defined within the range $E \leq 10$ GPa as shown in figure 4.10.

These results from the thickness modification of the composites indicate that although highly elastic materials like the encapsulation material, UV-IF-010, with E = 2.8 MPa are characteristically flexible, they require very high optimised thicknesses up to 3.3 mm for the NA engineering of an e-textile. This significantly increases the resultant stiffness and thickness of the e-textile. For example, the optimised encapsulation thickness in composite 6 (where $h_6 = 3300$ µm) increases the initial stiffness by almost 80 times and also increases the initial composite thickness by more than 25 times. This contrasts the results for composite 10 (where $h_5 = 550$ µm), whose the optimising encapsulation thickness increased the initial composite thickness and stiffness to only 5 and 14 times the initial values. This shows that stiff polymeric materials like the top adhesion, UV-IF-1 with E = 100 MPa are better; requiring lower optimising thickness that only reasonably increases the total e-textile stiffness and thickness as in composite 10, relative to high increase from using elastic polymers as in composite 6.

4.5.1 Stress optimization of an e-textile

The normal stress on the "i^{th}" layer in a multi-layer beam is given as:

$$\sigma_i = E_i \varepsilon_i = \frac{E_i\left(\sum_{j=1}^{i} h_j - \bar{y}\right)}{r} \qquad (4.13)$$

Where σ_i and ε_i are the normal stress and strain in the i^{th} layer, and "r" is the bending radius of the beam.

Table 4.4 gives the stress values across the layers of the differently optimised e-textile composites in Table 4.3 when bent at $r = 5$ mm. The resulting stress profiles are illustrated in figure 4.14. Since the neutral axis position is independent of the bending radius, r of a beam, as shown in equation 4.5, $r = 5$ mm bending radius was chosen for the modelling and the experiments based on the literature review. At this radius printed conductors on woven fabrics show significant response to bending stress [94]. The profiles in figure 4.14 depict zero stress on the interconnect layer for optimised composites 2 - 10 which contrasts with the bending stress of 1.21 MPa that it experienced in the un-optimised composite 1.

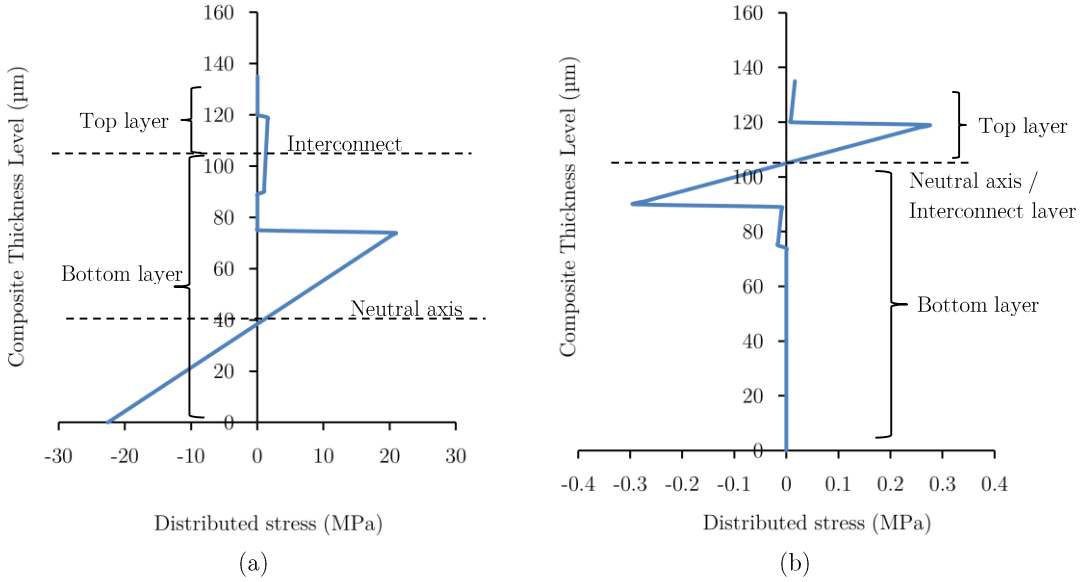

Figure 4.14: Stress distribution within (a) composite 1 (b) composite 2 due to $r = 5$ mm. The steps in the graph shows the transition between layers

The stress profiles also show the maximum stress that can be induced in the layers of the composite during bending which is important for:

i. Identifying and limiting potential locations of failures or cracks in the e-textile before fabrication.

ii. Estimating the maximum bending radius that an e-textile can survive.

Table 4:4: Minimum and maximum stresses across the layers of different e-textiles at a bending radius of 5 mm. The interconnect layer/ neutral axis, layer 4 has been omitted since it has zero stress. The negative sign show compressive stresses while asterisked *cells have inputted units and values*.

E-textile Composites	Layer 1 Kapton Substrate			Layer 2 UV – IF - 010			Layer 3 UV – IF - 1			Layer 5 UV – IF - 010			Layer 6 Polyurethane (39)		
	Min. (MPa)	Max (MPa)	UTS (MPa)	Min. (kPa)	Max. (kPa)	UTS (MPa)	Min. (kPa)	Max. (MPa)	UTS (MPa)	Min. (MPa)	Max. (MPa)	UTS (MPa)	Min. (kPa)	Max. (kPa)	UTS (MPa)
Stresses at bending radius of 5 mm															
1	-29	22.6	236	-27.7	-20.1		-10^3	-1.3		-1.3	-1.6		-44.8	-53.0	
2	18.2 (pPa)	61.7 (pPa)	-	8.8	16.5	25	19.6	0.29		-0.27	0	64	-16.5	-8.2	
3	3.8	47.2		- 5.1 $\times 10^5$	3.2 $\times 10^5$	-	-0.46 $\times 10^5$	-0.2		-0.76	-0.48		-29.9	-21.7	25
4										-40.3	8.8	-	-16.3	-8.1	
5	18.4	61.9		8.9	16.6		25.5	0.30		-0.27	0.006	64	-291 $\times 10^3$	-144 $\times 10^3$	-
6			236			25			64	-0.29			-1820	-8.8	
7										-9.3			-957	-261	
8	17.6	61.7		8.2	15.9		*265 pPa	0.27		-10.4	-19.6	64	-552	-292	25
9										-10.7	$\times 10^{-3}$		-391	-300	
10										-10.8			-310	-302	
Stresses at bending radius of 1.3 mm and 1.2 mm respectively															
10	64.1	224		29.9	57.8		*965 pPa	1.0		-39.1	-0.07		-1098	-1126	
10	69	241	236	32.2	62.2	25	*1 nPa	1.1	64	-42.1	-0.08	64	-1212	-1182	25

Also, the maximum induced stress in any layer is shown to increase as the layer thickness increases and as the bending radius of the composite reduces as shown by the stress values in Table 4.4. This prohibits the use (i.e. screen printing) of thicknesses or bending radii that make the maximum bending stress in any layer greater than its ultimate tensile strength/stress (UTS), i.e. the maximum stress it can withstand.

$$UTS = \frac{F_{\max}}{A} \tag{4.14}$$

Where F_{max} and A are the maximum force at breaking point and the initial cross sectional area of the material respectively. It should be noted that equation 4.14 gives the engineering stress on the material which is only an exaggerated measure of the true stress on the beam. To calculate the true stress, the final cross sectional area of the beam at the point of failure will be required and this can often be difficult to obtain [141].

Since composite 10 showed the lowest flexural stiffness, the minimum bending radius it could survive was investigated. Theoretically it can survive up to $r = 1.3$ mm below which the induced stress in the Kapton substrate, 241 MPa at $r = 1.2$ mm will become greater than its UTS value of 236 MPa which was obtained from its tensile test using equation 4.14.

4.5.2 Quantifying the strain in an e-textile due to bending stress

The strain induced in any layer from a bending stress can be estimated by exploiting the piezo-resistive properties of strain gauges which enable them to change their electrical resistances upon an applied strain. Strain gauges can be empirically useful for locating the neutral axis of an e-textile.

The relationship between the applied strain, ε and the change in electrical resistance, ΔR of the gauge is given by:

$$GF = \frac{\Delta R/R}{\varepsilon} \tag{4.15}$$

Where GF is the gauge factor which is a measure of the sensitivity of the transducer to an applied strain.

4.6 Experimental validation of the beam theory model on Kapton and textile

To empirically verify the beam theory model results, piezoresistive strain gauges were screen printed on Kapton and Bari, a polyester cotton fabric, substrates of the same dimensions: 150 mm x 150 mm which was chosen to fit the size of sub-holder of DEK 248 semi-automatic screen printer, shown in section 3.2.

In figure 4.15, each substrate is shown to contain three pairs of twin strain gauges, SG-1, SG-2 and SG-3 whose dimensions are 5.1 cm x 2.6 cm, 6.6 cm x 6.2 cm and 5.5 cm x 2.0 cm respectively. The gauges were meandered to maximise the gauge length and therefore change in resistance. The resistance change, ΔR of the gauges during bending at a radius of 5 mm were measured to locate the NA. At the NA, $\Delta R = 0$ but during tension and compression $\Delta R > 0$ and $\Delta R < 0$ respectively.

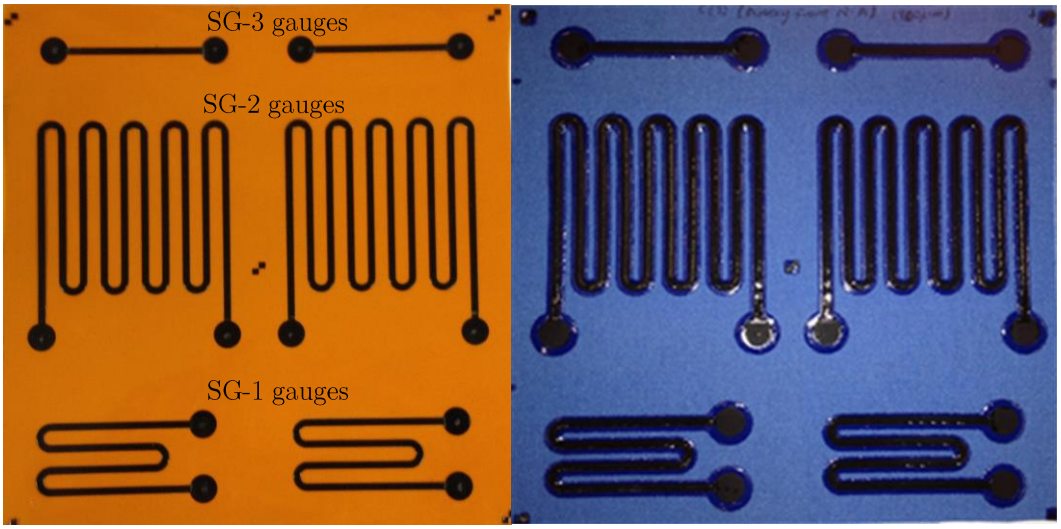

Figure 4.15: Screen printed strain gauges on Kapton (left) and Bari fabric (right)

4.6.1 Fabrication process

The composites on the Bari fabric were fabricated following the printing process described in figure 3.9. However in this case, the silver paste is replaced with a piezoresistive paste, Fabink-TC-PolyPR1. For the Kapton composites, the Fabink-TC-PolyPR1 ink was screen printed directly on the Kapton substrate. For both substrates i.e. Bari and Kapton, an average gauge thickness of 5 µm was achieved after oven curing of the ink for 5 minutes at 100 °C.

Some of the gauges were encapsulated with the Fabink UV-IF-1 paste and others, the UV-IF-010 ink which has a lower elastic modulus compared to the UV-IF-1 as shown in Table 4.1. This was done to differentiate how these inks influence the mechanical and electrical performances of the encapsulated gauges. In this case, the encapsulation does not only protect the strain gauge but it also enables the positioning of the gauge on the NA of the composite. The different thicknesses of encapsulation printed on Kapton and Bari are shown in Table 4.5.

Table 4.5: Thickness distribution of e-textile composites of Kapton and Bari fabric

Layer	Material	Average thickness (µm)					
		Tile 1	Tile 2	Tile 3	Tile 4	Tile 5	Tile 6
Substrate	Kapton	75					
Interface	UV-IF-010	-	-	-	-	-	-
Bottom adhesion	UV-IF-1	-	-	-	-	-	-
Strain gauge	Fabink-TC-PolyPR1	5					
Top adhesion	UV-IF-1	-	18	100	200	560	-
Encapsulation	UV-IF-010	-	-	-	-	-	595
Total thickness		80	98	180	280	640	675
Substrate	Bari fabric	324					
Interface	UV-IF-010	-	-	-	-	-	-
Bottom adhesion	UV-IF-1	109					
Strain gauge	Fabink-TC-PolyPR1	5					
Top adhesion	UV-IF-1	40	100	200	400	600	800
Encapsulation	UV-IF-010	-	-	-	-	-	-
Total thickness		478	538	638	838	1038	1238

4.6.2 Device testing and analysis of results

The gauges were bent in negative and positive bending orientations as shown in figure 4.16 to also ascertain if the elastic characteristics of the composite in both orientations are the same.

Figure 4.16: Negative bending (left) and positive bending (right) orientations of the strain gauges

Figure 4.17 shows that on Kapton, the gauge is closest to the NA in the composite with UV-IF-1 encapsulation thickness, $H_T = 560$ µm during negative bending since the smallest resistance change of $\Delta R \approx 2\%$ in both SG-1 and SG-2 gauges occurred at this thickness. This does not correlate with the $H_T = 411$ µm predicted by the model having used the values $E_T = 100$ MPa, $E_B = 3$ GPa and $H_B = 75$ µm in equation 4.6.

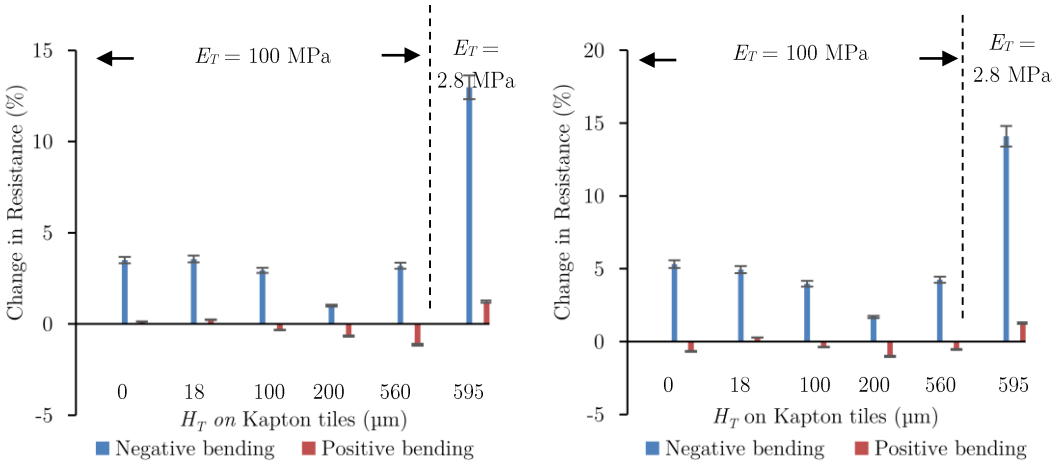

Figure 4.17: In-bending resistance changes of (a) SG -1 and (b) SG-2 strain gauges on Kapton tiles at a bending radius of 5 mm in negative and positive bending. Two samples were averaged for each result.

This inconsistency in the empirical and theoretical H_T values most likely ensues from a change in the values of the elastic moduli of the printed polymers due to changes in the ambient temperature during the fabrication process and possibly during testing. Changes in ambient temperature have been shown to affect the elastic modulus of materials and for polymers; the elastic modulus can increase significantly by a factor of 10^3 for a temperature change of up to 30 °C [149]. This is equivalent to a factor of 33.33 for every 3 °C change in temperature which perhaps explains the high error margins in the elastic modulus values of the UV-IF-1 and UV-IF-010 pastes obtained from the tensile test as 100 ± 30 MPa and 2.8 ± 1 MPa respectively. Also during the fabrication process, these pastes were put through a 100 °C heat for 5 minutes to cure the strain gauges and also 14 cycles of 30 seconds UV heating for curing the polymers. These were unaccounted for in the preliminary tensile testing of the pastes. Hence by using the lower modulus $E_T = 70$ MPa, the theoretical $H_T = 525$ µm which is reasonably consistent with the experiment.

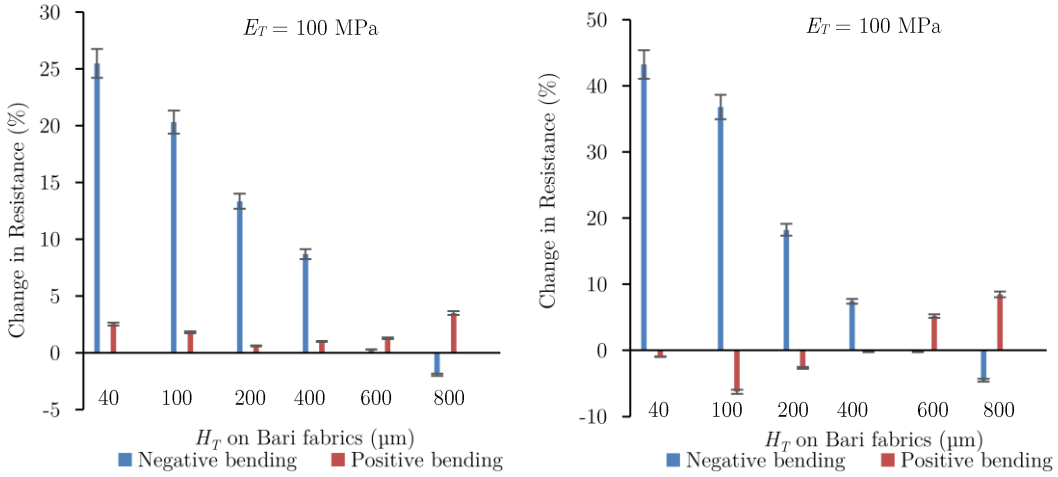

Figure 4.18: In-bending resistance changes of (a) SG -1 and (b) SG-2 strain gauges on Bari fabrics at a bending radius of 5 mm in negative and positive bending. Two samples were averaged for each result.

Nonetheless, figure 4.17 clearly agrees with the model that the use of stiff encapsulations rather very elastic encapsulations minimise the thickness that is required to engineer interconnects on the NA of composites. This is indicated by the smaller $\boldsymbol{\Delta R}$ in both positive and negative bending in the strain gauge with the UV-IF-1 encapsulation, $H_T = 560$ µm than the gauge with UV-IF-010 encapsulation despite its comparable thickness $H_T = 595$ µm.

For the composites on fabric, the model estimated an $H_T = 840$ µm given that the elastic modulus of the fabric is 400 MPa; but in practice $H_T \approx 600$ µm as shown in figure 4.18. With the lower and upper elastic modulus values of UV-IF-1 i.e. $E_T =$ 70 MPa and $E_T =$130 MPa, $H_T = 740$ µm and 1000 µm respectively and these are still very inconsistent with the experiment. The inconsistency is attributed to the following:

i. Fabrics are stiff in tension but very compliant in compression. Therefore there is vast difference between their tensile and compressive elastic properties [130]. This makes the use of the tensile modulus of the fabric in the mathematical model insufficient to characterise its elastic behaviour.

ii. The interface material alters the elastic properties of the fabric because the sinking of the interface paste into the fabric limits the movement of the loosely interlocked yarns of the fabric.

Finally, the results also show that the NA is different for negative and positive bending. This indicates that the elastic properties of the e-textile changes with its bending orientation and must be considered in the subsequent mathematical model.

4.7 Conclusions

The NA of a screen printed e-textile is initially located within its textile substrate away from the interconnect layer which must be printed on the surface the textile. The results show that the NA is best engineered into the interconnect position by increasing the elastic modulus or thickness of the encapsulating layers that are directly printed above it. This ensures that the stiffness or thickness of the e-textile is significantly increased respectively.

The optimizing values for these parameters are impossible to calculate from the generic NA equation based on beam theory because it does account for the different elastic properties exhibited by fabrics in tension and compression respectively. This therefore necessitates the need for characterising the bending properties of fabric in e-textiles to improve the model. This forms the discussion of chapter 5.

CHAPTER 5
IMPLICATIONS OF THE BENDING BEHAVIOUR OF WOVEN FABRICS FOR SCREEN PRINTED INTERCONNECTIONS

5.1 Introduction

This chapter aims to correlate results from the NA equation in equation 4.5 with empirical results by integrating the bending properties of woven fabrics obtained from Pierce's cantilever bending theory of fabrics into the beam theory model. An analytical model for the bending characteristics of fabrics is initially developed to obtain the parameter that differentiates the bending from the beams assumed in equation 4.5. This parameter, called the asymmetric factor, is derived for four different fabrics from Pierce's cantilever test. The investigated fabrics are Bari (see appendix A), Polyester, Escalade (see appendix C) and Lagonda (see appendix D). These were selected for their use as industrial work wears and apparel garments. The asymmetric factors of these fabrics are inserted into the analytical model to obtain an integrated model for calculating their NA positions. The resulting NAs are empirically verified on composites of these fabrics each consisting of a woven fabric substrate, a thermoplastic polyurethane (TPU) interface layer, the gauge and TPU encapsulation layers depicted in figure 5.1. The NAs are ascertained by subjecting the composites to the same test conditions described in section 4.6. Also, the effect of the interface layer on the elastic characteristics of the fabrics, and on

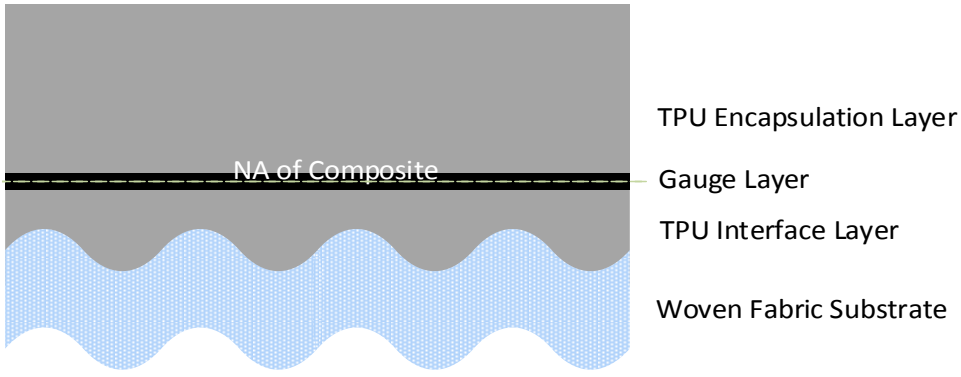

Figure 5.1: Assembly of a four layer textile composite

the correlation between the theoretically and empirically obtained NA positions are investigated.

5.2 Modelling the bending of woven fabrics

In symmetric beams the NA naturally coincides with the central axis due to equal tensile and compressive modulus values. In fabrics these values are unequal [110]. In pure bending, the tensile and compressive moduli of the fabric illustrated in figure 5.2 are defined as E_T and E_C respectively. If this modular difference shifts the NA i.e. plane EF from the central axis, GH of the fabric by a distance δ, then the bending strain, ε on any arbitrary plane AB of elemental dA in the bent fabric is given by [138]:

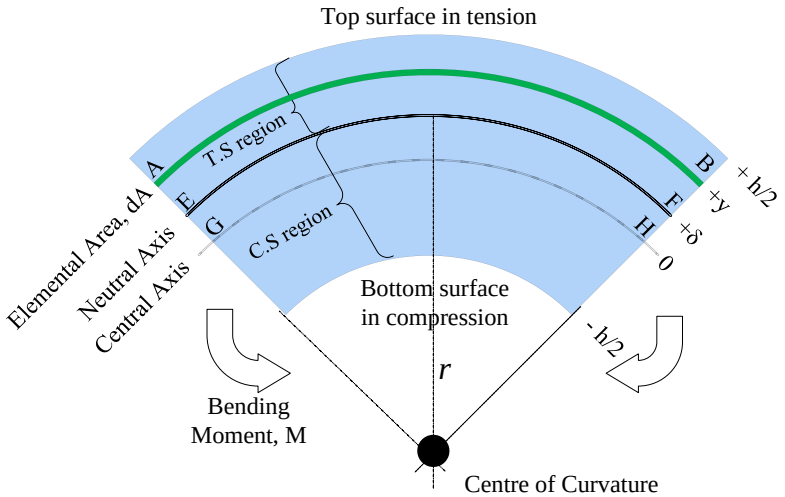

Figure. 5.2: Deformation of a fabric under pure negative bending moments. T.S and C.S regions are the tensile and compressive stress regions respectively.

$$\varepsilon = \frac{\textit{change in length of plane } AB}{\textit{undeformed length of plane } AB} = \frac{(r+y-\delta)\theta - r\theta}{r\theta}$$

$$\varepsilon = \frac{y-\delta}{r} \tag{5.1}$$

Where r and $r+(y-\delta)$ are the radius of curvature of planes EF and AB relative to the centre of curvature respectively.

The bending stress is obtained from elastic modulus, E in (tension or compression) of the fabric by:

$$\sigma = \frac{dF}{dA} = E\varepsilon = \frac{E(y-\delta)}{r} \tag{5.2}$$

As the beam attains force equilibrium across its entire area, the force becomes zero:

$$F = \int_{-\frac{h}{2}}^{\delta} E_C\left(\frac{y-\delta}{r}\right)xdA + \int_{\delta}^{\frac{h}{2}} E_T\left(\frac{y-\delta}{r}\right)xdA = 0 \tag{5.3}$$

To enable the calculation of the position and distance of the NA from the central axis of the fabric using equation 5.3, the following are initially defined:

$$k = \frac{1-\beta}{1+\beta} \quad ; \quad \beta = \frac{E_C}{E_T} \quad \Leftrightarrow \quad E_C \le E_T \tag{5.4}$$

Where "k" and "β" are the relative modular difference (i.e. the normalised difference between tensile and compressive modulus values of the fabric) and the bi-modular ratio of the fabric. These will also be used to:

i. Differentiate the bending characteristics of fabrics from that of its symmetric equivalent which was assumed in equation 4.5.
ii. Show how the modular difference affects the NA positions of the fabric and its composite.

By inserting equation 5.4 into equation 5.3, the distance δ of the NA from the central axis is given in equation 5.5 [130]. It is important to note that equation 5.5 is only a scalar description of "δ" and it is therefore insufficient for locating the exact position of the NA because it presupposes that the NA and the elemental area, dA are located above the central axis of the fabric. If this is changed such that the NA and dA are now located below the central axis in figure 5.2, then equation 5.5 becomes equation 5.6.

$$\delta = n\left(\frac{h}{2}\right) \quad ; \quad n = \frac{1-\sqrt{\beta}}{1+\sqrt{\beta}} \tag{5.5}$$

$$\delta = -n\left(\frac{h}{2}\right) \tag{5.6}$$

Where "n" is the fractional change in the NA from its initial central axis position and "h" is the thickness of the fabric.

By substituting equation 5.4 into equation 5.5, the relationship between "n" and the relative modular difference, k in the fabric is derived as:

$$k = \frac{2n}{n^2+1} \quad \Leftrightarrow \quad 0 \le k \le 1\,;\, 0 \le n \le 1 \tag{5.7}$$

A plot of equation 5.7 shown in figure 5.3 indicates that as the modular difference of a fabric increases, the fractional change, n in its NA position also increases and introduces a degree of asymmetry in the fabric about its central axis. This asymmetry is indicated by the k-value of the fabric which ranges from the completely symmetric, $k = 0$ to the completely asymmetric value, $k = 1$. This elastic asymmetry contrasts the bending behaviour of the fabric from that of a symmetric equivalent by reducing the bending rigidity, G (a parameter that describes the compliance of fabrics to bending loads) as shown below in the bending moment equation of the fabric [138]:

$$M = \int_{-\frac{h}{2}}^{\delta} yE_C\left(\frac{y-\delta}{r}\right)xdA + \int_{\delta}^{\frac{h}{2}} yE_T\left(\frac{y-\delta}{r}\right)xdA = 0 \tag{5.8}$$

$$M = \frac{\eta E_T I}{r}\,;\, \eta = (1-n)^2 \tag{5.9}$$

$$G = \frac{\eta E_T I}{x}\,;\, I = \frac{xh^3}{12} \tag{5.10}$$

$$B = \eta E_T \tag{5.11}$$

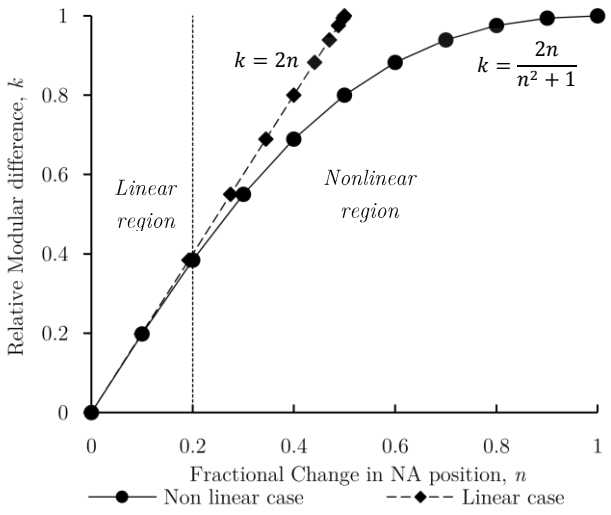

Figure 5.3. The effect of a relative modular difference, k of fabrics on the fractional change in the NA, n relative to the central axis of the fabric.

B is the bending modulus defined as the ability of the fabric to resist deformation under a bending load. η is the asymmetric factor which reduces the values of B and G in fabrics as shown in equations 5.10 and 5.11.

This explains why woven fabrics are readily compliant to bending in that the resistance of the fabrics to bending is moderated by η, a factor that has no effect in the symmetric case i.e. $\eta = 1$. The value of η is obtained from the Pierce's cantilever bending test of fabrics discussed below.

5.2.1 Pierce's bending theory of fabrics

Pierce's bending theory relates in equation 5.12, the deformation of a fabric to its bending rigidity per unit width, G as the fabric bends under its own weight in the cantilever bending test depicted in figure 5.4 [109].

$$G = WL^3\left(\frac{\cos(\theta/2)}{8\tan(\theta)}\right) \tag{5.12}$$

W, L and θ are the weight per unit area, overhang length and the bending angle of the fabric respectively.

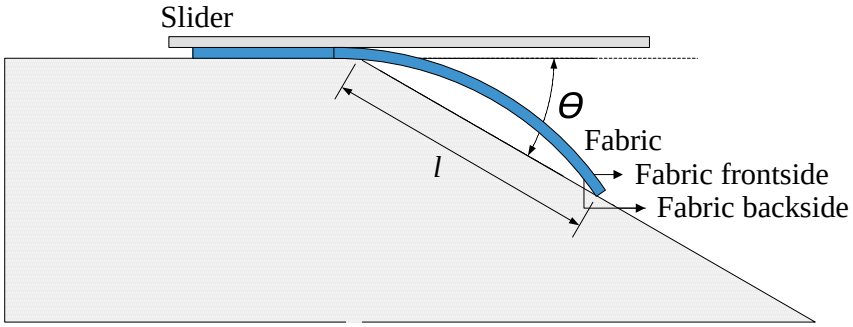

Figure 5.4. The Pierce cantilever test of a 75mm × 10mm specimen of Bari fabric inclined at 41.5° after being slid with an alumina plate on a horizontal platform

The bending angle, θ was set to 41.5° to replicate that used in a standard commercial tool, the Shirley tester, and also to reduce the effect of overhang length and too small or too large bending angle on the flexural rigidity of the fabrics [102].

Then 100 mm × 10 mm sized strips of the four examined fabrics were cut along their warp and weft weave directions. These were slid on a low-friction horizontal platform in the direction parallel to the long dimension of the strip. To obtain overhang lengths, the front-side and backside of the fabrics as shown in figure 5.4

Table 5.1: Physical Properties of fabrics

Fabric	Bari		Lagonda		Escalade		[1]Polyester	
Supplier	Klopman							
Thickness (µm)	324		290		400		60	
Twill	2 × 1		2 × 1		3 × 1		2 × 1	
Colour	Blue		Cream		Cream		White	
Percentage Blend, % (Polyester/Cotton/Lycra)	65 / 35 / 0		30 / 40 / 30		16 / 46 / 38		100 / 0 / 0	
Direction of Measurement	Warp / Weft		Warp		Weft		Warp	
Bending orientation	Neg.	Pos.	Neg.	Pos.	Neg.	Pos.	Neg.	Pos.
Tensile Modulus, E_T (MPa)	400		622		79		550	
[2] Weight (N/m^2)	2.0		2.1		2.1		3.0	
Overhang Length (m)	0.041	0.043	0.055	0.066	0.037	0.045	0.059	0.077
Compressive Modulus, E_C (MPa).	2.0	2.0	6.84	12.95	2.37	4.82	4.4	11
Bending Modulus, B (MPa)	6.4	7.6	22.82	39.2	6.87	12.4	15.4	34.1
[3] Bending rigidity, G (µNm)	18.2	21.0	46.2	79.8	14.0	25.3	81.4	180.9
Asymmetric factor, η	0.016	0.019	0.037	0.067	0.087	0.157	0.028	0.062
Fractional change in NA position, n	0.874	0.862	0.808	0.735	0.705	0.603	0.833	0.751

Direction of Measurement	Weft		Warp / Weft	
Bending orientation	Neg.	Pos.	Neg.	Pos.
Tensile Modulus, E_T (MPa)	102		617	
[2] Weight (N/m^2)	3.0		0.5	
Overhang Length (m)	0.05	0.059	0.033	0.035
Compressive Modulus, E_C (MPa).	3.26	5.92	55.53	70.34
Bending Modulus, B (MPa)	9.28	15.3	131.4	157.34
[3] Bending rigidity, G (µNm)	49.5	81.4	2.37	2.83
Asymmetric factor, η	0.091	0.150	0.213	0.255
Fractional change in NA position, n	0.698	0.613	0.538	0.495

[1] The cantilever test values were influenced by surface properties of the fabric. The electrostatic force between the substrate and the inclined plane caused the fabric to bend which is not necessarily under its own weight.

[2] Weight per unit area of test sample of size 10 cm × 1 cm used for Pierce Cantilever test

[3] Bending rigidity per unit width of test sample

were slid on the platform similar to how they would have been bent in a printed e-textile in positive and negative bending orientations respectively. The overhang lengths, L of the strips were measured as the fabrics touched the inclined plane after bending the fabric and were substituted into equation 5.12 to obtain the corresponding bending rigidities which are shown in Table 5.1.

The bending rigidity of the fabrics changes with the bending orientation and this can be inferred from equation 5.10 to mean that the asymmetric factor,η changes with bending direction of the fabric since all other parameters in the equation 5.10 are known constants.

By equating equations 5.10 and 5.12, the values of η corresponding to these bending rigidities are calculated from:

$$\eta = G\frac{x}{E_T I} \tag{5.12}$$

From these values of η, the bending and compressive modulus (B and E_C) values of the fabrics shown in Table 5.1 were calculated from equation 5.4 after the value of β - the bi-modular ratio of the fabrics was obtained from equations 5.5 and 5.9. These values are in the order of more than 10^2 MPa lower than the E_T values which clearly explains the compliance of the fabrics in bending.

5.2.2 Effect of the asymmetric factor on the NA of fabrics

The multiple asymmetric factors, η obtained from the cantilever bending test meant that the NA of each of the fabrics is at different distances, δ from the central axis depending on the bending orientation. The relationship between η and δ in figure 5.5 shows that as η increases, the NA moves closer to the central axis of the fabrics i.e. δ decreases. It also shows the different locations of the NA in negative and positive bending orientations of the fabrics.

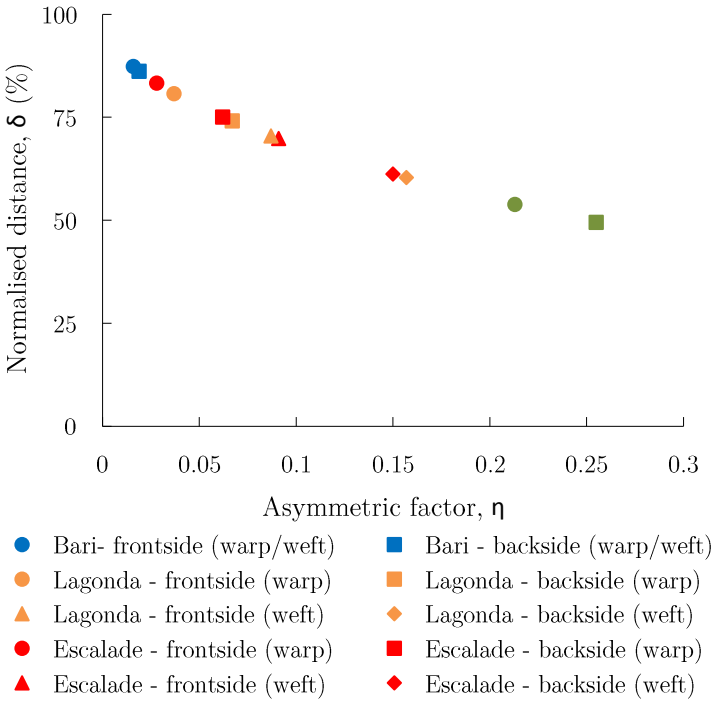

Figure 5.5: Relationship between the asymmetric factor, η and the normalised NA distance, δ from the central plane using measured bending factors of all fabrics. The top and back sides denote negative and positive bending respectively.

For the fabrics, Bari and Polyester, that have equal elastic modulus along their warp and weft weave directions, only two bending-oriented NAs are noticed and these are unaffected by the weave direction along in which the fabrics are bent. When the warp and weft elastic modulus values are unequal, the fabrics have four bending-oriented NAs which is the case with Lagonda and Escalade. These fabrics contain Lycra in their weft weave, an elastic material that makes the weft more stretchable than the warp which is polyester cotton [150]. Hence the pair of bending oriented NAs from negative and positive bending along the warp direction are different from those along the weft direction.

Since distance, δ is only a scalar variable, it is necessary to define the tensile and compressive regions of the fabrics so as to pinpoint the position of the NA in any bending orientation. This is because the boundary between these regions is the NA. In positive bending, the fabric bends inwards as in figure 5.6. The resulting compression in the fabric largely characterises its bending which results in a larger compressive region. This is represented by shifting the NA below the central axis by the distance, δ, as shown in figure 5.6. Conversely in negative bending, the region of tensile stress is larger. Now, the NA positions due to η are calculated and

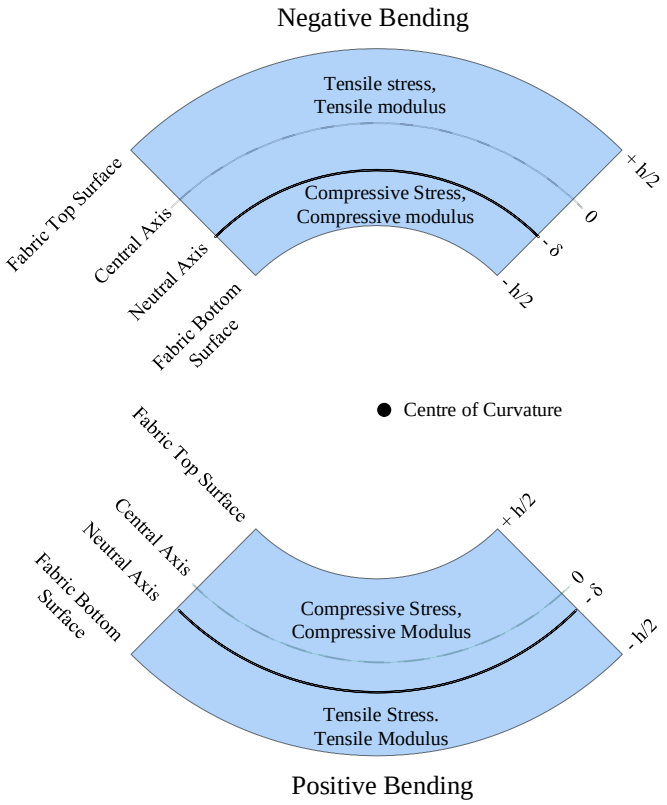

Figure 5.6: NA positions of a fabric in negative and positive bending.

contrasted with the central axes of the fabrics (i.e. the NA in the symmetric case) in Table 5.2.

Table 5.2: NA positions of investigated fabrics

Fabrics	Central Axis (Warp/Weft) µm	Asymmetric NA (µm)			
		Warp direction		Weft direction	
		Negative bending	Positive bending	Negative bending	Positive bending
Bari	162	20.4	22.4	20.4	22.4
Polyester	30	13.9	15.2	13.9	15.2
Lagonda	145	27.8	38.4	42.8	57.6
Escalade	200	33.4	49.8	60.4	77.4

5.2.3 Effect of fabric asymmetry on the NA of screen printed e-textiles

The asymmetry in fabrics is accounted for in the generic NA equation 4.5 by modelling the fabric as a two-layer material. The four layer e-textile in figure 5.1 is now treated as a five layer structure as shown in figure 5.7.

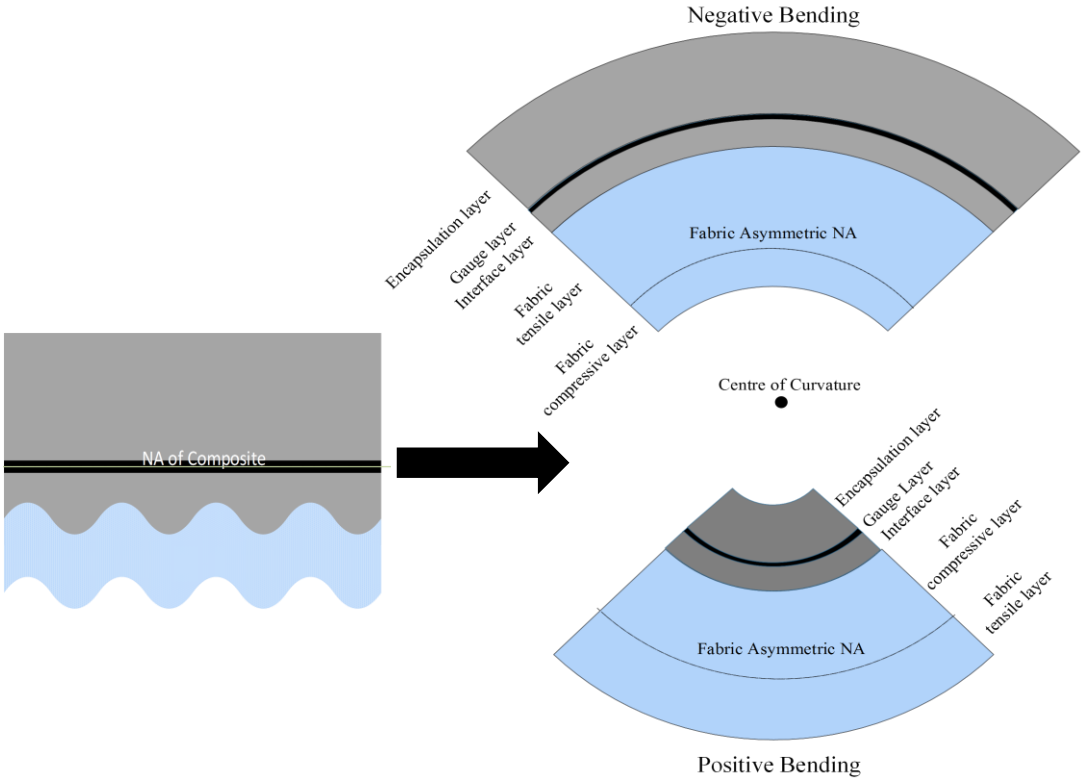

Figure 5.7: The five layer equivalent (right) of a four layer e-textile (left) in negative and positive bending orientations due to the asymmetry of fabrics.

The two fabric layers are its compressive and tensile regions of which the elastic properties are characterised by the compressive and tensile modulus values of the fabric respectively. The bottom fabric layer has a thickness equivalent to the asymmetric NAs shown in Table 5.2 at the given bending orientations.

5.2.3.1 Calculating the NA of the screen printed e-textile composites

The NA of screen printed e-textile composites can be pre-set to the position of the printed conductor with an optimised thickness of encapsulation. For the composites examined in this work, the optimised encapsulation thicknesses, h_T that were calculated from equation 4.5 are shown in Table 5.3. These results show that the different optimised encapsulations thicknesses for negative and positive bending orientations in the asymmetric case are unlike the symmetric case where they are equal. Also apparent is the lower asymmetric encapsulation requirement in positive bending than in negative bending. This is because the fabric offers little bending resistance in positive bending since it is largely characterised by the low compressive modulus of the fabric. Also since its NA is closer to the position of the conductor than in negative bending as illustrated in figure 5.7, a smaller h_T is needed to shift the NA from within the fabric to the conductor's position.

Table 5.3: Symmetric and Asymmetric encapsulation thickness for the FLC structures on all fabrics

Fabric	Bari		Polyester		Lagonda				Escalade			
Fabric Weave	Warp/Weft		Warp/Weft		Warp		Weft		Warp		Weft	
Bending Orientation	Neg.	Pos.	Neg.	Pos.	Neg.	Pos.	Neg.	Pos.	Neg.	Pos.	Neg.	Pos.
Pre-set Neutral Axis (µm)	433		169		399				509			
Symmetric Encapsulation value h_T (µm)	840		335		960		353		1165		510	
Asymmetric Encapsulation value, h_T (µm)	799	292	295	217	886	450	315	220	1090	542	450	305
Rough estimate of empirical encapsulation (µm)	600	400	400	300	1000	600	1000	300	1000	600	1000	400

5.3 Experimental validation of the optimised encapsulation thicknesses from the integrated model

The asymmetric NAs in Table 5.3 were verified following the same fabrication process and bending test conditions for the Bari fabric described in sections 4.6.1 and 4.62 respectively. In this case however, the strain gauges were also printed aligned with the warp and weft weave of the fabrics to demonstrate the effect of the elastic property of the fabric on the NA. The encapsulation thickness, h_T printed on the gauge was varied between 100 µm and 800 µm on each fabric. A cross-section of the complete four layer composite (FLC) structure is shown in figure 5.8.

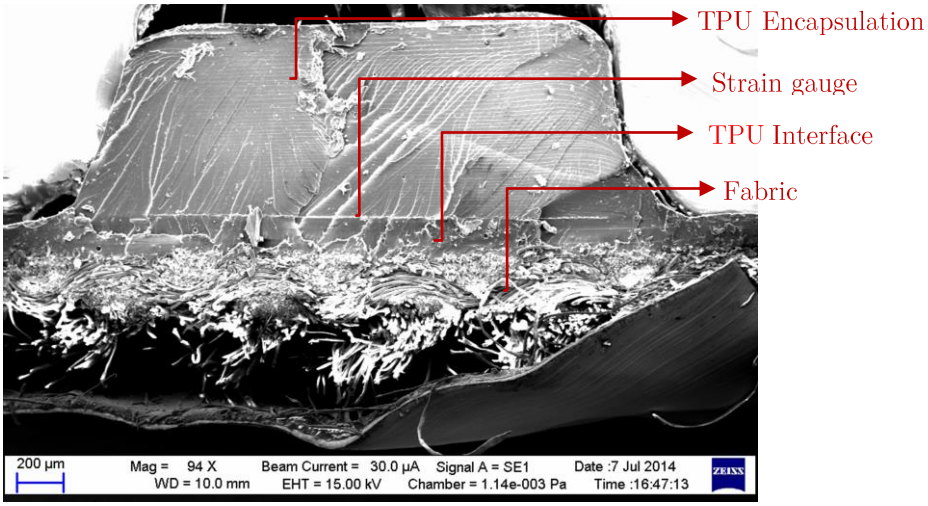

Figure 5.8: A SEM cross section of a strain gauge sandwiched between two TPU layers on Bari fabric

5.3.1 Device testing and results

The composites were bent around a 5 mm radius rod in negative and positive bending orientations as in section 4.6.2. The results validate the possible number of NA positions in the fabric composites indicated in figure 5.5. It also affirms that the NA of the composites change when their bending orientation and the elastic characteristics change.

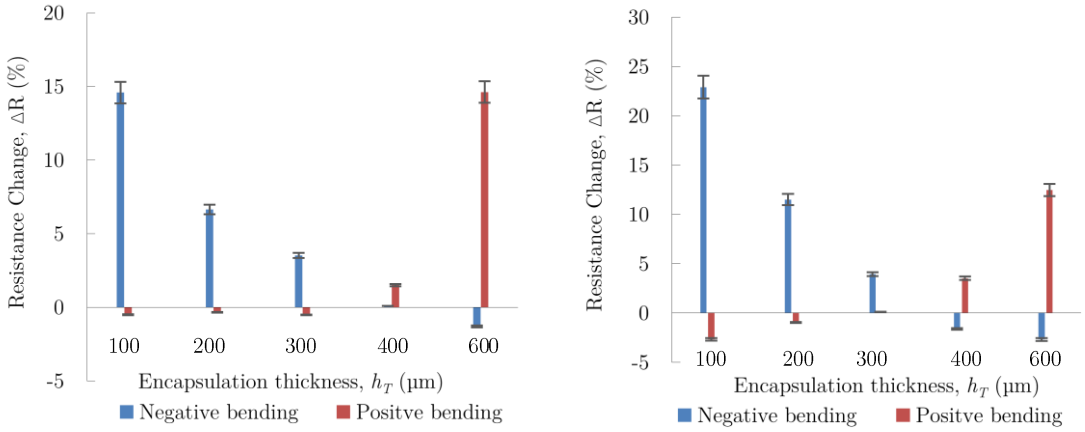

Figure 5.9: In-bending responses of SG-1 (left) and SG-2 (right) strain gauges printed in FLC structures of Polyester fabric during one bending cycle.

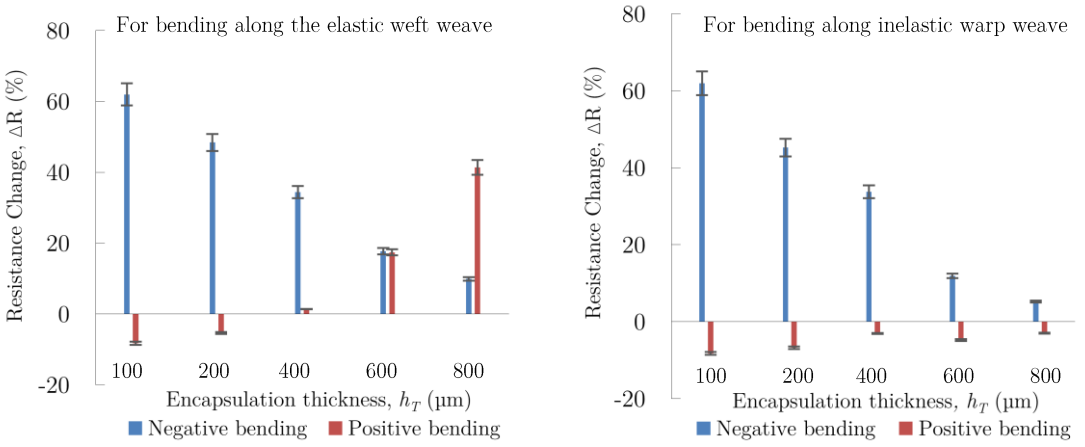

(a) Lagonda composites

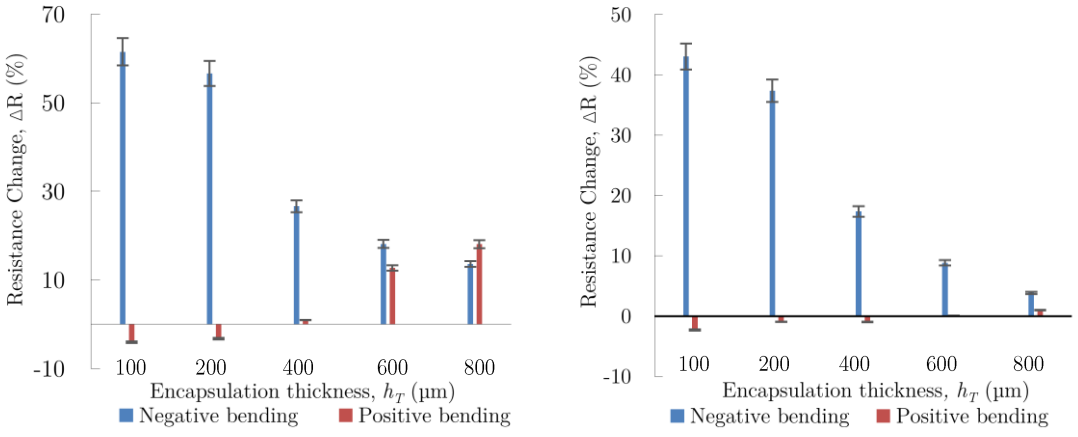

(b) Escalade composites

Figure 5.10: The in-bending responses of SG-1 and SG-2 strain gauges printed in FLC structures of Lagonda and Escalade fabrics along their elastic weft and inelastic warp weave during one bending cycle.

This is corroborated by the two bending-oriented NAs (i.e. where $\Delta R \approx 0$) noticed in the Bari and Polyester fabric composites, each in positive and negative bending orientations as shown in figures 4.15 and 5.9.

Lagonda and Escalade composites fabrics have very distinct elastic moduli along the warp and weft weave so four NAs are seen as predicted in the integrated model. Each pair of NAs is seen during positive and negative bending along the warp and weft weave of the fabrics as shown in figure 5.10. Also, the empirical encapsulation thicknesses, h_T required to locate these NAs are comparable to the theoretical asymmetric thicknesses. For example, the NAs in the Bari composites were empirically located with $h_T \approx 400$ µm and $h_T \approx 600$ µm encapsulations during positive and negative bending respectively. These values show no correlation with the symmetric thickness of 840 µm.

While the empirical thicknesses are dissimilar to the asymmetric equivalents (292 µm and 799 µm), both sets of thicknesses agree that a smaller encapsulation is required to locate the NA in positive bending. This trend is consistent across all the fabrics except in the negative bending of the Lagonda and Escalade composites along their elastic weft directions. The bending test showed that both fabrics seemed to behave as though they were bent along their warp direction where the fabrics are stiffer. This anomaly primarily stems from the limiting effect of the interface layer on the bending dynamics of the fabrics. In woven fabrics, the warp and weft yarns are typically interlocked in a way that both yarns are still able to slide across each other, shear, stretch or contract about their woven position. With the interface, this movement becomes hindered because the interface layer impregnates the fabric during printing and in some cases rigidly bonds the yarns together and grips them to their initial woven position. Consequently, the fabric behaves like a bimetallic strip where the yarn with the higher elastic modulus (i.e. with lower expansion under stress) mainly influences the bending of the fabric just as with a bimetallic strip where the metal with the lower thermal coefficient determines the bending behaviour of the strip. This also explains why the asymmetric thicknesses are not close the empirical equivalents.

5.4 Effect of the interface on the elastic characteristics of the fabric

If the elastic modulus of the interface - impregnated fabric is approximated to the value when the fabric just contained a single layer of interface UV-IF-1, then the asymmetric thicknesses can be recalculated from equation 4.5 with new elastic modulus values. Table 5.4 shows the new tensile modulus of the four fabrics examined in this work. Due to the difficulty in obtaining the compressive modulus of the samples from the Tinius Olsen's benchtop tester, the new compressive moduli were chosen to fit the electrical resistance changes of the strain gauges.

The recalculated asymmetric encapsulation thicknesses of the composites based of the new tensile and compressive modulus values of the fabric are shown in Table 5.5.

Table 5.4: Elastic modulus of UV-IF-1 impregnated fabrics

Fabrics		Fabric + UV-IF-1 average thickness	Width	Gauge length	[1]Average tensile modulus, E_{TE} of impregnated fabric	[2]Approximate compressive modulus, E_C of impregnated fabric in	
						Negative bending	Positive bending
Bari		348 µm	1 cm	3.5 cm	220 ± 19 MPa	80 MPa	
Lagonda	Warp	365 µm	0.4 cm	3 cm	599 ± 29 MPa	90 MPa	
	Weft	350 µm			36 ± 2 MPa	90 MPa	20 MPa
Escalade	Warp	441 µm			443 ± 14 MPa	90 MPa	60 MPa
	Weft	434 µm			56 ± 3 MPa	90 MPa	52 MPa
Polyester		75 µm			615 ± 44 MPa	95 MPa	

[1]Fabric-interface modulus was averaged over four samples.

[2]Values were deduced from the electrical resistance changes of the strain gauges

Table 5.5: Asymmetric encapsulation thicknesses of the FLC structures due to the interface effect

Fabric	Bari		Polyester		Lagonda				Escalade			
Fabric Weave	Warp/Weft		Warp/Weft		Warp		Weft		Warp		Weft	
Bending Orientation	Neg.	Pos.	Neg.	Pos.	Neg.	Pos.	Neg.	Pos.	Neg.	Pos.	Neg.	Pos.
Previous asymmetric encapsulation thickness	799	292	295	217	886	450	315	220	1090	542	450	305
New asymmetric encapsulation value (µm)	605	418	295	217	852	525	280	245	980	580	406	373
Rough estimate of empirical Encapsulation, (µm)	600	400	400	300	1000	600	1000	300	1000	600	1000	400

To simultaneously verify these thicknesses and demonstrate the interface effect, the theoretically normalised distances of the strain gauges from the NA position were contrasted with the empirically obtained resistance changes as shown in figure 5.11.

Figure 5.11 shows that, when the interface effect is not modelled, the normalised distance, δ of the strain gauge from the NA of the composites will not correlate with the measured changes in its resistance ΔR during bending. For instance in the negative bending of the Bari composites, the minimum $\Delta R \approx$ - 0.3 % which should normally indicate the proximity of the gauge to the NA, is implying a separation of $\delta \approx 18$ % between the gauge and the NA. This disproportionality is corrected in the improved model by characterising the interface effect which then translates this resistance change to a distance, $\delta \approx 0.5$ % which reasonably reflects the measured change in resistance.

Similarly in positive bending, a $\Delta R \approx$ - 0.3 % in the gauge is also translated to $\delta \approx$ - 1.4 % and $\delta \approx 10$ % when modelled with and without the interface effect respectively. The new asymmetric encapsulation thicknesses for these bending orientations are 605 µm and 415 µm respectively. These values also correlate with the empirical $h_T \approx 600$ µm and $h_T \approx 400$ µm respectively shown in table 5.5. This is also consistent with results from the Lagonda and Escalade composites except during negative bending along the weft weave of the fabric. In Lagonda for example, the minimum $\Delta R \approx 10$ % is disproportionately translated to a large normalised distance of $\delta \approx$ - 35 % between the gauge and the NA. This happened because the composites behaved as though they were in bent along the inelastic warp weave of the fabrics as highlighted and explained in section 5.3. Consequently, the tensile and compressive moduli of the fabrics along the weft were replaced with their warp weave equivalents which correctly translated $\Delta R \approx 10$ % to a distance of $\delta \approx 4$ %. This was also the case for the Escalade composite.

The asymmetric thicknesses for Lagonda and Escalade during negative bending along the weft weave are 851 µm and 980 µm. These values are validated by the experiment since none of the gauges in both composites was positioned on the NA at the highest encapsulation thickness, $h_T = 800$ µm. The smaller $\Delta R \approx 10$ % (where $\delta \approx 4$ %) in the gauges in Lagonda at $h_T = 800$ µm compared to the $\Delta R \approx 14$ %

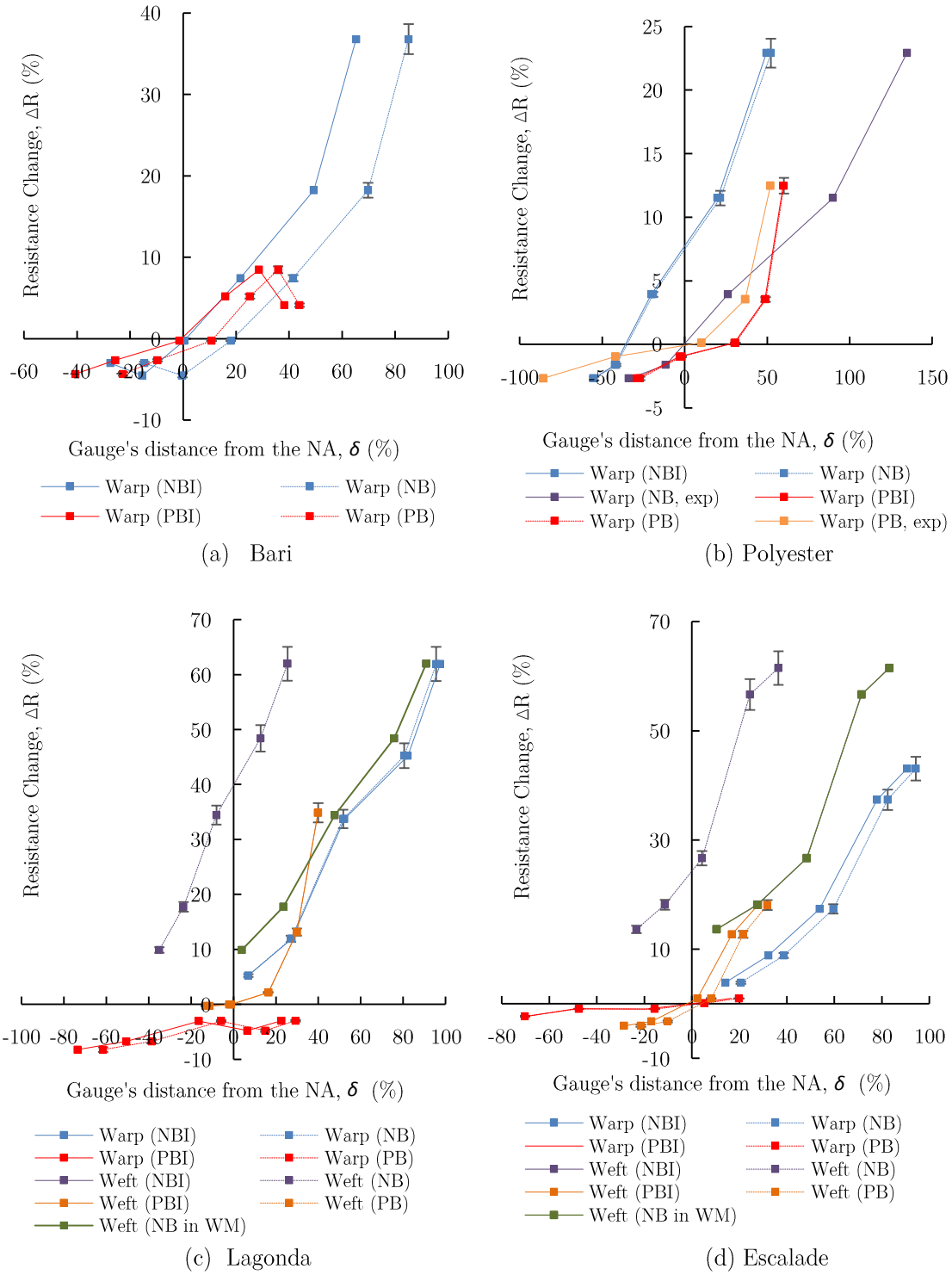

Figure 5.11: A comparison of the resistance changes of the strain gauge after one bending cycle its normalised distance from the NA of the composites. NB, PB, and NBI, PBI denote the negative and positive bending results before and after modelling the interface effect. The warp weave mode (WM) bending behaviour only occurs in the negative bending of Lagonda and Escalade fabrics along their weft weave. Also plots derived purely from experimental results are indicated in the Polyester fabrics as (exp).

(where $\delta \approx 10$ %) in Escalade also validate the higher encapsulation that is required for the escalade composite as was calculated.

The model however failed to characterise the bending behaviour of the polyester fabric composites. Empirical results indicate that the elastic property of the polyester fabric is different from the one obtained from the tensile test. By extrapolating these results, the tensile and compressive modulus values of the fabric were obtained as 2.25 GPa and 95 MPa respectively. These values, in particular the tensile modulus clearly contradicts the 617 MPa from the Tinius Olsen tensile tester and used to characterise the polyester fabric. This discrepancy emphasises the unusual bending characteristics of fabrics and the need for further characterization of the mechanical properties of fabrics.

5.4.1 Effect of the interface on the correlation between the theoretical and empirical strains on the gauges

The theoretical and empirical strains can be calculated from equations 4.13 and 4.15 respectively. Only the strains on Bari, Lagonda and Escalade composites will be discussed in this section due to the difficulty in characterising the Polyester fabric as indicated earlier in the concluding paragraph of section 5.4.

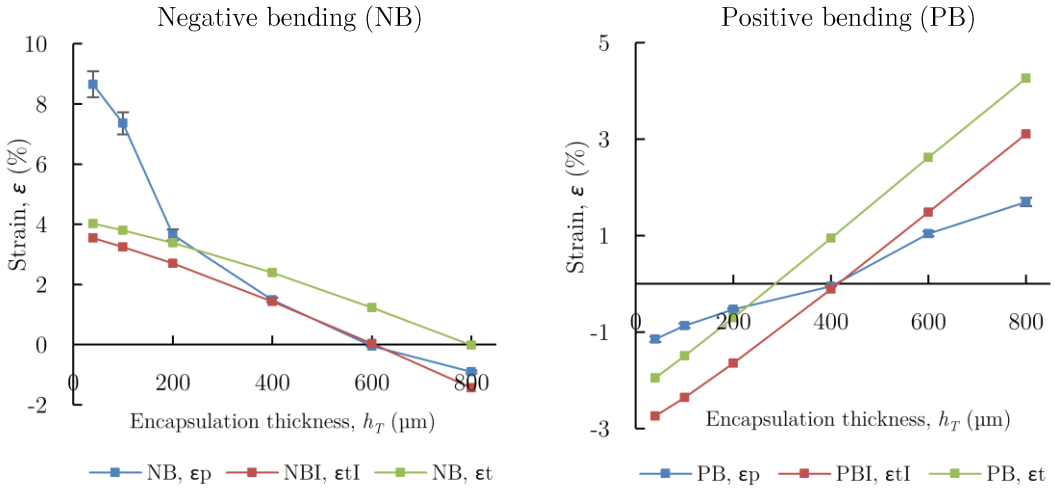

(a) (b)

Figure 5.12: Effect of the interface effect on the correlation of the empirical strain ε_P with the theoretical strains ε_t and ε_{tI} calculated before and after the interface effect characterisation on the SG 2 strain gauges in Bari composites. NB, PB, and NBI, PBI denote the negative and positive bending results before and after modelling the interface effect.

Figures 5.12, 5.13 and 5.14 contrast the empirical strain, ε_P with the theoretical strains, ε_t and ε_{tI} calculated before and after characterising the effect of the interface layer on the bending behaviour of the Bari, Lagonda and Escalade composites. The graphs show that theoretical strains calculated before the characterising the interface effect in all the composites do not correlate with the empirical strains in the gauge especially at the NA where all strains should be zero.

For example, a comparison of the strain values, $\varepsilon_t \approx 1.23$ %, $\varepsilon_{tI} \approx 0.04$ % and $\varepsilon_P \approx$ - 0.05 % at the NA of the Bari composite in negative bending i.e. where $h_T = 600$ µm in figure 5.12a, shows that ε_P better correlation with ε_{tI} than ε_t. The graph also

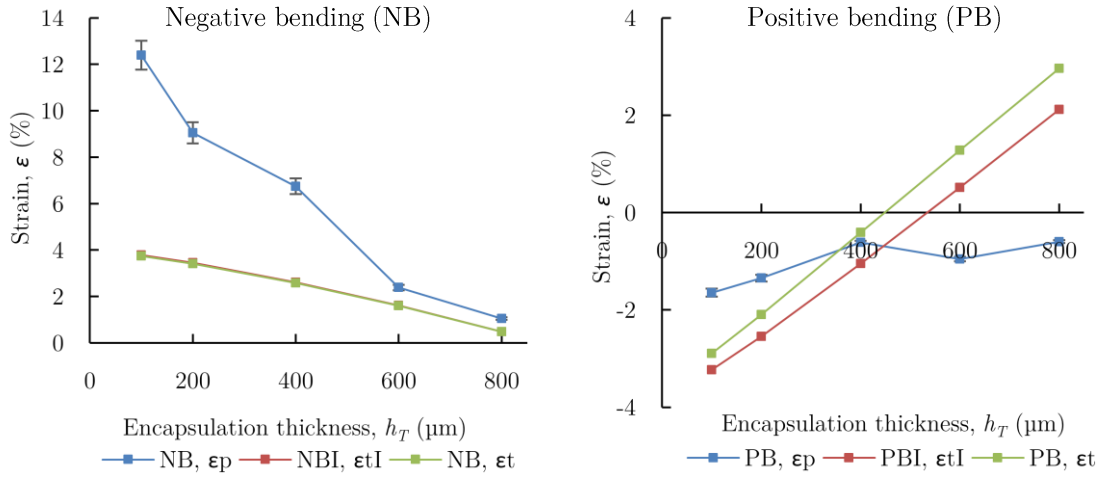

(a) Lagonda SG 1 strain gauges along the warp weave

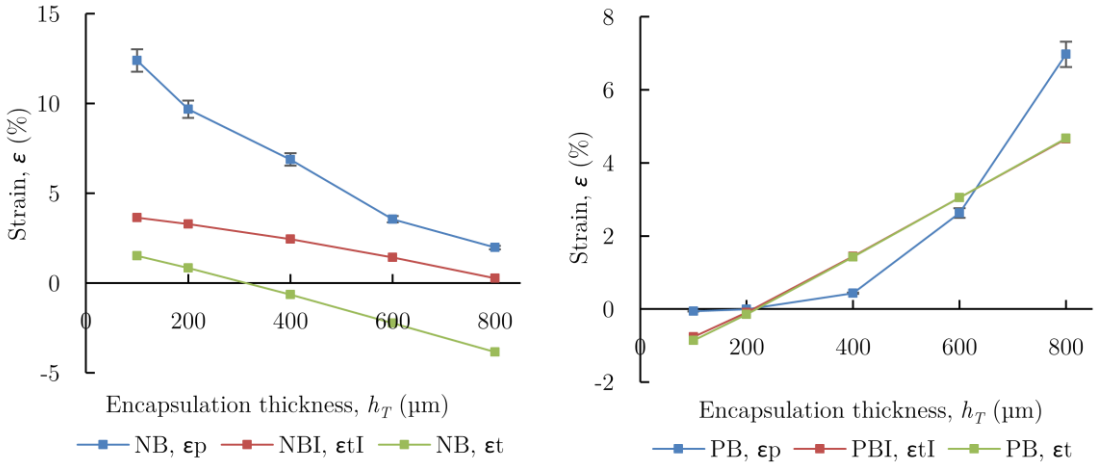

(b) Lagonda SG 2 strain gauges along the weft weave

Figure 5.13: Effect of the interface effect on the correlation of the empirical strain ε_P with the theoretical strains ε_t and ε_{tI} calculated before and after the interface effect characterisation on the SG 2 strain gauges in Lagonda composites. NB, PB, and NBI, PBI denote the negative and positive bending results before and after modelling the interface effect.

shows that model predicts the strains close to the NA better than those far from the NA. This is evidenced by the huge difference between the values of ε_P and ε_{tI} when $h_T < 200$ µm also in negative bending. This is because the position of the strain gauge varies across within the composite due to the non-uniformity of the printed thickness of the layer which is influenced by the uneven surface of the interface layer as shown in section 3.3.4. This is why the e average thicknesses were reported. This difference is also significant because the measurements are micro-strains. Although similar correlation is also observed in the positive bending of the

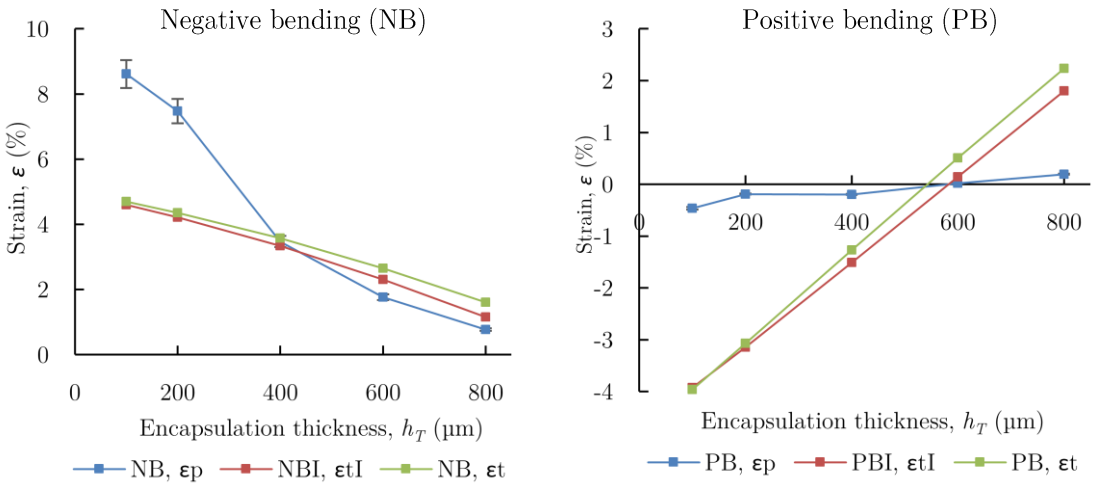

(a) Escalade SG 1 strain gauges along the warp weave

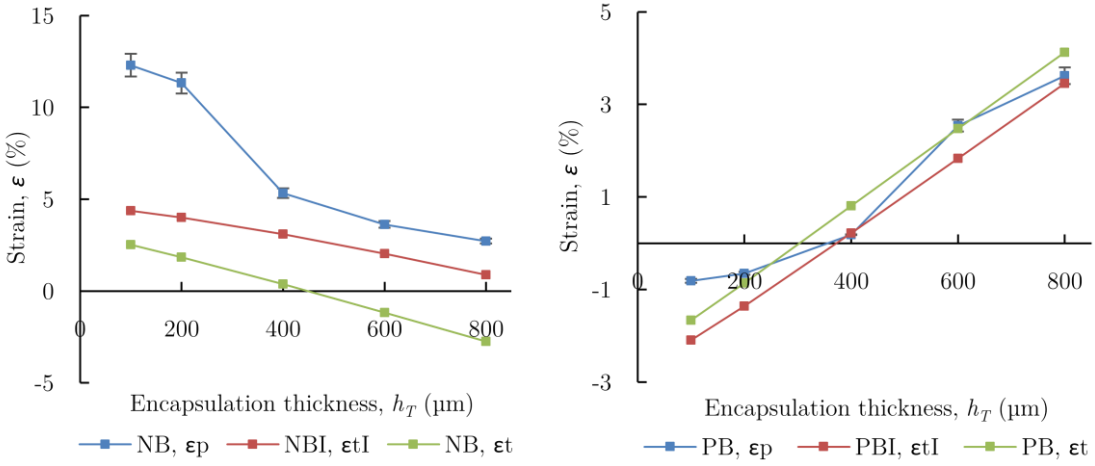

(b) Escalade SG 2 strain gauges along the weft weave

Figure 5.14: Effect of the interface effect on the correlation of the empirical strain ε_P with the theoretical strains ε_t and ε_{tI} calculated before and after the interface effect characterisation on the SG 2 strain gauges in Escalade composites. NB, PB, and NBI, PBI denote the negative and positive bending results before and after modelling the interface effect.

composites in figure 5.12b, the graph shows that the model predicts strains in negative bending better than positive bending. Like the Bari composites, the integrated model was also used to closely predict the strains on the gauges in Lagonda and Escalade fabrics as shown in figures 5.13 and 5.14 respectively.

5.5 Conclusions

The contrasting elastic properties of fabrics in tension and compression create an elastic asymmetry in the fabric. This asymmetry alters the bending characteristics of the fabric and changes its NA position whenever the bending orientation of the fabric changes. It is therefore essential to properly characterise this asymmetry when modelling the NA of a screen printed e-textile. To do this, the fabric must be modelled as a two layer material containing two sublayers that are bounded by the asymmetric NA of the fabric.

For screen printed e-textiles containing an interface layer, it is also necessary to characterise the effect of the interface on the fabric's elastic properties. This is because the fabric behaves like bimetallic strip after it's been impregnated by the interface. The stiffer yarn in the fabric now controls the bending of the fabric. This behaviour is approximately characterised by the elastic modulus of the fabric when it just contains a single layer of interface.

While this chapter achieved its goal of characterising and empirically validating the NA and the strains developed within the screen printed e-textiles described herein, the model developed in this chapter is still not exhaustive in its approach as was shown in the difficulty in characterising the Polyester fabric composite. Hence more characterisation of the mechanical properties of fabrics is still needed to enable a perfect model.

CHAPTER 6
DURABILITY OF SCREENPRINTED INTERCONNECTS ON WOVEN FABRICS

6.1 Introduction

The bending characteristics of screen printed e-textiles has been modelled in the previous chapter to theoretically determine the NA of the e-textiles. The optimised strain gauges positioned close to the theoretical NA demonstrated minimal changes of less than 0.1 % in their electrical resistances during bending. However the results do not show how the electrical performance of the optimised gauge is affected as it relaxes from bending.

This chapter examines the implications of this when screen printing e-textiles by investigating the post bending effects on these gauges. This is assessed by comparing the resistance changes and empirical strains on the gauge during and after bending. An examination of the effect of the bending orientation of the e-textile on the magnitude of the strains developed on the gauges. The effects of washing on the gauges are also be assessed to demonstrate their washability. Based on this, potential solutions to optimising electrical interconnects for better durability in positive and negative bending e-textile applications are proposed. The failure modes that could potentially arise from engineering electrical interconnects on the NA of an e-textile using encapsulations as thick as 700 µm are also discussed.

6.2 Experimental testing of the durability of e-textiles by bending and washing

The two composite structures investigated are the four layer composite (FLC) and six layer composite (SLC) structures. The impact of bending on the electrical performances of printed strain gauges and LED circuits are first assessed with the FLC structures before using the SLC Only the SLCs were used to examine the effect of washing on the sandwiched circuits. This is because it is more waterproof than the FLC. It used the Fabink-UV-IF-010 as the interface and encapsulation layers on the fabrics to improve the water resistance of the composite as discussed

in section 3.6.1.2. The poor adhesion of Fabink-UV-IF-010 to the Fabink-TC-PolyPR1 (piezo-resistive) and Electrodag PF-410 silver inks necessitated the use of Fabink-UV-IF-1 before and after the inks were printed. This improves the adhesion within the composite as reported in [95].

6.2.1 Fabrication process

The fabrication process for the FLC structures is as described in section 4.6.1. The printed thicknesses are also detailed in table 4.5 (page 95). For the SLC structures, the interface and encapsulation materials are replaced with UV-IF-010 while new adhesion layers of UV-IF-1 are introduced as shown in figure 6.1. An interface

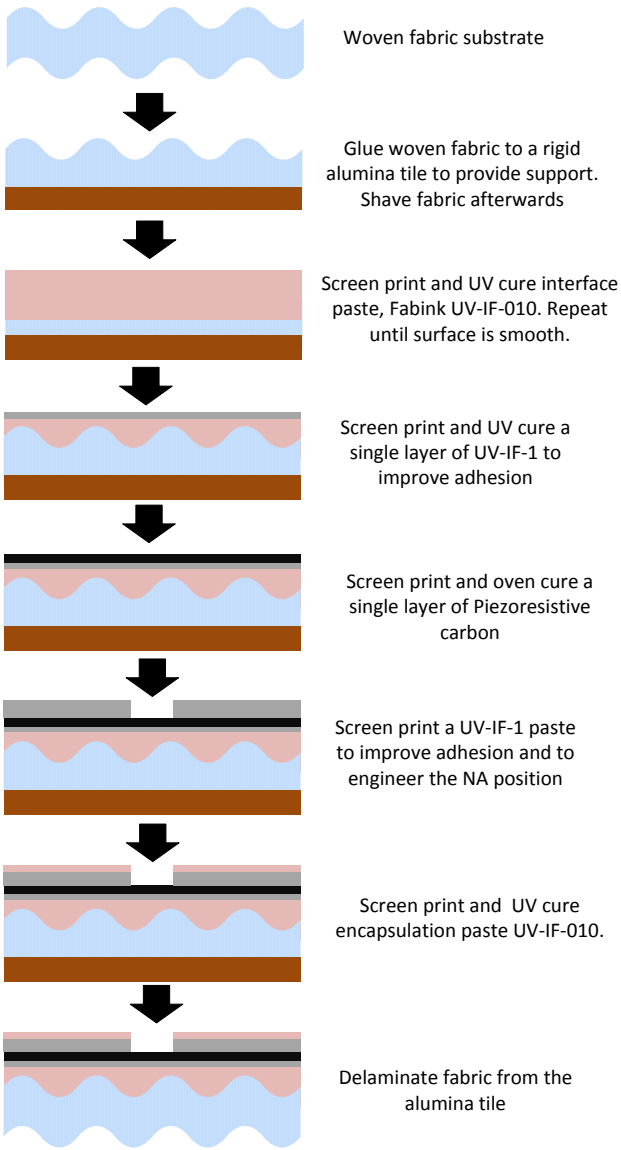

Figure 6.1: Fabrication process for a six layer composite (SLC) e-textile

thickness of 109 µm was realised. The UV-IF-1 adhesion layer on the interface had an average thickness of 22 µm while the value for the top adhesion layer on the gauge was 22 µm for the un-optimised gauge and 676 µm for the optimised gauge. The UV-IF-010 encapsulation has an average thickness of 24 µm.

6.3 Bending test and results

The primary conclusion from the bending test results of all the composites shown in figures 6.2 and 6.3 is that gauges closest to the NA of their composites experience the least strains and show the least changes in electrical resistance during and after bending i.e. in-bending and post-bending. These graphs also indicate other results which are best discussed by the dividing the composites into two groups, each containing composites showing similar behaviour in bending.

6.3.1 Bari, Lagonda (warp) and Escalade (warp) fabrics

These fabrics are similar because they are stiff, that is they have a high elastic modulus in the direction in which the screen printed gauges are oriented as indicated in Table 5.1. The in-bending and post-bending results for gauges printed on these fabrics shown in figure 6.2 can be summarised as follows:

(a) In negative bending, the magnitude of the in-bending changes in resistance and strain is greater than the post-bending equivalent.

(b) Compared to negative bending situations, the gauges in positive bending experience more stress after bending and therefore show higher changes in resistance after bending than during bending.

These conclusions are illustrated with figure 6.2c which shows the results for the gauges along the warp weave of the Escalade fabric. In negative bending, the magnitude of both the in-bending and post-bending changes in resistance and strain of the gauges are shown to reduce as the encapsulation thickness h_T approaches the value that places the gauge at the NA. The in-bending changes are also shown to be a magnitude higher than the post bending changes. For the gauge closest to the NA of the composite, with $h_T = 800$ µm, the in-bending resistance change $|\Delta R| \approx$

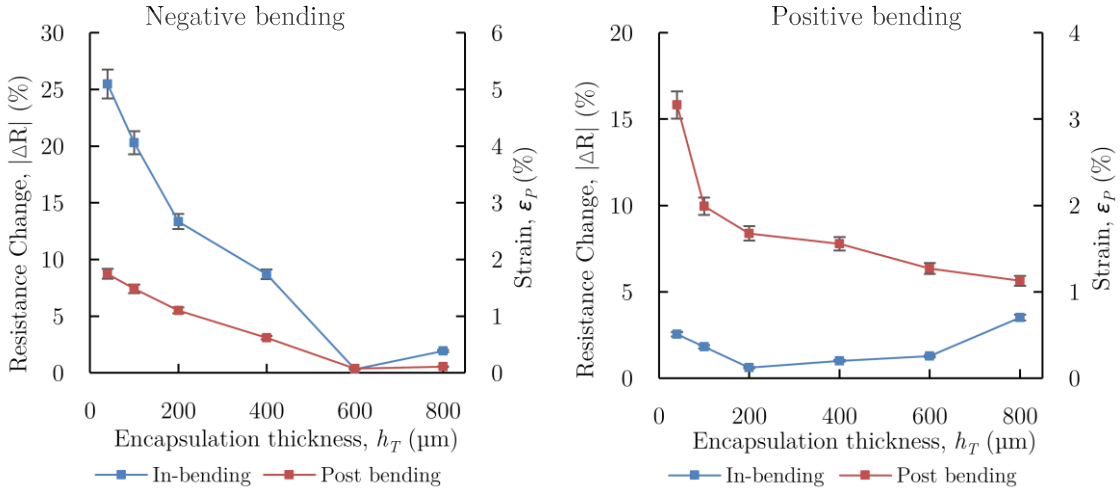

(a) Bari composite: SG-1 gauges

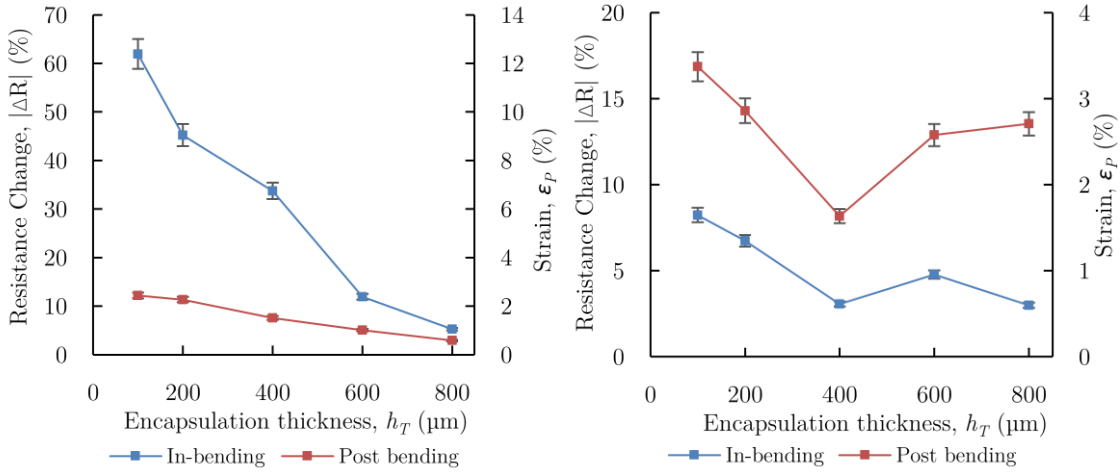

(b) Lagonda composite: SG 1 gauges along the warp weave

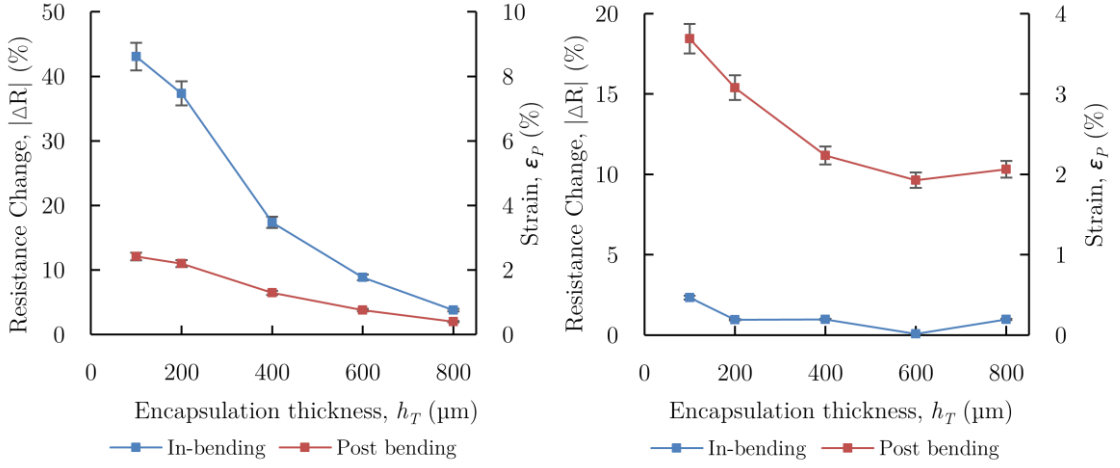

(c) Escalade composite: SG-1 gauges along the warp weave

Figure 6.2: In-bending and post-bending resistance changes and empirical strains from negative and positive bending of gauges in Bari, Lagonda (warp) and Escalade (warp) composites. The encapsulation thickness, h_T on the graph correlates to the values on both vertical axes.

3.76 % and the equivalent empirical strain, $\varepsilon_P \approx 0.75$ %, are almost twice the post-bending values $|\Delta R| \approx 2$ % and $\varepsilon_P \approx 0.4$ %. Conversely, at the NA in positive bending where $h_T \approx 600$ µm, the in-bending values $|\Delta R| \approx 0.08$ % and $\varepsilon_P \approx 0.02$ % of the gauge are almost 120 times less than its corresponding post-bending values, $|\Delta R| \approx 9.64$ % and $\varepsilon_P \approx 1.93$ %. This means that for e-textiles, fabricated using these stiff fabrics, the electrical resistances of interconnections will degrade more quickly in positive bending applications than in negative bending even when in close proximity to the NA.

6.3.2 Polyester, Lagonda (weft) and Escalade (weft) fabrics

Except for the polyester fabric, these fabrics are elastic in the directions in which the gauge was oriented. The Polyester fabric seems to be the odd fabric in this category since its tensile modulus automatically classifies it as a stiff fabric, in Table 5.1. Similarly, its empirically extrapolated tensile modulus value of 2.25 GPa in section 5.4 also suggests the same. However based on the comparison of the similar trends in the graphs in figure 6.3, it can be deduced that the polyester fabric behaves as though it were elastic. The results from the bending tests of gauges printed on fabrics shown in figure 6.3 are hence summarised as follows:

(a) In negative bending, the magnitude of the in-bending resistance changes and strains is always greater than in post-bending.

(b) In positive bending, as h_T exceeds the value that places the gauge on the NA, the magnitude of the in-bending resistance changes and strains of the gauge becomes higher than its corresponding post-bending values. The converse is also true.

The results from the Lagonda (weft) composite in figure 6.3b are used to illustrate these inferences. The gauges showed similar electrical characteristics as those of the first set of fabrics in negative bending. In positive bending however, the gauges show higher post-bending changes in resistance and strain than in-bending resistance and strain changes when $h_T < 400$ µm (i.e. 400 µm is the thickness that places the gauge on the NA of this composite). As this value is exceeded, the in-bending changes becomes greater.

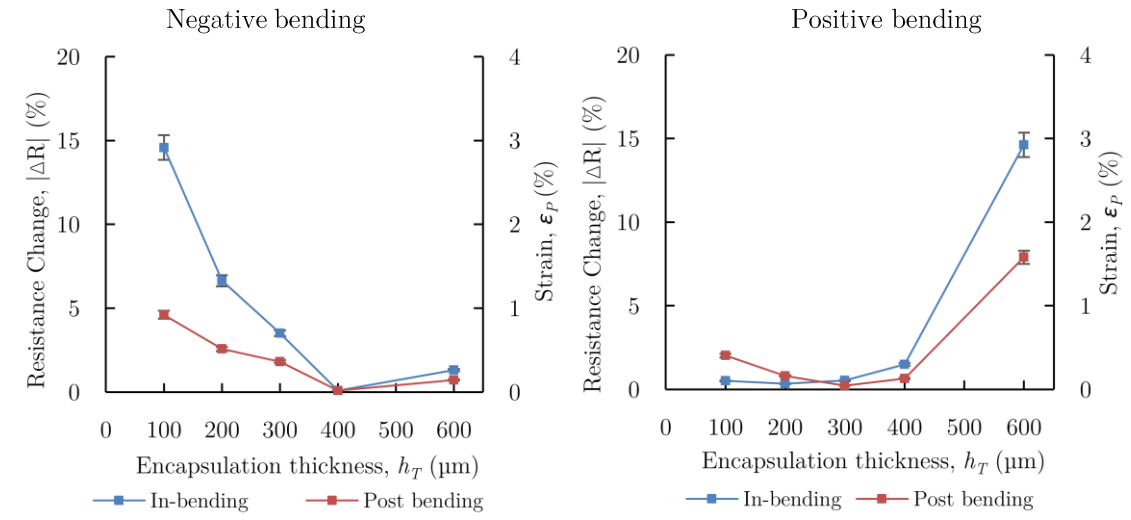

(a) Polyester composite: SG-1 gauges

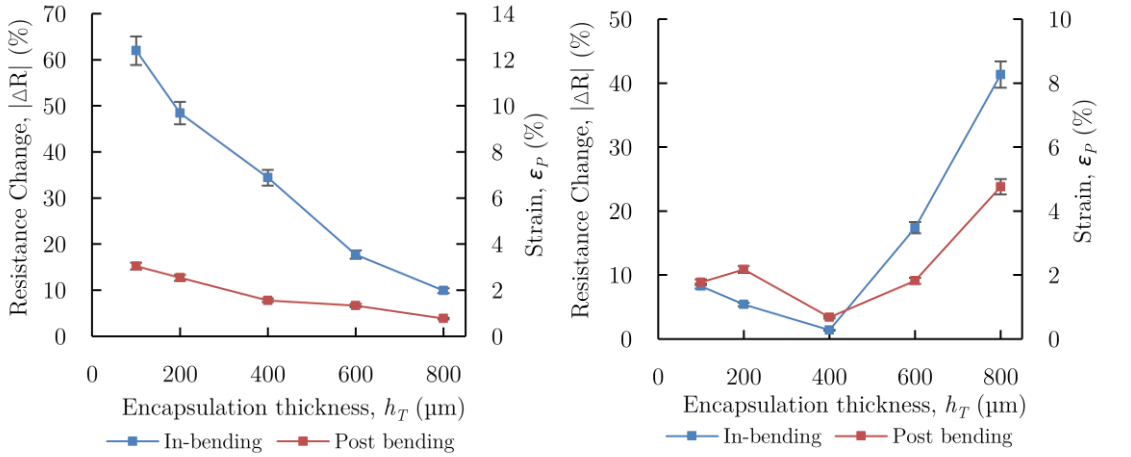

(b) Lagonda composite: SG 2 gauges along the weft weave

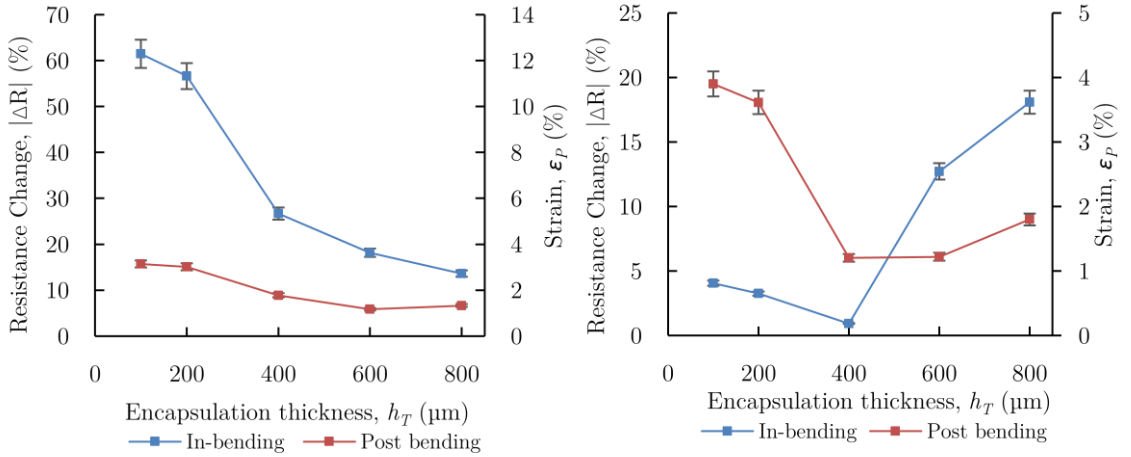

(c) Escalade composite: SG-2 gauges along the weft weave

Figure 6.3: In-bending and post-bending resistance changes and empirical strains from negative and positive bending of gauges in Polyester, Lagonda (weft) and Escalade (weft) composites. The encapsulation thickness, h_T on the graph correlates to the values on both vertical axes.

For example, at $h_T = 100$ µm for example the in-bending and post bending changes of the gauge were almost identical with values $|\Delta R| \approx 8.27$ %, $\varepsilon_P \approx 1.65$ % and $|\Delta R| \approx 8.88$ %, $\varepsilon_P \approx 1.78$ % respectively. While these values reduced at the NA when $h_T \approx 400$ µm, the post-bending change was still almost twice the in-bending change and as h_T increased to 800 µm, the in-bending changes also increased to almost twice the post bending changes. However, this is 60 times better than the performance of the gauges printed on the first set of fabrics in section 6.3.1 where the post-bending resistance changes are almost 120 times greater than the in-bending resistance changes.

This result indicates that printed interconnections perform better in both positive and negative bending when printed on elastic fabrics. This contrasts their behaviour on the stiff fabrics in section 6.3.1 where they only perform better in negative bending.

6.3.3 Implications of bending test results for durable e-textiles

Durability of electrical interconnections is critical for screen printed e-textiles but the dependence of the NA position on the bending orientation and elastic properties of the fabric substrate of the e-textile make this challenging. Electrical interconnections may only be effectively placed at one NA at a time as indicated in the bending test where the NA in positive and negative bending orientations are different. These conductors can therefore be situated very close to the NA positions in both orientations. In the Bari fabric for example, an optimised encapsulation thickness, $h_T = 500$ µm would suffice since it averages the h_T values in both positive and negative bending. While this compromises the durability of the conductors when printed on the NA in either bending orientation, this approach should minimise the effective stress experienced the conductor hence optimizing it in long term for both bending orientations. Positive bending applications are not recommended for screen printed interconnections with stiff fabrics since the fabric experiences more stress than in negative bending. But in such cases, interconnect materials that show high resilience to stresses could be used to achieve better durable performance.

6.3.4 Effect of the optimised encapsulation thickness of electrical interconnections on e-textile wearability

The bending tests have shown that a high optimised encapsulation thickness, h_T is almost inevitable when thermoplastic polyurethanes elastomers (TPU) are used to engineer electrical interconnects close to the NA. The elastic modulus of TPUs is between 0.015 - 0.7 GPa [127] and for the UV-IF-1 TPU (100 MPa) used in this work, h_T was as high as 0.8 mm. Obtained results indicate that the h_T value for optimizing an e-textile of thickness, t and elastic modulus, E, can be reduced by using thinner fabrics with a higher or comparable elastic modulus.

A trade-off to this is that the proportion of the printed materials or films to that of the fabric can increase significantly if the fabric is too thin. This could consequently alter the textural feel and comfort of the fabric. Table 6.1 shows this increase in the film/fabric mass ratio when Bari was replaced with the thinner polyester fabric. An e-textile wearer could become more aware of the printed film.

Table 6.1: Deposit to fabric mass ratios for optimised Bari and Polyester composites

[1]Strain Gauge	Fabric	Fabric Thickness (µm)	Fabric Mass (g)	Film Mass (g)	Total Mass (g)	Film /Fabric Mass ratio
	Polyester	60	0.17	0.43	0.60	2.53
SG - 1	Bari	324	0.76	0.72	1.48	0.95
	Polyester	60	0.30	1.29	1.59	4.30
SG - 2	Bari	324	1.35	2.26	3.61	1.67

[1]The strain gauges are positioned close to the NA

6.3.5 Bending test for the SLC structures

To properly investigate the effect of washing on gauges positioned close to the NA, gauges in SLC structures of Bari and Polyester with printed encapsulation of average thicknesses of h_T = 700 µm and h_T = 400 µm were subjected to bending. These fabrics were used because the gauges require smaller optimised encapsulation thicknesses compared to Escalade and Lagonda fabrics as shown in section 5.3.1. The bending result shown in figure 6.4 also correlates with the results from the FLC structures in that the post-bending changes in the electrical resistances of the strain gauges are more than the in-bending changes after positive bending. The gauge in Bari for example showed in-bending changes of $\Delta R \approx$ -2 % in negative

bending. This reduced to $\Delta R \approx$ - 0.07 % after bending. In positive bending, the in-bending resistance, $\Delta R \approx 0.5$ % increase to $\Delta R \approx 3.33$ % after bending. This result indicates the gauges are not exactly located on the NA of the SLCs but in its proximity.

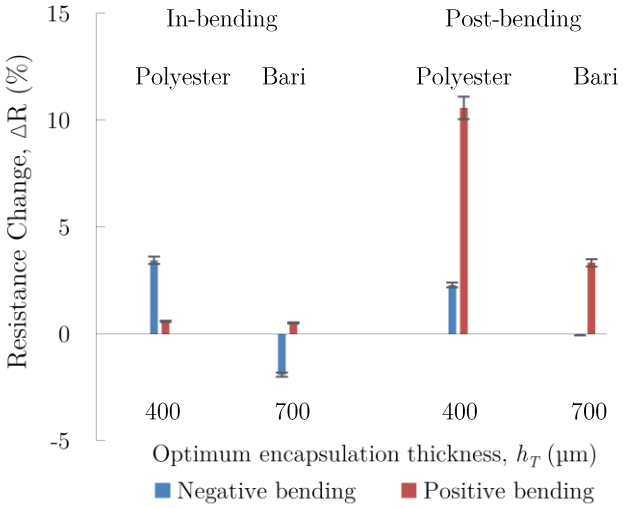

Figure 6.4: In-bending and Post-bending responses of SG-1 strain gauges printed in SLC structures of Bari and Polyester at the optimum encapsulation thickness due to bending radius of 5mm

6.4 Wash test

To replicate practical applications, the SLCs were stapled to a T-shirt as shown in figure 6.5 and were loaded with other clothes in a domestic washing machine for

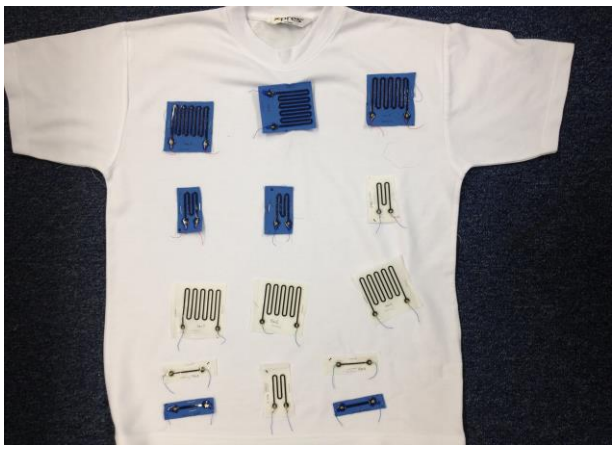

Figure 6.5: Strain gauge patches stapled on a T-Shirt

five washing cycles that consisted a 58 minute wash at a temperature of 40 °C with a 1000 rpm spin dry followed by oven drying at 100 °C for 5 minutes per washing cycle. This wash cycle was chosen to closely replicate the normal washing procedure as stated in the ISO 6330:2000-6A washing standard shown in Appendix E.1. While the oven drying of the gauges at this temperature does not in any way reflect real life drying conditions for fabrics, it presents a harsher condition to assess the performance and survival of the e-textile. A total of twenty eight samples consisting of fourteen optimised and un-optimised strain gauge samples.

The resistance measurement of the gauge after washing was done by using 240 µm thick wires that were attached to the terminals of the strain gauges using isotropic silver–loaded epoxy adhesive as shown in figure 6.6. These were cured at room-temperature for a day. These terminals were also glob-topped with UV-IF-010 and UV-cured for 120 seconds to protect the wires during washing. Further protection was also ensured by hand sewing the wires to the fabric to prevent them from peeling off.

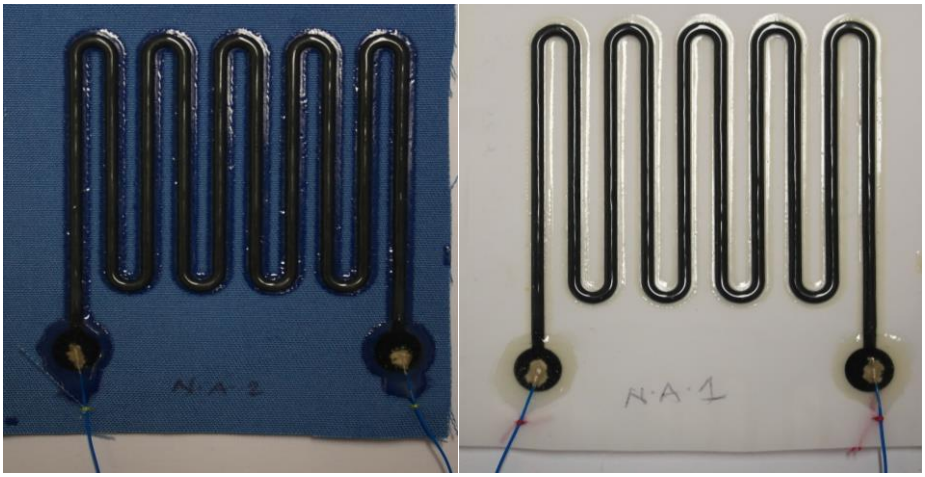

(a) Wired SG-1 on Bari Fabric (b) Wired SG-1 on Polyester Fabric

Figure 6.6: Strain gauge wiring and glob topping.

6.4.1 Discussion of results

A comparison of the resistance changes after washing is reported in figure 6.7 for the optimised and un-optimised gauges in the Polyester fabric and Bari SLC structures. The actual resistance change in the gauges after each wash and dry cycle is shown in Table 6.2 (see page 127). As expected the resistance changes of the optimised strain gauges were smaller than the values obtained for the un-optimised

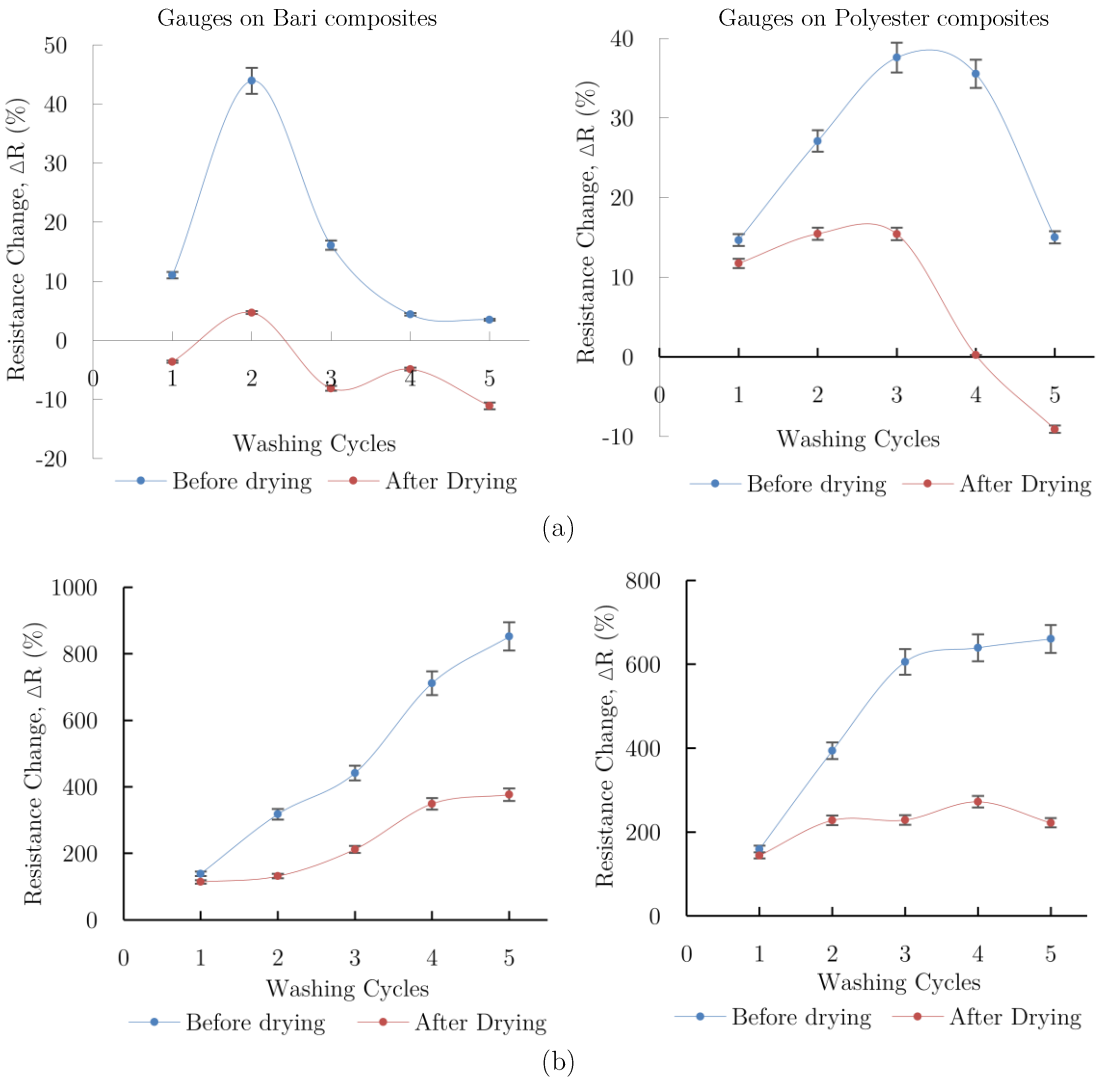

Figure 6.7: Effect of washing and drying on the resistance of (a) optimised strain gauges closest to the NA and (b) un-optimised strain gauges farthest from the NA of Bari (right) and Polyester fabric (left) SLC structures. Plots are based on the average resistance change of two samples.

gauges after five washing cycles. The optimised samples exhibited a resistance change of $|\Delta R| \approx 10\%$ after drying compared to a resistance change of $|\Delta R| \approx 200\%$ in the un-optimised strain gauges of both the Polyester fabric and Bari composites.

Figure 6.7 also showed that the resistance change measured just after washing the gauges, i.e. before drying is almost twice the resistance change after drying. This shows that the UV-IF-010 polyurethane encapsulant also absorbs water during washing and expands as a consequence. This stretches the strain gauge and increases its resistance just after washing as shown in figure 6.8.

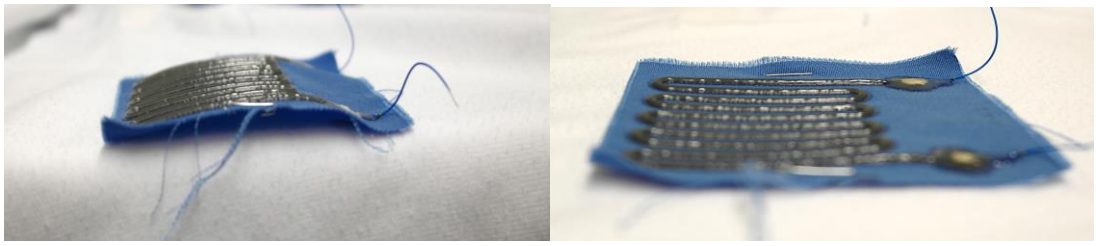

Figure 6.8: Pre-drying (left) and post-drying (right) of the strain gauge after washing

Drying eliminates the absorbed water and any residual washing stresses by relaxing the gauge and reducing its resistance. However, drying parameters such as the temperature and drying time must also be carefully controlled to minimise residual stresses in the samples. This explains the negative post-drying resistance changes seen in the optimised gauges in figure 6.7 which showed that though the drying process had removed the residual tensile stresses in the gauges, it had also produced residual compressive stresses in the gauges.

Table 6.2: Actual resistances of strain gauges after each wash and dry cycle.

Fabric	Gauge location	Samples	Initial Resistance before washing (Ω)	Actual resistance in (Ω) after 1^{st} wash & drying	2^{nd} wash & drying	3^{rd} wash & drying	4^{th} wash & drying	5^{th} wash & drying
Bari	NA	1	719	708	858	720	690	655
		2	897	846	808	750	846	778
	Away from NA	1	92.6	167.5	224.8	218.8	323.4	318
		2	66.3	164	146.2	257.5	364	404
Polyester	NA	1	801	869	869	835	745	688
		2	740	851	906	937	795	710
	Away from NA	1	54.5	108.6	163.9	166	146.6	152.9
		2	61.9	179	220	218.7	294.3	225

6.4.2 Encountered failure modes after washing

Only 36 % (i.e. 10 samples) of the 28 strain gauge samples that were washed survived the five washing cycles. This statistic consists of the 43 % of the optimised samples (i.e. 6 out of 14) and the 29 % of un-optimised samples (i.e. 4 out of 14).

The failed samples did not survive because of structural defects induced in them during washing. These failure modes are described as follows:

6.4.2.1 Peeling of the glob-top at the power supply terminals

The peeling of the glob-top encapsulation at the contact pads during washing either broke the gauges or soaked its pads which made it impossible to measure the resistances of these gauges as shown in figure 6.9. This failure is attributed to poor bonding between the glob-top and the interface layer. While the glob-top and the interface layer are both of the same material, curing them separately meant they were only able to make a interfacial bonding rather than the seamless bonding that

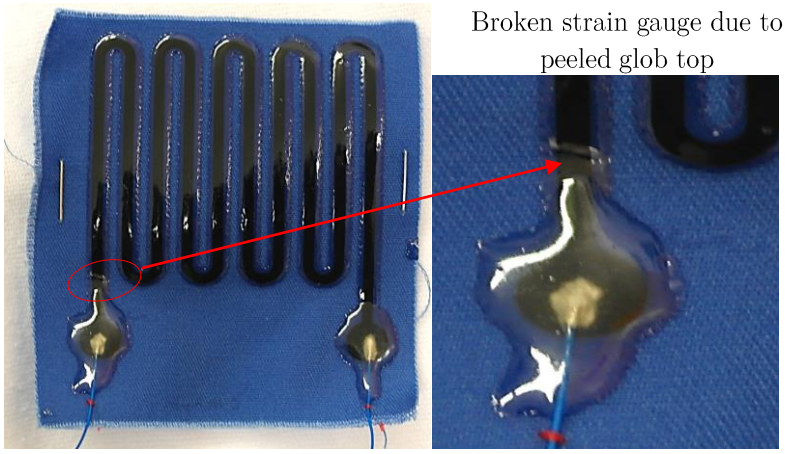

(a)

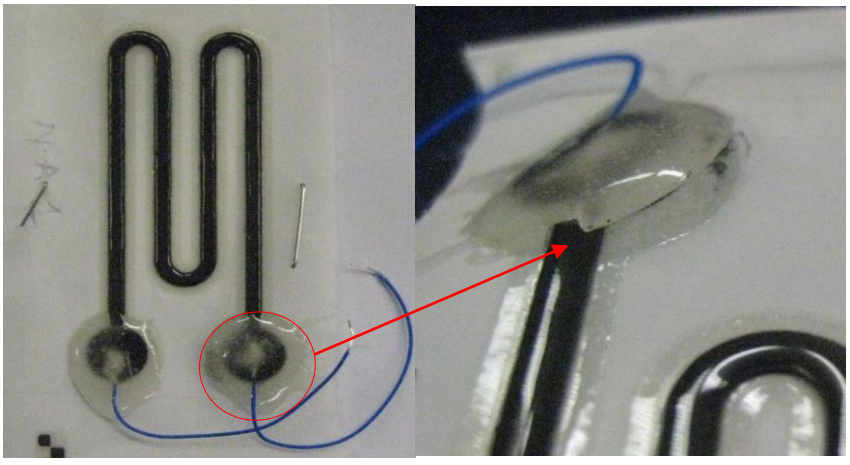

(b)

Figure 6.9: Peeling of glob top from (a) un-optimised and (b) optimised strain gauges on Bari and PES fabrics after the 1st and 3rd washing cycle respectively.

would have occurred if they were cured at the same time. Consequently, in washing, this interfacial bond is stressed to failure.

6.4.2.2 Mismatch between the thickness of the encapsulation and its underlying layers

The optimised SLC Bari sample has a total thickness of about 1.2 mm. The encapsulating layer (i.e. the UV-IF-1 top adhesion and UV-IF-010 encapsulation) constitutes 61 % of this thickness. This huge difference between the encapsulating layer and the underlying layers (i.e. the interface, bottom adhesion and strain gauge layers) created potential stress risers at the terminating sites of the encapsulation on the strain gauge. This unfurled during washing when the encapsulating layer peeled off by breaking the glop top and peeling the strain gauge together with it as shown in figure 6.10. This failure mechanism was not encountered when the encapsulation thickness was as low as 24 µm in section 3.6.1 (page 63). This shows that the adhesive bond between the encapsulating layer and the underlying layers decreases as the encapsulation thickness is increased.

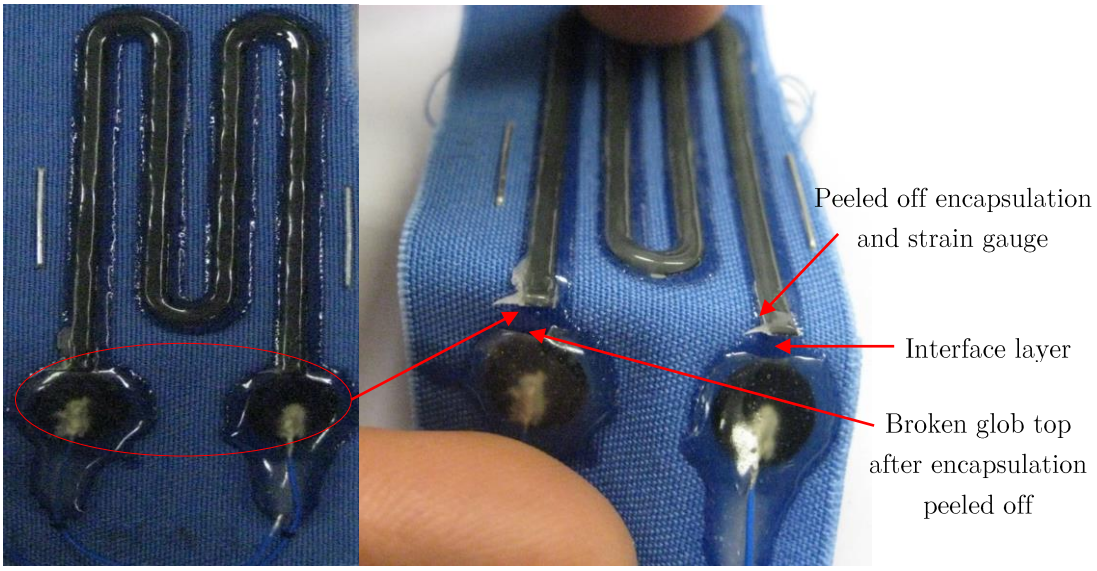

Figure 6.10: Encapsulating layer and strain gauge peeling off the interface after the 3rd wash

6.5 Application circuit

The simple resistor and LED circuits investigated in section 3.4.1 were screen printed on the NA of SLC Bari composites to determine if the circuits will endure

more wash cycles. An encapsulation thickness $h_T = 700$ µm was used to locate the interconnections on the NA as shown in figure 6.11.

Figure 6.11: Screen Printed resistive circuit on neutral axis on a Bari- textile patch

6.5.1 Component attachment

Following the recommendation in section 3.6.1.2 to use anisotropic adhesive, the LEDs and resistors were attached pads of the printed circuit using an anisotropic conductive achieve, Elecolit 3061 as pictured in figure 6.12. To achieve this anisotropy, a force of 0.51 N was exerted on the components in the orientation of conduction during curing. The samples were oven cured for 5 mins at 100 °C.

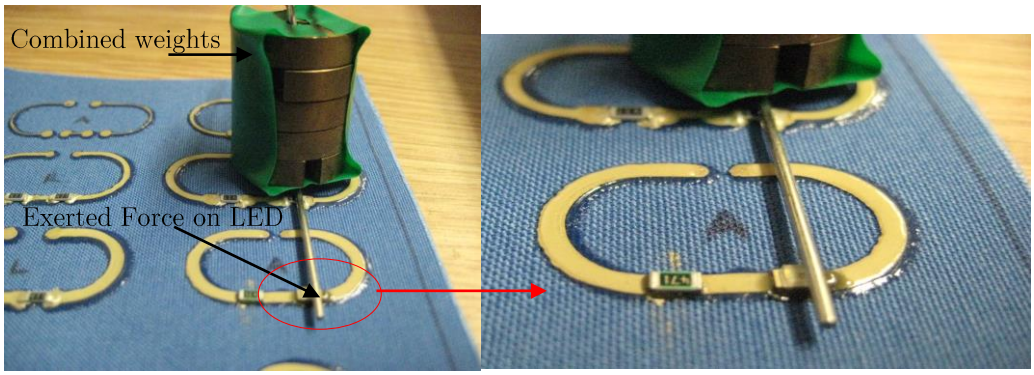

Figure 6.12: Application of anisotropic conductive adhesive on an LED textile patch

Isotropic silver-loaded epoxy adhesive was used to attach the wires to circuits following the detailed process in section 3.5.2.

6.5.2 Bending and wash tests

The LED and resistor circuits did not survive bending and washing because of mechanical failures at the termination sites of the encapsulating layer at the contact pads as illustrated in figure 6.13.

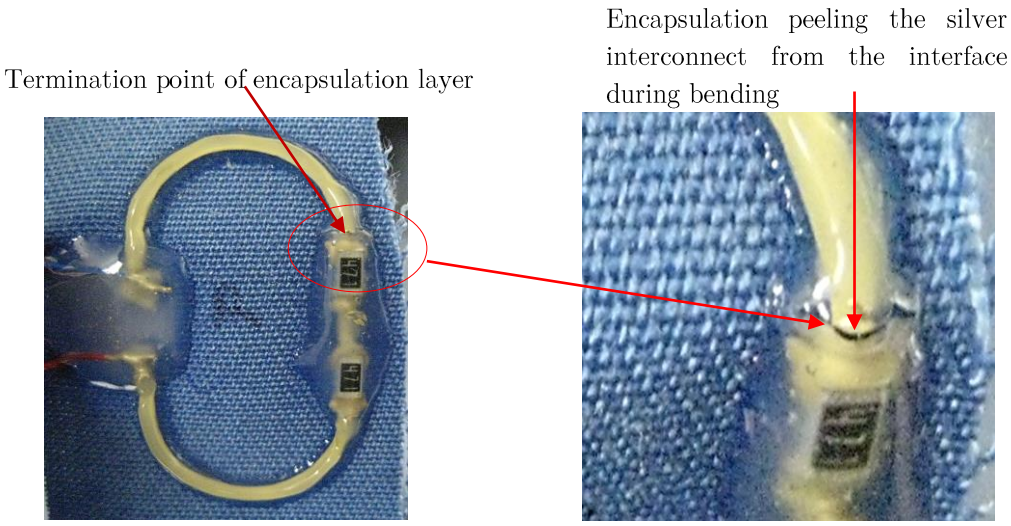

Figure 6.13: Circuit failure due to the high thickness of the encapsulation layer.

This was due to the stiffness mismatch at these locations. This is because the encapsulation does not bend equally as the underlying layers, consequently during flexing or bending, the mechanical bond between both layers breaks down. In contrast to the wash test in section 3.6, this results shows that by only increasing the thickness of the encapsulation to optimise the electrical performance of printed conductors, the probability of incurring failures at the interfaces also increases during bending and washing.

6.6 Conclusions

So far, the concept of the neutral axis has been explored to improve the durability of an e-textile by optimising the position its electrical interconnects. The findings of this work from chapters 3 to 6 lead to the conclusion that electrical interconnects of improved durability in both positive and negative bending orientations are best achieved when oriented along the fabric weave of higher stiffness. Results show that when printed on elastic fabrics, these interconnects degrade faster in performance after bending except when on the NA. Failure modes and the increased wearer

sensitivity of printed films also arise when high TPU encapsulation thicknesses are used to optimise interconnects on the NA. To avoid this, it then becomes necessary to use stiffer encapsulations so that these interconnects and the integrated electronics are optimised with lower encapsulation thicknesses.

The durability of e-textiles can also be enhanced by reducing the size of the circuit integrated on the fabric while its interconnections are still positioned on the neutral axis. This potentially minimises the stress areas on the e-textiles because the electronic component sizes are also reduced along with the track widths of the electrical interconnects. Consequently thick film processes like screen printing are no longer suitable. Hence the next chapter focuses on the fabrication of very fine thin film interconnections and circuits for e-textiles.

CHAPTER 7
THIN FILM INTECONNECTIONS ON TEXTILES

7.1 Introduction

This chapter investigates the design and fabrication of very fine circuits for e-textiles. Screen printing is an easy and time effective approach for making interconnections on fabrics unlike other the fabrication techniques discussed in Chapter 2. This is because it requires lesser fabrication processes than the others. However with screen printing, only printed circuits with feature sizes greater than or equal to 100 µm can be integrated on the textile [128].

The minimum feature size of a circuit becomes critically important when the electronic functionality to be integrated within a small fabric space requires a dense or very fine circuitry. By scaling down the size or minimum feature of the integrated electronics, the wearability of the e-textile is enhanced because the circuitry becomes less conspicuous to the wearer. The reduction in component size, especially by using the bare die versions of components also minimises the e-textile stiffness [8]. With packaged components such as the LEDs and resistors used in section 6.5, the fabric loses it flexibility and becomes effectively rigid in the areas where the components are integrated.

Thin film interconnections are suitable for fabricating such fine circuits that require resolutions higher than 100 µm [138]. Section 2.2.2 indicates that thin film processes have been successfully used to make electronic circuits on flexible plastic substrates such as Kapton. After fabrication, these substrates are cut into strips and are woven into textiles but at the moment these have poor wearability. This is why printed circuits on Kapton was not considered in great detail in the previous chapters. Although thin film processes like evaporation and sputtering have been used to directly coat fabrics, they are yet to be used to make functional electronic circuits on them. Hence in this work, the suitability of conducting thin film processes on a UV-IF-1 coated fabric is initially investigated. The UV-IF-1 coating is used to minimise the surface roughness of the fabric as explained in section 3.3.3.

The functionalisation of a Kapton substrate with a temperature sensor circuit is also investigated with the thin film processes of photolithography and thermal evaporation deposition since they are commonly used in the literature. The sensor circuit is composed of aluminium interconnects, surface mount resistors, thermistor, bare die LED chips and a wafer level chip scale packaged (WLCSP) microcontroller of sizes less than 1 mm^3. The aluminium interconnections are of line widths and spacings of 30 µm to allow for cutting the Kapton thin strips to improve their wearability and concealment on fabrics. The strips can be initially assembled with other textile fibres to make an electronic yarn before they are woven into a fabric. The thin strips are encapsulated before washing to determine their electrical and mechanical reliability. This is because the bending test results in figure 4.17 (see page 93) indicate encapsulated conductors on Kapton perform better than un-encapsulated conductors especially when they are located on the neutral axis.

7.2 Fabrication of thin film interconnections on substrates

Thermal evaporation deposition is a cost effective technique for depositing conductive thin films on substrates as discussed in section 2.2.2. To realise useful thin film interconnections/circuits for e-textiles with the technique, the following processes are necessary:

7.2.1 Surface treatment of substrates

Evaporated thin films adhere poorly to their substrates. To improve their adhesion, a surface treatment of the substrates is often required. This work uses the plasma surface modification which is one of the cleanest and hazard-free of improving adhesion of a material because it produces little to no toxic or unwanted byproducts [155, 156]. It entails exposing the substrate to an ionised gas or gases, called plasma which adds or replaces the organic functional groups at the surface of the substrate to increase its adhesion strength. Some of the gases that have been used in this process include oxygen, nitrogen and argon [155].

7.2.2 Surface patterning of substrates

It is necessary to define the areas where electrical interconnections are to be located on the substrate before depositing any thin film on it. Photolithography enables

the transfer of patterns from a mask to the surface of a substrate during its exposure to ultra violet (UV) light [157]. The substrate surface is initially coated with a photosensitive material called photoresist before UV exposure. The choice of photoresist applied on the substrate determines the photolithographic process that will be used to realise thin film on the substrate.

Figure 7.1 shows two photolithographic patterning processes; etch and lift-off. The etch process uses a negative photoresist which becomes insoluble in a developer solution when exposed to UV through the mask. The unexposed (dark field) area dissolves in the developer and makes it possible to etch the underlying substrate

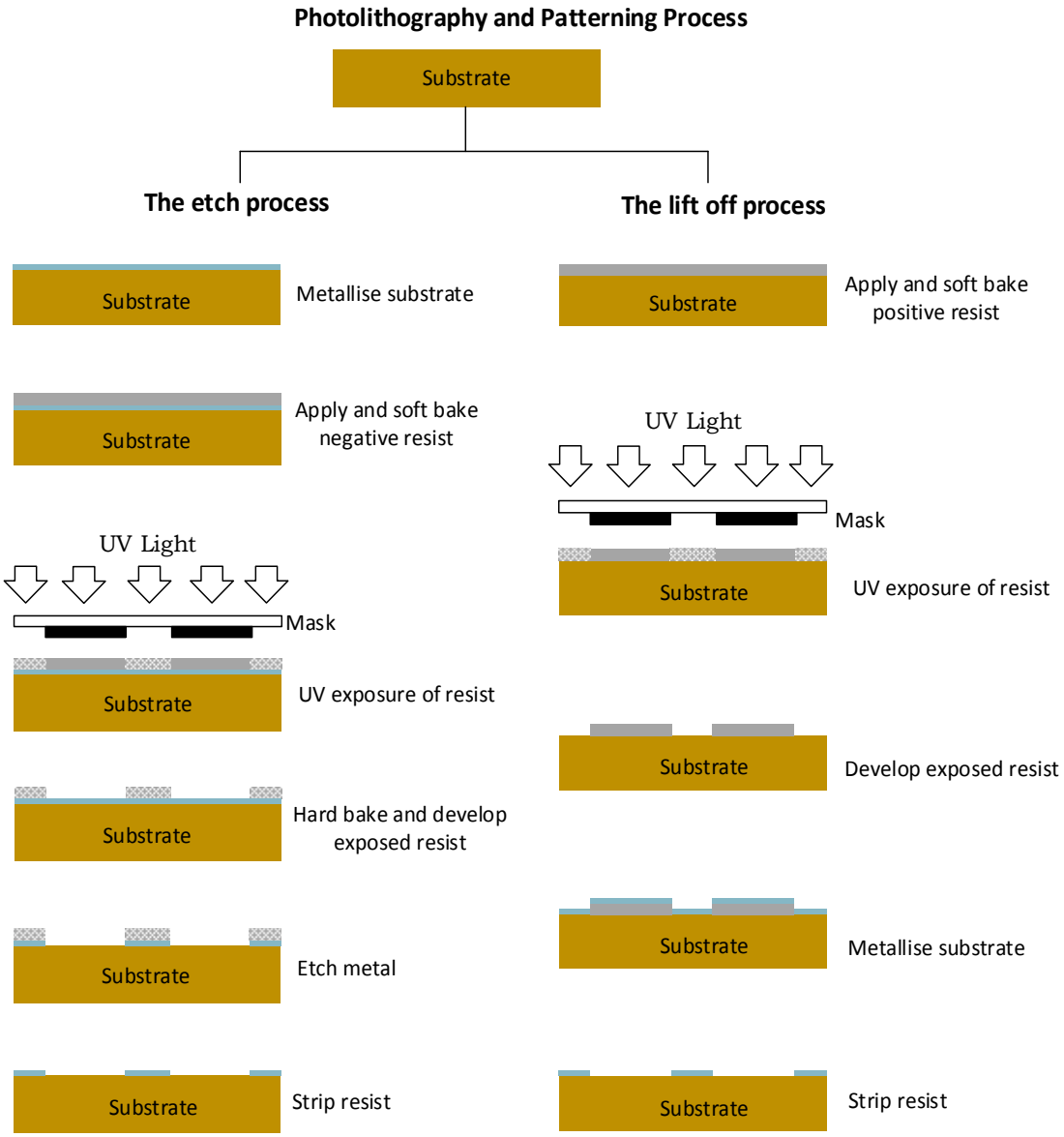

Figure 7.1: The photolithographic process for etching and lift off

area. For lift-off, a positive photoresist is used. The masked area of the resist is insoluble while the exposed area dissolves in a developer solution which makes it possible to metallise the underlying substrate area. The main advantage of the lift-off is the ability to control the linewidth unlike in wetting etching where overcutting of deposited patterns is possible [158].

Some of the chemicals for performing the etch and lift-off processes at the University of Southampton nanofabrication clean room are listed in table 7.1. While these chemicals are suitable for processing on Kapton substrates [154], their suitability on fabrics is unknown. The effects of processing these chemicals on fabric at room temperature is assessed in section 1.3 to determine the practicality of etch and lift off process on fabrics.

Table 7.1: Chemical solutions for the etch and lift off processes

Photolithographic process	Chemical solutions	Use
Etch process	AZ nLOF 2070 photoresist	Negative resist solution
	AZ 726 MIF Developer solution	To develop AZ nLOF 2070 after UV-exposure
	Ferric Chloride solution	To etch copper film
	Chrome etchant UN0398	To etch chromium film
Lift – Off process	AZ 9260 photoresist	Positive resist solution
	AZ 400K developer	To develop positive resist after UV-exposure
	N-Methyl-2-pyrrolidone (NMP)	To strip positive resist after metallisation of substrate
	Acetone	To strip positive resist after metallisation of substrate
General	De-ionised water	To clean substrate after developing

7.3 The feasibility of fabricating thin film circuits in fabrics

Conductive thin films that are fabricated directly on fabric lack durability under mechanical stresses, hence the surface of the fabric is often treated to improve durability and electrical performance [9, 102]. Although Silva et al. [9] fabricated 300 nm thick aluminium film on polymer coated textile, nothing has been published

Figure 7.2: Samples of UV-IF-1 coated (top) and uncoated (bottom) fabric samples before testing

in literature on the suitability of thin film fabrication processes for patterning interconnections on polymer coated fabrics especially when printed circuits are to be fabricated.

This section therefore investigates the effects of the chemicals listed in 7.1 on a polymer coated fabric by immersing two 10 mm x 85 mm rectangular samples of UV-IF-1 coated and uncoated fabrics shown in figure 7.2 in the chemical solutions. Table 7.3. The results from the test after five minutes are discussed as follows:

7.3.1 Effect of de-ionised water, AZ 726 MIF and AZ 400K developer solutions on UV-IF-1 coated and uncoated fabrics

Figure 7.3 shows a twist in the UV-IF-1 coated fabric after 5 minutes of submerging it de-ionised water. The uncoated fabric remained unchanged. This confirms the results in 3.6.1.1 that the UV-IF-1 interface absorbs water which is responsible for the twist in the sample. Similar behaviour was also observed with the UV-IF-1 coated samples that were submerged in AZ 726MIF and AZ 400K developer solutions as shown indicated in figure 7.4.

Figure 7.3: Samples of UV-IF-1 coated fabrics after submerging it de-ionized water for 5 minutes

(a) (b) (c)

Figure 7.4: Samples of UV-IF-1 coated (left) and uncoated fabrics after submerging them in (a) AZ 726 MIF, (b) AZ 400K developer solutions for 5 minutes. Figure (c) shows the delamination samples from alumina tiles after 5 minutes.

The UV-IF-1 coated samples also twisted despite being glued to an alumina tile. This is because the adhesive glue was weakened by the developer solutions. While the samples do not appear to be physically damaged, this result shows that the lithographic process on a UV-IF-1 coated fabric might be possible by using a chemically resistant adhesive that is able to overcome the twisting force in the fabric and hold it firm to its alumina tile.

7.3.2 Effect of chrome, ferric chloride, acetone and NMP solutions on the UV-IF-1 coated and uncoated fabrics

The UV-IF-1 coated fabric twisted after 5 minutes of submerging it into a chrome etchant as shown in figure 7.5a. Unlike in figures 7.3 and 7.4, more rounds of twist are noticed which possibly indicates that the UV-IF-1 polymer either greatly

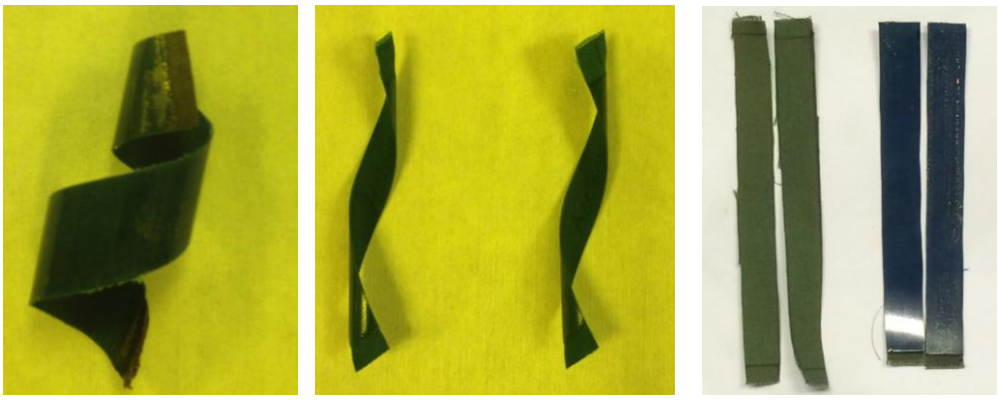

(a) (b) (c)

Figure 7.5: Samples of UV-IF-1 coated fabrics after submerging them in (a) chrome etchant (b) acetone and (c) ferric chloride for 5 minutes. In (c) the uncoated fabric (left) is also shown.

absorbs the chrome etchants or is attacked by it. Similar twist is also seen with acetone in figure 7.5c. While the coated and uncoated samples dipped in the ferric chloride solution showed no twist during the same time, these were stained by the colour of the etchant thereby changing its colour from blue to a tarnish brown. The UV-IF-1 coated part of the fabrics can be readily cleaned with a wipe as evident in figure 7.5b.

This result shows that the chrome etchant can be suitable for fabricating thin films on UV-IF-1 coated fabrics only if a chemically resistant adhesive that is strong enough to firmly hold the fabric in position during the processing time. Ferric chloride etchant offer a better alternative except for the stain it introduces in the fabric. This can be curbed by masking the exposed area of the fabric before etching with a disposable material such as a polyvinylchloride (PVC) material.

The effect of NMP solution on the UV-IF-1 interface at room temperature is shown in figure 7.6. After 20 minutes, the 95 mm x 95 mm sample of a UV-IF-1 coated fabric folded up completely. Also the NMP is shown to attack the UV-IF-1 polymer by peeling it off the fabric.

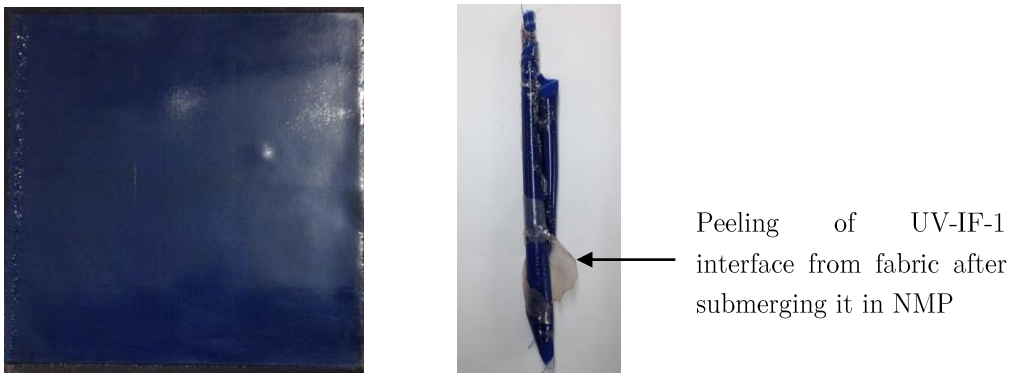

Figure 7.6: Effect of NMP on a 95 mm x *95 mm of UV-IF-1 fabric coated fabric after submerging it for twenty minutes.*

7.3.3 Conclusions on the suitability of the lift-off or etch process on a UV-IF-1 coated fabric

The results in section 7.3.2 show that the lift-off process is unsuitable for making thin film interconnects on a UV-IF-1 interface on fabric. The NMP solution attacks and destroys the UV-IF-1 interface even before the metal can be lifted off. Acetone, another lift-off solution, twists the fabric. Lift-off chemicals that are gentle on the

interface coating are necessary to make the lift-off process suitable for interface coated fabrics.

The etch process is a potential alternative but its suitability entirely depends on the type of metal to be deposited and the etchant to be used. This work has considered the etching of copper and chromium films with ferric chloride and chrome etchants respectively. While chrome etchant twist the fabric, the ferric chloride proves a better alternative for deposition copper interconnections on UV-IF-1 coated fabrics but the decolourisation of the fabric during the etching process could be a deterrent especially where aesthetics is necessary for the end user e-textile application. Therefore an extensive study of the effect of other metal etchants on the UV-IF-1 or any polymer coated fabric is still needed before any definitive conclusions can be made on the suitability of the etch process for such substrates.

This results shows that unlike Kapton substrates, for photolithographic patterning of thin film metals on fabrics coated with polymers like Fabink UV-IF-1 becomes highly process selective and restrictive. To this end, this work will focus on fabricating thin film interconnects on Kapton substrates.

7.4 Design and fabrication of thin film circuits on Kapton for e-textile applications

The design considerations for electrical interconnections on Kapton for e-textiles depends on its method of integration into the textile. Two forms of integration have been reported in literature and these are by:

i. Sandwiching etched metallised Kapton strips between two screen-printed PDMS polymers on textiles [59, 60]. A 0.1 mm wide horse shoe strip was only used as interconnects and connected in pairs to rigid interposer circuits.

ii. Weaving of laser cut metallised Kapton strips or fibres with textile yarns to make a fabric [53, 54, 60]. The strips in [53 - 55] and [61] are 2 mm and 5 mm wide respectively. In both cases the strips were functionalised with packaged sensors and/or LEDs of similar width.

The drawback to these techniques is that the electronic strips are still visible to the user even after integrating them to a textile as shown in figures 2.16 - 2.18. To compensate for this visibility, the strips would have to be designed or positioned aesthetically within the fabric and this can become challenging as the circuit complexity increases. Otherwise the width of the strips needs to be significantly reduced to make them less conspicuous. In [59, 60], the strip width was reduced to 20 µm but this was used only as an electrical interconnection for rigid interposer circuits. These interposers were ten times heavier that the fabric and can increase the user's awareness of the integrated electronics in the textile.

In this work, the width of the Kapton strip is reduced to 0.8 mm while ensuring:

i. The strip retains its electronic functionality

ii. It is small enough to be assembled into an electronic yarn illustrated in figure 7.7 where the thin film interconnections and electronic modules are first encapsulated before textile fibres are woven around it to conceal the areas of electronic modules that should not be assessed by the user.

iii. The resulting electronic yarn can be woven into a textile

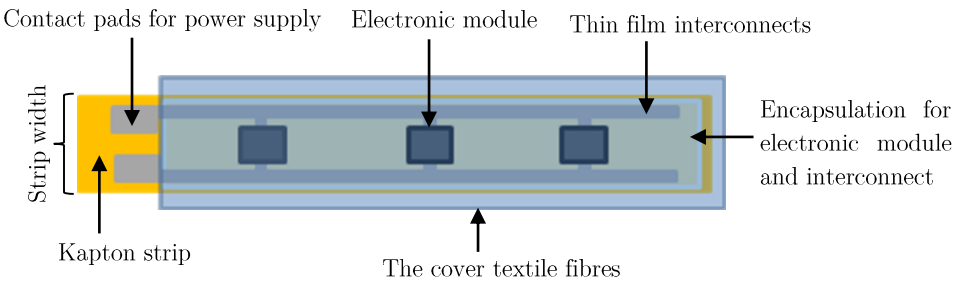

Figure 7.7: A simple cross sectional description of the electronic yarn. The cover textile fibre is made transparent to be make the layers underneath it visible.

The choice of using a strip width of 0.8 mm was based on the maximum width of strip that can be woven in the Jacquard weaving tool at Nottingham Trent University which will be used to manufacture the electronic yarn. This strip width is still 2.5 times smaller than the state of the art.

7.4.1 The design of a re-programmable temperature sensing strip

A programmable temperature sensing circuit shown in figure 7.8 was fitted in the 0.77 mm wide strip of lengths of 75 mm and 135 mm designed in L-Edit as shown

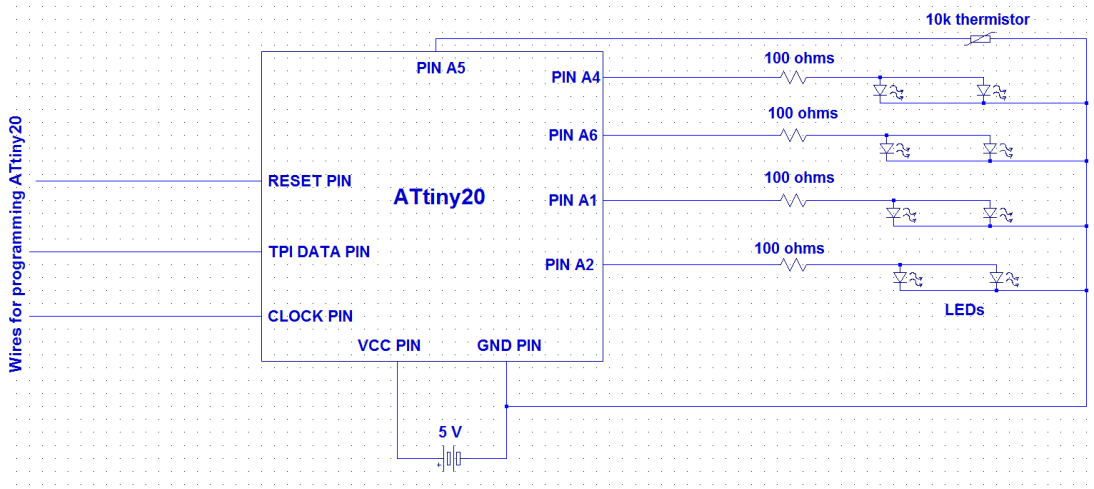

Figure 7.8: Schematic for a re-programmable temperature sensor

in figure 7.8. The circuit function is to detect and classify ambient temperature into four different temperature ranges (5 - 15 °C, 16 - 25 °C, 26 - 35 °C and 36 - 45 °C). These temperature ranges will be indicated by a pair of blue, green, yellow and red LED lights respectively as shown in figure 7.9.

The circuit contains four major components, a microcontroller, LEDs, resistors, and a thermistor (see appendix F.1 for dimensions). These components are interconnected by 30 µm wide aluminium thin film conductors while parallel conductor lines were also spaced by 30 µm. This conductor width and line spacing ensure that the sensing circuit (without the microcontroller) is less than 0.8 mm wide which can then be woven into a yarn. It was impossible to fit the microcontroller into the 0.8 mm strip width because it was difficult to find a commercially available microcontroller with a smaller width than 1.403 mm.

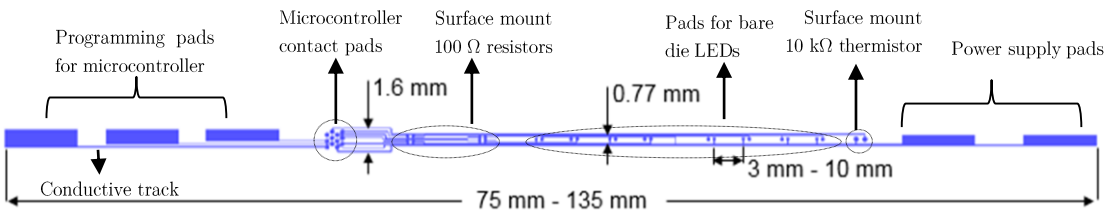

Figure 7.9: Temperature sensing circuit layout for a 0.8 mm wide Kapton strip

The circuit was also designed in two different lengths of 75 mm and 135 mm, to demonstrate how closely packed the components can be without failing during use.

The maximum separation between components corresponding to this lengths are 3 mm and 10 mm. The power supply and programming pad were positioned at opposite ends of the strips to provide the option of reducing the length of the strip after the microcontroller has been programmed. The spacing between the 5 mm x 0.67 mm rectangular power supply pads are 3.3 mm and 5 mm for the short and long strips respectively.

The temperature sensor circuit patterns in appendix F.2 were replicated on a 7-inch glass mask by JD Photo Data Ltd, UK. The glass mask also contained square sized patterns with resolutions of 10 µm, 20 µm, 40 µm, 60 µm, 80 µm, 100 µm, 200 µm, 400 µm, 600 µm and 800 µm. This was done to test empirically ascertain the best pattern resolution that can be achieved with the photolithographic process.

7.4.2 Fabrication of the temperature sensing circuit on Kapton

The fabrication process is divided into two parts: (a) the fabrication of the circuit pattern in figure 7.9 and (b) the attachment of the components to their circuit pads.

7.4.2.1 Fabrication process for the deposition of thin aluminium interconnections on Kapton

The lift-off process was used to fabricate the temperature circuit on the Kapton substrate for better control the interconnect linewidth [158]. Although the process is standard, this is the first to be developed on Kapton in the University of Southampton clean room facility.

Six Kapton sheets were initially adhesively bonded to a 6 inch silicon wafer using Tesla double sided adhesive tape. This was to ensure the Kapton sheet remained flat and rigid during the lift-off process. The Tesla adhesive was also chosen because it could survive the process temperatures and chemicals. To improve its adhesion, a plasma treatment of the Kapton surface with O^{2-} (oxide ions) for 5 minutes was performed in Plasmalab 80Plus etcher by Oxford instruments, USA. This was validated by a tape test performed on a subsequently deposited 1 µm film of aluminium by evaporation as shown in figure 7.10.

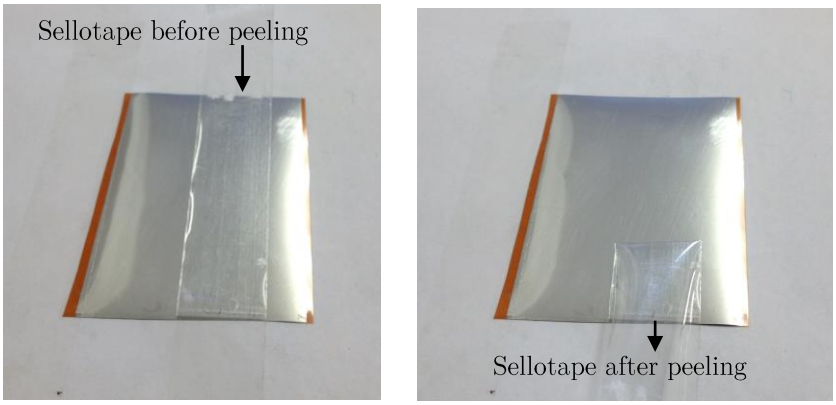

Figure 7.10: Tape test on 1 μm thick aluminium film deposited on a plasma treated Kapton

The plasma treated surfaces were spin coated with AZ 9260 positive photoresist for thirty seconds using a Brewer Cee200 spin coater at a spin speed of 3000 rpm. This achieved a resist thickness of 6 µm on each substrate. The resist was patterned by with the glass mask using the EVG 620T UV mask aligner. The substrates were exposed to UV light of energy density of 8.81 eV for 20 seconds. Then they were immersed in a 1:4 solution of AZ 400K developer and water, and were gently agitated while they developed for 5 minutes.

After inspecting the developed patterns in a microscope, the substrates were plasma treated again before aluminium films of thicknesses of 500 nm, 1 µm and 1.5 µm thermally evaporated on them at deposition rate of 2.5 Å/sec and an applied

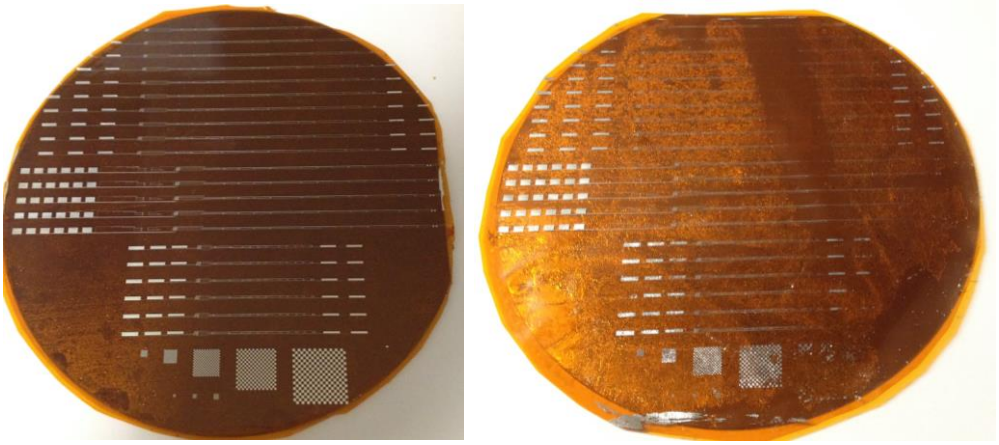

(a) (b)

Figure 7.11: Patterned substrate after lift-off for substrate (a) with plasma re-treatment and (b) without plasma re-treatment after photolithography

pressure of 10^{-5} torr. The process lasted 35 minutes for every 500 nm film that was deposited. The metallised substrates were dipped in a solution of NMP for 12 hours to lift-off the remaining resist on the resist. Afterwards the substrates were was rinsed with de-ionized water. The patterned substrate is shown in figure 7.11a. Similarly, an initial experiment indicated the poor adhesion of aluminium thin films after lift-off to Kapton substrates that were not re-plasma treated as shown in figure 7.11b. The photolithography processes before lift-off mostly likely re-modified the surface characteristics of the Kapton substrate after the first plasma treatment.

7.4.2.2 Resolution of the evaporated aluminium films

After lift-off, the patterns were inspected through a Nikon microscope at 10x magnification. All the patterns were clearly defined down to a resolution of 10 µm on all substrates, as shown in figure 7.12.

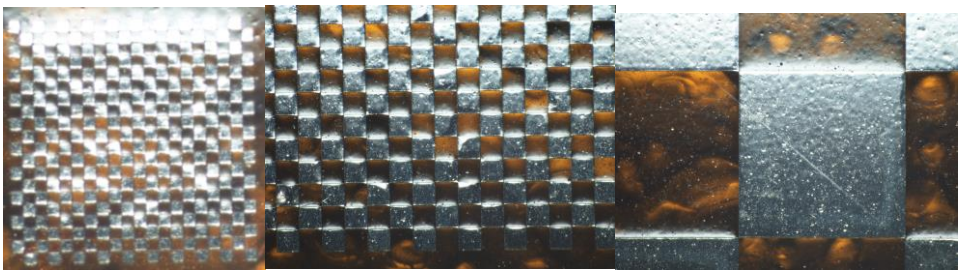

(a) (b) (c)

Figure 7.12: Clearly defined square patterns at 10X magnification on 1.5 µm thick aluminium substrates for resolutions of (a) 10 µm (b) 40 µm and (c) 800 µm after lift-off

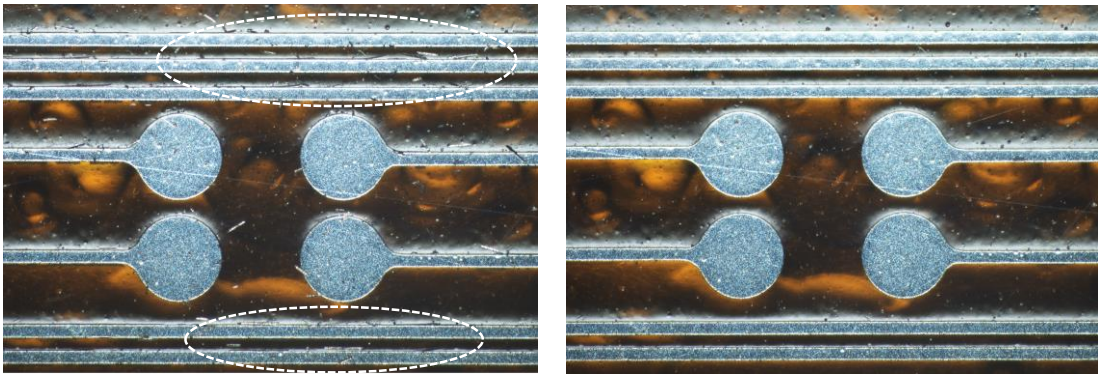

(a) *(b)*

Figure 7.13: 10X magnification of circuit interconnections (a) before and (b) after acetone clean. The equivalent positions in (b) of the circled portions in (a) are cleaner and devoid of stray aluminium films.

Further inspection of the circuit interconnections showed that it was necessary to clean the substrates with acetone after rinsing off the NMP from the substrates

with de-ionised water. Figure 7.13 shows that while the interconnections were clearly defined, the circuit can still be shorted by stray aluminium films that were not completed lifted off as shown. It was necessary to clean the substrates with acetone to remove the stray films otherwise electrical integrity of the circuit will be compromised.

7.4.2.3 Electrical resistivity of the evaporated aluminium film

The resistance, R of a uniform rectangular conductor of a length, l, thickness, t and width w, shown in figure 7.14 is given by the equation (7.1):

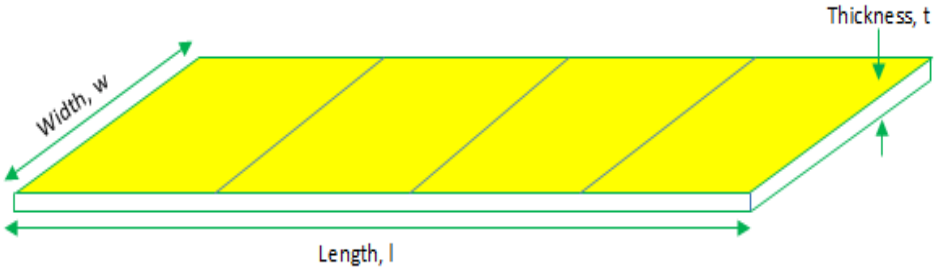

Figure 7.14: A uniform conductor divided into a number of squares [159]

Where: ρ = electrical resistivity of the conductor, a material property independent of the geometry of the conductor which determines how much current a conductor can resist. It is the resistance of a material of unit length and unit cross-sectional area. The term $\frac{\rho}{t}$ is referred to as Sheet Resistance, R_{sq} of the conductor while the second term $\frac{l}{w}$ is called the aspect ratio and it gives the number of squares that can be taken found in the conductor, figure 7.14.

The electrical resistivity of the evaporated aluminium interconnects at room temperature calculated based the average measurements of the electrical resistances from six different circuits of same length and thickness is shown in Table 7.2.

The electrical resistivity of the aluminium interconnections is shown to vary between the values of 1.2 x 10^{-6} Ωm and 2.92 x 10^{-7} Ωm. Although these values correlate with the resistivity value of 10^{-7} Ωm obtained in [9], they also indicate an unevenness in the film thickness across the entire length of the interconnects which is one of the disadvantages of the thermally evaporated films [157]. The resistivity values are in an order of 10^{-1} higher than the bulk resistivity of aluminium, 2.65 x

Table 7.2: Electrical resistivity of evaporated aluminium interconnect

Film thickness, t (µm)	Film length, l (mm)	Film width, w (µm)	[1]Measured electrical resistance, R (Ω)	Calculated electrical resistivity, ρ (Ωm)	Typical electrical resistivity of aluminium at 20 °C (Ωm)[158]
0.5	36.7 mm	30 µm	2994.5	1.2 x 10^{-6}	2.65 x 10^{-8}
	81.3 mm		9045	1.67 x 10^{-6}	
1	36.7 mm		268.8	2.20 x 10^{-7}	
	81.3 mm		791. 33	2.92 x 10^{-7}	
1.5	36.7 mm		149.97	1.84 x 10^{-7}	
	81.3 mm		364.18	2.02 x 10^{-7}	

[1]*Average resistance measurements from six different circuits*

10^{-8} Ωm [160]. Thin metallic films generally have higher resistivity than their corresponding bulk metal because of defects that displace atoms from their lattice sites hence annealing might often be required after deposition to minimise this effect [160]. In this case, the aluminium films were not annealed since their conductivity was high enough for the temperature circuit.

7.4.2.4 The component bonding process

The pitch size between parallel conductors in the circuit is 30 µm. To avoid short circuiting, component bonding to the circuits was initially attempted with a thermally cured anisotropic conductive adhesive, Elecolit 3061 as described in section 6.5.1. The anisotropic adhesive ensures electrical conductivity is only achieved vertically between the pads of the components and the interconnection pads.

This process requires the use of a flip-chip bonder with resolution of up to 100 µm for proper placement due to the small scale of the component especially the resistors, see table 7.4. Due to the unavailability of the tool, the component placement were manually attempted. The small size of the components necessitated the use of flat weights (weighing 8 N) that covered the entire substrate area as shown in figure 7.15.

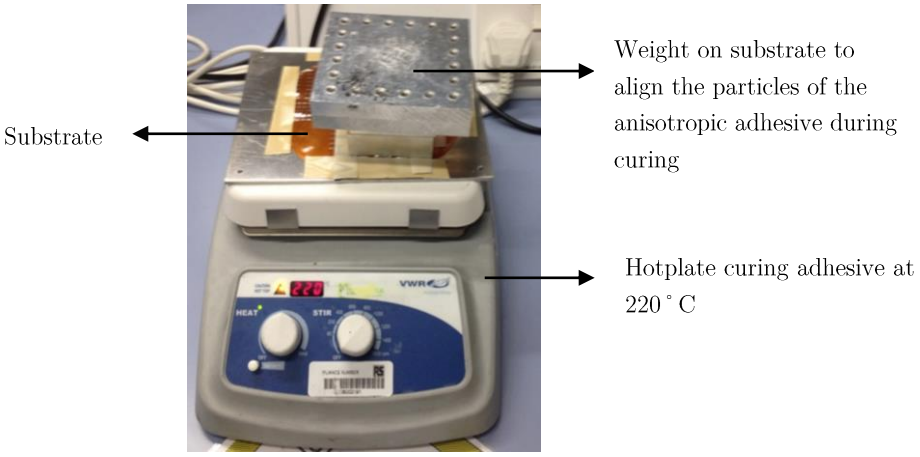

Figure 7.15: Component bonding using anisotropic adhesive

The adhesive was manually dispensed using a 100 µm thick needle tip. To enable proper heat transfer between the adhesive and component, a hot plate curing at 220 °C for 10 minutes was used in place oven curing. While occasional precision placements of the resistors, in particular, were possible as shown in figure 7.16a, it was not repeatable to ensure proper testing. The failure modes encountered include:

i. Misalignment of resistors with the contact pads, as shown in figure 7.16b. This mainly occurred during the placement of a load on the component before it is cured since it is firmly held in place. The misalignment results in a short circuit.

ii. Poor heat transfer between the component and the adhesive. The adhesive was uncured after 10 minutes of heating it while the weight is still firmly placed on the component. But without the weight, the adhesive cures in less than a 1 minute. This was the reason for using a

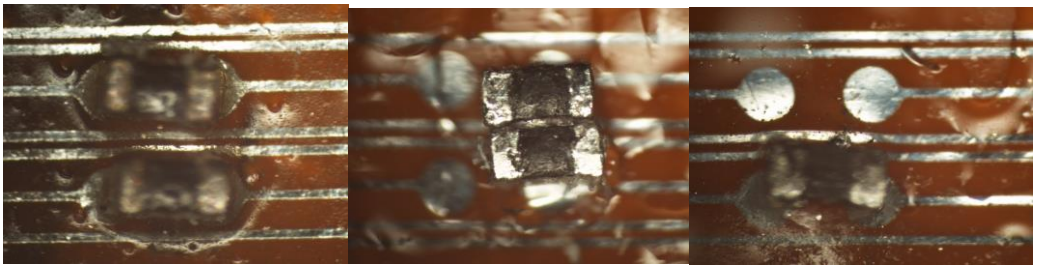

(a) (b) (c)

Figure 7.16: Anisotropically mounted resistors at 10X magnification when (a) properly aligned with interconnect pads (b) and (c) misaligned with interconnect pads

temperature as high as 220 °C but the process was still unrepeatable. It should be noted that this problem was not encountered in section 6.5.1 because the components were not of sub-millimetre dimensions. Conventional flip chip bonding ensures uniformly heat distribution to ensure proper heat transfer within the adhesive [161].

To address the misalignment, a stencil containing apertures with sizes equivalent to the components was designed. The adhesive was dispensed through the apertures before positioning the component in the aperture. While the components firmly remained in position after curing, they stuck to the stencil and peeled off the substrate as the stencil was removed. This led to the use of isotropic conductive adhesive.

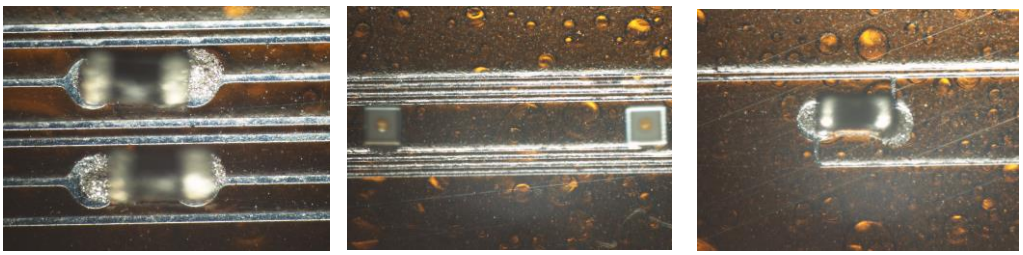

(a) (b) (c)

Figure 7.17: Successfully mounted (a) resistors (b) LEDs and (c) thermistor on interconnect pads. Images are at 5X magnification

All the components were successfully mounted on the temperature sensing strip as shown in figure 7.17 using silver loaded epoxy adhesive which was also dispensed with the 100 µm tip of a needle. The components were mounted and oven cured on the strip in batches for 5 minutes, first the four resistors, eight LEDs and the thermistor and microcontroller.

Following this, the gold contact pad at the top of the LED (which can be seen in figure 7.17b) is required to be wire bonded to the ground (i.e –ve) terminal pad on the strip. Attempts to do this with an ultrasonic wedge wire bonder failed because the 25 µm thick aluminium wire from that should be ultrasonically bonded did not stick on the contact pad on the aluminium interconnection or the LED bond pads at a bonding force of 100 US energy. This is called the non-stick effect in wire bonding and it is attributed to insufficient bonding force [162]. The initial bonding force was increased to 160 US energy which did not resolve the problem.

Hence attempts were made to manually wire bond the LEDs with the silver load epoxy adhesive to bond the 25 µm thick aluminium wire to bond pads on the LED and interconnect. The unrepeatability and difficulty of the process led to a few LEDs wire bonds.

7.5 Circuit testing

To test the circuit, wires were bonded to the power supply and programing contact pads on the strip using the silver epoxy. Due to the difficulty in wire bonding all the LEDs, the microcontroller was programmed to just turn on, and/or blink an LED on the strip. Figure 7.18 shows a blue LED lighting on the strip after the microcontroller was successfully programmed.

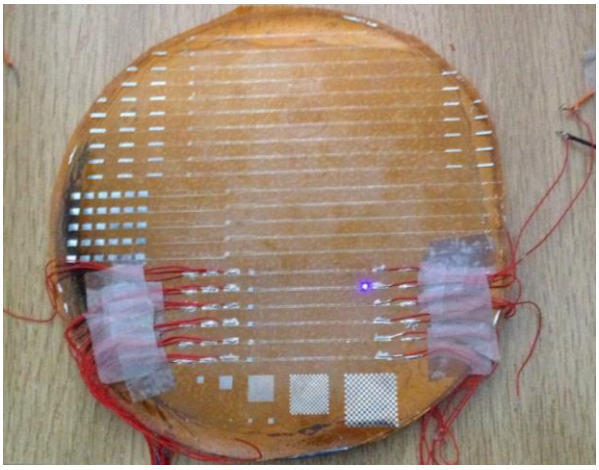

Figure 7.18: A blued LED turned on by a microcontroller on the 0.8 mm sized circuit

7.5.1 Reliability testing of the of electronic strip

To place the interconnects and components on two working strips on the NA, an encapsulation thickness of up to 0.6 mm is required based on the previous experiment in section 4.6. The strip was manually glob topped from a 5 ml syringe with UV-IF-1 and UV-IF-010 inks to test them for washing. To avoid any interfacial failures that could result by glob-topping the components in isolation, the entire circuit was glob-topped. The inks were UV-cured for sixty seconds. Due to the bleeding of the inks during dispensing, the encapsulation extended to neighbouring circuits on the strip. An encapsulation thickness of 1.1 mm was achieved which is

0.5 mm more than the thickness required. Nonetheless, after encapsulation, the LED lightings became too dim and unnoticeable hence they were not washed since they had already failed. This failure could have resulted from a poor contact at the wire bonds on the LEDs.

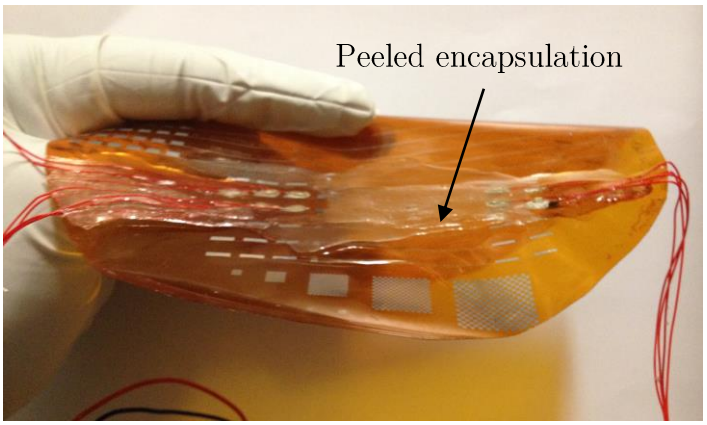

(a) Peeling of encapsulation from Kapton substrate

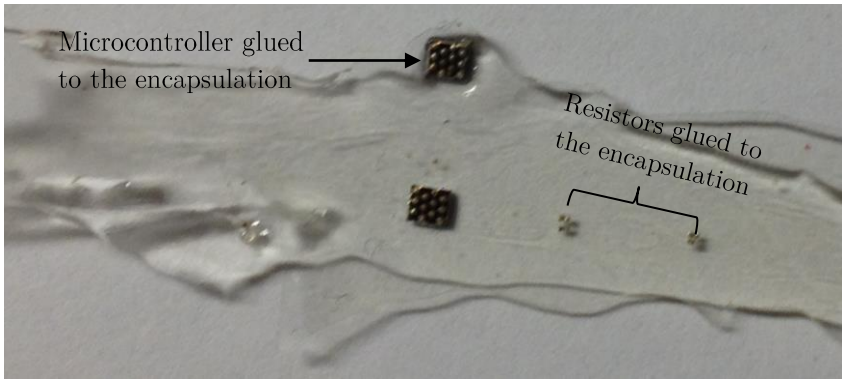

(b) Peeling of components by the encapsulation

Figure 7.19: Failure modes on temperature sensing strip after encapsulation

Furthermore, the Kapton sheet was separated from the silicon wafer at a temperature 130 °C from a hotplate. This was done at this temperature to weaken the glue strength of the Tesla adhesive tape so that the Kapton can be peeled off easily. However during delamination, the TPU encapsulation peeled off from the Kapton substrate and also peeled the components with it as shown in figure 7.19.

7.6 Conclusions

The integration of very fine functional circuits on textiles with feature sizes below 100 µm can be achieved with thin film interconnections. While it is easy to realise thin films on fabric or a polymer coated fabric, photolithographic patterning of thin

film interconnects on these substrates is complicated by the effects of the photolithographic processes on them. This work demonstrated showed that a UV-IF-1 (or a TPU) coated fabric would not survive a lift-off process based on NMP solution while the use of etchants like ferric chlorides causes a discolouration of the fabric. To conduct any photolithography on TPU polymer coated fabrics, the processing liquids that are gentle on such polymers are required.

Conventional flexible substrates such as Kapton are an alternative means of integrating fine circuits on fabrics but when functionalised, these substrates are too wide and often not concealed within the fabric after integration. By reducing their width, they can be better concealed by a cover textile fibre when woven into a yarn before integrating them on the fabric. This was successfully demonstrated with a 0.8 mm wide programmable Kapton strip that was functionalised with LED lightings. However, the prototype was not robust enough and didn't survive full processing.

CHAPTER 8
CONCLUSIONS AND FUTURE WORK

E-textiles are a potential solution for integrating electronic functionalities into a textile without significantly compromising its traditional function. The state of the art indicates that the transition of e-textiles from research prototypes to mass produced commercial products is hampered by their short-lived durability. This is because the incorporated electrical interconnections and the electronic components fail when they are exposed to real application stresses such as washing and bending. The durability of the e-textiles reviewed from the literature was initially enhanced by improving material properties such as the flexural rigidity and elasticity of the electrical interconnections so that they are still electrically reliable under flexural stresses. Waterproof and abrasion-proof features were also incorporated into the e-textiles to make them more durable under washing by using thermoplastic polymers to encapsulate or sandwich the interconnections and electronic components on the textile.

This thesis furthered these contributions by examining the reliability of electrical interconnections and electronic components for printed circuits on textiles. The findings of this work and its implications for achieving durable and wearable e-textiles are summarised below.

8.1 Suitable electrical interconnections for e-textiles

The electrical interconnections used for e-textiles can be categorised into electrical conductive threads/yarns, and electrically conductive films and laminates which consist of conductive inks, thin films and metal cladded or coated flexible plastics.

Electrically conductive threads/yarns are integrated into fabrics using any of the traditional textile techniques such as weaving, knitting, sewing and embroidery. They derive their conductivity from flexible metal yarns or coatings and can offer conductivities in the range of 0.01 Ω/m - 500 Ω/m respectively. Their durability are often improved by increasing their mechanical strength or by encapsulating them. Electronic components are more reliably bonded to them with the use of flexible or rigid interposer circuits to which the interconnections may be sewn but

this can potentially alter the textural feel of the e-textile. Conductive threads/yarns are best suited for realising only simple circuits on fabrics since they are limited by their integration process to the weave structure of the host fabric. This constraint also complicates their use for designing and integrating complex circuits on the fabric.

Electrically conductive films and laminates offer more flexibility in designing any circuit due to the design freedom and simplicity afforded by their integration process. Hence they are suitable for making large area (> 100 cm^2) planar circuits or concealing and localising circuits within a small fabric space (< 10 cm^2). Some of the common methods for realising these interconnections on fabrics include the screen printing of conductive inks, thermal evaporation of metallic films on fabrics or flexible plastics, and the weaving of conductive flexible plastics to fabrics. Although these interconnections are not as conductive as conductive yarns (containing metallic fibres or yarns), they still offer conductivities as high as 1 Ω/m for metal clad plastic substrates or a sheet resistivity as low as 0.01 Ω/sq. for 25 µm thick conductive films.

Electronic components can be easily bonded to them by using conductive (isotropic or anisotropic) adhesives or with flexible interposer circuits. Their durability can also be enhanced with the aforementioned methods used for conductive yarns. It is also possible to limit the stress induced in them during use by positioning them on the neutral axis (NA) of the e-textile. Unlike the previous durability solutions, this has the advantage of optimising the electrical performance of the interconnection irrespective of its material property. This approach is impractical with conductive threads/yarns because they are always interlocked to the fabric by weaving or knitting them in and out the fabric and this places them across all the stress planes of the fabric. For this reason, this thesis discussed the reliability of printed circuits realised by the screen printing and thermal evaporation deposition of conductive films.

8.2 Durable screen printed circuits for e-textiles

The current durability solution from the literature for screen printed interconnections on textiles sandwiched the screen printed interconnect between two screen printable thermoplastic polyurethanes (TPU) which act as:

i. an interface between the fabric and the interconnections to minimise the surface roughness of the fabric and to increase the flexibility of the interconnect by reducing its thickness to values as low as 5 µm.

ii. an encapsulant to protect the interconnect from abrasion and oxidation from air and water.

This thesis indicated, through a theoretical model developed in this work to characterise the bending behaviour of printed e-textiles, that these interconnects will be more electrically reliable and durable when they are positioned on or close to NA of the e-textile. Empirical verification of the model results obtained by screen printing a piezoresistive strain gauge in close proximity to the NA of four screen printed e-textiles of different woven fabric substrates - Bari, polyester, Escalade and Lagonda, showed resistance changes of $|\Delta R| \leq 10$ % for bending at a radius of 5 mm and five cycles of washing. However, a high TPU encapsulation thickness is often needed to engineer the screen printed interconnect on the NA due to its low stiffness. Thermoplastic polyurethanes elastomers (TPU) generally have elastic modulus defined in the range 0.015 - 0.7 GPa [125] and for the Fabink UV-IF-1 TPU (100 MPa) used in this work, the encapsulation thickness was as high as 0.8 mm. A disadvantage of using such a high thickness is that it can lead to failures in screen printed circuits due to stress risers that develop in the neighbourhood of the termination points of the encapsulant on the screen printed interconnect. Failure modes arising from the washing of screen printed LED circuits based on this encapsulation thickness also show that glob topped components are prone to failure unlike the circuits with small encapsulation thickness of 24 µm.

Another disadvantage is the effect of using such a high encapsulation on the wearability of the e-textile. An e-textile wearer can become more aware of the screen printed circuit. Nonetheless a compromise between the stiffness and flexibility of the encapsulating material can minimise the encapsulation thickness. By using flexible materials with elastic modulus as high as 3 GPa such as Kapton, an

encapsulation thickness less than 30 µm would be sufficient to position the interconnect on the NA of these fabrics based on the model.

Related results also showed that the different elastic modulus values of fabrics in tension and compression changes the NA position of e-textile as the bending orientation of the fabric changes from positive to negative bending and vice versa. Hence it is recommended that screen printed interconnects are located close to the NA positions in both bending orientations so as to improve the longevity of the interconnect.

8.3 Durable and wearable thin film circuits for e-textiles

The suitability of screen printed interconnects for e-textiles is limited by the resolution of the screen printing process to the integration of circuits with a minimum feature size of 100 µm. Very fine functional circuits with features sizes down to 20 µm are initially achieved on flexible plastic strips with photolithographic patterning and thin film deposition techniques before they are integrated into the fabric by weaving. While the emerging e-textile prototypes show good durability by surviving five washing cycles, the integrated plastic strips are too wide (≥ 2 mm) and are hence visible to the wearer. This potentially limits their wearability especially in aesthetic oriented field such as the fashion industry.

In this thesis, the width of the electronic strip is reduced to 0.8 mm which is small enough to be concealed by a cover textile yarn before it can be woven into a fabric. A functional strip was demonstrated with a reprogrammable circuit which contained a microcontroller to flash a bare die square sized LED that is 0.3 mm wide. Although the circuit was not robust enough for testing because the components were manually bonded to the strip due to the unavailability of the standard flip-chip and wire bonding processing tools, the working strip demonstrates some potential for this technology.

A related experiment in thesis also showed that the fabrication thin film circuits directly on a polymer coated fabric can be limited by the inability of the fabric to survive the photolithography patterning processes. This makes the use of flexible plastic ideal for integrating thin film circuits on fabrics.

8.4 Future work

To advance the findings of this research for the design and manufacture of durable e-textiles, further investigations in the following areas would be beneficial.

8.4.1 Modelling the mechanical behaviour of printed e-textiles

The mechanical behaviour of printed e-textiles in real applications determines the span of their durability. Therefore to customise and optimise their performance over the application lifetime, it is essential to have a theoretical model that is representative of this practical behaviour as a guide to designing them. This research presented a theoretical model that characterised the mechanical behaviour of printed e-textiles based on their elastic properties. Screen printed e-textiles were used as a case study for the model. The model was however only able to approximate the behaviour of three of the four experimented screen printed e-textiles on Bari, Polyester, Lagonda and Escalade woven fabrics. The mechanical actions such as bending, tensile extensibility, compression and washing that limit e-textile durability was simplified to a bending action. Hence the mechanical property of the e-textiles was characterised from their bending behaviour based on their elastic property in tension and compression. It also assumed a uniform geometry across the cross-section of the e-textile for simplicity hence the effects of the structural geometry and shear properties of the fabric substrate on e-textile durability were not investigated. The physiochemical effect of other washing parameters such as hydrodynamic flow actions [117] and the detergent flux [116] on the e-textile behaviour was also not considered. A model incorporating these parameters should improve the correlation between empirical results and model predictions. The new model should nonetheless be easy to use and cost effective for e-textile design.

8.4.2 Neutral axis engineering of printed e-textiles

The results presented in this work showed that the positioning of the printed circuits on the neutral axis of an e-textile improve its durability. However thermoplastic polyurethane (TPU) encapsulations of thicknesses as high as 0.8 mm are still needed to achieve this depending on the fabric substrate. Besides the increased sensitivity of the wearer to printed encapsulation, the e-textile also

becomes easily prone to mechanical failures especially at the interfaces. New screen printable materials of elastic modulus up to 3 GPa are needed to significantly reduce the encapsulation thickness.

Similarly more work is still needed in providing durable encapsulations to the electronics attached to these printed interconnections. The glob-top encapsulations experimented in this work resulted in structural failures along the interfaces between the glob top encapsulation on the component and the interconnect encapsulation. To avoid this, it is recommended that the encapsulation is stencil printed so that the components and interconnects are all encapsulated at once. This is because it is still at the moment impractical to screen print the encapsulation after the component has been bonded to the interconnects.

8.4.3 Durable thin film circuits on textiles

This work presented a proof of concept thin film temperature sensor circuit that has a minimum feature size of 30 µm. The circuit is contained on a 0.8 mm wide Kapton strip and could be potentially concealed in a textile as an electronic yarn. However, its robustness still has to be improved before any integration on textiles can be contemplated. Some aspects in the fabrication process of thin film circuits on textiles that would benefit from further investigation include:

1. Reliable techniques and automated tools for precision placement of electronic components of widths and lengths less than 0.3 mm on the strip. This is because manual placements of such components on the strip proved challenging and requires an excellent hand-eye co-ordination from the technician. Commercial flip chip bonders are promising but expensive tools. They will often need to be customised as the component size decreases.

2. Dispenser modules for depositing a small droplet volume of conductive adhesive on the contact pads on the strip. For the smallest contact pad (i.e. 0.2 mm x 0.2 mm) fabricated in this work, a minimum of 1 nano-litre droplet of conductive adhesive is required if a 25 microns adhesive thickness is assumed. This can be manually cumbersome and unrepeatable. Besides manual dispensing can be

fraught with short circuiting challenges especially where isotropic adhesives are dispensed.

3. Making reliable wire-bonds on thin film interconnects on Kapton and on the bare die chips integrated on them. This is perhaps on area that mainly limited the robustness and reliability of the fabricated temperature sensor in this work. Non-stick of aluminium wire to the evaporated aluminium film on Kapton was encountered during a wedge bonding. Gold – gold ball bonding have been shown in literature to be effective for its reliability [69] but this has yet to be investigated on flexible substrates.

Finally, the Functional ElecTronic Textiles (FETT) project by the University of Southampton and Nottingham Trent University seeks to further this technology by investigating reliable bonding electronics on thin film circuits on plastic substrates. Commercial flip-chip tools are investigated for adhesively mounted components alongside the suitability of wire-bonding (i.e. wedge and ball bonding) techniques for thin film circuits on plastics.

REFERENCES

[1] G. Cho, S. Lee and J. Cho, "Chapter 1: Review and Reappraisal of Smart Clothing", Smart Clothing and technology application textbook, published by CRC Press 2010, pg. 2.

[2] C. Dalsgaard and A. Jensen, "White Paper on Smart Garments: A market overview of intelligent textile technology in apparel", January 2011, pg. 1-11.

[3] D. Meoli and T. May-Pumlee, "Interactive Electronic Textile Development", Journal of Textile and Apparel, Technology and Management, Vol. 2 spring 2002, pg. 1-9.

[4] http://www.virtualworldlets.net/Shop/ProductsDisplay/VRInterface.php?ID=49

[5] M. Engin, A. Demirel, E. Z. Engin and M. Fedakar, "Recent developments and trends in biomedical sensors", Measurement Vol. 37 (2), March 2005, pg. 173-188.

[6] N. Taccini, G. Loriga, A. Dittmar and R. Paradiso, "Knitted Bioclothes for Health Monitoring", 6th Annual International Conference of the IEEE-EMBS, San Francisco, CA, USA, September 2004, pg. 2165-2168.

[7] E. R. Post, M. Orth, P. R. Russo, and N. Gershenfeld, "E-broidery: Design and Fabrication of textile-based computing", IBM Systems Journal, Vol. 39, 2000, pg. 840-860.

[8] Y. Kim, H. Kim and H. Yoo, "Electrical Characterization of Screen Printed Circuits on the Fabric", IEEE Trans. Advanced Packaging, Vol. 33 (1), February 2010, pg. 196 – 205.

[9] Silva, N. L., Gonçalves, L. M., & Carvalho, H. (2013). Deposition of conductive materials on textile and polymeric flexible substrates. Journal of Materials Science: Materials in Electronics, 24(2), 635-643.

[10] L. Buechley and M. Eisenberg, "Fabric PCBs, electronic sequins and socket buttons: Techniques for e-textiles craft", Pers Ubiquit Comput 2007, pg. 1-18.

[11] C. R. Merritt, H. T. Nagle, and E. Grant, "Fabric-Based Active Electrode Design and Fabrication for Health Monitoring Clothing", IEEE Trans. Info., Tech., in Biomedicine, Vol. 13 (2), March 2009, pg. 274 – 280.

[12] http://www.cutecircuit.com/ accessed on the 22nd of November 2015.

[13] Clevertex, Development of a strategic Master plan for the transformation textile and clothing into a knowledge driven industrial sector by 2015 – "Report on the intelligent Textiles State of the Art". http://109.2.243.201/documents/State_of_the_art.pdf: accessed on the 22nd of November 2015.

[14] Paul, G. (2014). Screen printed textile based wearable biopotential monitoring (Doctoral dissertation, University of Southampton).

[15] Mattila, H. (Ed.). (2006). Intelligent textiles and clothing. Woodhead Publishing.

[16] M. Suh, K. Carroll and N. Cassill, "Critical Review on Smart Clothing Product Development", Journal of Textile and Apparel, Technology and Management, Vol. 6(4), Fall 2010, pg. 1-18.

[17] S. Baurley, "Interactive and experiential design in smart textile products and applications", Pers Ubiquit Comput (2004) 8: 274-281.

[18] J. Berzowska, "Electronic Textiles: Wearable Computers, Reactive Fashion and Soft Computation", Textile Vol. 3 (1), pg. 2-19.

[19] L. Van Langenhove, M. Catrysse and F. Pirotte, "Chapter 5: The Use of Electronics in Medical textiles", Smart textiles for medicine and healthcare – Materials, systems and application, published by Woodhead Publishing Limited, England, 2007.

[20] S. Lam Po Tang, G. K. Stylios, "An Overview of smart technologies for clothing design and engineering", International Journal of Clothing Science and Technology, Vol. 18(2), 2006, pg. 108-208

[21] S. S. Mohammed, A. Ramasmy and T. Shanmuganantham, "Wireless Power transmission – A Next Generation Power Transmission System", International Journal of Computer Applications, Vol. 1(13), 2006, pg. 100-103.

[22] http://www.wirelesspowerconsortium.com/technology/how-it-works.html

[23] Li, Y., Grabham, N., Torah, R., Tudor, J., & Beeby, S. (2015). Data for the figures in Smart Textile Based Flexible Coils for Wireless Inductive Power Transmission.

[24] Zhu, D., Grabham, N. J., Clare, L., Stark, B. H., & Beeby, S. P. (2015, May). Inductive power transfer in e-textile applications: Reducing the effects of coil misalignment. In Wireless Power Transfer Conference (WPTC), 2015 IEEE (pp. 1-4). IEEE.

[25] R. Brock, "Terms and Definitions of Textiles", Available at www.textilelinks.com/author/rb/blterms.html: accessed 22nd of November 2015.

[26] M. Sun, "E-Textiles for Wearability: Review of Integration technologies", Textile world, April 2012.

[27] L. A. Buechley, "An investigation of Computational Textiles with Applications to Education and Design", PhD Thesis, University of Colorado, Boulder USA, 2007.

[28] Bhattacharya, R., Van Pieterson, L., & Van Os, K. (2012). Improving conduction and mechanical reliability of woven metal interconnects. Components, Packaging and Manufacturing Technology, IEEE Transactions on, 2(1), 165-168.

[29] Hegemann, D., Amberg, M., Ritter, A., & Heuberger, M. (2009). Recent developments in Ag metallised textiles using plasma sputtering. Materials Science and Technology, 24(1), 41-45.

[30] http://cactus-needle.blogspot.com/2013/11/more-from-kaffe-fassett-exhibit.html: accessed 22nd of November 2015.

[31] http://www.cstsales.com/popular_weave_styles.html: accessed 22nd of November 2015.

[32] I. Locher and G. Troster, "Fundamental Building Blocks for Circuits on Textiles", IEEE Trans. Advanced Packaging, Vol. 30(3), August 2007, pg. 541-550.

[33] S. Jung, C. Lauterbach and W. Weber, "A Digital Music Player Tailored for Smart Textiles: First Results", Avantex Symposium 2002.

[34] T. K. Ghosh, A. Dhawan and J. F MUTH, "Chapter 14: Formation of electrical circuits in textile structures", Intelligent textile and clothing Textbook, published by Woodhead Publishing Company, England, 2006.

[35] S. Jung, C. Lauterbach and W. Weber, "A Digital Music Player Tailored for Smart Textiles: First Results", Avantex Symposium 2002.

[36] S. Jung, C. Lauterbach, M. Strasser and W. Weber, "Enabling Technologies for Disappearing Electronics in Smart Textiles", IEEE International Solid-State Circuits Conference, 2003.

[37] W. Weber, R. Glaser, S. Jung, C. Lauterbach, G. Stromberg and T. Strum, "Electronics in Textiles, The Next Stage in Man Machine Interaction", Proceedings of the 2nd CREST Workshop on Advanced Computing and Communicating Techniques for Wearable Information Playing, Nara Institute of Science technology, Nara, Japan, 23-24 May 2003.

[38] Learn How to Knit, http://www.learn2knit.co.uk/knitting/decreasing.php: accessed 22nd of November 2015.

[39] N. Taccini, G. Loriga, A. Dittmar and R. Paradiso, "Knitted Bioclothes for Health Monitoring", 6th Annual International Conference of the IEEE-EMBS, San Francisco, CA, USA, September 2004, pg. 2165-2168.

[40] M. Soleimani, "Knitted Switches for Smart Clothing using double electrode technology," Sensor Review 28(3), 2008, pg. 229-232.

[41] T. Linz, "Analysis of Failure Mechanisms of Machine Embroidered Electrical Contacts and Solutions for Improved Reliability", PhD Dissertation, UGent, October 2011.

[42] T. Linz, C. Kallmayer, R. Aschenbrenner and H. Reichl, "Fully Integrated EKG Shirt based on Embroidered Electrical Interconnections with Conductive Yarn and Miniaturized Flexible Electronics", Proceedings of the International Workshop on Wearable and Implantable Body Sensor Networks (BSN'06), 2006.

[43] T. Linz, C. Kallmayer, R. Ashenbrenner and H. Reichl, "Embroidering Electrical Interconnects with Conductive Yarn for the Integration of Flexible Electronic Modules into Fabric", Proceedings of the Ninth IEEE International Symposium on Wearable Computers (ISWC'05), 2005.

[44] J. Taelman, T. Adriaensen, C. van der Horst, T. Linz and A. Spaepen, "Textile Integrated Contactless EMG Sensing for Stress Analysis", Proceedings of the 29th Annual International Conference of the IEEE EMBS, Cite Internationale, Lyon, France, August 2007.

[45] N. Noury, A. Dittmar, C. Corroy, R. Baghai, J.L. Weber, D. Blanc, F. Klefsat, A. Blinovska, S. Vaysse and B. Cornet, "VTAMN – A Smart Clothe for Ambulatory Remote Monitoring of Physiological Parameters and Activity", Proceedings of the 26th Annual International conference of the IEEE EMBS, San Francisco, CA, USA, September 2004, pg. 3266-3269.

[46] L. Buechley, "A Construction Kit for Electronic Textiles", Wearable Computers, 10th IEEE International Symposium, Montreux, Switzerland, October 2006, pg. 83.

[47] Du, Y. E. (Ed.). (2013). Biometrics: from fiction to practice. CRC Press, pg. 173.

[48] J. Cho, J. Moon, K. Jeong and G. Cho, "An Exploration of Electrolessly Cu/Ni Plated Polyester Fabrics as E-Textiles", Proceedings of the IEEE International Symposium on Wearable Computers, (ISWC'05), 2005.

[49] R. S. Khandpur, Textbook on Printed Circuit Boards – Design, Fabrication and Assembly, Published by McGraw-Hill Companies, USA, 2006.

[50] J. Cho, J. Moon, K. Jeong and G. Cho, "Application of PU-sealing into Cu/Ni Electroless Plated Polyester Fabrics for E-Textiles", Fibers and Polymers, Vol. 8 (3), 2007, pg. 330 – 334.

[51] J. Cho, J. Moon, M. Sung, K. Jeong and G. Cho, "Design and Evaluation of Textile –Based Signal Transmission Lines and Keypads for Smart Wear", HCI'07 Proceedings of the 12th international conference on Human – computer interaction: Interaction platforms and techniques, 2007, pg. 1078-1085.

[52] Wasa, K. (2012). Handbook of Sputter Deposition Technology: Fundamentals and Applications for Functional Thin Films, Nano-materials and MEMS. William Andrew, pg. 14.

[53] C. Zysset, K. Cherenach, T. Kinkeldei and G. Troster, "Weaving Integrated Circuits into Textiles", Wearable Computers (ISWC), International Symposium, 2010, pg. 1-8.

[54] Zysset, C., Kinkeldei, T. W., Münzenrieder, N., Cherenack, K., & Tröster, G. (2012). Integration Method for Electronics in Woven Textiles. Components, Packaging and Manufacturing Technology, IEEE Transactions on, 2(7), 1107-1117.

[55] K. H. Cherenack, T. Kinkeldei, C. Zysset and G. Troster, "Woven Thin-Film Metal Interconnects", IEEE Electron Device Letters, Vol. 31(7), July 2010, pp. 740-742.

[56] S. Shin, B. Kim, Y. K. Son, J. E. Kim, and I. Cho, "A Flexible Textile Wristwatch Using Transfer Printed Textile Circuit Technique", IEEE International Conference on Consumer Electronics (ICCE), Las Vegas , NV, USA, March 2012, pg. 21

[57] T. Vervust, G. Buyle, F. Bossuyt and J. Vanfletern, "Integration of Stretchable and washable electronic modules for smart textile applications", The Journal of the Textile Institute, iFirst, 2012, pg. 1-12.

[58] D. Brosteaux, F. Axisa, M. Gonzalez and J. Vanfleteren, "Design and Fabrication of Elastic Interconnections for Stretchable Electronic Circuits", IEEE Electron Device Letters, Vol. 28 (7), July 2007, 552-554.

[59] T. Loher, D. Manessis, R. Heinrich, B. Schmied, J. Vanfleteren, J. DeBaets, A. Ostmann, and H. Reichl, "Stretchable Electronic Systems", IEEE Electronics Packaging Technology Conference, 2006, pg. 271-276.

[60] F. Bossuyt, T. Vervust, F. Axisa and J. Vanfletern, "Improved Stretchable Electronics Technology for Large Area Applications", Proceedings of MRS Spring meeting 2010, Symposium JJ, (San Francisco USA), April 2010.

[61] S. Takamatsu, T. Yamashita and T. Itoh (2015). Fabrication of fabric LED array. Symposium on Design Test Integration and Packaging of MEMS and MOEMS. pp. 269 – 272.

[62] J. Slade, M. Agpaoa-Kraus, J. Bowman, A. Riecker, T. Tiano, C. Carey and P. Wilson, "Washing Electrotrxtiles", Proceedings of the Materials Research Society Symposium (MRS), 736:99-108.

[63] Sivasankar, Engineering Chemistry textbook, Published by Tata McGraw-Hill Publishing Company Limited, New Delhi, India, 2008.

[64] Cummins, G., & Desmulliez, M. P. (2012). Inkjet printing of conductive materials: a review. Circuit World, 38(4), 193-213.

[65] K. Gilleo, Polymer Thick Film textbook, published by International Thomson Publishing, Inc., 1996.

[66] B. Karaguzel, "Printing Conductive Inks on Nonwovens: Challenges and Opportunities", PhD thesis, North Carolina State University, USA, 2006.

[67] Gamota, D. R., Brazis, P., Kalyanasundaram, K., & Zhang, J. (Eds.). (2013). Printed organic and molecular electronics. Springer Science & Business Media.

[68] Minges, M. L. (1989). Electronic materials handbook: packaging (Vol. 1). Asm International.

[69] C. P. Wong, K. Moon and Y. Li, "Chapter 1: Nano-conductive Adhesives for Nano-electronics Interconnection", Nano-Bio-Electronic, Photonic and MEMS Packaging textbook, published Springer Science and Business media, 2010.

[70] J. M. Lowe and J. DevonPort, "Method for Making Printed Circuits", United States Patent, September 1992.

[71] D. Li, D. Sutton, A. Burgess, D. Graham and P. D. Calvert, "Conductive Copper and nickel lines via reactive inkjet printing", Journals of Materials Chemistry, Vol. 19, 2009, pg. 3719-3724.

[72] P. Markowski, W. Pinczakwoski, L. Straszewski and A. Dziedzic, "Thick-film thermoelectric microgenerators based on nickel, silver and PdAg-based compositions" Electronics Technology, International Spring Seminar, May 2007, pg. 223-228

[73] Li, Y. (2014). Direct write printed flexible electronic devices on fabrics (Doctoral dissertation, University of Southampton).

[74] Li, Y., Torah, R., Beeby, S. P., & Tudor, J. (2012). Inkjet printed flexible antenna on textile for wearable applications.

[75] Rothe, H., Usbeck, A., Cibis, D., & Krueger, K. (2005, August). Characterization of drop-on-demand printed conductive silver tracks. In Optics & Photonics 2005 (pp. 587812-587812). International Society for Optics and Photonics.

[76] Li, Y., Torah, R., Beeby, S., & Tudor, J. (2015). Fully direct-write dispenser printed dipole antenna on woven polyester cotton fabric for wearable electronics applications. Electronics Letters, 51(17), 1306-1308.

[77] Li, Y., Torah, R., Yang, K., Wei, Y., & Tudor, J. (2015). Fully direct write dispenser printed sound emitting smart fabrics. Electronics Letters, 51(16), 1266-1268.

[78] Wei, Y., Torah, R., Li, Y., & Tudor, J. (2015, April). Dispenser printed proximity sensor on fabric for creative smart fabric applications. In Design, Test, Integration and Packaging of MEMS/MOEMS (DTIP), 2015 Symposium on (pp. 1-4). IEEE.

[79] de Vos, M., Torah, R., & Tudor, J. (2015, April). A novel pneumatic dispenser fabrication technique for digitally printing electroluminescent lamps on fabric. In Design, Test, Integration and Packaging of MEMS/MOEMS (DTIP), 2015 Symposium on (pp. 1-4). IEEE.

[80] Pan, J., Tonkay, G. L., & Quintero, A. (1999). Screen printing process design of experiments for fine line printing of thick film ceramic substrates. Journal of Electronics Manufacturing, 9(03), 203-213.

[81] J. Lewis and A. Ryan, "Chapter 20: Printing as an Alternative Manufacturing Process for Printed Circuit Boards", New Trends in Technologies: Devices, Computer, Communication and Industrial Systems textbook, published by Sciyo, November 2010.

[82] T. Kang, C. R. Merritt, E. Grant, B. Pourdeyhimi and H. T. Nagle, "Nonwoven Fabric Active Electrodes for Bipotential Measurement During Normal Daily Activity", IEEE Trans. On Biomedical Engineering, Vol. 55 (1), January 2008, pg. 188 – 195.

[83] Paul, G., Torah, R., Beeby, S., & Tudor, J. (2014). The development of screen printed conductive networks on textiles for biopotential monitoring applications. Sensors and Actuators A: Physical, 206, 35-41.

[84] Paul, G. M., Cao, F., Torah, R., Yang, K., Beeby, S., & Tudor, J. (2014). A smart textile based facial EMG and EOG computer interface. Sensors Journal, IEEE, 14(2), 393-400.

[85] Yang, K., Freeman, C., Torah, R., Beeby, S., & Tudor, J. (2014). Screen printed fabric electrode array for wearable functional electrical stimulation. Sensors and Actuators A: Physical, 213, 108-115.

[86] B. Karaguzel, C. R. Merritt, T. Kang, J. M. Wilson, H. T. Nagle, E. Grant and B. Pourdeyhimi, "Utility of nonwovens in the production of integrated electrical circuits via printing conductive inks", Journal of the Textile Institute, Vol. 99 (1), 2008, pg. 37-45.

[87] B. Karaguzel, C. R. Merritt, T. Kang, J. M. Wilson, H. T. Nagle, E. Grant and B. Pourdeyhimi, "Flexible, durable printed electrical circuits", Journal of the Textile Institute, Vol. 100 (1), 2009, pg. 1-9.

[88] F. De Flaviis, "Chapter 5: Guided Waves",The Electrical Engineering Handbook, published by Elsevier Academic Press, 2005.

[89] http://websupplements.net/projects/virtual_labs/: accessed on 22nd November 2012.

[90] S. Merilampi, T. Laine-Ma and P. Ruuskanen, "The characterization of electrically conductive silver ink patterns on flexible substrates", Microelectronics Reliability, Vol. 29, 2009, pg. 782-790.

[91] T. Araki, M. Nogi, K. Suganuma, M. Kogure, and O. Kirihara, "Printable and Stretchable Conductive Wirings Comprising Silver Flakes and Elastomers", IEEE Electron Device Letterss, Vol. 32 (10), October 2011, pg. 1424 – 1426.

[92] S. Merilampi, T. Bjorninen, V. Haukka, P. Ruuskanen, L. Ukkonen and L. Sydanhemo, "Analysis of electrically conductive silver inks on stretchable substrates under tensile load", Microelectronics Reliability, Vol. 50, 2010, pg. 2001-2011.

[93] I. Kazani, C. Hertleer, G. De Mey, A. Schwarz, L. Van Langenhove, "Electrically Conductive Textiles Obtained by Screen Printing", Fibres and Textiles in Eastern Europe, Vol. 20(90), 2012, pg. 57-63.

[94] Paul, G., Torah, R., Yang, K., Beeby, S., & Tudor, J. (2014). An investigation into the durability of screen-printed conductive tracks on textiles. Measurement Science and Technology, 25(2), 025006.

[95] Yang, K., Torah, R., Wei, Y., Beeby, S., & Tudor, J. (2013). Waterproof and durable screen printed silver conductive tracks on textiles. Textile Research Journal, 0040517513490063.

[96] I. Kazani, C. Hertleer, G. De Mey, G. Guxho and L. Van Langenhove, "Dry cleaning of electroconductive layers screen printed on flexible substrates", Textile Research Journal, June 2012, pg. 1-8.

[97] M. Inoue, Y. Yamasaki and K. Suganuma, "Development of Super-Flexible Wires Using Conductive Adhesives for Artificial Skin Applications of Robots and Related Equipments", Polytronic 2005 – 5th International Conference on Polymers and Adhesives in Microelectronics and Photonics, 2005, pg. 90-95.

[98] Yang, K., Torah, R. N., Beeby, S., & Tudor, J. (2013). Investigation of screen printed flexible silver to achieve washable conductors on textiles.

[99] Suh, M., Carroll, K. E., Grant, E., & Oxenham, W. (2013). Effect of fabric substrate and coating material on the quality of conductive printing. Journal of the Textile Institute, 104(2), 213-222.

[100] Cao, J., Akkerman, R., Boisse, P., Chen, J., Cheng, H. S., De Graaf, E. F., ... & Lee, W. (2008). Characterization of mechanical behavior of woven fabrics: experimental methods and benchmark results. Composites Part A: Applied Science and Manufacturing, 39(6), 1037-1053.

[101] Lahey, T. J., & Heppler, G. R. (2004). Mechanical modeling of fabrics in bending. Journal of applied mechanics, 71(1), 32-40.

[102] Sun, M. N. (2008). A new tester and method for measuring fabric stiffness and drape. Textile Research Journal, 78(9), 761-770.

[103] Süle, G. (2012). Investigation of bending and drape properties of woven fabrics and the effects of fabric constructional parameters and warp tension on these properties. Textile Research Journal, 82(8), 810-819.

[104] Abbott, N. J. (1951). The measurement of stiffness in textile fabrics. Textile Research Journal, 21(6), 435-441.

[105] Bassett, R. J., & Postle, R. (1990). Fabric mechanical and physical properties: Part 4: The fitting of woven fabrics to a three-dimensional surface. International Journal of Clothing Science and Technology, 2(1), 26-31.

[106] Hu, J. (2004). Structure and mechanics of woven fabrics. Elsevier.

[107] Jeon, B. S., Chun, S. Y., & Hong, C. J. (2003). Structural and mechanical properties of woven fabrics employing Peirce's model. Textile research journal, 73(10), 929-933.

[108] Lammens, N., Kersemans, M., Luyckx, G., Van Paepegem, W., & Degrieck, J. (2014). Improved accuracy in the determination of flexural rigidity of textile fabrics by the Peirce cantilever test (ASTM D1388). Textile Research Journal, 0040517514523182.

[109] Kenkare, N., & May-Plumlee, T. (2005). Evaluation of drape characteristics in fabrics. International Journal of Clothing Science and Technology, 17(2), 109-123.

[110] W. R. Yu, M. Zampaloni, F. Pourboghrat, K. Chung, & T. J. Kang (2005, Jun.). Analysis of flexible bending behavior of woven preform using non-orthogonal constitutive equation. Composites Part A: Applied Science and Manufacturing. 36(6), pp. 839-850.

[111] Tan, P., Tong, L., & Steven, G. P. (1997). Modelling for predicting the mechanical properties of textile composites—A review. Composites Part A: Applied Science and Manufacturing, 28(11), 903-922.

[112] Hallal, A., Younes, R., & Fardoun, F. (2013). Review and comparative study of analytical modeling for the elastic properties of textile composites. Composites Part B: Engineering, 50, 22-31.

[113] Dixit, A., & Mali, H. S. (2013). Modeling techniques for predicting the mechanical properties of woven-fabric textile composites: A review. Mechanics of Composite Materials, 49(1), 1-20.

[114] Sankar, B. V., & Marrey, R. V. (1997). Analytical method for micromechanics of textile composites. Composites Science and Technology, 57(6), 703-713.

[115] Lee, A., Seo, M. H., Yang, S., Koh, J., & Kim, H. (2008). The effects of mechanical actions on washing efficiency. Fibers and Polymers, 9(1), 101-106.

[116] Yun, C., Cho, Y., & Park, C. H. (2016). Washing efficiency and fabric damage by beating and rubbing movements in comparison with a front-loading washer. Textile Research Journal, 0040517516636005.

[117] Park, S., Yun, C., Kim, J., & Park, C. H. (2013). The effects of the fabric properties on fabric movement and the prediction of the fabric movements in a front-loading washer. Textile Research Journal, 0040517512468810.

[118] Peirce, F. T. (1930). 26—The "handle" of cloth as a measurable quantity. Journal of the Textile Institute Transactions, 21(9), T377-T416.

[119] Naujokaitytė, L., Strazdienė, E., & Fridrichova, L. (2007). Comparative Analysis of Fabrics' Bending Behavior Testing Methods. Tekstil: Journal of Textile & Clothing Technology, 56(6).

[120] S. Lee, J.Y. Kwon, D. Yoon, H. Cho, J. You, Y. T. Kang, D. Choi and W. Hwang, "Bendability optimization of flexible optical nanoelectronics via neutral axis engineering" Nanoscale Research Letters, May 2012, pg. 7:256.

[121] M. C. Reid, "Electronic Textile-Based Sensors and Systems for Long-Term Health Monitoring", PhD Thesis, North Carolina State University, USA, March 2008.

[122] N. Karak, "Chapter 5: Structure and Properties of Polymers", Fundamentals of Polymers: Raw Materials to Finished Products, Published by PHI Private Limited, New Delhi, 2009, pg. 102.

[123] M. Maccioni, E. Orgiu, P. Cosseddu, S. Locci, and A. Bonfiglio, "Towards the textile transistor: Assembly and characterization of an organic field effect transistor with a cylindrical geometry", Applied Physics Letters, Vol. 89 (143515), 2006, pg. 1-3.

[124] J. B. Lee and V. Subramanian, "Weave Patterned Organic Transistors on Fiber for E-Textiles", IEEE Trans. Electron Devices, Vol. 52 (2), February 2005, pg. 269 – 275.

[125] S. Lee, B. Kim and H. Yoo, "Planar Fashionable Circuit Board Technology and its Applications", Journal of Semiconductor Technology and Science, Vol. 9 (3), September 2009, pg. 174 – 180.

[126] H. Kim, Y. Kim, Y. Kwon, and H. Yoo, "A 1.12mW Continuous Healthcare Monitor Chip integrated on a Planar Fashionable Circuit Board", IEEE International Solid-State Circuits Conference, 2008, pg. 150.

[127] I. Locher, "Technologies for System-on-Textile Integration", PhD Dissertation, Swiss Federal Institute of Technology, Zurich, 2006.

[128] T. Velten, H. Schuck, M. Richter, G. Klink, K. Bock, C. K. Malek, S. Polster, and P. Bolt, "Microfluidics on foil", 4M Proceedings of the 2nd International Conference on Multi-Material Micro Manufacture, 2006, pg. 313-317.

[129] H. Lin, C. Chang, W. Hwu, and M. Ger, "The rheological behaviours of screen-printing pastes", Journal of Material Processing Technology, Vol. 197, 2008, pg. 284 – 291.

[130] M. Pudas, J. Hagberg, and S. Leppavuori, "Printing parameters and ink components affecting ultra-fine-line gravure-offset printing for electronics applications", Journal of European Ceramic Society, Vol. 24, September 2004, pg. 2943 – 2950.

[131] Drobny, J. G. (2010). Radiation technology for polymers. CRC press.

[132] Foster, C. W., Kadara, R. O., & Banks, C. E. (2016). Fundamentals of Screen-Printing Electrochemical Architectures. In Screen-Printing Electrochemical Architectures (pp. 13-23). Springer International Publishing.

[133] M. P. Groover, "Chapter 16: Powder Metallurgy", Fundamentals of Modern Manufacturing: Materials, Processes, and Systems Textbook, Third Edition, Published by John Wiley & Sons. Inc., Hoboken, USA, 2007, pg. 337-361.

[134] Klauk, H. (2012). Organic electronics II: more materials and applications (Vol. 2). John Wiley & Sons.

[135] Degarmo, E. Paul; Black, J.; Kohser, Ronald A. (2007), Materials and Processes in Manufacturing (10th ed.), Wiley, p. 937, ISBN 13-978-0470-05512-0.

[136] J. Fjelstad, "Chapter 5: Practical Design Guidelines for Flex", Flexible Circuit Technology Textbook, Third Edition, Published by BR Publishing, Inc. Seaside, USA, 2006, pg. 75 -116.

[137] Silver epoxy adhesive datasheet by RS components, "http://docs-europe.electrocomponents.com/webdocs/04ad/0900766b804aded0.pdf; last accessed 22nd November 2015.

[138] E. J. Hearn, "Chapter 4: Bending", Mechanics of Materials textbook, Third Edition, Published by Butterworth –Heinemann, 1997, pg. 62-88.

[139] R. Huston and H. Josephs, "Chapter 8: Beams, bending Stresses (Flexure)", Practical Stress Analysis in Engineering Design, Third Edition, Published by CRC Press, New York, USA, 2009, pg. 103 – 110.

[140] R.G. Ballas, in Piezoelectric Multilayer Beam Bending Actuators: Static and Dynamic Aspects of Senosr Integration, Springer, 2007, pg. 54.

[141] Davis, J. R. (Ed.). (2004). Tensile testing. ASM international.

[142] N. Karak, "Chapter 5: Structure and Properties of Polymers", Fundamentals of Polymers: Raw Materials to Finished Products, Published by PHI Private Limited, New Delhi, 2009, pg. 102.

[143] Z. Zupin and k. Dimitrovski, "Chapter 2: Mechanical Properties of Fabrics from Cotton and Biodegradable Yarns Bamboo, SPF, PLA in Weft", Woven Fabric Engineering, Published by Sciyo, Croatia, 2010 pg. 25.

[144] J. Malzbender, J.M.J. den Toonder, A. R. Balkenende, G. de With, "Measuring mechanical properties of coatings: a methodology applied to nano-particle filled sol-gel coatings on glass" Material Science and Engineering, Vol. 36, 2002, pg. 47 – 103.

[145] National Centre for Advanced Tribology (nCAT), University of Southampton, UK, http://www.southampton.ac.uk/ncats/Downloads/Equipment/Nano-Indentation.pdf

[146] Ward, I. M., & Sweeney, J. (2012). Mechanical properties of solid polymers. John Wiley & Sons, pg. 381.

[147] Chandrasekhar, P. (2013). Conducting polymers, fundamentals and applications: a practical approach. Springer Science & Business Media, pg. 243.

[148] http://www-materials.eng.cam.ac.uk/mpsite/properties/non-IE/stiffness.html

[149] Hosford, W. F. (2010). Mechanical behavior of materials. Cambridge University Press, pg. 345.

[150] Betzina, S. (2004). More fabric savvy: a quick resource guide to selecting and sewing fabric. Taunton Press, pg. 82.

[151] Ugur, Ş. S., Sariişik, M., & Aktaş, A. H. (2010). The fabrication of nanocomposite thin films with TiO2 nanoparticles by the layer-by-layer deposition method for multifunctional cotton fabrics. Nanotechnology, 21(32), 325603.

[152] Liston, E. M., Martinu, L., & Wertheimer, M. R. (1993). Plasma surface modification of polymers for improved adhesion: a critical review. Journal of Adhesion Science and Technology, 7(10), 1091-1127.

[153] Ghosh, M. (1996). Polyimides: fundamentals and applications. CRC Press, pg. 389

[154] Wong, W. S., & Salleo, A. (Eds.). (2009). Flexible electronics: materials and applications (Vol. 11). Springer Science & Business Media.

[155] Inagaki, N., Tasaka, S., & Hibi, K. (1994). Improved adhesion between plasma-treated polyimide film and evaporated copper. Journal of adhesion science and technology, 8(4), 395-410.

[156] Dunn, D. J. (2004). Engineering and structural adhesives (Vol. 15). iSmithers Rapra Publishing.

[157] Madou, M. J. (2002). Fundamentals of microfabrication: the science of miniaturization. CRC press.

[158] Dell'Acqua-Bellavitis, L. M. (2007). Lab-on-a-chip Devices with Nanophase Surface Topography for Neural Electrophysiological Applications. ProQuest.

[159] Franssila, S. (2004). Front Matter (pp. i-xv). John Wiley & Sons, Ltd, pg. 19.

[160] Machlin, E. S. (2006). Materials Science in Microelectronics: The relationships between thin film processing and structure. Elsevier.

[161] Datta, M., Osaka, T., & Schultze, J. W. (Eds.). (2004). Microelectronic packaging. CRC press.

[162] Chauhan, P. S., Choubey, A., Zhong, Z., & Pecht, M. G. (2014). Copper wire bonding (pg. 11 - 38). Springer New York.

APPENDIX A

Datasheet of Bari fabric

workwear ◆ protectivewear ◆ casual apparel

www.klopman.com

FABRIC INFORMATION

FABRIC:	**SBM-S**
FINISH:	**Bacteriostatic finish silver based (P309 AG)**
END USE:	**Workwear Industrial Wash**

FABRIC DESCRIPTION	CHARACTERISTICS
Fibre Content	65 % Polyester 35 % Cotton
Finished Weight	210 g/m²
Yarn Count (Nm)	Warp 44 Nm Weft 27 Nm
Finished Construction (cm)	Warp 48 cm Weft 23 cm
Weave	2x1 twill
Minimum Usable Width	150 cm

PHYSICAL PERFORMANCE		TEST METHODS AND RESULTS			
		Klopman Tests	Results	International Tests	Results
Tensile Strength	Warp Weft	T.M. KI 711	Warp 1100 N Weft 600 N	ISO 13934-1	Warp 1100 N Weft 600 N
Pilling ICI Box (36000 Rev)		T.M. KI 720	Grade :4	ISO 12945-1	Grade :4
Shrinkage in washing 75°C 5 x		T.M. KI 743-TT	+/- 3.0%	ISO 15797	+/- 3.0%

COLOUR PERFORMANCE		TEST METHODS AND RESULTS			
Rubbing Dry		T.M. KI 750	Grade :4	ISO 105 X12	Grade :4
Washing:	Colour Change Colour Staining (Pes + Cot)	T.M. KI 770-A T.M. KI 770-A	Grade :4 Grade :3/4	ISO 105 C06 E1S ISO 105 C06 E1S	Grade :4 Grade :3/4
Dry Cleaning	(Colour Change)	T.M. KI 754	Grade :4	ISO 105 D01	Grade :4
Perspiration:	Colour Change Colour Staining (Pes + Cot)	T.M. KI 757 T.M. KI 757	Grade :4 Grade :3/4	ISO 105 E04 ISO 105 E04	Grade :4 Grade :3/4
Light Fastness		T.M. KI 760	Grade :5	ISO 105 B02	Grade :5

OTHER PERFORMANCES	TEST METHODS AND RESULTS			
Antibacterial efficiency (Dynamic contact test) Tested by Sanitized®			ASTM E 2149-01	30X ISO 15797, t2, p4: > 99%

Dark and special colours may not fulfil quoted figures.
Characteristics may vary within commercial tolerances.
Sanitized is a Registered Trademark

PRODUCT CARE - ALL FABRICS ARE TESTED TO KLOPMAN TEST METHODS.

Domestic Laundering:

Industrial Laundering - see Klopman Laundering Recommendation.

ISO 9001:2000 REGISTERED COMPANY

THIS DOCUMENT IS FOR INFORMATION ONLY.
FOR A CONTROLLED DOCUMENT PLEASE CONTACT THE KLOPMAN "PRODUCT MANAGER" - FROSINONE.

Oct-08 English

Figure A.1: Datasheet of Bari fabric

APPENDIX B

B.1 Proof of neutral axis equation

Taking into consideration the elastic modulus of the different materials that make up the n – layered composite in figure 4.1, the resultant force acting across the cross-section of the beam in pure bending about its neutral axis position is given by:

$$F = \sum_{i}^{n} E_i x_i \int_{lower\ limit}^{upper\ limit} \frac{y}{R} dy = 0 \qquad (B.1)$$

From figure 4.2, the lower and upper limits of the integral is obtained about the i-th layer as:

$$Lower\ limit = \bar{y} - \sum_{j=1}^{i-1} h_j$$

$$Upper\ limit = \bar{y} - \sum_{j=1}^{i} h_j \qquad (B.2)$$

Hence equation B.1 can be reduced as:

$$\sum_{i}^{n} E_i x_i \int_{\bar{y} - \sum_{j=1}^{i-1} h_j}^{\bar{y} - \sum_{j=1}^{i} h_j} \frac{y}{R} dy = 0$$

$$\sum_{i}^{n} E_i x_i \left[\frac{y^2}{2} \right]_{\bar{y} - \sum_{j=1}^{i-1} h_j}^{\bar{y} - \sum_{j=1}^{i} h_j} = \sum_{i}^{n} E_i x_i \left[\left(\bar{y} - \sum_{j=1}^{i} h_j \right)^2 - \left(\bar{y} - \sum_{j=1}^{i-1} h_j \right)^2 \right] = 0 \qquad (B.3)$$

Applying the difference of two squares, then

$$\sum_{i}^{n} E_i x_i \left[\left(2\bar{y} - \sum_{j=1}^{i-1} h_j - \sum_{j=1}^{i} h_j \right) \left(\sum_{j=1}^{i-1} h_j - \sum_{j=1}^{i} h_j \right) \right] = 0$$

But

$$\sum_{j=1}^{i-1} h_j - \sum_{j=1}^{i} h_j = \left(h_1 + h_2 + ... + h_{i-1} \right) - \left(h_1 + h_2 + ... + h_{i-1} + h_i \right) = -h_i$$

$$\sum_i^n E_i x_i \left[\left(2\bar{y} - \sum_{j=1}^{i-1} h_j - \sum_{j=1}^{i} h_j \right) (-h_i) \right] = 0$$

$$\sum_i^n E_i x_i \left[-2\bar{y}h_i + h_i \left(\sum_{j=1}^{i-1} h_j + \sum_{j=1}^{i} h_j \right) \right] = 0$$

Also,

$$\sum_{j=1}^{i-1} h_j + \sum_{j=1}^{i} h_j = (h_1 + h_2 + ... + h_{i-1}) + (h_1 + h_2 + ... + h_{i-1} + h_i) = 2\sum_{j=1}^{i-1} h_j + h_i = 2\sum_{j=1}^{i} h_j - h_i$$

$$\sum_i^n E_i x_i \left[-2\bar{y}h_i + h_i \left(2\sum_{j=1}^{i} h_j - h_i \right) \right] = 0$$

$$\sum_i^n E_i x_i \left[2\bar{y}h_i - 2h_i \sum_{j=1}^{i} h_j + h_i^2 \right] = 0 \qquad (B.4)$$

$$2\sum_i^n E_i x_i h_i \bar{y} = \sum_i^n E_i x_i h_i \left(2\sum_{j=1}^{i} h_j - h_i \right)$$

$$\bar{y} = \frac{\sum_i^n E_i x_i h_i \left(2\sum_{j=1}^{i} h_j - h_i \right)}{2\sum_i^n E_i x_i h_i} \qquad (B.5)$$

B.2 Apparent modulus of a multi-layer beam

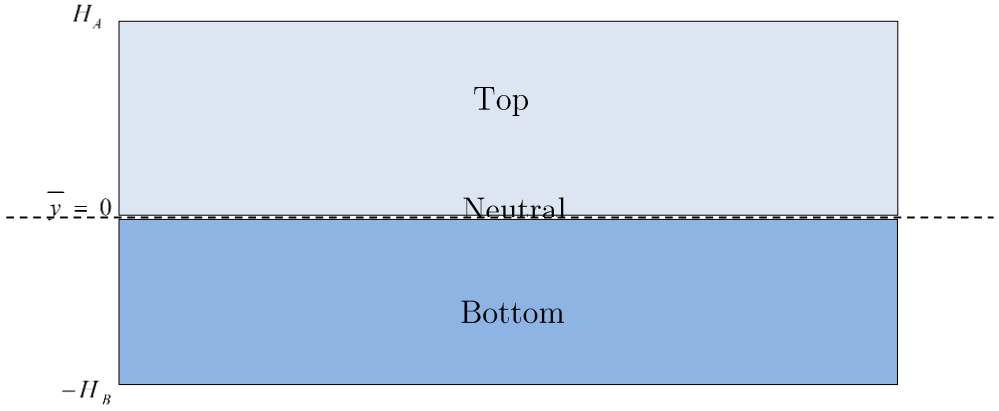

Figure B.1: Bilayer equivalent of a multi-layer beam

If the neutral axis position of this multi-layer becomes the new origin, i.e. $\bar{y} = 0$, so that it has k bottom layers and n-k top layers about this point, then equation (B.4) can be rewritten as:

$$\sum_{i}^{k} E_i x_i \left[2\bar{y}h_i - 2h_i \sum_{j=1}^{i} h_j + h_i^2 \right] + \sum_{i=k+1}^{n} E_i x_i \left[2\bar{y}h_i - 2h_i \sum_{j=k+1}^{i} h_j + h_i^2 \right] = 0 \qquad (B.6)$$

From equation 4.13,

$$-E_B H_B^2 + E_A H_A^2 = 0 \qquad (B.7)$$

By comparing both equations then,

$$-E_B H_B^2 = \sum_{i}^{k} E_i x_i \left[2\bar{y}h_i - 2h_i \sum_{j=1}^{i} h_j + h_i^2 \right] \qquad (B.8a)$$

$$E_A H_A^2 = \sum_{i=k+1}^{n} E_i x_i \left[2\bar{y}h_i - 2h_i \sum_{j=k+1}^{i} h_j + h_i^2 \right] \qquad (B.8b)$$

If the following parameters are defined as follows:

$$t_i = \frac{h_i}{H_B}; \sum_{i=1}^{k} t_i = 1 \quad \forall\ i \le k$$

$$t_i = \frac{h_i}{H_A}; \sum_{i=k+1}^{n} t_i = 1 \quad \forall\ i \ge k+1 \qquad (B.9)$$

For $\bar{y} = 0$ then equations B.8a and B.8b can be rewritten as:

$$E_B = \sum_{i=1}^{k} E_i t_i \left(2\sum_{j=1}^{i} t_j - t_i \right) \qquad (B.10a)$$

$$E_A = \sum_{i=k+1}^{n} E_i t_i \left(t_i - 2\sum_{j=k+1}^{i} t_j \right) \qquad (B.10b)$$

APPENDIX C

Datasheet of Escalade fabric

workwear ◆ protectivewear ◆ casual apparel

www.klopman.com

FABRIC INFORMATION

FABRIC:	**Escalade**
FINISH:	**Regular Finish (4176 16)**
END USE:	**Apparel Garment**

FABRIC DESCRIPTION	CHARACTERISTICS	
Fibre Content	46% Cotton 38%T400 16%Polyester	
Finished Weight	295g/m²	
Yarn Count	Warp 25 Nm	Weft 330 Dtex
Finished Construction	Warp 43 cm	Weft 23,5 cm
Weave	3x1 twill	
Minimum Usable Width	140 cm	

PHYSICAL PERFORMANCE		TEST METHODS AND RESULTS			
		Klopman Tests	Results	International Tests	Results
Tensile Strength	Warp Weft	T.M. KI 711	Warp 1200 N Weft 600 N	ISO 13934-1	Warp 1200 N Weft 600 N
Tear Strength-Elmendorf (gr.)	Warp Weft	T.M.KI 713	Warp 2500gr Weft 3500gr	ISO 13937-1	Warp 2500gr Weft 3500gr
Pilling (11000 Rev)		T.M. KI 721	Grade :3/4	ISO 12945-1	Grade :3/4
Shrinkage in washing 1 x 60°C T.D.		T.M. KI 741-TD	+1/-2.5%	ISO 6330 /2A-E	+1/-2.5%

COLOUR PERFORMANCE		TEST METHODS AND RESULTS			
Rubbing Dry		T.M. KI 750	Grade :4	ISO 105 X12	Grade :4
Washing:	Colour Change Colour Staining	T.M. KI 774-A T.M. KI 774-A	Grade :4 Grade :3/4	ISO 105 C06 C1S ISO 105 C06 C1S	Grade :4 Grade :3/4
Dry Cleaning	Colour Change	T.M. KI 754	Grade :4	ISO 105 D01	Grade :4
Perspiration:	Colour Change Colour Staining	T.M. KI 757 T.M. KI 757	Grade :4 Grade :3/4	ISO 105 E04 ISO 105 E04	Grade :4 Grade :3/4
Light Fastness		T.M. KI 761	Grade :5	ISO 105 B02	Grade :5

OTHER PERFORMANCES		TEST METHODS AND RESULTS		
% Stretch	Elongation	T.M. KI 737	>16%	ASTMD 3107-80	>16%
	Growing	T.M. KI 737	2,5%	ASTMD 3107-80	2,5%

For dark, black & special colours, minimum fastness expected values have to be negotiated at first sampling order.
If any additional minimum colour fastness requirements are specifically needed, please contact your Klopman representative.
For any customised minimum fastness requirements please contact your Klopman representative.
Due to a special construction we should consider +/-5% weight tolerance.

PRODUCT CARE - ALL FABRICS ARE TESTED TO KLOPMAN TEST METHODS.

Domestic Laundering:

ISO 9001:2000 REGISTERED COMPANY

THIS DOCUMENT IS FOR INFORMATION ONLY.
FOR A CONTROLLED DOCUMENT PLEASE CONTACT THE KLOPMAN "PRODUCT MANAGER" - FROSINONE.

Jan-07 English

Figure C.1: Datasheet of Escalade fabric

APPENDIX D

Datasheet of Lagonda fabric

workwear • protectivewear • casual apparel

www.klopman.com

FABRIC INFORMATION

FABRIC:	**LAGONDA (Provisional)**
FINISH:	**Regular A909 16**
END USE:	**Apparel Garment**

FABRIC DESCRIPTION	CHARACTERISTICS	
Fibre Content	40% Cotton 30% T400 30% Polyester	
Finished Weight	205 g/m²	
Yarn Count	Warp 34 Nm	Weft 165 Dtex
Finished Construction	Warp 47 cm	Weft 28 cm
Weave	2x1 twill	
Minimum Usable Width	138 cm	

PHYSICAL PERFORMANCE		TEST METHODS AND RESULTS			
		Klopman Tests	Results	International Tests	Results
Tensile Strength	Warp	T.M. KI 711	Warp 800 N	ISO 13934-1	Warp 800 N
	Weft		Weft 400 N		Weft 400 N
Tear Strength- Elmendorf (gr.)	Warp	T.M.KI 713	Warp 2000gr	ISO 4674/B	Warp 2000gr
	Weft		Weft 1500gr		Weft 1500gr
Pilling (11000 Rev)		T.M. KI 722	Grade :3/4	ISO 12945-1	Grade :3/4
Shrinkage in washing 1 x 60°C (%) T.D.		T.M. KI 741-TD	+1/-2.5%	ISO 6330 /2A-E	+1/-2.5%

COLOUR PERFORMANCE		TEST METHODS AND RESULTS			
Rubbing Dry		T.M. KI 750	Grade :4	ISO 105 X12	Grade :4
Washing:	Colour Change	T.M. KI 774-A	Grade :4	ISO 105 C06 C1S	Grade :4
	Colour Staining	T.M. KI 774-A	Grade :3/4	ISO 105 C06 C1S	Grade :3/4
Dry Cleaning	Colour Change	T.M. KI 764	Grade :4	ISO 105 D01	Grade :4
Perspiration:	Colour Change	T.M. KI 757	Grade :4	ISO 105 E04	Grade :4
	Colour Staining	T.M. KI 757	Grade :3/4	ISO 105 E04	Grade :3/4
Light Fastness		T.M. KI 761	Grade :5	ISO 105 B02	Grade :5

OTHER PERFORMANCES		TEST METHODS AND RESULTS			
% Stretch	Elongation	T.M. KI737	25 +/-5%	ASTMD 3107-80	25+/-5%
	Growing	T.M. KI737	2%	ASTMD 3107-80	2%

For dark, black & special colours, minimum fastness expected values have to be negotiated at first sampling order.
If any additional minimum colour fastness requirements are specifically needed, please contact your Klopman representative.
For any customised minimum fastness requirements please contact your Klopman representative.
Due to a special construction we should consider +/-5% weight tolerance.

PRODUCT CARE - ALL FABRICS ARE TESTED TO KLOPMAN TEST METHODS.

Domestic Laundering:

ISO 9001:2000 REGISTERED COMPANY

THIS DOCUMENT IS FOR INFORMATION ONLY.
FOR A CONTROLLED DOCUMENT PLEASE CONTACT THE KLOPMAN "PRODUCT MANAGER" - FROSINONE.

Nov 08 English

Figure D.1: Datasheet of Lagonda fabric

APPENDIX E

E.1 ISO washing standard 6330:2000

The washing procedure by the International Organization for standardization is described in the Table below:

Table E.1: ISO 6330: 2000 Washing Standard for horizontal rotating drum machine – Type A.

Procedure No	Agitation during heating, washing and rinsing	Total load (dry mass)	Washing				Rinse 1		Rinse 2			Rinse 3			Rinse 4		
			Temp b °C	Liquor level c, d cm	Wash time e min	Cool Down f	Liquor Level c min	Rinse time e, g min	Liquor Level c cm	Rinse time e, g min	Spin time e min	Liquor Level d cm	Rinse time e, g min	Spin time e min	Liquor Level d cm	Rinse time e, g min	Spin time e min
1A[h]	Normal	2 ± 0,1	92 ± 3	10	15	Yes[i]	13	3	13	3	-	13	2	-	13	2	5
2A[h]	Normal	2 ± 0,1	60 ± 3	10	15	No	13	3	13	3	-	13	2	-	13	2	5
3A[h]	Normal	2 ± 0,1	60 ± 3	10	15	No	13	3	13	2	-	13	2	2[j]	-	-	-
4A[h]	Normal	2 ± 0,1	50 ± 3	10	15	No	13	3	13	2	-	13	2	2[j]	-	-	-
5A	Normal	2 ± 0,1	40 ± 3	10	15	No	13	3	13	3	-	13	2	-	13	2	5
6A	Normal	2 ± 0,1	40 ± 3	10	15	No	13	3	13	2	-	13	2	2[j]	-	-	-
7A	Gentle[K]	2 ± 0,1	40 ± 3	13	3	No	13	3	13	3	1	13	2	6	-	-	-
8A[l]	Gentle[K]	2 ± 0,1	30 ± 3	13	3	No	13	3	13	3	-	13	2	2[j]	-	-	-
9A[l]	Gentle	2	92 ± 3	10	12	Yes[i]	13	3	13	3	-	13	2	2[j]	-	-	-
Simulated Hand Wash	Gentle[K]	2	40 ± 3	13	1	No	13	2	13	2	2	-	-	-	-	-	-

a – For procedures 1A, 2A and 5A an alternative load of 5kg and for procedure 7A an alternative load of 1kg is recommended where articles are being tested for washing efficiency, possible abrasion sensitivity or similar effects.

b – All filling temperatures for wash and rinse are (20±5) ºC.

c – Liquor level is measured from the bottom of the cage after the machine has been run for 1 min and allowed to stand for 30s

d – The volumes of liquor corresponding to the quoted levels are determined by a separate test using a graduated measuring vessel.

e – The stated times may have a tolerance of ±20s

f – Cool down; top up with cold water to 13cm level and agitate for a further 2 min.

g – Rinse time is measured when liquor level is reached.

i – For safe laboratory practice only

J – Short spin or drip dry

k – No agitation during heating

l – This programme is retained because it is part of 1SO 3758

APPENDIX F

F.1 List and dimensions of components for temperature sensing strip

Table F.1: List of circuit components

S/N	Component	Function	Number used	Package	Dimension length x width x thickness (mm^3)
1.	Attiny20 Microcontroller, supplied by Digi-key, USA	To program to the ambient temperature to be detected by the circuit	1	Wafer level chip scale package (WLCSP)	1.555 x 1.403 x 0.538
2.	LEDs (blue, red, green and yellow) supplied by Cree lightings INC, USA	To indicate the temperature sensed	8	Wire bondable bare die	0.3 x 0.3 x 0.27
3	100 Ω resistor	To prevent the LEDs from drawing too much current from the microcontroller.	4	Surface mount	0.4 x 0.2 x 0.13
4	10 kΩ thermistor	To detect changes in ambient temperature changes	1	Surface mount	0.6 x 0.3 x 0.3
5	CBC005, supplied by Cymbet corporation	To store energy of 5μAh useful for clocking and as a switch over power	1	Wire bondable bare die	2.25 x 1.7 x 0.175
6	CBC910, supplied by Cymbet corporation	Power management for module	1	Wire bondable bare die	1.36 x 0.96 x 0.15

F.2 Screen design of the photolithography glass mask for the temperature sensing strip

Glass mask for photolithographic patterning of a temperature sensor circuit on Kapton. Section 1 contains 10 square patterns of resolution ranging from 800 µm to 10 µm to determine highest resolution of the thin film technique. Sections 2 and 4 contain temperature sensing circuits with lengths of 75 mm and 135 mm. Section 3 contains 142 mm long temperature sensing circuits that contain a rechargeable 5 µAh (micro-amp-hour) bare die energy storage and power management chips. This was designed to investigate the potential of a self-powered strip by a battery. However since the power provided by the battery is too low to power the microcontroller, it can be used to power the thermistor.

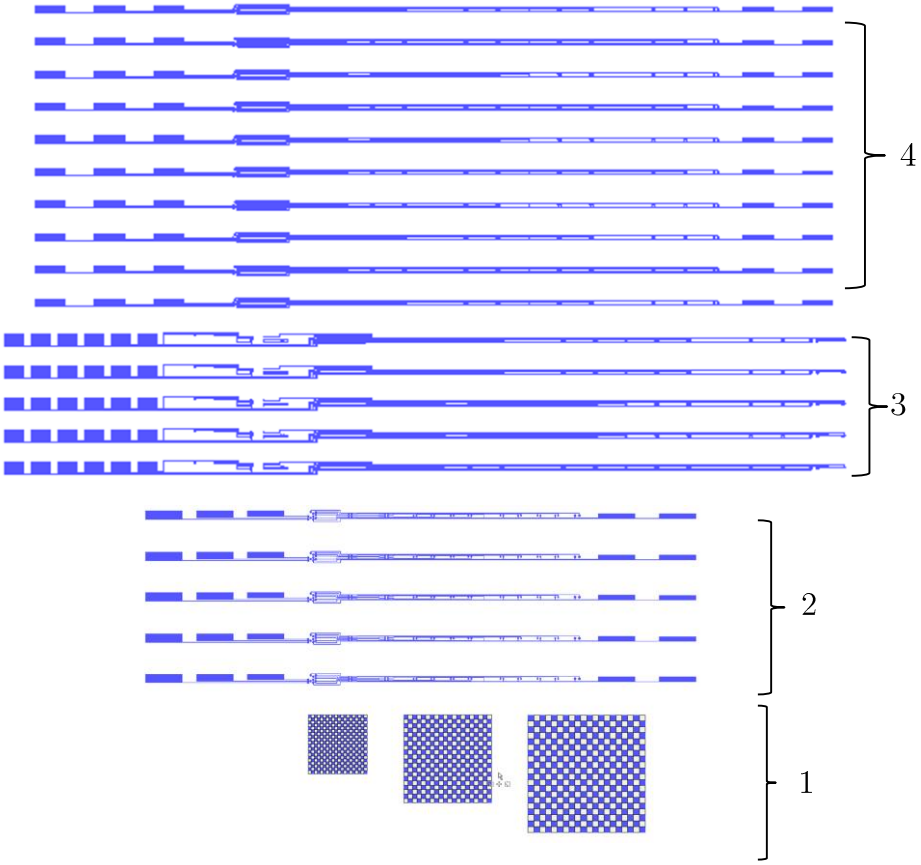

Figure F.1: Screen design for patterning thin film temperature sensor circuit on Kapton